






Universitat Autònoma de Barcelona

ADVERTIMENT. L'accés als continguts d'aquesta tesi queda condicionat a l'acceptació de les condicions d'ús establertes per la següent llicència Creative Commons:  http://cat.creativecommons.org/?page_id=184

ADVERTENCIA. El acceso a los contenidos de esta tesis queda condicionado a la aceptación de las condiciones de uso establecidas por la siguiente licencia Creative Commons:  <http://es.creativecommons.org/blog/licencias/>

WARNING. The access to the contents of this doctoral thesis it is limited to the acceptance of the use conditions set by the following Creative Commons license:  <https://creativecommons.org/licenses/?lang=en>

Synthesis and characterization of curcuminoids and their derived polymeric systems

Laura Rodríguez Cid

Doctoral Thesis

Ph.D. in Chemistry

Supervisor: ICREA Prof. Núria Aliaga Alcalde

Supervisor: Prof. Concepción Domingo Pascual

Tutor: Dr. José A. Ayllón Esteve

Departament de Química-Facultat de Ciències (UAB)

Institut de Ciència de Materials de Barcelona (ICMAB-CSIC)

2021



Universitat Autònoma de Barcelona
Departament de Química-Facultat de Ciències
Pograma de doctorado: Doctorado en Química

Synthesis and characterization of curcuminoids and their derived polymeric systems

Thesis presented to aspire to the Doctorate in
Chemistry degree by

RODRIGUEZ Firmado digitalmente
por RODRIGUEZ CID
CID LAURA - LAURA - 44659536E
44659536E Fecha: 2021.08.31
17:09:37 +02'00'

Laura Rodríguez Cid

ALIAGA Firmado digitalmente
por ALIAGA ALCALDE
ALCALDE NURIA NURIA - 44179637H
- 44179637H Fecha: 2021.08.31
17:22:33 +02'00'

Supervisor

ICREA Prof. Núria Aliaga Alcalde

DOMINGO Firmado digitalmente
por DOMINGO PASCUAL
PASCUAL M.CONCEPCION - DNI
M.CONCEPCION 40971685Z
- DNI 40971685Z Fecha: 2021.09.01
14:21:53 +02'00'

Supervisor

Prof. Concepción Domingo Pascual

JOSÉ ANTONIO Firmado digitalmente
por JOSÉ ANTONIO
AYLLÓN ESTEVE AYLLÓN ESTEVE - DNI
- DNI 33901452G
33901452G Fecha: 2021.09.01
09:58:38 +02'00'

Tutor

Dr. José A. Ayllón Esteve

Bellaterra, September 2021

Abstract

Curcuminoids (CCMoids) are a group of molecules that display two aromatic rings joined by a seven-carbon conjugated chain (diarylheptanoids) and a β -diketone moiety in the central position of their structures. The straightforward synthesis of this type of molecules allows their thorough design depending on the final purpose, mainly by modifying the lateral substituents, but also the chain length and/or the β -diketone unit. Despite of the number of CCMoids that have been synthesized until now, and the presence in many of them of functional groups susceptible to react with other species, the use of CCMoids as building blocks for the creation of highly dimensional structures is scarce. This, together with the properties shown by this family of molecules (biomedical, electronic...) and their versatile chemistry, motivated the development of the ideas presented in this doctoral thesis.

In this sense, nine CCMoids, including four not previously described in the literature, are presented in this doctoral thesis. Moreover, their detailed characterization has been carried out, probing not only the achieving of the desired molecules in high purity but also how their structural differences may affect their physicochemical properties.

Regarding the formation of extended structures, several coordination polymers (CPs) have been achieved from the reaction with transition metal ions and first steps in the synthesis of organic polymers (OPs) are also shown.

For the studies of CPs, two CCMoids were tested: a natural one, the bisdemethoxycurcumin (BDMC), with phenol groups at the sites of the molecule, and a synthetic CCMoid, 3pyCCMoid, with pyridines as aromatic substituents.

The reaction between BDMC and zinc acetate, performed under mild conditions in EtOH, provides a new 1D system. In addition, dimensionality and porosity of this network have been expanded by studying the reaction occurring between three species: BDMC, Zn(II) salts, and a ditopic co-linker (1,2-bis(4-pyridyl)ethylene, 1,3-bis(4-pyridyl)propane or 4,4'-bipyridine). In total, here seven new CPs are presented. The structures of five of them were elucidated by single-crystal X-ray diffraction. Moreover, we show that the combination of solid state ^{13}C NMR and conventional techniques (elemental analysis, FTIR.) can provide useful information about the coordination modes of BDMC, in the cases of unresolved structures.

The coordination of 3pyCCMoid with Zn(II) centres results in three CPs with different architectures and dimensionalities (from 1D to 3D). Here it is examined how synthetic methods and some slightly changes, in the reaction conditions, affect the formation of the final materials. In addition, an effective method for the exfoliation of a 2D CP was optimized and the characterization of the few layer nanosheets performed. Using the same CCMoid but reacting with a Co(II) salt, an isostructural 2D CP was synthesized, being the first CCMoid-CP with a metal different than Zn(II).

For the synthesis of OPs, two approaches have been proposed: (i) the formation of extended structures by the use of a CCMoid with boronic acids (BOHCCMoidBF₂) at the sites that reacts with commercial polyols and, (ii) the in-situ synthesis of CCMoid units that evolve together forming high dimensional materials. Regarding this part, preliminary results are presented in this Thesis, proving the formation of expanded structures, and encouraging future work to continue with this study.

Here, the variety of structures, different dimensionalities and conformations adopted by the studied CCMoids probe the potential of these molecules to form extended structures by themselves or with the assistance of metal coordination and/or co-linkers.

Resumen

Los curcuminoides (CCMoids) son un grupo de moléculas que presentan dos anillos aromáticos unidos por una cadena conjugada de siete carbonos (diarilheptanoides) y una β -dicetona en la posición central de sus estructuras. La síntesis sencilla de este tipo de moléculas permite su diseño minucioso en función del propósito final, principalmente modificando los sustituyentes laterales, pero también la longitud de la cadena y / o la β -dicetona. A pesar de la cantidad de CCMoids que se han sintetizado hasta ahora, y la presencia en muchos de ellos de grupos funcionales susceptibles de reaccionar con otras especies, el uso de CCMoids como bloques de construcción para la creación de estructuras altamente dimensionales es escaso. Esto, unido a las propiedades mostradas por esta familia de moléculas (biomédicas, electrónicas...) y su polivalente química, motivó el desarrollo de las ideas presentadas en esta tesis doctoral.

En este sentido, en esta tesis doctoral se presentan nueve CCMoids, incluidos cuatro no descritos previamente en la literatura. Además, se ha llevado a cabo su caracterización detallada, comprobando no solo que se habían conseguido las moléculas deseadas en alta pureza sino también cómo sus diferencias estructurales pueden afectar sus propiedades fisicoquímicas.

En cuanto a la formación de estructuras extendidas, se han logrado varios polímeros de coordinación (CP) a partir de la reacción con iones de metales de transición y también se muestran los primeros pasos en la síntesis de polímeros orgánicos (OP).

Para los estudios de CPs, se probaron dos CCMoides: uno natural, la bisdemetoxicurcumina (BDMC), con grupos fenol en los laterales de la molécula, y un CCMoid sintético, 3pyCCMoid, con piridinas como sustituyentes aromáticos.

La reacción entre BDMC y acetato de zinc, realizada en condiciones suaves en EtOH, proporciona un nuevo sistema 1D. Además, la dimensionalidad y la porosidad de esta red se han ampliado mediante el estudio de la reacción que se produce entre tres especies: BDMC, sales de Zn (II) y un co-ligando ditópico (1,2-bis (4-piridil) etileno, 1, 3-bis (4-piridil) propano o 4,4'-bipiridina). En total, aquí se presentan siete nuevos CPs. Las estructuras de cinco de ellos se resolvieron mediante difracción de rayos-X de monocristal. Además, mostramos que la combinación de ^{13}C NMR en estado sólido y técnicas convencionales (análisis elemental, FTIR.) Puede proporcionar información útil sobre los modos de coordinación de BDMC, en los casos de estructuras no resueltas.

La coordinación de 3pyCCMoid con centros de Zn (II) da como resultado tres CP con diferentes arquitecturas y dimensionalidades (de 1D a 3D). Aquí se examina cómo los métodos sintéticos y algunos cambios leves en las condiciones de reacción afectan la formación de los materiales finales. Además, se optimizó un método eficaz para la exfoliación de un CP 2D y se realizó la caracterización de los sistemas de pocas capas.

Utilizando el mismo CCMoid pero reaccionando con una sal de Co (II), se sintetizó un CP 2D isoestructural, siendo el primer CCMoid-CP con un metal diferente a Zn (II).

Para la síntesis de OPs, se han propuesto dos enfoques: (i) la formación de estructuras extendidas mediante el uso de un CCMoid con ácidos borónicos en los laterales (BOHCCMoidBF₂) que reaccionan con polioles comerciales y, (ii) la síntesis in situ de unidades CCMoid que evolucionan juntas formando materiales de altas dimensiones. Con respecto a esta parte, en esta tesis doctoral se presentan resultados preliminares que prueban la formación de estructuras expandidas y alientan el trabajo futuro para continuar con este estudio.

Aquí, la variedad de estructuras, diferentes dimensionalidades y conformaciones adoptadas por los CCMoids estudiados demuestran el potencial de estas moléculas para formar estructuras extendidas por sí mismas o con la ayuda de coordinación de metales y / o co-ligandos.

Outline

In this doctoral thesis, a group of organic molecules that belong to the family of the curcuminoids (CCMoids) have been synthesized, together with a set of extended structures (coordination polymers, CPs, and organic polymers, OPs) based on them. The **general introduction** displays a brief explanation of all the topics addressed in this work elaborated later in the rest of chapters. In the **objectives** section, the principal aims are presented and, in the **methodology, and characterization techniques** section, the synthetic procedures presented in the different chapters are described, as well as specifics on the characterization techniques applied.

In **chapter I**, the synthetic protocols for the different CCMoids are described. Some of these units are later used as linkers, and therefore, special attention is paid to the analysis of the different substituents in the lateral positions and unit lengths of these CCMoids, hence the influence of the skeleton structure in the CCMoid properties is discussed.

Chapter II shows the synthesis of CPs based on a natural CCMoid, the so-called bisdemethoxycumin, BDMC, containing exclusively phenol groups as lateral substituents. The most part of the structures of such CPs were completed by the use of a set of bipyridine molecules as co-linkers. The results presented in this chapter were published in a publication (appendix II):

Rodríguez-Cid, L., Sañudo, E. C., López-Periago, A. M., González-Campo, A., Aliaga-Alcalde, N., & Domingo, C. (2020). Novel Zn (II) Coordination Polymers Based on the Natural Molecule Bisdemethoxycurcumin. *Crystal Growth & Design*, 20(10), 6555-6564.

Chapter III describes the CPs obtained using a synthetic CCMoid that contains pyridine moieties at the sides (3pyCCMoid). This work describes the achievement of a new 3D structure, where this CCMoid coordinates to Zn(II) centres, and compares it with two additional systems (1D and 2D) prepared in the past. In addition, a robust methodology established for the exfoliation of the 2D-CP based on this curcuminoid is also shown. The results presented in this chapter were published in a publication (appendix II):

Rodríguez-Cid, L., Qian, W., Iribarra-Araya, J., Etcheverry-Berrios, Á., Martínez-Olmos, E., Choquesillo-Lazarte, D., Sañudo, E.C., Roubeau, O., López-Periago, A. M., González-Campo, A., Planes, J.G., Soler, M., Domingo, C. & Aliaga-Alcalde, N. (2021). Broadening the scope of high structural dimensionality nanomaterials using pyridine-based curcuminoids. *Dalton Transactions*, 50(20), 7056-7064.

Chapter IV, describes the explorative work performed with the aim of creating OPs based on CCMoids. Preliminary results in the synthesis of such extended structures are discussed here together with general feedback for future studies.

Finally, the **general conclusions** section provides final considerations of the achievements of this doctoral thesis.

Acronyms

2,3,6,7,10,11-hexahydroxytriphenylene	HHTP
Attenuated total reflection	ATR
Acetonitrile	ACN
Acetylacetone	acac
Atomic force microscope	AFM
Benzene-1,4-diboronic acid	BDBA
Bi-O-demethyl curcumin	BODMC
Biological metal organic frameworks	bioMOFs
Bisdemethoxycurcumin	BDMC
Brunauer, Emmett, and Teller	BET
Cambridge crystallographic data center	CCDC
Coordination polymer	CPs
Counter electrode	CE
Covalent organic framework	COF
Critical pressure	P _c
Critical temperature	T _c
Curcumin	CCM
Curcuminoid	CCMoid
Cyclic voltammetry	CV
Demethoxycurcumin	DMC
Deoxyribonucleic acid	DNA
Deuterated chloroform	CDCl ₃
Dichloromethane	DCM
Diethylacetamide,	DEE
Diethylformamide	DEF
Diethylpropionamide	DEP:
Dimethylacetamide	DMA
Dimethylformamide	DMF
Dimethylsulfoxide	DMSO
Electrochemistry	EC
Elemental analysis	EA
Energy-dispersive X-ray spectroscopy	EDS
Ethanol	EtOH
Ethyl acetate	EtOAc
Fourier transform	FT
Gel permeation chromatography	GPC
High resolution transmission electron microscope	HR-TEM
Highest occupied molecular orbital	HOMO

Immunodeficiency Virus	VIH
Infrared spectroscopy	IR
International union of pure and applied chemistry	IUPAC
Lowest unoccupied molecular orbital	LUMO
Matrix-assisted laser desorption/ionization- Time of flight	MALDI-TOF
Metal-organic framework	MOF
Methanol	MeOH
Microwave	MW
Mass spectrometry	MS
Nuclear magnetic resonance spectroscopy	NMR
Organic polymer	OP
Powder X-rays diffraction	PXRD
Randles-Sevcik equation	RA equation
Reference electrode	RE
Room temperature	RT
Scanning electron microscopy	SEM
Secondary building units	SBU _s
Single crystal X-ray diffraction	SCXRD
Supercritical carbon dioxide	scCO ₂
Ultraviolet-Visible	UV-Vis
Transmission electron microscope	TEM
Working electrode	WE
X-ray diffraction	XRD

Acknowledgment

Gracias a mis directoras, Nuria y Concha por todo lo que me han enseñado y por toda la paciencia. Aunque no siempre hemos estado de acuerdo en todo, esto no habría sido posible sin vosotras. También a Ana y Aránzazu, por todo lo que me han enseñado y ayudado. Os admiro mucho.

Gracias a toda la gente presente y pasada del grupo Funnanosurf y Fluidos Supercríticos (Raúl, Wejie, Ezhil, Niki, Pablo, Josep, Ona, Italo, Álvaro, Maripaz, Yolimar, Beltzane, Kenia, Martí, David L., Albert T. y Sandra F.C....), fuese mucho o poco tiempo siempre te llevas algo de cada persona. Gracias especialmente a Eulalia, Marc y Víctor, me ha encantado formar parte de vuestro TFG, un poquito de esta tesis es vuestra también.

Gracias a Rossella y Daniel por estar siempre ahí, dispuestos a dar consejos y a ayudar, ojalá mucha más gente fuese como vosotros.

Gracias al Dr. Josep Puigmartí y a todo su grupo por el tiempo en Zúrich. Gracias también a toda la gente con la que hemos colaborado estos años y sin la que no hubiese sido posible mucho de lo que aparece en esta tesis y en los artículos, especialmente a la Dra. Carolina Sañudo por todo el trabajo cristalográfico. Gracias por confiar en nuestra ciencia.

También a todas aquellas personas que me han ayudado con el trabajo de caracterización, sobre todo a la gente de los servicios técnicos (RMN, DRX, TEM, SEM, fluorescencia, UV, IR...) del ICMAB, UAB, UB, el sincrotrón ALBA y otros centros de investigación, pero también a muchas otras personas que me han dedicado su tiempo para que todo saliese lo mejor posible.

Gracias a mi familia que siempre me han apoyado, por las visitas y por todos los esfuerzos que hacen para que nos podamos ver, aunque sea poquito. Gracias a mis padres, Luz y Sergio, porque soy lo que soy gracias a ellos, a todo lo que me han enseñado y transmitido. Gracias a mis hermanas Raquel e Iria y a mis sobrinos Roi, Brais y Lía porque no hay ningún mal que no se cure con un abrazo vuestro. Gracias por todo el amor.

Por último, gracias a toda esa gente que son mi familia, aunque no compartamos ADN. A todos aquellos que llevan tantos años conmigo que ya no se vivir sin ellos: Lara, Fran, Meli, Bea, Cintia, Denis, Cris, Laura C. A todas las que me regaló la carrera en Santiago: Leti, Elena, Angy y Ana y el máster en Barcelona: Sandra F., Laura M. y Ane. También, a todos los que, aunque parezca mentira, aparecieron

hace solo cuatro años o menos: Teresa, Sole, Sandra C., Jose, Amanda, Marta, Dani, Gloria, Nuria, Sandra G., Albert, Joseline, Raquel, Alex y David V. Se que para muchos es una decepción que aparezca solo una lista de nombres, pero si escribo aquí todas las razones me daría para otra tesis. No os preocupéis, tengo una sorpresa para todos vosotros.

Finalmente quiero terminar con algo que pensaba mientras escribía estos agradecimientos. En estas hojas hay una gran mayoría de nombres de mujer y pensando en todas ellas solo decir que: si hay alguien que todavía cree que son inferiores en cualquier sentido, que venga a conocer a cualquiera de ellas.

Table of content

Abstract -----	I
Resumen -----	II
Outline -----	III
Acronyms -----	IV
Acknowledgments -----	V
General introduction -----	1
1. Introduction-----	3
1.1 Curcuminoids (CCMoids)-----	3
1.1.1. Natural and synthetic CCMoids-----	3
1.1.2. CCMoids preparation: extraction and synthesis-----	5
1.1.3. CCMoids applications-----	6
1.2. Coordination chemistry of CCMoids-----	7
1.2.1. CCMoid-based mononuclear compounds-----	7
1.2.2. CCMoids coordination polymers-----	9
1.3. Coordination polymers (CPs)-----	10
1.3.1. Metal centres-----	11
1.3.2. Organic molecules as linkers-----	11
1.3.3. Natural molecules as linkers-----	14
1.3.4. Synthetic methods-----	15
1.3.5. 2D-CPs: properties and synthetic approaches-----	18
1.3.6. Applications of CPs-----	20
1.4. Organic extended structures-----	22
1.4.1. Organic polymers-----	22
1.5. Precedents and motivation of this thesis: CPs and polymers based on CCMoid-----	24
2. References-----	28
Objectives -----	37
Synthetic methods and characterization techniques -----	41
1. Equipment and methodology-----	43
1.1 Synthetic method-----	43
1.1.1 Solvothermal methodology-----	43
1.1.2 Layering methodology-----	44
1.1.3. scCO ₂ methodology-----	44
1.2. liquid-assisted exfoliation-----	46
2. Characterization techniques-----	46
2.1. Composition and structural information-----	47
2.1.1 Nuclear magnetic resonance(NMR)-----	47
2.1.2. Mass spectrometry-----	48
2.1.3. Elemental analysis (EA)-----	49
2.1.4. Fourier transformed infrared spectroscopy (FTIR)- attenuated total reflectance (ATR)-----	49
2.1.5. X-ray diffraction (XRD): powder and single-crystal. Synchrotron source-----	50

2.2 Morphology-----	51
2.2.1. Scanning electron microscopy (SEM)-----	51
2.3. Characterization techniques for nanosheets-----	52
2.3.1. Energy Dispersive X-rays Spectroscopy (EDS)-----	52
2.3.2. Transmission electron microscopy (TEM)-----	52
2.3.3. Atomic force microscopy (AFM)-----	52
2.4. Optical spectroscopic properties-----	53
2.4.1. Ultraviolet-visible (UV-Vis) absorption spectroscopy-----	53
2.4.2. Fluorescence spectroscopy-----	55
2.5. Electrochemistry-----	55
2.5.1. Cyclic voltammetry (CV)-----	56
2.5.2. Reversibility-----	57
2.5.3. Applications of the voltammetry technique-----	58
3. References-----	60
Chapter I. Synthesis and characterization of CCMoids-----	61
Chapter scope-----	63
1. Introduction-----	63
2. Materials and methods-----	64
2.1. Materials-----	64
2.2. Description and synthesis of CCMoids-----	64
2.2.1. CCMoids using Pabon's method-----	64
2.2.1.1. BDMC-----	64
2.2.1.2. 3pyCCMoid-----	66
2.2.1.3. 2-thphLCCMoid-----	67
2.2.2. BODMC-----	69
2.2.3. Synthesis of CCMoidBF ₂ -----	71
2.2.3.1. CCMoidBF ₂ from free CCMoid-----	71
2.2.3.2. CCMoidBF ₂ from acacBF ₂ -----	72
3. Characterization-----	75
3.1. ¹ H NMR-----	75
3.2. ¹³ C-NMR-----	79
3.3. Infrared spectroscopy (FTIR-ATR)-----	81
3.4. Mass spectroscopy-----	84
3.5. Crystal structures: powder and single crystal X-ray diffraction (XRD)-----	86
3.5.1. BDMC-----	86
3.5.2. 3pyCCMoid-----	90
3.5.3. BODMC-----	90
3.5.4. Other CCMoids-----	91
3.6. Solid state NMR (CPMAS ¹³ C)-----	92
3.7. Ultraviolet-Visible absorption spectroscopy and fluorescence emission	94
3.8. Electrochemistry-----	97
3.8.1. HOMO-LUMO energy bandgap estimation-----	100
4. Conclusions-----	102
5. References-----	104
Chapter II. CPs based on BDMC-----	109
1. Introduction-----	111

2. Objectives-----	113
3. Materials and methods-----	113
3.1 Materials-----	113
3.2. Methods. CPs synthesis-----	113
3.2.1. Solvothermal methods-----	113
3.2.2. scCO ₂ method-----	114
4. Results and discussion-----	114
4.1. Solvothermal synthesis-----	114
4.1.1. Crystallographic description-----	115
4.1.2. CPMAS ¹³ C Structural correlation studies-----	123
4.1.3. Elemental analysis-----	125
4.1.4. Powder XRD-----	126
4.1.5. General trends in BDMC CPs-----	128
4.1.5.1. Dipyridinic co-linkers-----	128
4.1.5.2. Adsorbed/coordinated solvent molecules-----	129
4.1.6. Supplementary structural analysis of CCMoid-CPs-----	132
4.1.6.1. Infrared spectroscopy (FTIR-ATR)-----	132
4.1.6.2. Morphology of the crystals. Optical microscope and SEM images-----	134
4.2. Synthesis in scCO ₂ -----	135
4.2.1. Powder XRD-----	135
4.2.2. Infrared spectroscopy (FTIR-ATR)-----	137
4.2.3. Elemental analysis-----	138
4.2.4. Morphology-----	139
4.3. Reactions of BDMC with other metals-----	139
5. Conclusions-----	140
6. References-----	141
Chapter III. CPs based on 3pyCCMoid-----	143
1. Introduction-----	145
2. Objectives-----	146
3. Materials and methods-----	146
3.1 Materials-----	146
3.2. Methods. CPs synthesis-----	147
3.2.1. Solvothermal methods-----	147
3.2.2. scCO ₂ method-----	147
3.2.3. Layering method-----	148
3.2.4 Exfoliation method-----	148
4. Results and discussion-----	149
4.1. CPs based on 3pyCCMoid. Solvothermal and layering method-----	149
4.1.1. Crystallographic description-----	149
4.1.2. Comparative studies of the 3pyCCMoidM-x structures-----	157
4.1.3. Additional characterizations-----	159
4.1.3.1. Powder XRD-----	159
4.1.4.2. Crystal morphology-----	160
4.1.5.3. CPMAS ¹³ C NMR-----	161
4.1.5.4. Infrared spectroscopy (FTIR-ATR) -----	162

4.1.5.5. Elemental analysis -----	164
4.2. CPs based on 3pyCCMoid. scCO2 procedure-----	164
4.2.1. Powder XRD-----	164
4.2.2. Infrared spectroscopy (FTIR-ATR) -----	165
4.2.3. Solubility test-----	166
4.3. Exfoliation studies of 3pyCCMoidZn-2 -----	167
5. Conclusions-----	170
6. References-----	172
Chapter IV. OPs based on CCMoid-----	173
1.Introduction-----	175
1.1. CCMoids as monomeric units-----	175
1.1.1. Boronic acid: definition and reactivity-----	175
1.1.2. Molecules used in this approach-----	177
1.2. Polymers with CCMoid-like structure-----	179
2.Objectives-----	180
3.Materials and methods-----	181
3.1 Materials-----	181
3.2. Synthetic methods-----	181
3.2.1. Boronic esters based on BOHCCMoidBF ₂ -----	181
3.2.1.1. BOHCCMoidBF ₂ -Pin (Bpin)-----	181
3.2.1.2. BOHCCMoidBF ₂ -cate (Bcate)-----	182
3.2.1.3. BOHCCMoidBF ₂ -pol-----	182
3.2.1.3. BOHCCMoidBF ₂ -HHTP (BHHTP)-----	183
3.2.2. Boronic esters based on BODMC-----	184
3.2.3. Polymers with CCMoid-like structures-----	185
4. Results and discussion-----	186
4.1. Boronic esters based on BOHCCMoidBF ₂ -----	186
4.2. Boronic esters based on BODMC-----	191
4.3. CCMoid like polymeric structures-----	193
5. Conclusions-----	194
6. Future work and perspectives-----	194
7.References-----	196
General conclusions-----	198
Appendix I. Supplementary figures-----	202
Appendix II. Publications-----	239



GENERAL INTRODUCTION

1. Introduction

At the heart of this doctoral thesis is the development of new coordination polymers (CPs), including 2D structures, and organic polymers (OPs), all of them extended structures involving known and newly synthesized curcuminoid molecules (CCMoids). Thereafter, this introductory chapter describes the synthetic protocols and main characteristics of the developed materials and CCMoid precursors.

1.1. Curcuminoids (CCMoids)

CCMoids are a group of molecules that present a conjugated carbon chain with different aromatic substituents in the corners and a β -diketone moiety in the central position (figure 1). As it is typical in molecules with a β -diketone, CCMoids could have the keto-enol and diketo forms in equilibrium, predominating in many cases the keto-enol form. This is the case of curcumin that displays mostly the later in organic solvents, acid media and solid state.¹

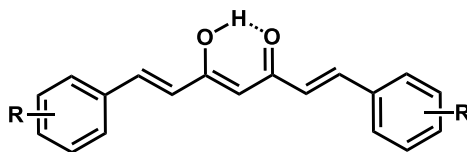


Figure 1. General structure of CCMoids in the enol form.

CCMoids can have a biological (natural) or synthetic origin, although all of them can be synthesized in the laboratory.² The chemical versatility and potential tritopic coordination of these molecules make them interesting candidates to develop coordination chemistry, including the generation of coordination polymers (CPs). The substituents present in the corners can react with organic molecules as well forming polymers (OPs). All these important aspects are developed in the core of this doctoral thesis and are illustrated in the following sections.

1.1.1. Natural and synthetic CCMoids

There are three known CCMoids available in nature, curcumin (CCM), demethoxycurcumin (DMC) and bisdemethoxycurcumin (BDMC). These three compounds are part of turmeric, a spice obtained from the rhizomes of the plant *Curcuma longa*. This plant is included in the Zingiberaceae family and it is cultivated in tropical and subtropical regions, mainly in Asia.³ In turmeric, CCMoids occur in a percentage between 2-8 wt%, being CCM the most abundant (70-80 wt%), followed by DMC (15-25 wt%) and BDMC (3-10 wt%). All of them have oxygen groups as substituents in the two aromatic rings (R in figure 1 and figure 2). CCM has one hydroxyl and one methoxy groups in each ring, in the positions *para*- and *meta*-, respectively. The structure

of BDMC is similar to that of CCM, but the two methoxy groups are missing; and, finally, DMC is an asymmetric CCMoid, since it has different substituents in the two aromatic rings, e.g., one side contains one hydroxyl and methoxy groups and the other only one hydroxyl unit.⁴ From them, CCM has been the most studied and used material. The first set of scientific studies dealing with the properties of the CCM molecule go back to 1748 in the publication of Loeber and Buechner;⁵ however, CCM was not isolated until 1842 by Vogel *et al.*⁶ and its chemical formula was described in 1910 by Milobedzka *et al.*⁷

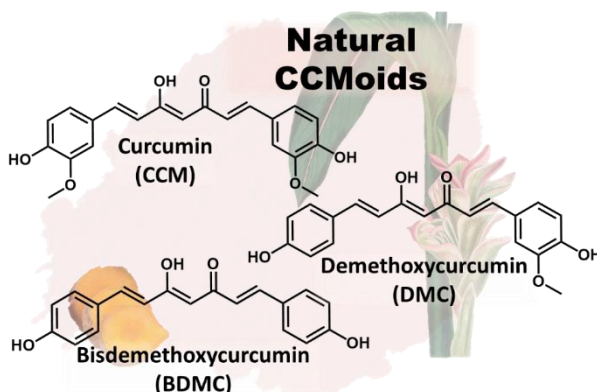


Figure 2. Molecular structures of natural CCMoids. Flowers, leaves and rhizomes of the plant *Curcuma Longa* are shown on the background.

Nowadays, different methodologies have been developed to increase the number of members of the CCMoid family by the use of synthetic methods, with a huge variety of lateral substituents that have been designed to answer the requirements of different applications. Figure 3 displays some examples of synthesized CCMoids.

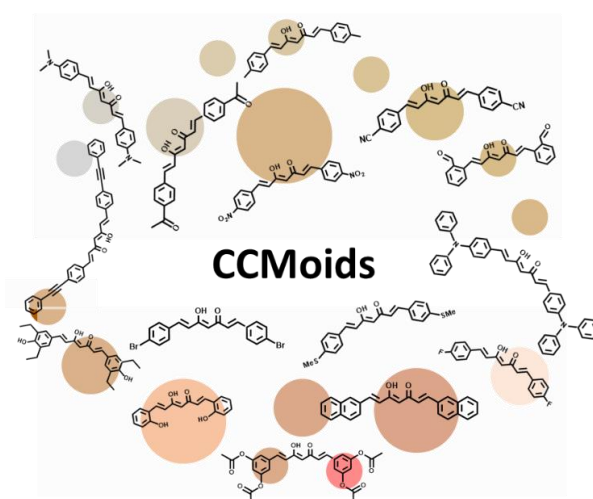


Figure 3. Examples of synthetic CCMoids with different lateral substituents.⁸⁻¹³

1.1.2. CCMoids preparation: extraction and synthesis

The increased historical interest in CCM and other natural CCMoids have boost the development of different extraction techniques from turmeric, going from conventional extraction with organic solvents^{14,15} to assisted with microwave technology¹⁶ and even the use of supercritical CO₂.¹⁷ Extraction is followed by separation using chromatographic methods to obtain each CCMoid individually.¹⁸ However, extraction techniques have the drawbacks of low percentages of recovery and low selectivity, which make difficult to obtain each single CCMoid highly pure. All these factors have promoted advanced research on synthetic approaches¹⁹ that, at the same time, allow the preparation of new CCMoids, with different substituents than the observed in the natural molecules.

For the synthesis of CCMoids, first attempts were based on a condensation reaction established between acetyl acetone (acac) and an aldehyde owning the desired substituent. Thus, vanillin was utilized to obtain CCM. In the first synthesis, performed in 1910, eight steps were necessary to obtain the final molecule, which resulted in very low yields.¹⁹ Later, in 1937, Pavolini *et al.*²⁰ proposed a fast one-pot reaction involving boron oxide, but still the yield was very low, approx. 10 wt%. Finally, in 1964, Pabon *et al.*²¹ managed to improve the yield up to values of 70 wt% by adding tributylborate and n-butylamine to the reaction medium, while using ethyl acetate as solvent. This synthetic protocol, summarised in figure 4, starts with the formation of a compound by the reaction of two molecules of acac and boron oxide (**1**, figure 4). This step avoids the undesired Knoevenager condensation occurring through the protons of the central C atom in the acac molecule, that are more acidic than those from the corners. Then, the aldehyde is added together with tributylborate and n-butylamine, the latter in catalytic quantities. The first is used to remove the molecules of water formed by condensation in the main reaction and the second, to facilitate the removal of the protons of the acac. Finally, the compound with the boron oxide (**2**, figure 4) is dissociate using water or acid media to obtain the desired CCMoid in high yields.¹⁵

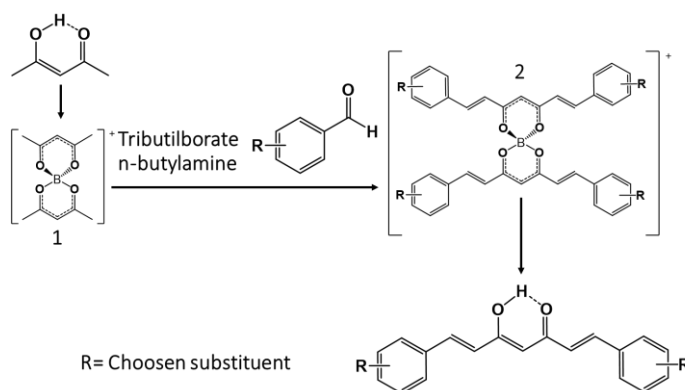


Figure 4. Schematic representation of the Pabon's method.

Using the Pabon's method or variations from this, it has been possible to obtain all the natural phenolic CCMoids, and also others with different substituents in the benzene rings,² for example, with aromatic cyclic substituents such as thiophenes.²² However, this method is not always the optimal to obtain all the CCMoids with reasonable yields. To solve this problem, new synthetic protocols have been proposed,² although most of them still keep the condensation between the acac and the aldehyde as initial main step. As an example, Rao *et al.*²³ have proposed the formation of a different intermediate by using boron trifluoride instead of boron oxide. Other authors suggested changes in the solvent, as Ferrari *et al.*²⁴ that used DMF instead of EtOAc. Finally, different molecules to remove protons in acac have been studied instead of n-butylamine, for instance piperidine or morpholine used by Babu *et al.*²⁴ Also, the use of microwave assisted synthesis has been proposed to reduce reaction time and the amount of solvent.²⁵

1.1.3. CCMoids applications

Turmeric has been employed since ancient time, mainly in China and India, as a dye, aromatic spice, food additive for preservation and in traditional medicine.²⁶ All these applications relate to the presence of CCMoids in this spice. These molecules confer to the turmeric the characteristic yellow-orange colour and, as many of other diarylheptanoids, give biomedical properties.²⁷ Most of the biomedical benefits can be attributed to their antioxidant and anti-inflammatory effects. Particularly CCM has been recognized and used worldwide in many different forms: in curries in India, served in tea in Japan, in cosmetics in Thailand, as a colorant in China, in drinks in Korea, as an anti-inflammatory and antiseptic agent in Malaysia and Pakistan, and as a preservative and a colouring agent in mustard, cheese, butter or chips in the United States.²⁸ In addition, all natural CCMoids have been tested as antioxidants, antiprotozoal, antibacterial, antiviral and antitumoral agents.^{28,29}

Some synthetic CCMoids have been studied in molecular electronics. In that sense, the team of Aliaga-Alcalde *et al.*^{30,31} have studied the use of anthracene based CCMoids in molecular break junction devices. In these works, the CCMoids were coupled by π - π stacking to few layer graphene electrodes; this way, measurements of the electron transport through the molecule were carried out, proving the potential of room-temperature operation of molecular-based devices.^{30,31} The same group have performed studies with gold electrodes and thiophene and methylthiophene based CCMoids by mechanically controllable break junction technique.²² For the family of thiophene CCMoids, HOMO (highest occupied molecular orbital) and LUMO (lowest unoccupied molecular orbital) studies in solution and anchored to a gold electrode have been performed.

In addition, the so-called pseudo-CCMoids are described as molecules that maintain some CCMoid features, but also present differences from the general structure, some

examples are shown in figure 5. Thus, pseudo-CCMoids could be CCMoids with substituents in the central carbon (in yellow), which confer interesting new functionalities to the molecules, including the possibility of anchoring them to substrates (nanoparticles, rigid or flexible surfaces, electrodes, etc.).³²⁻³⁴ Modifications in the number of carbons in the skeleton of the molecule are included here too (in blue).^{30,31} Finally, the presence of the β -diketone allows the coordination of metals and semimetals (in green, figure 5), intensively studied in coordination chemistry.³⁵ This last aspect is further discussed in the next sections.

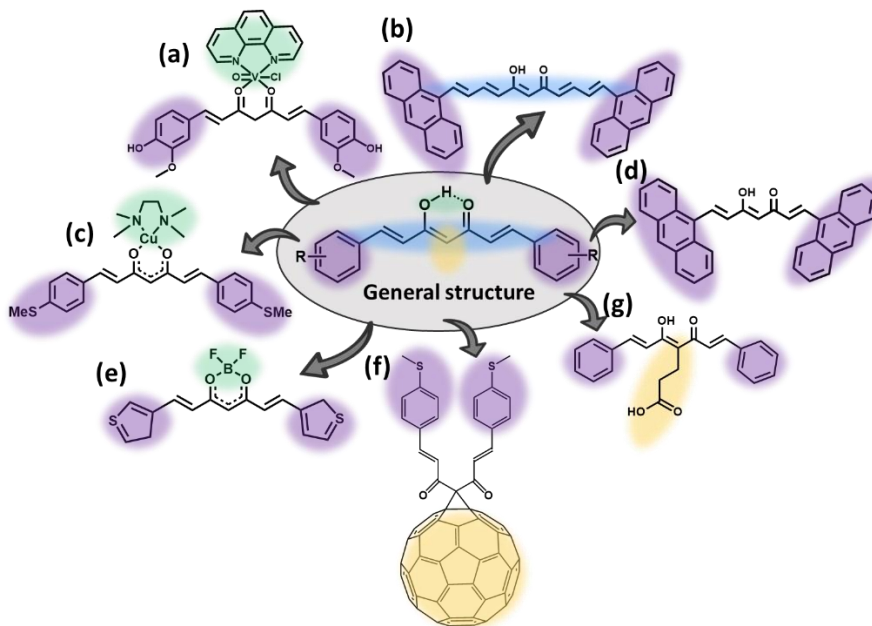


Figure 5. Examples of CCMoids with different moieties: (a) Wanninger *et al.*³⁶, (b) Burzuri *et al.*³¹ (c) Olavarría-Contreras *et al.*³⁵, (d) Prins *et al.*³⁰, (e) Olavarría-Contreras *et al.*³⁵, (f) Dulic *et al.*³⁴ and (g) Ohtsu *et al.*³⁷

1.2. Coordination chemistry of CCMoids

1.2.1. CCMoid-based mononuclear compounds

The β -diketone functionality has been intensively studied in coordination chemistry due to the easy formation of mononuclear compounds with a multitude of the elements of the periodic table.³⁸ The presence of a β -diketone in the central position of CCMoids makes feasible the formation of metal and semimetal coordination compounds thus, changing or adding new properties to the compounds, opening them to new applications. In general, these compounds include one divalent or trivalent metal centre

and a variable number of CCMoid entities (one to three), requiring sometimes additional molecules (*e.g.*, solvent and/or co-ligands) to complete the coordination sphere of the metal ion. Mononuclear CCM compounds have been synthesized with most of the elements in the periodic table, generally with metallic centres of the d-block, particularly Cu(II), Zn(II), Ni(II), Fe(II), Mn(II) and Ru(II); although there are also a good number of publications with vanadyl species, mainly with the V=O unit.³⁸ In addition, some examples of compounds can be found involving Na(II), Be(II), Mg(II), Ca(II), Ba(II), In(II), Sn(II), Pb(II), Y(II), La(II), Zr(II), Cr(II), Tc(II), Th(II) and U(II), among others.³⁹ Finally, many examples of coordination compounds have been also published with CCMoids, natural and synthetic, involving most of them metal ions of the groups eight to twelve in the periodic table.⁴⁰

In general, the synthetic path for the achievement of mononuclear CCMoid compounds involves the mixing and heating of the chosen CCMoid molecule and the metal salt often under the presence of a weak base to help the deprotonation of the former.⁴⁰ The heating method is usually by the use of conventional reflux setups or oven, but microwave-assisted synthesis can be used as well.⁴¹ In many cases, the precipitation of crystals containing only the CCMoid as the ligand in the coordination compound (homoleptic species) is difficult, being more common the achievement of crystal structures where, in addition to the CCMoid, other molecules participate in the coordination (heteroleptic compounds). These spectator ligands can be solvent molecules or small/capping molecules, among others.⁴²

CCMoid-based coordination compounds have been synthesized basically for medical purposes. For example, some compounds involving Zn(II) are proposed to reduce the levels of insulin in plasma,⁴³ to increase females fertility,⁴⁴ to act against gastric ulcers or to give hepatotoxicity protection.⁴⁵ Different CCMoid compounds involving Zn(II), Cu(II), Pd(II) or vanadate have shown encouraging properties in cancer treatments.⁴⁰ Some of these coordination compounds have been studied for the treatment of different diseases, such as Parkinson,⁴⁶ Alzheimer⁴⁷ or VIH.⁴⁸ Along with them, CCMoid-based coordination compounds containing Ga(III), Tc(I) or Re(I) metal centres have been developed as potential contrast agent in imaging diagnosis.^{49,50}

Besides biomedical purposes, CCMoid-based coordination compounds have found applications as sensors and/or capturing toxic heavy metal ions, such as Cu(II), Cr(II), Cd(II), Pb(II) or Hg(II).⁵¹ Advanced optical applications have been described for Ln(III)-CCMoid compounds.⁵² Co(II)-CCMoid compounds were synthesized to exploit the magnetic properties of the metal centres that vary depending on the disposition (E or Z) of the CCMoid ligands.⁵³ Finally, Ni(II)-CCMoid compounds have been studied for the modification of electrodes.⁵⁴

Moreover, it is also remarkable the number of publications based on compounds with CCM and boron species, particularly boron oxide, which have previously been analysed, and sometimes even isolated, as intermediate units in the synthesis of CCMoids (figure

4). In fact, the first two synthesized mononuclear coordination compounds based in CCM were two boron compounds (figure 6), rosocyanine⁵⁵ and rubrocurcumin.⁵⁶

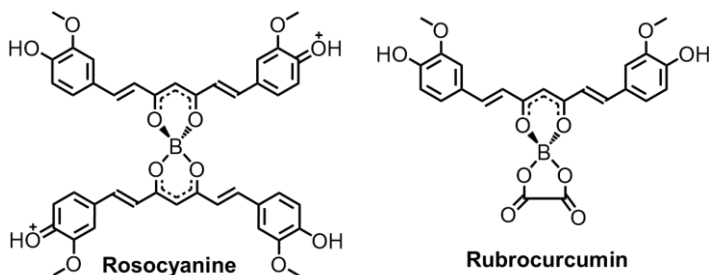


Figure 6. Molecular schemes of rosocyanine and rubrocurcumin.

The coordination of CCM and boron ions produce huge variations in the light absorption capacity of the final compounds vs. pristine CCM, which allows the development of boron detection methodologies in different media.⁵⁷ This colorimetric approach is still in use for the determination of boronic acid and derivatives, where the addition of CCM produces a clear colour change in the solutions.⁵⁸ In the family of boron compounds, the most studied are those containing boron difluoride moiety coordinated to the β -diketone group of the CCMoids. This type of “CCMoidsBF₂” systems are widely studied for their electron-accepting properties and strong fluorescence.⁵⁹ Indeed, the BF₂ unit enhances and promotes shifts in the absorbance and fluorescence properties of the CCMoid-based coordination compounds.⁶⁰ This effect is related to changes in the energy gap between HOMO and LUMO orbitals.⁶⁰ In general, CCMoids and coordinated CCMoids present a semiconductive behaviour and, usually, a reduction of the bandgap is observed when they are coordinated to BF₂ units.¹³

1.2.2. CCMoids coordination polymers

In addition to the β -diketone functionality, CCMoids may also contain other donor atoms, placed as aromatic substituents in the lateral positions, which are prone to coordinate with metal centres. Curiously, the possibility of having these additional interactions was already detected during the synthesis of mononuclear species, and the resulting polymers were considered undesired by-products.⁴⁰ Historically, this issue has been overlooked, although in some occasions the possibility of forming CPs was already suggested.⁴⁰ These precedents proves the capacity of the CCMoids family to act as exceptional candidates to synthesize new CP structures.^{61,62} This is the starting point and query that triggered the studies presented in this doctoral thesis. For this reason, this introductory chapter gives a general description of CPs, describing, in particular, the limited information of regarding the existing CCMoids-CP.

1.3. Coordination polymers (CPs)

CPs, and the subclass of metal-organic frameworks (MOFs), are extended infinite structures of different dimensionalities, *i.e.*, one-, two- or three-dimensional (1D, 2D or 3D) structures, formed by the coordination of metal centres or metal clusters with organic linkers (figure 7).⁶³ The dimensionality of the structure is defined by the number of directions in space where the infinite array extends, that in return, depends on the structure and number of coordination bonds established between the metal ions and the linkers. CPs are usually precipitated as highly ordered crystalline materials⁶⁴ that can be studied by single-crystal XRD. In general, due to the almost infinite existing structures and the strength of the coordination bonds, CPs are highly insoluble in most common solvents. In some cases, solubilisation is achieved by the use of strong coordinative solvents or extreme pH values.⁶⁵

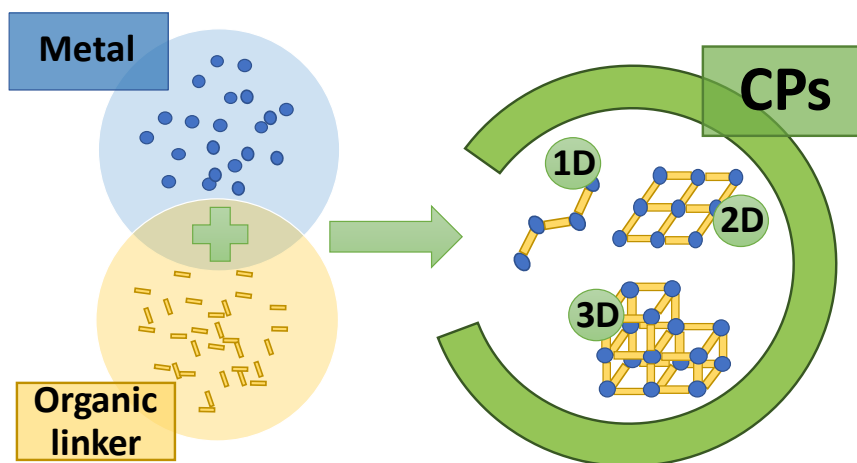


Figure 7. Schematic description of the formation of CPs.

Different bibliographical sources have suggested that the first synthesized CP is the compound known as Prussian blue, obtained between 1704 and 1705, although its structure was not elucidated until 1974.⁶⁶ The term "coordination polymer" appears in the decade of 1950 and the subject rapidly evolves in the 1960s and 1970s^{67,68} with the publication of several initial reviews about CPs. However, it was not until the 1980s, and, especially, since the elucidation of a 3D CP synthesized by Hoskin and Robson in 1989,⁶⁹ when the field triggers the interest of a vast part of the scientific community.

Since the beginning, the sub-class of MOFs has attracted most of the attention. The term MOF was popularized by Yaghi *et al.*⁷⁰ around 1995 to describe a microporous CP. Nowadays, the IUPAC recommended the use of MOF to name CPs that involve porosity, while CP can be utilized to name all the infinite structures formed by the coordination of metal centres and organic linkers.⁷¹

1.3.1. Metal centres

CPs have been synthesized with almost all the metal ions of the periodic table, although mainly transition metals (3d-5d) and lanthanides are used in most of the investigations. Metal ions are connected with their neighbours through the organic linkers. In many cases, the metal centre is pre-organized in secondary building units (SBUs), which are well-defined clusters containing two or more metals connected through donor atoms.⁷² Metal ions influence the final structure of the CP through their coordination number and adopted geometry. In CPs, the metal centres have basically coordination numbers from two to six, extensible to higher values in few cases, mainly for lanthanides. Besides, for a fixed coordination number, the metal can adopt different geometries (table 1). Multiple articles describe the possibility of controlling the final structures by conveniently choosing the metal geometry.⁷³ However, structural design is a complex process, since it can be affected by several parameters, such as the functional groups and length of the linkers, as well as the existence of counter ions, solvent molecules, or non-bonding guests that occupy some of the available coordination positions of the metal unit.⁷³ Stoppers are commonly used to control the number and orientation of the coordination of the metal ions.⁷³ The metal centres, as the linkers, contribute to the properties of the CP, therefore, depending on their nature the CP may present magnetic properties,⁵⁴ by involving paramagnetic metals, or luminescence, due to antenna effects, caused by the presence of lanthanides.⁷⁴

1.3.2. Organic molecules as linkers

The principal requirement for an organic molecule to act as a CP linker is to have at least two donor atoms that promote coordination to metal ions. Taking into account this broad definition, the number of molecules accomplishing this requirement is extremely high.⁶³ Figure 8 depicts some examples of linkers often used to build CPs, showing oxygen and nitrogen units as the most typical donor atoms. Molecular bridges with only one type of coordination group are called homotopic linkers, in contrast to heterotopic linkers that possess at least two different coordinative groups. The latter are less common than the former and increases the serendipity in the prediction of the final structures (due to the combination of more than one functional group, having different reactivity within the same linker, *e.g.*, charged and neutral).⁷⁵⁻⁷⁷ One interesting strategy to obtain new CPs is the use of isorecticular synthesis, also known as the node spacer strategy. In this methodology the coordinative part of the ligand (node) remains unchanged, varying the nature/length between the coordinative part (spacer).⁷⁸ Some examples are shown in figure 8.

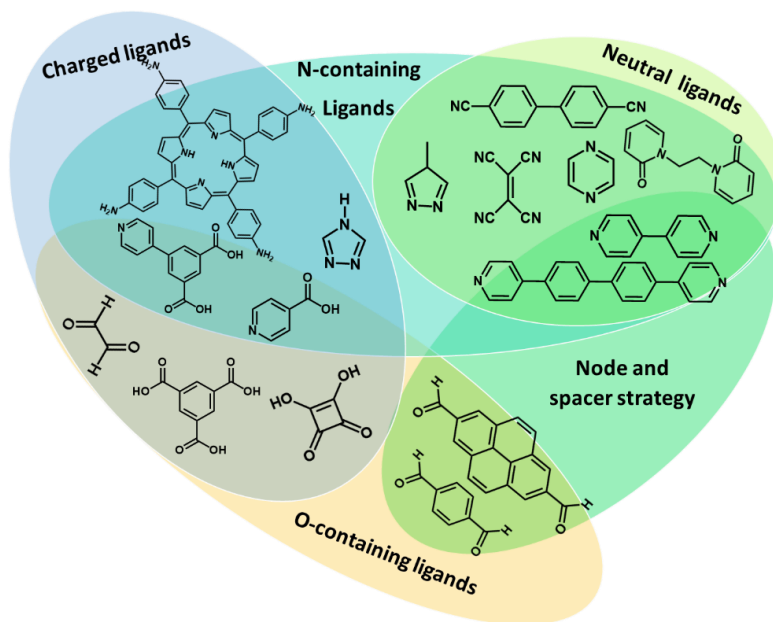


Figure 8. Examples of linkers used in CPs classified by the neutral or charged nature of the donor atom, including examples of heterotopic linkers and the strategy of node and spacer.

In the case of oxygen-containing linkers, the most well-known systems are a family of carboxylic ligands. Actually, many of the most famous MOFs contain carboxylates, *e.g.*, HKUST, MOF-5, MIL-100 and the IRMOF family (table 1).⁷⁹ Other oxygen containing linkers incorporate alcohol, catechol or β -diketone functional groups.⁷⁹ From the nitrogen-containing linkers, pyridine-based molecules have been extensively studied. Within this family, the linkers have in common at least two pyridine groups with the N atoms in different positions (*ortho-meta*- or *para*-). Between the two rings, spacers are located, such as other aromatics groups or carbon chains with different lengths and saturation degree. As bipyridines are neutral ligands and the metal centres have, most of the time, two or more positive charges, the resulting CPs need to incorporate other entities to compensate the charge, which can be counterions from the metal salt or additional ligands.⁸⁰ Inside of the pyridine family, also molecules with three pyridine rings, tripyridines, have been used as linkers in CPs.^{81,82}

Table 1. Organic linkers, secondary building units and structures of some well-known MOFs.

Name	Organic linker	SBU	Structure
HKUST			
MOF-5			
MIL-100			
IR-MOF16			
UIO-66			
ZIF-8		Zn ²⁺	

The most common CPs are those formed by metal centres connected through one type of linkers. Despite of this, the combination of two or more linkers is a common practice too, leading to compounds known as mixed-linker systems. Related to this, a number of CPs formed by the mixing of ditopic and tritopic linkers⁸³ or anionic and neutral linkers⁸⁴ can be found in the literature. A frequently reported combination is the mixing of carboxylic acids and rigid bipyridine co-linkers; this way, even structures like helical chains have been described.⁸⁵⁻⁸⁷ The approach of using a co-linker is often applied to drastically modify the structure of the CP, for instance to obtain CPs with two or more types of pores or to increase the dimension of the final structure.⁸⁸

1.3.3. Natural molecules as linkers

Efforts to synthesize new molecules that could be used as organic linkers have risen together with the scientific interest in CPs. In this respect, they have been performed many studies in molecules present in nature to establish their potential use linkers. For instance, amino acids,⁸⁹ peptides,^{90,91} nucleobases,^{92,93} proteins⁹⁴ and saccharides^{95,96} have been extensively used. Some investigations have also been carried out with porphyrins⁹⁷ or even with small biomolecules present in living organisms (figure 9).^{98,99}

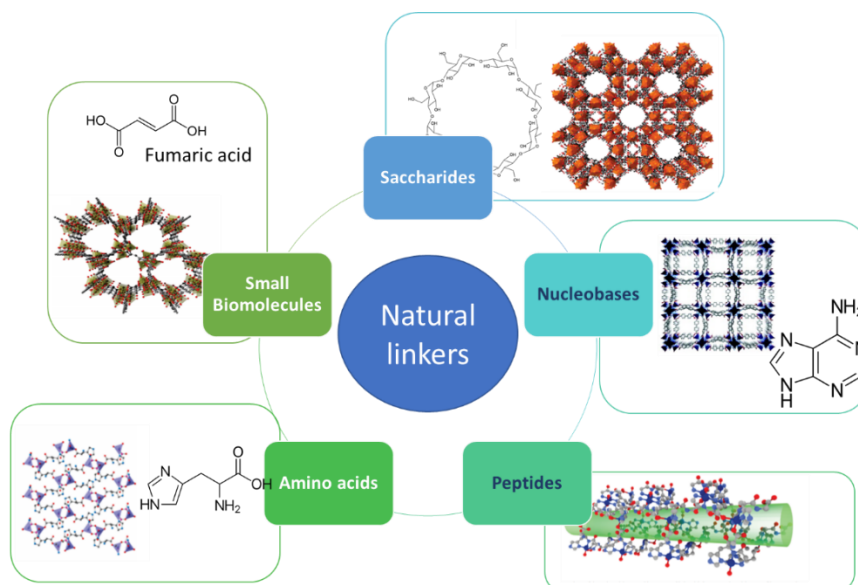


Figure 9. Examples of natural linkers used for the synthesis of CPs.¹⁰⁰

Most of the natural molecules are heterotopic linkers, which confers asymmetry to the molecule and can hamper the achievement of infinite structures. Moreover, they often have more flexibility than designed synthetic linkers, being this a drawback to achieve crystalline structures.⁶¹ Nevertheless, they bring interesting properties, such as biocompatibility, facilitating relevant biological applications. In recent years, it has been developed a new sub-class of CPs called biological metal organic frameworks (BioMOFs) that present biomolecules as linkers, thus ensuring the biocompatibility.¹⁰¹ For synthetic CCMoids, the biological capabilities of each system should be addressed depending on the design. Regarding this matter and taking into account that natural CCMoids have been used in medical trials thanks to their low toxicity and absence of side effects, these CCMoids meet the criteria toward the synthesis of BioMOFs.

1.3.4. Synthetic methods

The literature related to CPs and MOFs synthesis displays multiple methods. In this section, a short description of the different synthetic approaches is given, paying special attention to the three methodologies applied in this doctoral thesis: (i) layering, (ii) reaction at high temperature (solvothermal and non-solvothermal syntheses) and (iii) synthesis in supercritical CO₂.

1.3.4.1. Direct precipitation (open and close vessels) and layering

In the *direct precipitation* method (performed in open vessels), reagents are mixed at room temperature in a fixed concentration, slightly below than the corresponding to their supersaturation level. Factors such as nucleation are thus reduced, and high-quality crystals are formed by slow solvent evaporation.¹⁰²

The *layering* approach is similar, but in this case, crystallization is produced by the slow diffusion of the reagents. In this methodology, represented in figure 10, two miscible solvents are used, the organic linker is dissolved in one and the metal salt in the other. Here the densities of each solvent organise the layers, the densest is placed at the bottom of the vial meanwhile the other is carefully added on the top, forming two different layers. The vials are kept unaltered during a period of time enough to allow solvents diffusion and gradual mixing of the reagents, with the idea again of favouring crystal growth versus nucleation.¹⁰⁴ This technique has been traditionally used to obtain crystals of organic molecules, coordination compounds and proteins,¹⁰³ and it was also used in early works for the synthesis of CPs.¹⁰⁴

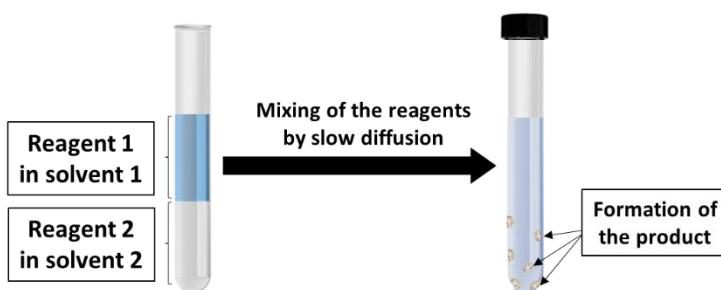


Figure 10. Schematic representation of the layering method.

In the *solvothermal* technique, temperature and pressure are used to accelerate the kinetics of the process and, at the same time, to achieve high quality crystals. Indeed, solvothermal methods are the most commonly used in the synthesis of CPs and MOFs. Solvothermal reactions take place in closed vessels under autogenous pressure above the boiling point of the solvent.¹⁰⁵ Experiments are performed in teflon-lined autoclaves

or even sealed glass vials when the filling volume and the temperature are relatively low. There are variations of the method used in this doctoral thesis, displaying soft conditions that involve the use of closed glass vials using again low temperatures and filling volumes (figure 11a). For the solvothermal reaction, the recipient is typically introduced in an oven at RT and the temperature is raised to the desired value either straightforwardly or with a complex ramp.¹⁰⁶

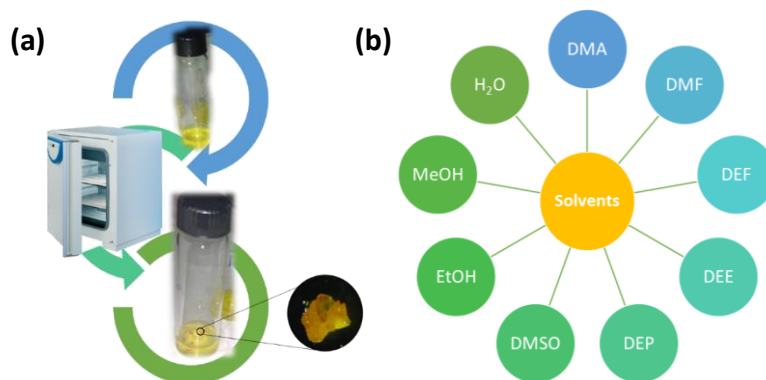


Figure 11. Schematic solvothermal method: (a) a vial with hermetic closure and the reagents completely solubilized is introduced in an oven used for the solvothermal synthesis, recovering a vial with the precipitated crystals; (b) Examples of solvents used in CP syntheses: DMA: dimethylacetamide, DMF: dimethylformamide, DEF: diethylformamide, DEE: diethylacetamide, DEP: diethylpropionamide, DMSO: dimethylsulfonamide, EtOH: ethanol, MeOH: methanol, H₂O: water.

In the solvothermal method, heating can also be performed with a *microwave*, and with a precise optimization of the parameters (e.g.: temperature, pressure, power, solvent and time), it is possible to increase the yield of the reaction and improve crystallinity and product purity. It is particularly remarkable the effectiveness that have shown this heating technique in the achievement of nanoscale products.¹⁰⁶ Indeed, the fast-heating in microwave favours nucleation vs. crystal growth.

It is important to emphasize that many net and mixed solvents have been used in CPs synthesis (figure 11, right). The physico-chemical properties of the solvent play a key role in the synthesis; for example, the boiling point is important in solvothermal methods, the density is relevant in layering approaches and the dipole moment in microwave heating. The basic treat of some of the solvents, such as dimethylformamide (DMF) or dimethylacetamide (DMA)¹⁰⁷, is often necessary to deprotonate the linker, triggering the formation of the CP. In addition, some solvents, such as MeOH, EtOH, DMF, DMA or H₂O have the ability of coordinating with the metal ions becoming part of the structure.¹⁰⁸ In other cases, the solvent remains in the structure as a guest molecule, without forming strong bonds with the metal centre, but interacting with different parts of the structure through electrostatic forces.¹⁰⁹ Even when the solvent is not included in the structure,

different CPs can be obtained by changing this factor in the synthetic protocol, thus they can act as structural directing agents.¹¹⁰ The use of mixtures of solvents has also been extensively tested to favour crystallization.¹¹¹

Regarding other conditions, the pH effect has been extensively studied in aqueous reactions, either in pure water or mixed with alcohols, particularly in compounds involving carboxylic acids.¹¹² Clearly, here the deprotonation of the linker would favour the coordination with the metal units. Following the strategy of playing with the pH, the selective deprotonation within the linkers (e.g.: tricarboxylic acids) can be attained giving place to different structures.¹¹³

Finally, reagent's concentration is a basic parameter to define not only the crystal quality, but also the precipitated phase. In that sense, high concentration can trigger fast precipitation, leading to small crystals. On the contrary, low concentration can significantly increase the reaction time, hindering precipitation and the achievement of crystalline materials.¹¹⁴ The search of the successful concentration of reagents is frequently performed based on a trial-and-error method. Variations in the molar ratio between metal salts and linkers can easily produce changes in the structure as well.

1.3.4.2. Synthesis in supercritical CO₂

A supercritical fluid is a system that can be liquefy at temperatures and pressures above its critical point. In these conditions, the fluid have intermediate properties between the gas and liquid phases.¹¹⁵ In their supercritical conditions, fluids present some interesting properties, such as high diffusivity that facilitates mass transfer, gas-like viscosity and null surface tension.¹¹⁵ ScCO₂, the most used supercritical fluid, has a relatively low critical pressure and temperature (73 bar and 31 °C, respectively, figure 12), as well as low cost, non-flammability, and negligible toxicity.

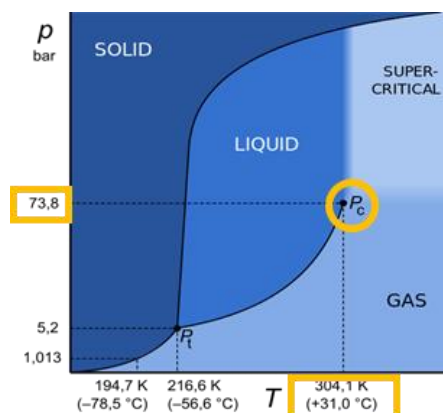


Figure 12. Phase diagram of CO₂, remarking in yellow the critical point and conditions.

scCO₂ has been extensively used in the post-synthesis activation of MOFs to eliminate residual reagents and/or solvents remaining in the structure, while avoiding the collapse of the porous structure.¹¹⁶ This is especially problematic when solvents with high boiling point are used in the synthesis. In these cases, it is necessary the exchange of these solvents with more volatile liquid solvents (e.g., alcohols) before scCO₂ activation. In addition, scCO₂ is considered a green methodology that avoid toxic solvents generally used in the synthesis of CPs.¹¹⁷ The first CP achieved using scCO₂ was published by the team of Domingo *et al.* in 2015¹¹⁸ and since that, the effectiveness of this methodology in the synthesis of previously reported¹¹⁹ and new compounds have been probed.¹²⁰ The main drawback in the use of this technique is the low solubility of many reagents in scCO₂. Different approaches can be applied to solve this limitation, as it is the use of co-solvents, in which a small quantity of a solvent miscible with scCO₂ (EtOH, DMSO...) is added to the reaction media.¹²¹ Some basic additives, such as tert-butylpyridine, have also been used to increase the solubility by forming an intermediate specie with the metal ions.¹²² Moreover, in many cases the products are obtained as powder crystalline precipitates in contrast to the single crystals obtained with other techniques.⁶² Overall, nowadays the use of scCO₂ for the synthesis of CPs is increasing.¹²³

1.3.4.4. Additional synthetic methods

Electrochemistry: metal ions are continuously produced by the oxidation of a metallic electrode introduced in a solution that contains the organic linker and a conducting salt. This methodology was developed for large scale production, since it allows the continuous formation of a large quantity of material, while avoiding the presence of the contra ions in the salt sources.¹²⁴

Mechanochemistry: the driving force that makes possible the reaction is mechanical, *e.g.*, pressure or grinding. The use of this method avoids the need of high external temperatures or/and high boiling point solvents, while open the possibility of using reagents with low solubility in typical solvothermal solvents. In some cases, it becomes necessary the addition of small quantities of salts or solvents (ion or liquid assisted grinding, respectively) to obtain crystalline products.¹²⁵

Sonochemistry: ultrasonic waves are used to induce the reaction by cavitation, *i.e.*, by the formation of microbubbles in the solvent containing the reagents, due to the high negative pressure produced on it by the waves.¹²⁶

1.3.5. 2D-CPs: properties and synthetic approaches.

Since the exfoliation of graphene in 2004, 2D layered materials have attracted much attention because of their especial characteristics giving by the dimensionality, such as huge aspect ratio, quantum-size effect and plain surface conformation.¹²⁷ In 2D materials, the layers are constituted by covalent or coordination bonds, while they are stacked together in 3D products through weak interactions, such as π - π stacking or H-

bonding and electrostatic forces. The name nanosheets is used for 2D structures stacked from few layers to a thickness of approx. 100 nm. In general, nanosheets present high flexibility and resistance to mechanical stress, and higher specific surface area than the non-exfoliated bulk materials. Currently, many different families of 2D materials are under study, including graphene-based products, transition metal dichalcogenides (MoS₂, TiS₂, TaS₂, WS₂, MoSe₂, WSe₂, etc.), layered metal oxides, layered double hydroxides and black phosphorus, and more recently 2D CPs, MOFs and COFs (covalent organic frameworks).¹²⁸ Due to the great technological interest of these nanomaterials, many different methods have been developed to obtain nanosheets, which are here divided in two groups: bottom up and top down.

Bottom-up approach: the nanosheets are formed by controlling and limiting the growth of the material in one direction.¹²⁹ Actually, for CPs the restriction of the growth in one direction is challenging, but some strategies have been developed. One of the most popular is the interlayer growth, where the structure is moulded in a liquid-liquid interphase of immiscible solvents, such as water or DCM,¹³⁰ or in air-liquid interphase.¹³¹ Recently, methodologies based on the use of surfactants, which avoid the vertical growth of the nanosheet and the staking, or the intercalation of small molecule between the layers have been successfully tested.¹³² Related techniques are vapour deposition and sonication.¹²⁸

Top-down approach: layers are separated from the bulk material by breaking the supramolecular interactions that keep them together.¹²⁸ For this, the most used techniques are mechanical cleavage by sonication, mechanical force-assisted liquid exfoliation, ion intercalation-assisted and selective etching-assisted methods.¹³³ In this doctoral thesis, the liquid exfoliation technique using sonication as the mechanical force has been used (figure 13), as it has been described previously for other CPs.¹³⁴

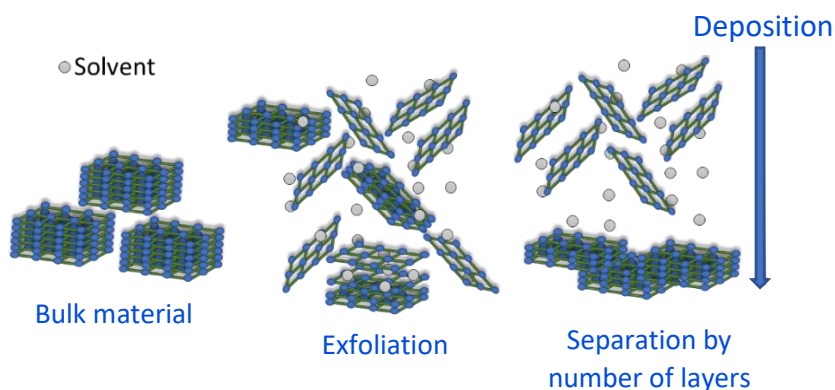


Figure 13. Schematic representation of the liquid-assisted exfoliation method using ultrasounds as the mechanical force.

This technique is straightforward, fast and effective, although the exfoliation yield is low, and problems related to re-aggregation of the layers are common.¹³⁵ The selection of the solvent is one of the key points in this method. The studied material must be insoluble in the solvent, but still weak interactions between the solvent and the nanosheets are required to avoid re-stacking. Nanosheets are basically characterized by atomic force microscopy (AFM) and high-resolution transmission electron microscopy (HR-TEM) microscopies. Additionally, with TEM the electron diffraction pattern of the nanosheets can sometimes be obtained and transformed in the XRD pattern, thus proving that the structure of the bulk crystals is maintained after exfoliation. TEM also provides an idea of the thickness of the nanosheets by using the contrast of the images. However, for this matter AFM gives a more precise information regarding the material thickness.¹³⁵

1.3.6. Applications of CPs

One of the advantages of CPs is that they can afford the best properties of their two components, the organic linker and the metal centre, and for this reason they can be applied in multiple fields. Some examples are presented in figure 14.

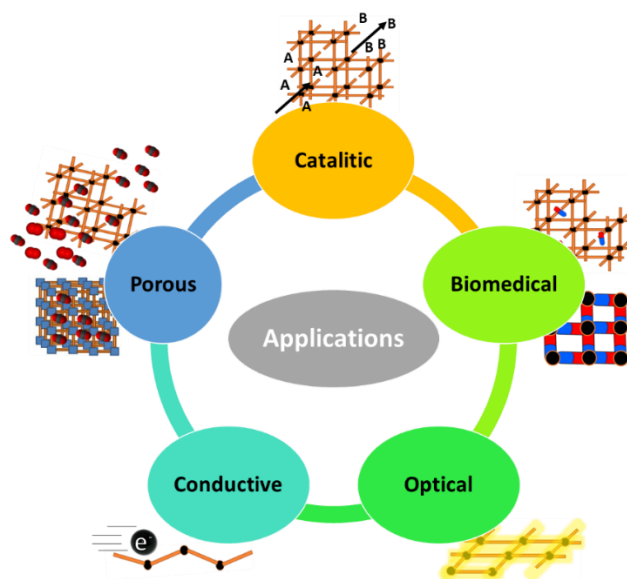


Figure 14. Examples of the application fields of CPs.

For *catalytic applications*, it is crucial the role of the transition-metal centre, that should be catalytically active. This property is especially interesting in open and porous MOF structures, due to the high number of metal centres accessible to the reagents that participate in the catalysis. This topic has been extensively considered and several MOFs have been studied toward oxidation, condensation, alkylation and reduction reactions.¹³⁶

For *conduction applications*, conductive CPs are divided according to the charge carrier in the studied material, being possible electronic or ionic conduction. From these two, proton conduction is the most important. In these materials, apart from the components of the CP, the counter ions and/or molecules surrounding the structure/occupying voids are also important. For example, to obtain high proton conductivity, organic linkers with $-\text{OH}$, $-\text{SO}_3\text{H}$, $-\text{PO}_3\text{H}$, $-\text{SH}$ or $-\text{NH}$ groups¹³⁷ as substituents are proposed, together with the inclusion of Lewis acid molecules or counter ions.¹³⁷ For electronic conductivity, significant overlapping between the orbitals of the metal ions and the organic molecules facilitates the charge transport. In this regard, conductive CPs open the application of these extended structures to the fabrication of ion batteries, supercapacitors, field effect transistors, etc.¹³⁸

For *optical applications*, the luminescence properties of some CPs have been taken into consideration.¹³⁹ For this, the selection of linkers is crucial, although the metal centre also plays a role because it can quench or increase this property. For example, lanthanides have been recurrently chosen for this application, due to their antenna effect that increases luminescence emission.¹⁴⁰

For *biomedical applications*, bioMOFs and bioCPs are being proposed too. Uses have been found in biomedicine and/or as biosensors. For all these applications, it is necessary the used of non-toxic and biocompatible components.¹⁴¹ In medicine, the most studied CPs have been porous structures (MOFs) used for drug encapsulation and delivery. Many articles propose the placement of different therapeutic drugs inside the pores of these compounds and the further delivery of the drugs inside the body.¹⁴² In most cases, there is a decomposition of the MOF, which also implies the release of their components (figure 15). For that reason, it is especially important the use of innocuous organic molecules and metals in the synthesis of BioMOFs.¹⁴³ Recently, Miller *et al.*¹⁴⁴ have proposed that the organic linker may be also the drug of interest. This last approach reduces toxicity and the drawback of needing a porous material to encapsulate the drug, since the active agent is already part of the CP structure (figure 16).¹⁴⁵ In addition, some BioMOFs have shown antimicrobial properties¹⁴⁶ or even biomimetic catalysis.¹⁴⁷ BioMOFs display encouraging properties as biosensors for the selective detection of metal ions^{148,149} or other species.¹⁵⁰ Regarding this matter, as has been previously explained, many CCMoids have shown relevant medical properties and low or null toxicity, being considered suitable for the formation of CPs with biological applications and a new member of the BioMOFs family.

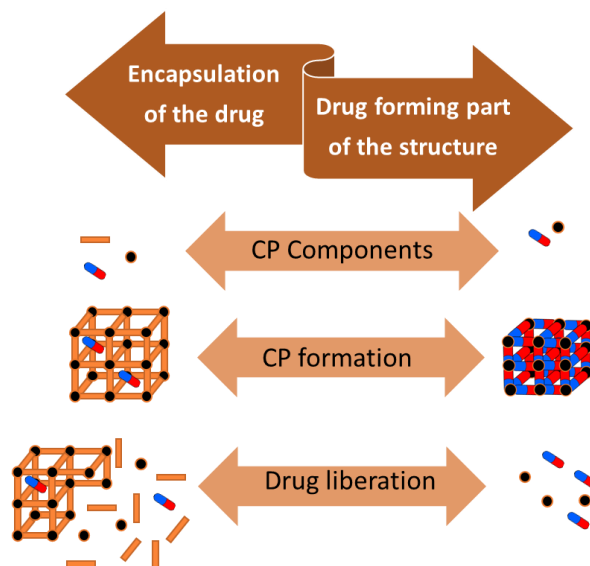


Figure 15. Drug encapsulation in porous CPs and forming part of the structure.

1.4. Organic extended structures

1.4.1. Organic polymers (OPs)

OPs are formed by the repetition of sub-elements involving covalent bonds among these monomeric units.¹⁵¹ Many OPs are available in nature and have been used since ancient times.¹⁵² Very well-known examples are wool and cotton. Bakelite, the first organic synthetic polymer, was already described in 1909, followed by polyethylene, poly(vinyl chloride) and polyamide between 1930 and 1950. This discovery supposed a complete revolution in human society, leading to the development of the plastic industry in the 1950s. The development of synthetic polymers has represented a huge impact for industry, with the development of highly important materials such as nylon or polyethylenopolystyrene.¹⁵³ During this period, the research on OPs was of great importance, leading to several Nobel prizes (e.g., Flory, de Gennes, Ziegler and Natta).¹⁵⁴ Since then, the number of articles related to OPs continues growing. The functional groups and the structure of the monomers are of great relevance and affect the rigidity, the capacity of establishing interchain interactions and crosslinking.¹⁵⁵

The methodology chosen to achieve polymerization would depend on the functional groups implicated in the formation of the covalent bond, being distinguished in the literature two types: addition and condensation polymerizations (figure 16).

Addition or chain-growth polymerisation: here, the polymer contains all the atoms of the starting monomer. This is the typical reaction for monomers with double or triple bonds in the carbon chain, as for example polyethylene, propylene, polypropylene or polyvinyl

chloride. In many cases, this polymerization follows a radical, cationic or anionic, mechanism with three steps, denominated initiation, propagation and termination. There is only one point of the chain where the next monomer can react.¹⁵⁵

Condensation or step growth polymerisation: this process is done by the reaction of the lateral functional groups of the reactive monomer (carboxylic acids, amines, alcohols...). In many cases, the formation of the bond produces the elimination of a small molecule, frequently water. Examples of this type of polymers are polyester, nylon, proteins and even DNA.¹⁵⁵

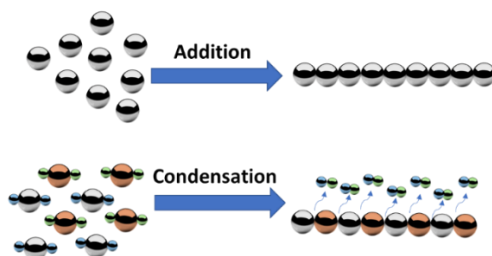


Figure 16. Schematic representation of the addition and condensation polymerization processes.

The properties and applications of OPs depend on the constituent monomers and the connection between them. This is one of the most used material around the world, from packing to transportation, with more added-value applications in the biological and electronical fields.¹⁵⁴

In the case of biological and biomedical applications, biological OPs play an important role in living organisms. DNA or proteins are examples of these OPs with essential functions, as well as some polysaccharides (cellulose, chitin, starch and agar).¹⁵⁶ Many of these polymers have been used for different industrial purposes, including the pharmaceutical, where they are often used as excipients, i.e., inactive substances that act as vehicle or medium for an active substance.¹⁵⁷ In the biomedical field, OPs, natural or synthetic, are used in biosensors,¹⁵⁸ drug encapsulation¹⁵⁹ or tissue regeneration.¹⁶⁰

In another matter, conductive polymers are of great relevance for the construction of electronic devices because of their high electrical conductivity, mechanical flexibility, and low cost. In many cases, they are doped to increase the conductivity. The first conductive polymer was described in 1977 by Shirakawa *et al.*¹⁶¹ by doping polyacetylene with halogens. Further on, many polymers have shown interesting conductive properties that, in many cases, are also combined with magnetic, wetting, optical or mechanical features.¹⁶¹ This allows the fabrication of field effect transistors, diodes, thermoelectrics, sensors, solar cells, and supercapacitors, among others.¹⁶¹

As it occurs in the area of CPs, the formation of ordered materials with porosity creates a new type of OPs, called covalent organic frameworks (COFs) that opens the door to new applications.¹⁶² These structures can be used for absorption and separation of molecules and gases, as they can be design with specific pores size and specific moieties in the voids allowing selectivity. Many applications have been proposed based in this capacity, such as the fabrication of selective membranes, contaminant entrapment, drug encapsulation, separation of chiral compounds, gas storage and transport.¹⁶²

1.5. Precedents and motivation of this doctoral thesis: CPs and polymers based on CCMoids.

One of the main novelties of this doctoral thesis relays in the preparation of highly dimensional structures based on CCMoids. For that, we take advantage of the coordination capabilities of the central β -diketone moiety and lateral substituents to form CPs or, in the case of the OPs, the ability of the lateral substituents to react with organic molecules. In this section the state of the art of this topic is explained to emphasize the motivation of this work.

In 2015, Su *et al.*⁶¹ reported the first CP based on CCM, involving Zn(II) metal centre, depicted in figure 17a. This is a porous structure where three Zn(II) form a SBU through oxo bridges from lateral hydroxy groups of nearby CCM molecules. Within the CP, the central Zn(II) atom is coordinated to six oxygens of four different lateral moieties, two methoxy and four phenolic groups. The lateral Zn(II) atoms are pentacoordinated, where two of the five oxygen atoms are from a β -diketone and the rest from neighbouring moieties, two phenolic and one methoxy groups, respectively. The phenol groups are acting as bridges between the central and the lateral metal atoms.

More recently, the synthesis of a new CCM-Zn(II) MOF structure was achieved in $scCO_2$ by the team of Domingo *et al.*⁶² Here, it is worth to mention that CCM is typically extracted from turmeric roots using $scCO_2$ and EtOH as a solvent and co-solvent, respectively.¹⁶³ In this new structure, shown in figure 17b, all the Zn(II) atoms are equivalent, constituting a SBU formed by two metal atoms connected through oxo phenyl bridges. Here, the Zn(II) atoms are pentacoordinated to one β -diketone of one CCMoid and three oxygen atoms of two substituents of the aromatic ring being one methoxy and two phenolic oxygens, the latter are shared between both metal ions. In this case, only one of the corners of the molecule is coordinated and the other remains protonated forming, despite of this, an ordered extended porous structure.

Additional CPs based on different CCMoids than CCM have been described by the team of Aliaga-Alcalde *et al.*⁵³ Figure 18 shows two isostructural CPs with Co(II) an Ni(II) ions, respectively, coordinated to the β -diketone of a CCMoid with anthracene substituents in the corners. In this case, as this CCMoid does not have donor atoms in the corners, the

coordination was completed with bipyridine co-linkers to achieve the extension of the structure forming 1D chains.

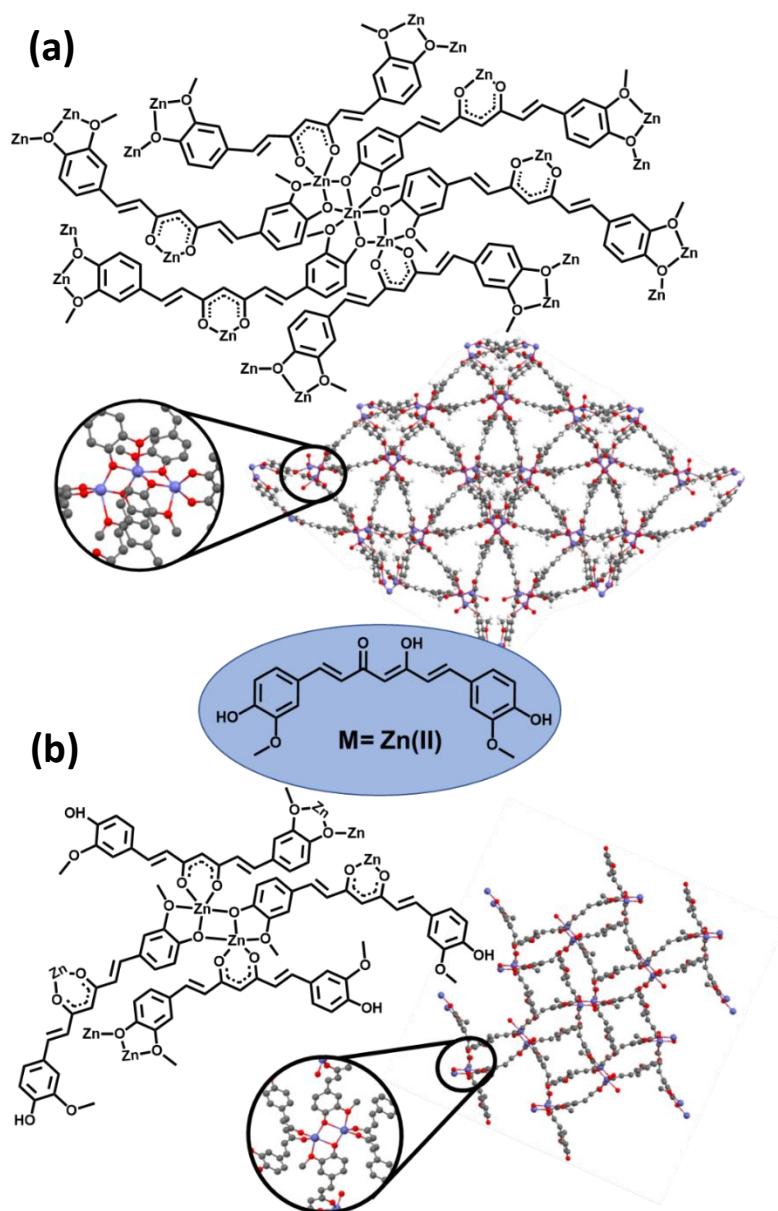


Figure 17. Published CPs based on CCM: a) Su *et al.*,⁶² b) Portoles-Gil *et al.*⁶² and the CCM structure and metal used emphasized in the centre of the figure.

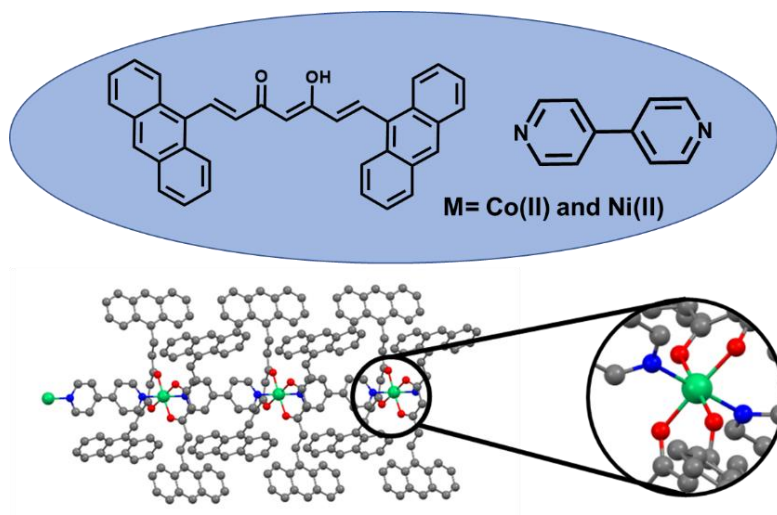


Figure 18. Published CPs based on other CCMoid different to CCM.

This doctoral thesis aims to enlighten in the knowledge on the design of CPs based on different CCMoids by using additional reactive lateral moieties, that can affect the dimensionality of the final structures as well as their chemical characteristics, thus, their potential properties.

In the subject of OPs, most of the research performed so far with CCMoids relates to the inclusion of these molecules in preformed polymeric structures, approach often used to increase the biodisponibility of synthesized polymers.¹⁶⁴⁻¹⁶⁶ Hence, the CCMoid is not normally used as a monomer in the formation of the polymer. This idea has been only explored in few works where CCM or derivatives have been used as co-monomers to form polymers (figure 19).^{167,168}

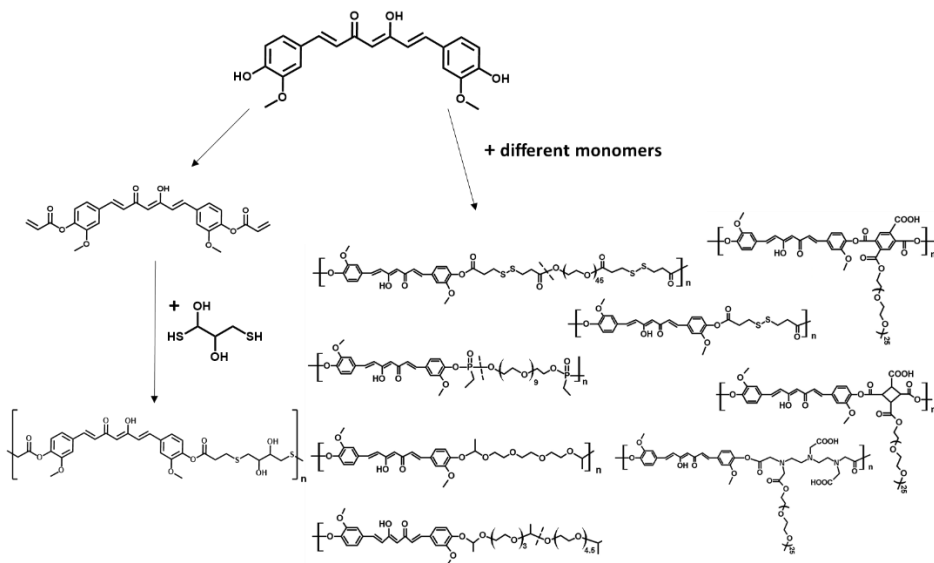


Figure 19. Organic polymers based on CCM and derivatives.^{167,168}

Also related, in 2019 Liu *et al.*¹⁶⁹ published an organic polymer using as monomers acetylacetonate boron difluoride and tris(4-formylphenyl)amine (figure 20). Even though the monomers were not CCMoids, the condensation between them gave as a result a CCMoid-based network and, therefore, the repeated unit in the end product is a CCMoid, forming a CCMoid-like OP (figure 20).

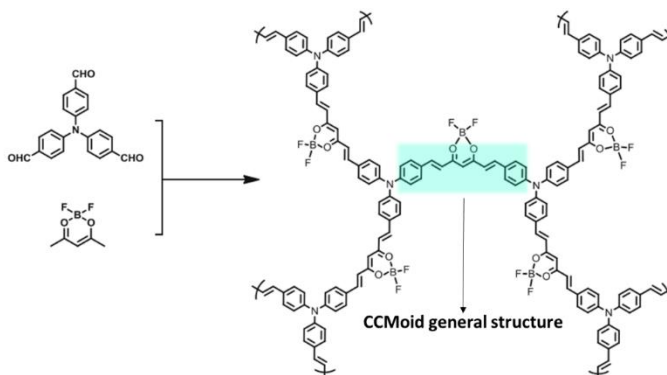


Figure 20. Organic polymer synthesized by Liu *et al.*¹⁶⁹

This doctoral thesis aims to provide insight on the above topics, obtaining polymers based in new CCMoids and new covalent bonds. Moreover, new CCMoid units have been also synthesized toward their future use in the creation of CCMoids-based polymer (1D-3D). Each chapter of the present doctoral thesis evaluate different aspects of CCMoids applied in the field of CPs.

2. References

- (1) Manolova, Y., Deneva, V., Antonov, L., Drakalska, E., Momekova, D., & Lambov, N. (2014). The effect of the water on the curcumin tautomerism: A quantitative approach. *Spectrochimica Acta Part A: Molecular and Biomolecular Spectroscopy*, 132, 815-820.
- (2) Pedersen, U., Rasmussen, P. B., & Lawesson, S. O. (1985). Synthesis of naturally occurring curcuminoids and related compounds. *Liebigs Annalen der Chemie*, 1985(8), 1557-1569.
- (3) Priyadarsini, K. I. (2014). The chemistry of curcumin: from extraction to therapeutic agent. *Molecules*, 19(12), 20091-20112.
- (4) Jayaprakasha, G. K., Rao, L. J. M., & Sakariah, K. K. (2005). Chemistry and biological activities of *C. longa*. *Trends in Food Science & Technology*, 16(12), 533-548.
- (5) Bandyopadhyay, D. (2014). Farmer to pharmacist: curcumin as an anti-invasive and antimetastatic agent for the treatment of cancer. *Frontiers in chemistry*, 2, 113.
- (6) Vogel A Jr. *J. Pharm. Chem.* 1842; 3:20.
- (7) Miłobędzka, J., v. Kostanecki, S., & Lampe, V. (1910). Zur kenntnis des curcumins. *Berichte der deutschen chemischen Gesellschaft*, 43(2), 2163-2170.
- (8) Deck, L. M., Hunsaker, L. A., Vander Jagt, T. A., Whalen, L. J., Royer, R. E., & Vander Jagt, D. L. (2018). Activation of anti-oxidant Nrf2 signaling by enone analogues of curcumin. *European journal of medicinal chemistry*, 143, 854-865.
- (9) Sherin, D. R., & Rajasekharan, K. N. (2016). Studies on the antioxidant activities of mechanochemically synthesized 1-aryl-3, 5-bis (styryl) pyrazoles as curcuminoids derived CNB 001 analogs. *Indian J. Heterocycl. Chem*, 26, 81-86.
- (10) Lee, K. H., Ishida, J., Ohtsu, H., Wang, H. K., Itokawa, H., Chang, C., & Shih, C. C. Y. (2003). Curcumin analogs for the treatment of cancers and androgen-related diseases. *PCT Int Appl, USA*, 36.
- (11) Lozada-García, M. C., Enríquez, R. G., Ramírez-Apán, T. O., Nieto-Camacho, A., Palacios-Espinosa, J. F., Custodio-Galván, Z.,... & Pérez-Villanueva, J. (2017). Synthesis of curcuminoids and evaluation of their cytotoxic and antioxidant properties. *Molecules*, 22(4), 633.
- (12) Sudarmanto, B. A., & Oetari, R. A. (2007). Application of quantum chemical descriptors in QSAR analysis of curcumin derivatives as ethoxyresorufin o-dealkylation inhibitor. *Indonesian Journal of Pharmacy*, 147-153.
- (13) Canard, G., Ponce-Vargas, M., Jacquemin, D., Le Guennic, B., Felouat, A., Rivoal, M., ... & Fages, F. (2017). Influence of the electron donor groups on the optical and electrochemical properties of borondifluoride complexes of curcuminoid derivatives: a joint theoretical and experimental study. *RSC advances*, 7(17), 10132-10142.
- (14) Vergheze, J., & Joy, M. T. (1989). Isolation of the colouring matter from dried turmeric (*Curcuma longa* L.) with ethyl acetate. *Flavour and Fragrance Journal*, 4(1), 31-32.
- (15) Xianchun, W., Xie, J., Shan, C., & Qi, Z. (1993). Extraction of curcumin from Jianghuang (*Curcuma longa*) by ethanol reflux. *Shipin Kexue (Beijing)*, 165, 45-47.
- (16) Dandekar, D. V., & Gaikar, V. G. (2002). Microwave assisted extraction of curcuminoids from *Curcuma longa*. *Separation science and technology*, 37(11), 2669-2690.
- (17) Chassagnez-Mendez, A. L., Machado, N. T., Araujo, M. E., Maia, J. G., & Meireles, M. A. A. (2000). Supercritical CO₂ extraction of curcumins and essential oil from the rhizomes of turmeric (*Curcuma longa* L.). *Industrial & engineering chemistry research*, 39(12), 4729-4733.
- (18) Schieffer, G. W. (2002). Pressurized liquid extraction of curcuminoids and curcuminoid degradation products from turmeric (*Curcuma longa*) with subsequent HPLC assays. *Journal of liquid chromatography & related technologies*, 25(19), 3033-3044.
- (19) Lampe, V., & Miłobędzka, J. (1913). Studien über curcumin. *Berichte d. D. Chem Gesellschaft*, 46(2), 2235-2240.
- (20) Pavolini, T. (1937). Nuova sintesi della Curcumina. *Riv. Ital. Essenze, Profumi, Piante Officinali*, 19, 167-168.
- (21) Pabon, H. J. J. (1964). A synthesis of curcumin and related compounds. *Recueil des Travaux Chimiques des Pays-Bas*, 83(4), 379-386.

- (22) Etcheverry-Berriós, A., Olavarría, I., Perrin, M. L., Díaz-Torres, R., Jullian, D., Ponce, I., ... & Dulić, D. (2016). Multiscale Approach to the Study of the Electronic Properties of Two Thiophene Curcuminoid Molecules. *Chemistry—A European Journal*, 22(36), 12808-12818.
- (23) Rao, E. V., & Sudheer, P. (2011). Revisiting curcumin chemistry part I: A new strategy for the synthesis of curcuminoids. *Indian journal of pharmaceutical sciences*, 73(3), 262.
- (24) Ferrari, E., Lazzari, S., Marverti, G., Pignedoli, F., Spagnolo, F., & Saladini, M. (2009). Synthesis, cytotoxic and combined cDDP activity of new stable curcumin derivatives. *Bioorganic & medicinal chemistry*, 17(8), 3043-3052.
- (24) Babu, K. D., & Rajasekharan, K. N. (1994). Simplified condition for synthesis of curcumin I and other curcuminoids. *Organic preparations and procedures international*, 26(6), 674-677.
- (25) Pore, D., Alli, R., SC Prabhakar, A., R Alavala, R., Kulandaivelu, U., & Boyapati, S. (2012). Solid-Phase Microwave Assisted Synthesis of Curcumin Analogs. *Letters in Organic Chemistry*, 9(6), 447-450.
- (26) Gopinath, H., & Karthikeyan, K. (2018). Turmeric: A condiment, cosmetic and cure. *Indian Journal of Dermatology, Venereology, and Leprology*, 84(1), 16.
- (27) Keserü, G. M., & Nógrádi, M. (1995). The chemistry of natural diarylheptanoids. In *Studies in natural products chemistry* (Vol. 17, pp. 357-394). Elsevier.
- (28) Hewlings, S. J., & Kalman, D. S. (2017). Curcumin: a review of its effects on human health. *Foods*, 6(10), 92.
- (29) Maheshwari, R. K., Singh, A. K., Gaddipati, J., & Srimal, R. C. (2006). Multiple biological activities of curcumin: a short review. *Life sciences*, 78(18), 2081-2087.
- (30) Prins, F., Barreiro, A., Ruitenbergh, J. W., Seldenthuis, J. S., Aliaga-Alcalde, N., Vandersypen, L. M., & van der Zant, H. S. (2011). Room-temperature gating of molecular junctions using few-layer graphene nanogap electrodes. *Nano letters*, 11(11), 4607-4611.
- (31) Burzurí, E., Island, J. O., Díaz-Torres, R., Fursina, A., González-Campo, A., Roubeau, O., ... & van der Zant, H. S. (2016). Sequential electron transport and vibrational excitations in an organic molecule coupled to few-layer graphene electrodes. *ACS nano*, 10(2), 2521-2527.
- (32) Díaz Torres, R. (2018). Synthesis, characterization and deposition on surfaces of curcuminoids-based systems. Doctoral dissertation, Universitat de Barcelona.
- (33) Etcheverry Berriós, Á. F. (2018). Diseño y síntesis de sistemas curcuminoides para aplicaciones en electrónica molecular. Doctoral dissertation, Universidad de Chile.
- (34) Dulic, D., Rates, A., Castro, E., Labra-Muñoz, J., Aravena, D., Etcheverry-Berrios, A., ... & van der Zant, H. S. (2019). Single-molecule transport of fullerene-based curcuminoids. *The Journal of Physical Chemistry C*, 124(4), 2698-2704.
- (35) Olavarría-Contreras, I. J., Etcheverry-Berriós, A., Qian, W., Gutiérrez-Cerón, C., Campos-Olguín, A., Sañudo, E. C., ... & Van Der Zant, H. S. (2018). Electric-field induced bistability in single-molecule conductance measurements for boron coordinated curcuminoid compounds. *Chemical science*, 9(34), 6988-6996.
- (36) Wanninger, S., Lorenz, V., Subhan, A., & Edelmann, F. T. (2015). Metal complexes of curcumin—synthetic strategies, structures and medicinal applications. *Chemical Society Reviews*, 44(15), 4986-5002.
- (37) Ohtsu, H., Xiao, Z., Ishida, J., Nagai, M., Wang, H. K., Itokawa, H., ... & Lee, K. H. (2002). Antitumor agents. 217. Curcumin analogues as novel androgen receptor antagonists with potential as anti-prostate cancer agents. *Journal of medicinal chemistry*, 45(23), 5037-5042.
- (38) Bray, D. J., Clegg, J. K., Lindoy, L. F., & Schilter, D. (2006). Self-assembled metallo-supramolecular systems incorporating β -diketone motifs as structural elements. *Advances in Inorganic Chemistry*, 59, 1-37.
- (39) Zhang, Y., Khan, A. R., Fu, M., Zhai, Y., Yu, A., & Zhai, G. (2019). The progresses in curcuminoids-based metal complexes: especially in cancer therapy. *Future medicinal chemistry*, 11(09), 1035-1056.
- (40) Khorasani, M. Y., Langari, H., Sany, S. B. T., Rezayi, M., & Sahebkar, A. (2019). The role of curcumin and its derivatives in sensory applications. *Materials Science and Engineering: C*, 109792.
- (41) Díaz-Torres, R., Menelaou, M., Roubeau, O., Sorrenti, A., Brandariz-de-Pedro, G., Sañudo, E. C., ... & Aliaga-Alcalde, N. (2016). Multiscale study of mononuclear Co II SMMs based on curcuminoid ligands. *Chemical science*, 7(4), 2793-2803.
- (42) Mendiguchia, B. S., Aiello, I., & Crispini, A. (2015). Zn (II) and Cu (II) complexes containing bioactive O, O-chelated ligands: homoleptic and heteroleptic metal-based biomolecules. *Dalton Transactions*, 44(20), 9321-9334.

- (43) Al-Ali, K., Fatah, H. S. A., & El-Badry, Y. A. M. (2016). Dual effect of curcumin–zinc complex in controlling diabetes mellitus in experimentally induced diabetic rats. *Biological and Pharmaceutical Bulletin*, 39(11), 1774-1780.
- (44) Lu, W. P., Mei, X. T., Wang, Y., Zheng, Y. P., Xue, Y. F., & Xu, D. H. (2015). Zn (II)–curcumin protects against oxidative stress, deleterious changes in sperm parameters and histological alterations in a male mouse model of cyclophosphamide-induced reproductive damage. *Environmental toxicology and Pharmacology*, 39(2), 515-524.
- (45) Yu, C., Mei, X. T., Zheng, Y. P., & Xu, D. H. (2014). Zn (II)–curcumin protects against hemorheological alterations, oxidative stress and liver injury in a rat model of acute alcoholism. *Environmental toxicology and pharmacology*, 37(2), 729-737.
- (46) Abbaoui, A., Chatoui, H., El Hiba, O., & Gamrani, H. (2017). Neuroprotective effect of curcumin-I in copper-induced dopaminergic neurotoxicity in rats: A possible link with Parkinson's disease. *Neuroscience letters*, 660, 103-108.
- (47) Ferrari, E., Benassi, R., Saladini, M., Orteca, G., Gazova, Z., & Siposova, K. (2017). In vitro study on potential pharmacological activity of curcumin analogues and their copper complexes. *Chemical biology & drug design*, 89(3), 411-419.
- (48) Sui, Z., Salto, R., Li, J., Craik, C., & de Montellano, P. R. O. (1993). Inhibition of the HIV-1 and HIV-2 proteases by curcumin and curcumin boron complexes. *Bioorganic & medicinal chemistry*, 1(6), 415-422.
- (49) Asti, M., Ferrari, E., Croci, S., Atti, G., Rubagotti, S., Iori, M., ... & Versari, A. (2014). Synthesis and characterization of ⁶⁸Ga-labeled curcumin and curcuminoid complexes as potential radiotracers for imaging of cancer and Alzheimer's disease. *Inorganic chemistry*, 53(10), 4922-4933.
- (50) Pignedoli, F., Zobi, F., Saladini, M., & Alberto, R. (2010). New ^{99m}Tc (I) and Re (I) Curcumin derivatives for molecular imaging. *Nuclear Medicine and Biology*, 6(37), 683.
- (51) García-Niño, W. R., & Pedraza-Chaverrí, J. (2014). Protective effect of curcumin against heavy metals-induced liver damage. *Food and Chemical Toxicology*, 69, 182-201.
- (52) Menelaou, M., Ouharrou, F., Rodríguez, L., Roubeau, O., Teat, S. J., & Aliaga-Alcalde, N. (2012). DyIII-and YbIII-Curcuminoid Compounds: Original Fluorescent Single-Ion Magnet and Magnetic Near-IR Luminescent Species. *Chemistry—A European Journal*, 18(37), 11545-11549.
- (53) Díaz-Torres, R., Menelaou, M., González-Campo, A., Teat, S. J., Sañudo, E., Soler, M., & Aliaga-Alcalde, N. (2016). Comparative Magnetic Studies in the Solid State and Solution of Two Isostructural 1D Coordination Polymers Containing CoII/NiII-Curcuminoid Moieties. *Magnetochemistry*, 2(3), 29.
- (54) Elahi, M. Y., Heli, H., Bathaie, S. Z., & Mousavi, M. F. (2007). Electrocatalytic oxidation of glucose at a Ni-curcumin modified glassy carbon electrode. *Journal of Solid State Electrochemistry*, 11(2), 273-282.
- (55) Schlumberger, M. E. (1866). Sur la réaction de l'acide borique sur la curcumine. *Bull. Soc. Chim. Paris*, 5, 194.
- (56) Roth, H. J., & Miller, B. (1964). Zur Kenntnis der Farbreaktion zwischen Borsäure und Curcumin. II. Zur Konstitution des Rosocyanins und Rubrocurcumins. *Archiv der Pharmazie*, 297(11), 660-673.
- (57) Aznarez, J., Bonilla, A., & Vidal, J. C. (1983). Spectrophotometric and fluorimetric determination of boron in soils, plants and waters by extraction with 2-methylpentane-2, 4-diol in isobutyl methyl ketone. *Analyst*, 108(1284), 368-373.
- (58) Lawrence, K., Flower, S. E., Kociok-Kohn, G., Frost, C. G., & James, T. D. (2012). A simple and effective colorimetric technique for the detection of boronic acids and their derivatives. *Analytical Methods*, 4(8), 2215-2217.
- (59) Margar, S. N., Rhyman, L., Ramasami, P., & Sekar, N. (2016). Fluorescent difluoroboron-curcumin analogs: an investigation of the electronic structures and photophysical properties. *Spectrochimica Acta Part A: Molecular and Biomolecular Spectroscopy*, 152, 241-251.
- (60) Bai, G., Yu, C., Cheng, C., Hao, E., Wei, Y., Mu, X., & Jiao, L. (2014). Syntheses and photophysical properties of BF₂ complexes of curcumin analogues. *Organic & biomolecular chemistry*, 12(10), 1618-1626.
- (61) Su, H., Sun, F., Jia, J., He, H., Wang, A., & Zhu, G. (2015). A highly porous medical metal–organic framework constructed from bioactive curcumin. *Chemical Communications*, 51(26), 5774-5777.
- (62) Portolés-Gil, N., Lanza, A., Aliaga-Alcalde, N., Ayllón, J. A., Gemmi, M., Mugnaioli, E., ... & Domingo, C. (2018). Crystalline curcumin bioMOF obtained by precipitation in supercritical CO₂ and structural

- determination by electron diffraction tomography. *ACS Sustainable Chemistry & Engineering*, 6(9), 12309-12319.
- (63) Janiak, C. (2003). Engineering coordination polymers towards applications. *Dalton Transactions*, (14), 2781-2804.
- (64) Olafson, K. N., Li, R., Alamani, B. G., & Rimer, J. D. (2016). Engineering crystal modifiers: bridging classical and nonclassical crystallization. *Chemistry of Materials*, 28(23), 8453-8465.
- (65) Batten, S. R., Neville, S. M., & Turner, D. R. (2008). *Coordination polymers: design, analysis and application*. Royal Society of Chemistry.
- (66) Buser, H. J., Ludi, A., Fischer, P., Studach, T., & Dale, B. W. (1974). A Neutron Diffraction Study of Prussian Blue, Fe₄[Fe(CN)₆]₃·14 D₂O.
- (67) Vinogradova, S. V., & Vinogradova, O. G. V. (1975). Coordination polymers with inorganic main chains. *Russian Chemical Reviews*, 44(6), 510.
- (68) Bailar, J. C., & Trotman-Dickenson, A. F. (Eds.). (1973). *Comprehensive inorganic chemistry* (Vol. 3, pp. 491-551). Oxford: Pergamon press.
- (69) Hoskins, B. F., & Robson, R. (1989). Infinite polymeric frameworks consisting of three dimensionally linked rod-like segments. *Journal of the American Chemical Society*, 111(15), 5962-5964.
- (70) Yaghi, O. M., & Li, H. (1995). Hydrothermal synthesis of a metal-organic framework containing large rectangular channels. *Journal of the American Chemical Society*, 117(41), 10401-10402.
- (71) Batten, S. R., Champness, N. R., Chen, X. M., Garcia-Martinez, J., Kitagawa, S., Öhrström, L., ... & Reedijk, J. (2013). Terminology of metal-organic frameworks and coordination polymers (IUPAC Recommendations 2013). *Pure and Applied Chemistry*, 85(8), 1715-1724.
- (72) Eddaoudi, M., Moler, D. B., Li, H., Chen, B., Reineke, T. M., O'keeffe, M., & Yaghi, O. M. (2001). Modular chemistry: secondary building units as a basis for the design of highly porous and robust metal-organic carboxylate frameworks. *Accounts of chemical research*, 34(4), 319-330.
- (73) Fujita, M., Fujita, N., Ogura, K., & Yamaguchi, K. (1999). Spontaneous assembly of ten components into two interlocked, identical coordination cages. *Nature*, 400(6739), 52-55.
- (74) Junker, A. K. R., Hill, L. R., Thompson, A. L., Faulkner, S., & Sørensen, T. J. (2018). Shining light on the antenna chromophore in lanthanide based dyes. *Dalton transactions*, 47(14), 4794-4803.
- (75) Feller, R. K., & Cheetham, A. K. (2006). Fe (III), Mn (II), Co (II), and Ni (II) 3, 4, 5-trihydroxybenzoate (gallate) dihydrates; a new family of hybrid framework materials. *Solid state sciences*, 8(9), 1121-1125.
- (76) Zhou, H., Li, M., Li, D., Zhang, J., & Chen, X. (2014). Thermal expansion behaviors of Mn (II)-pyridylbenzoate frameworks based on metal-carboxylate chains. *Science China Chemistry*, 57(3), 365-370.
- (77) Catarineu, N. R., Schoedel, A., Urban, P., Morla, M. B., Trickett, C. A., & Yaghi, O. M. (2016). Two principles of reticular chemistry uncovered in a metal-organic framework of heterotritopic linkers and infinite secondary building units. *Journal of the American Chemical Society*, 138(34), 10826-10829.
- (78) Eddaoudi, M., Kim, J., Rosi, N., Vodak, D., Wachter, J., O'Keeffe, M., & Yaghi, O. M. (2002). Systematic design of pore size and functionality in isorecticular MOFs and their application in methane storage. *Science*, 295(5554), 469-472.
- (79) Furukawa, H., Cordova, K. E., O'Keeffe, M., & Yaghi, O. M. (2013). The chemistry and applications of metal-organic frameworks. *Science*, 341(6149), 1230444.
- (80) Haldar, R., & Maji, T. K. (2013). Metal-organic frameworks (MOFs) based on mixed linker systems: structural diversities towards functional materials. *CrystEngComm*, 15(45), 9276-9295.
- (81) Portolés-Gil, N., López-Periago, A. M., Borrás, A., Fraile, J., Solano, E., Vallcorba, O., ... & Domingo, C. (2020). Tuning the Structure and Flexibility of Coordination Polymers via Solvent Control of Tritopic Triazine Conformation during Crystallization. *Crystal Growth & Design*, 20(5), 3304-3315.
- (82) Portolés-Gil, N. (2019). *Green synthesis of coordination polymers using supercritical carbon dioxide* Doctoral dissertation, Universitat Autònoma de Barcelona.
- (83) Haldar, R., & Maji, T. K. (2013). Metal-organic frameworks (MOFs) based on mixed linker systems: structural diversities towards functional materials. *CrystEngComm*, 15(45), 9276-9295.
- (84) Xiao, D. R., Wang, E. B., An, H. Y., Li, Y. G., Su, Z. M., & Sun, C. Y. (2006). A Bridge between Pillared-Layer and Helical Structures: A Series of Three-Dimensional Pillared Coordination Polymers with Multiform Helical Chains. *Chemistry—A European Journal*, 12(25), 6528-6541.

- (85) Wang, H., Zhang, D., Sun, D., Chen, Y., Wang, K., Ni, Z. H., ... & Jiang, J. (2010). Diverse Ni (II) MOFs constructed from asymmetric semi-rigid V-shaped multicarboxylate ligands: structures and magnetic properties. *CrystEngComm*, 12(4), 1096-1102.
- (86) Wang, H., Zhang, D., Sun, D., Chen, Y., Zhang, L. F., Tian, L., ... & Ni, Z. H. (2009). Co (II) metal-organic frameworks (MOFs) assembled from asymmetric semirigid multicarboxylate ligands: synthesis, crystal structures, and magnetic properties. *Crystal growth & design*, 9(12), 5273-5282.
- (87) Vaidhyanathan, R., Bradshaw, D., Rebilly, J. N., Barrio, J. P., Gould, J. A., Berry, N. G., & Rosseinsky, M. J. (2006). A family of nanoporous materials based on an amino acid backbone. *Angewandte Chemie International Edition*, 45(39), 6495-6499.
- (88) Zhang, S. Q., Jiang, F. L., Wu, M. Y., Ma, J., Bu, Y., & Hong, M. C. (2012). Assembly of discrete one-, two-, and three-dimensional Zn (II) complexes containing semirigid V-shaped tricarboxylate ligands. *Crystal growth & design*, 12(3), 1452-1463.
- (89) Shimazaki, Y., Takani, M., & Yamauchi, O. (2009). Metal complexes of amino acids and amino acid side chain groups. Structures and properties. *Dalton Transactions*, (38), 7854-7869.
- (90) Emami, S., Paz, F. A. A., Mendes, A., & Gales, L. (2014). Toward the Construction of 3D Dipeptide-Metal Frameworks. *Crystal Growth & Design*, 14(9), 4777-4780.
- (91) Navarro-Sanchez, J., Argente-Garcia, A. I., Moliner-Martinez, Y., Roca-Sanjuan, D., Antypov, D., Campins-Falco, P., ... & Marti-Gastaldo, C. (2017). Peptide metal-organic frameworks for enantioselective separation of chiral drugs. *Journal of the American Chemical Society*, 139(12), 4294-4297.
- (92) Zhang, M., Gu, Z. Y., Bosch, M., Perry, Z., & Zhou, H. C. (2015). Biomimicry in metal-organic materials. *Coordination Chemistry Reviews*, 293, 327-356.
- (93) García-Terán, J. P., Castillo, O., Luque, A., García-Couceiro, U., Román, P., & Lezama, L. (2004). An unusual 3D coordination polymer based on bridging interactions of the nucleobase adenine. *Inorganic chemistry*, 43(15), 4549-4551.
- (94) Sontz, P. A., Bailey, J. B., Ahn, S., & Tezcan, F. A. (2015). A metal organic framework with spherical protein nodes: rational chemical design of 3D protein crystals. *Journal of the American Chemical Society*, 137(36), 11598-11601.
- (95) Patel, H. A., Islamoglu, T., Liu, Z., Nalluri, S. K. M., Samanta, A., Anamimoghadam, O., ... & Stoddart, J. F. (2017). Non-invasive substitution of K⁺ sites in cyclodextrin metal-organic frameworks by Li⁺ ions. *Journal of the American Chemical Society*, 139(32), 11020-11023.
- (96) Abrahams, B. F., Moylan, M., Orchard, S. D., & Robson, R. (2003). Zinc Saccharate: A Robust, 3D coordination network with two types of isolated, parallel channels, one hydrophilic and the other hydrophobic. *Angewandte Chemie International Edition*, 42(16), 1848-1851.
- (97) Wilcox, O. T., Fateeva, A., Katsoulidis, A. P., Smith, M. W., Stone, C. A., & Rosseinsky, M. J. (2015). Acid loaded porphyrin-based metal-organic framework for ammonia uptake. *Chemical Communications*, 51(81), 14989-14991.
- (98) Jain, P., Ramachandran, V., Clark, R. J., Zhou, H. D., Toby, B. H., Dalal, N. S., ... & Cheetham, A. K. (2009). Multiferroic behavior associated with an order-disorder hydrogen bonding transition in metal-organic frameworks (MOFs) with the perovskite ABX₃ architecture. *Journal of the American Chemical Society*, 131(38), 13625-13627.
- (99) Thushari, S., Cha, J. A., Sung, H. H. Y., Chui, S. S. Y., Leung, A. L. F., Yen, Y. F., & Williams, I. D. (2005). Microporous chiral metal coordination polymers: hydrothermal synthesis, channel engineering and stability of lanthanide tartrates. *Chemical communications*, (44), 5515-5517.
- (100) Sun, B., Bilal, M., Jia, S., Jiang, Y., & Cui, J. (2019). Design and bio-applications of biological metal-organic frameworks. *Korean Journal of Chemical Engineering*, 36(12), 1949-1964.
- (101) Huang, L., Wang, H., Chen, J., Wang, Z., Sun, J., Zhao, D., & Yan, Y. (2003). Synthesis, morphology control, and properties of porous metal-organic coordination polymers. *Microporous and mesoporous materials*, 58(2), 105-114.
- (102) Nishinaga, T. (Ed.). (2014). *Handbook of Crystal Growth: Fundamentals*. Elsevier
- (103) Hoskins, B. F., & Robson, R. (1990). Design and construction of a new class of scaffolding-like materials comprising infinite polymeric frameworks of 3D-linked molecular rods. A reappraisal of the zinc cyanide and cadmium cyanide structures and the synthesis and structure of the diamond-related frameworks [N (CH₃)

- 4][CuI₂ZnII (CN)₄] and CuI [4, 4', 4'', 4'''-tetracyanotetraphenylmethane] BF₄. xC₆H₅NO₂. *Journal of the American Chemical Society*, 112(4), 1546-1554.
- (104) Rabenau, A. (1985). The role of hydrothermal synthesis in preparative chemistry. *Angewandte Chemie International Edition in English*, 24(12), 1026-1040.
- (105) Stock, N., & Biswas, S. (2012). Synthesis of metal-organic frameworks (MOFs): routes to various MOF topologies, morphologies, and composites. *Chemical reviews*, 112(2), 933-969.
- (106) Klinowski, J., Paz, F. A. A., Silva, P., & Rocha, J. (2011). Microwave-assisted synthesis of metal-organic frameworks. *Dalton Transactions*, 40(2), 321-330.
- (107) Kaljurand, I., Lilleorg, R., Murumaa, A., Mishima, M., Burk, P., Koppel, I., ... & Leito, I. (2013). The basicity of substituted N, N-dimethylanilines in solution and in the gas phase. *Journal of Physical Organic Chemistry*, 26(2), 171-181.
- (108) Banerjee, D., Finkelstein, J., Smirnov, A., Forster, P. M., Borkowski, L. A., Teat, S. J., & Parise, J. B. (2011). Synthesis and structural characterization of magnesium-based coordination networks in different solvents. *Crystal growth & design*, 11(6), 2572-2579.
- (109) Yakovenko, A. A., Wei, Z., Wriedt, M., Li, J. R., Halder, G. J., & Zhou, H. C. (2014). Study of guest molecules in metal-organic frameworks by powder X-ray diffraction: analysis of difference envelope density. *Crystal growth & design*, 14(11), 5397-5407.
- (110) Seetharaj, R., Vandana, P. V., Arya, P., & Mathew, S. (2019). Dependence of solvents, pH, molar ratio and temperature in tuning metal organic framework architecture. *Arabian journal of chemistry*, 12(3), 295-315.
- (111) Wang, F. K., Yang, S. Y., Huang, R. B., Zheng, L. S., & Batten, S. R. (2008). Control of the topologies and packing modes of three 2D coordination polymers through variation of the solvent ratio of a binary solvent mixture. *CrystEngComm*, 10(9), 1211-1215.
- (112) Yuan, F., Xie, J., Hu, H. M., Yuan, C. M., Xu, B., Yang, M. L., ... & Xue, G. L. (2013). Effect of pH/metal ion on the structure of metal-organic frameworks based on novel bifunctionalized ligand 4'-carboxy-4, 2': 6', 4''-terpyridine. *CrystEngComm*, 15(7), 1460-1467.
- (113) Luo, L., Lv, G. C., Wang, P., Liu, Q., Chen, K., & Sun, W. Y. (2013). pH-Dependent cobalt (ii) frameworks with mixed 3, 3', 5, 5'-tetra (1 H-imidazol-1-yl)-1, 1'-biphenyl and 1, 3, 5-benzenetricarboxylate ligands: synthesis, structure and sorption property. *CrystEngComm*, 15(45), 9537-9543.
- (114) Growing Quality Crystals – MIT (2021). Chemistry. <https://chemistry.mit.edu/facilities-and-centers/x-ray-diffraction-facility/growing-quality-crystals/>.
- (115) Pascual, C. D., & Subra-Paternault, P. (2015). *Supercritical Fluid Nanotechnology: Advances and Applications in Composites and Hybrid Nanomaterials*. CRC Press.
- (116) Mondloch, J. E., Karagiari, O., Farha, O. K., & Hupp, J. T. (2013). Activation of metal-organic framework materials. *CrystEngComm*, 15(45), 9258-9264.
- (117) Anastas, P. T., & Warner, J. C. (1998). *Principles of green chemistry*. *Green chemistry: Theory and practice*, 29.
- (118) López-Periágo, A., Vallcorba, O., Frontera, C., Domingo, C., & Ayllón, J. A. (2015). Exploring a novel preparation method of 1D metal organic frameworks based on supercritical CO₂. *Dalton Transactions*, 44(16), 7548-7553.
- (119) López-Domínguez, P., López-Periágo, A. M., Fernández-Porras, F. J., Fraile, J., Tobias, G., & Domingo, C. (2017). Supercritical CO₂ for the synthesis of nanometric ZIF-8 and loading with hyperbranched aminopolymers. Applications in CO₂ capture. *Journal of CO₂ Utilization*, 18, 147-155.
- (120) López-Periágo, A. M., Portolés-Gil, N., Lopez-Dominguez, P., Fraile, J., Saurina, J., Aliaga-Alcalde, N., ... & Domingo, C. (2017). Metal-organic frameworks precipitated by reactive crystallization in supercritical CO₂. *Crystal Growth & Design*, 17(5), 2864-2872.
- (121) López-Periágo, A., López-Domínguez, P., Barrio, J. P., Tobias, G., & Domingo, C. (2016). Binary supercritical CO₂ solvent mixtures for the synthesis of 3D metal-organic frameworks. *Microporous and Mesoporous Materials*, 234, 155-161.
- (122) Portolés-Gil, N., Gowing, S., Vallcorba, O., Domingo, C., López-Periágo, A. M., & Ayllón, J. A. (2018). Supercritical CO₂ utilization for the crystallization of 2D metal-organic frameworks using tert-butylpyridine additive. *Journal of CO₂ Utilization*, 24, 444-453.

- (123) Dapaah, M. F., & Liu, B. (2020). Recent Advances of Supercritical CO₂ in Green Synthesis and Activation of Metal–Organic Frameworks. *Journal of Inorganic and Organometallic Polymers and Materials*, 30(3), 581-595.
- (124) Mueller, U., Puetter, H., Hesse, M., & Wessel, H. (2007). WO 2005/049892, 2005. BASF Aktiengesellschaft.
- (125) Friščić, T. (2010). New opportunities for materials synthesis using mechanochemistry. *Journal of Materials Chemistry*, 20(36), 7599-7605.
- (126) Mason, T. J., & Peters, D. (2002). *Practical sonochemistry: Power ultrasound uses and applications*. Woodhead Publishing.
- (127) Rafiei-Sarmazdeh, Z., Zahedi-Dizaji, S. M., & Kang, A. K. (2019). Two-Dimensional Nanomaterials. In *Nanostructures*. IntechOpen.
- (128) Yang, F., Song, P., Ruan, M., & Xu, W. (2019). Recent progress in two-dimensional nanomaterials: Synthesis, engineering, and applications. *FlatChem*, 100133.
- (129) Zhao, M., Huang, Y., Peng, Y., Huang, Z., Ma, Q., & Zhang, H. (2018). Two-dimensional metal–organic framework nanosheets: synthesis and applications. *Chemical Society Reviews*, 47(16), 6267-6295.
- (130) Liao, P. Q., Huang, N. Y., Zhang, W. X., Zhang, J. P., & Chen, X. M. (2017). Controlling guest conformation for efficient purification of butadiene. *Science*, 356(6343), 1193-1196.
- (131) Kambe, T., Sakamoto, R., Hoshiko, K., Takada, K., Miyachi, M., Ryu, J. H., ... & Nishihara, H. (2013). π -Conjugated nickel bis (dithiolene) complex nanosheet. *Journal of the American Chemical Society*, 135(7), 2462-2465.
- (132) Wang, Y., Zhao, M., Ping, J., Chen, B., Cao, X., Huang, Y., ... & Zhang, H. (2016). Bioinspired design of ultrathin 2D bimetallic metal–organic-framework nanosheets used as biomimetic enzymes. *Advanced Materials*, 28(21), 4149-4155.
- (133) Duan, J., Li, Y., Pan, Y., Behera, N., & Jin, W. (2019). Metal-organic framework nanosheets: An emerging family of multifunctional 2D materials. *Coordination Chemistry Reviews*, 395, 25-45.
- (134) Tran, M., Kline, K., Qin, Y., Shen, Y., Green, M. D., & Tongay, S. (2019). 2D coordination polymers: Design guidelines and materials perspective. *Applied Physics Reviews*, 6(4), 041311.
- (135) Coleman, J. N., Lotya, M., O'Neill, A., Bergin, S. D., King, P. J., Khan, U., ... & Shvets, I. V. (2011). Two-dimensional nanosheets produced by liquid exfoliation of layered materials. *Science*, 331(6017), 568-571.
- (136) Lee, J., Farha, O. K., Roberts, J., Scheidt, K. A., Nguyen, S. T., & Hupp, J. T. (2009). Metal–organic framework materials as catalysts. *Chemical Society Reviews*, 38(5), 1450-1459.
- (137) Meng X, Wei MJ, Wang HN, Zang HY, Zhou ZY (2018) Multifunctional luminescent Zn(II)-based metal–organic framework for high proton-conductivity and detection of Cr³⁺ ions in the presence of mixed metal ions. *Dalton Trans* 47:1383–1387
- (138) Deng, X., Hu, J. Y., Luo, J., Liao, W. M., & He, J. (2020). Conductive Metal–Organic Frameworks: Mechanisms, Design Strategies and Recent Advances. *Topics in Current Chemistry*, 378(2), 1-50.
- (139) Allendorf, M. D., Bauer, C. A., Bhakta, R. K., & Houk, R. J. T. (2009). Luminescent metal–organic frameworks. *Chemical Society Reviews*, 38(5), 1330-1352.
- (140) Serre, C., Millange, F., Thouvenot, C., Gardant, N., Pellé, F., & Férey, G. (2004). Synthesis, characterisation and luminescent properties of a new three-dimensional lanthanide trimesate: M ((C₆H₃)(CO₂)₃)(M= Y, Ln) or MIL-78. *Journal of Materials Chemistry*, 14(10), 1540-1543.
- (141) McKinlay, A. C., Morris, R. E., Horcajada, P., Férey, G., Gref, R., Couvreur, P., & Serre, C. (2010). BioMOFs: metal–organic frameworks for biological and medical applications. *Angewandte Chemie International Edition*, 49(36), 6260-6266.
- (142) Wang, P., Jin, Z., Song, G., & Zhang, X. B. (2021). Recent progress and strategies for precise framework structure-enabled drug delivery systems. *Materials Today Sustainability*, 100065.
- (143) Li, F., Li, B., Wang, C., Zeng, Y., Liu, J., Gu, C. Y., ... & Mei, L. (2016). Encapsulation of pharmaceutical ingredient linker in metal–organic framework: combined experimental and theoretical insight into the drug delivery. *RSC advances*, 6(53), 47959-47965.
- (144) Miller, S. R., Heurtaux, D., Baati, T., Horcajada, P., Grenèche, J. M., & Serre, C. (2010). Biodegradable therapeutic MOFs for the delivery of bioactive molecules. *Chemical Communications*, 46(25), 4526-4528.
- (145) Rojas, S., Devic, T., & Horcajada, P. (2017). Metal organic frameworks based on bioactive components. *Journal of Materials Chemistry B*, 5(14), 2560-2573.

- (146) Emam, H. E., Darwesh, O. M., & Abdelhameed, R. M. (2018). In-growth metal organic framework/synthetic hybrids as antimicrobial fabrics and its toxicity. *Colloids and Surfaces B: Biointerfaces*, 165, 219-228.
- (147) Chen, K., & Wu, C. D. (2019). Designed fabrication of biomimetic metal–organic frameworks for catalytic applications. *Coordination Chemistry Reviews*, 378, 445-465.
- (148) Shen, X., & Yan, B. (2015). Photofunctional hybrids of lanthanide functionalized bio-MOF-1 for fluorescence tuning and sensing. *Journal of colloid and interface science*, 451, 63-68.
- (149) Liang, Y. Y., Luo, L. J., Li, Y., Ling, B. K., Chen, B. W., Wang, X. W., & Luan, T. G. (2019). A Luminescent Probe for Highly Selective Cu²⁺ Sensing Using a Lanthanide-Doped Metal Organic Framework with Large Pores. *European Journal of Inorganic Chemistry*, 2019(2), 206-211.
- (150) Xu, R., Wang, Y., Duan, X., Lu, K., Micheroni, D., Hu, A., & Lin, W. (2016). Nanoscale metal–organic frameworks for ratiometric oxygen sensing in live cells. *Journal of the American Chemical Society*, 138(7), 2158-2161.
- (151) McNaught, A. D. (1997). *Compendium of chemical terminology* (Vol. 1669). Oxford: Blackwell Science.
- (152) Jensen, W. B. (2008). The origin of the polymer concept. *Journal of Chemical Education*, 85(5), 624.
- (153) Feldman, D., & Barbalata, A. (1996). *Synthetic polymers: technology, properties, applications*. Springer Science & Business Media.
- (154) Verdu, J., & Fayolle, B. (2011). *Organic polymers*.
- (155) Odian, G. (2004). *Principles of polymerization*. John Wiley & Sons.
- (156) Kulkarni Vishakha, S., Butte Kishor, D., & Rathod Sudha, S. (2012). Natural polymers—A comprehensive review. *International journal of research in pharmaceutical and biomedical sciences*, 3(4), 1597-1613
- (157) Spsychalska, K., Zając, D., Baluta, S., Halicka, K., & Cabaj, J. (2020). Functional polymers structures for (Bio) sensing application—A review. *Polymers*, 12(5), 1154.
- (158) Vilar, G., Tulla-Puche, J., & Albericio, F. (2012). Polymers and drug delivery systems. *Current drug delivery*, 9(4), 367-394.
- (159) Silva, S. S., Mano, J. F., & Reis, R. L. (2010). Potential applications of natural origin polymer-based systems in soft tissue regeneration. *Critical reviews in biotechnology*, 30(3), 200-221.
- (160) Shirakawa, H., Louis, E. J., MacDiarmid, A. G., Chiang, C. K., & Heeger, A. J. (1977). Synthesis of electrically conducting organic polymers: halogen derivatives of polyacetylene,(CH) x. *Journal of the Chemical Society, Chemical Communications*, (16), 578-580.
- (161) Das, T. K., & Prusty, S. (2012). Review on conducting polymers and their applications. *Polymer-plastics technology and engineering*, 51(14), 1487-1500.
- (162) Feng, X., Ding, X., & Jiang, D. (2012). Covalent organic frameworks. *Chemical Society Reviews*, 41(18), 6010-6022.
- (163) Baumann, W., Rodrigues, S. V., & Viana, L. M. (2000). Pigments and their solubility in and extractability by supercritical CO₂-i: The case of curcumin. *Brazilian Journal of Chemical Engineering*, 17(3), 323-328.
- (164) Guo, C., Yin, J., & Chen, D. (2018). Co-encapsulation of curcumin and resveratrol into novel nutraceutical hyalurosomes nano-food delivery system based on oligo-hyaluronic acid-curcumin polymer. *Carbohydrate polymers*, 181, 1033-1037.
- (165) Manju, S., & Sreenivasan, K. (2012). Gold nanoparticles generated and stabilized by water soluble curcumin–polymer conjugate: blood compatibility evaluation and targeted drug delivery onto cancer cells. *Journal of colloid and interface science*, 368(1), 144-151.
- (166) O'Toole, M. G., Soucy, P. A., Chauhan, R., Raju, M. V. R., Patel, D. N., Nunn, B. M., ... & Gobin, A. S. (2016). Release-modulated antioxidant activity of a composite curcumin-chitosan polymer. *Biomacromolecules*, 17(4), 1253-1260.
- (167) Xu, X., Lü, S., Wu, C., Wang, Z., Feng, C., Wen, N., ... & Ren, C. (2018). Curcumin polymer coated, self-fluorescent and stimuli-responsive multifunctional mesoporous silica nanoparticles for drug delivery. *Microporous and Mesoporous Materials*, 271, 234-242.
- (168) Tang, H., Murphy, C. J., Zhang, B., Shen, Y., Van Kirk, E. A., Murdoch, W. J., & Radosz, M. (2010). Curcumin polymers as anticancer conjugates. *Biomaterials*, 31(27), 7139-7149.
- (169) Liu, W., Wu, S., Su, Q., Guo, B., Ju, P., Li, G., & Wu, Q. (2019). Difluoroborate-based conjugated organic polymer: a high-performance heterogeneous photocatalyst for oxidative coupling reactions. *Journal of Materials Science*, 54(2), 1205-12.



Objectives

Objectives

This doctoral thesis focuses in the synthesis, characterization and further used of molecules that belong to the curcuminoid family (CCMoid). In general, CCMoids present a β -diketone moiety in the central position of the molecule and, additional functional groups in the lateral sides, some of the latter display the ability of forming more complex structures. In this doctoral thesis we present CCMoids as molecular units that contain three reactive points and examine their capabilities coordinating with metal centres as well as reacting with additional organic molecules. Hence, the principal objective of this doctoral thesis was to explore the use of CCMoids in the formation of extended structures, probing their ability to act as building blocks for the creation of new coordination and organic polymers (CPs and OPs), respectively. For that, it became necessary to achieve a series of objectives:

- The first goal involves the synthesis of a family of CCMoids used in a second step as monomeric units. The initial part includes natural and synthetic CCMoids, that could be also described as known CCMoids and new ones, the latter not previously published. Moreover, our purpose included the thorough analysis of the physicochemical properties of these CCMoids, to suggest possible applications and to direct our synthetic efforts.
- The consecutive objective of this doctoral thesis involves the creation of extended structures (coordination polymers, CPs) exploring, in a first step, the formation of coordination bonds between metal centres and the β -diketone moiety and phenol substituents of a natural CCMoid, bisdemethoxycurcumin, BDMC. The assistance of co-linkers is also included in the study. This way, we analyse changes in the dimensionality of the CPs using neutral bipyridine linkers.
- In parallel with the CP studies performed with BDMC an artificial CCMoid, so-called 3pyCCMoid, is also examined. This molecule was initially used in a previous thesis work, however, here the formation of new CPs is explored by modifying the synthetic approach and the exfoliation of a previous synthesized 2D system based on the same CCMoid tested.
- Following our aim of creating extended structures, and taking advantage of the molecular design, this doctoral thesis examines the formation of organic polymers (OPs) based on CCMoids using two basic routes: the first involves the use of a new CCMoid, containing boronic acids that later could react with diol molecules, and the second path includes the creation “in situ” of CCMoid-like extended structures.



**Methodology
and
characterization
techniques**

1. Equipment and methodology

1.1. Synthetic methods

This doctoral thesis encompasses the synthesis of a variety of products, from small organic molecules to extended materials. As a consequence, a number of different methodologies have been applied to obtain the final systems. In general, organic small molecules are obtained using traditional synthetic procedures and the specific conditions for each one are given in chapter I. However, some of the CPs and OPs, especially the ones where crystallinity was required, are synthesized with the use of specific approaches. In this section, these methodologies are explained.

1.1.1. Solvothermal methodology

The solvothermal synthesis of the different compounds, outlined in figure 1, is carried out at high temperature using an oven as the heating source. The reagents and solvents are placed in a Pyrex vial with hermetic closure and sonicated during few seconds. Once the complete solubilisation of the reagents is achieved, the vials are placed in the oven for a fixed period of time, usually 72 h. After that time, some crystals placed on the walls and at the bottom of the vial are observed. These crystals are recovered directly from the mother solution and washed with fresh solvent.

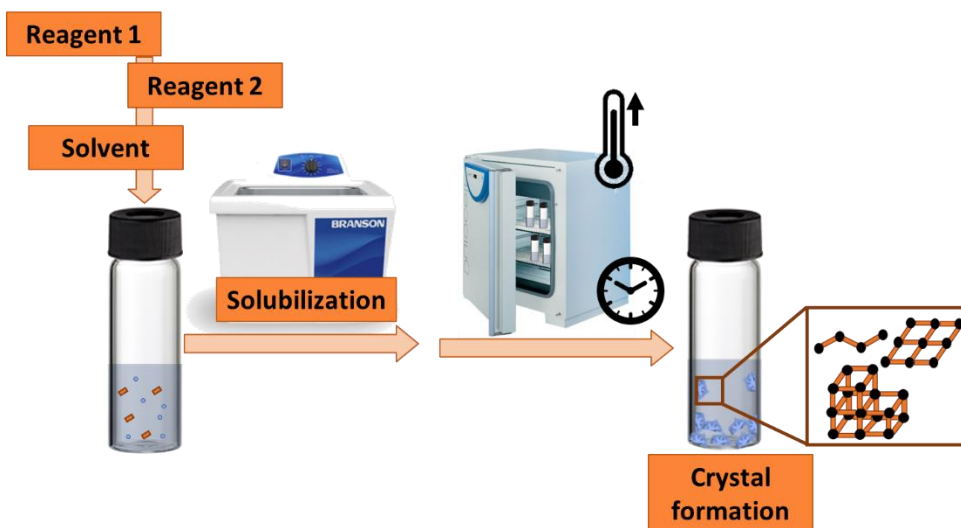


Figure 1. Schematic representations of the solvothermal methodology.

This methodology was used for the synthesis of CPs in chapters II and III, as well as for the formation of some boronic esters in chapter IV. The oven used is an Ecocell comfort.

1.1.2. Layering methodology

In this methodology, depicted in figure 2, two miscible solvents were used, and each reagent was solved in one of them. The denser solution was placed in the bottom part of a long vial and few mL of the less dense solvent were carefully added on the top, forming two different layers. Then, the second dissolution was added in the same way and the vial is kept unaltered the necessary time. The slow diffusion of the solvents allows a gradual mixing of the reagents appearing crystals in the mixture that were cleaned with fresh solvent. The intermedia layer of net solvent makes the mixing of the reagent slower assisting the formation of a clearer boundary.

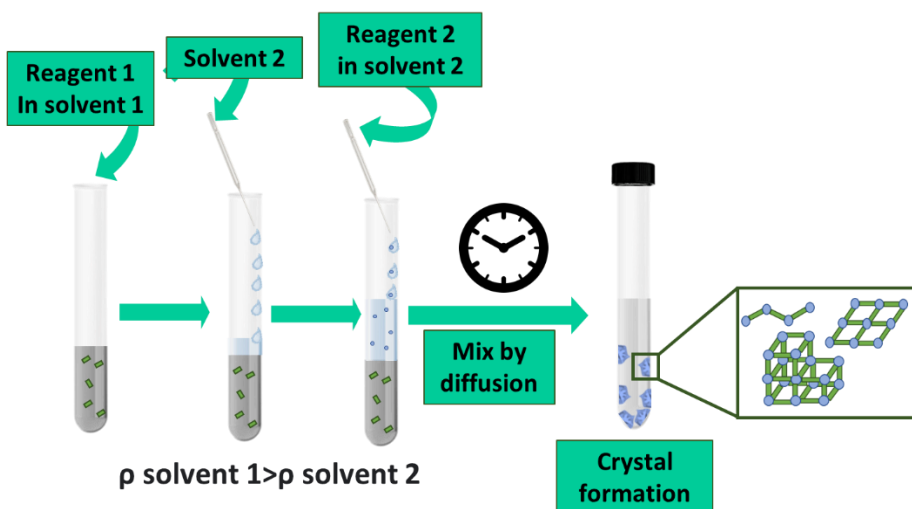


Figure 2. Schematic representations of the layering methodology followed in this doctoral thesis.

This methodology was used to crystallize the 3D CP described in chapter III.

1.1.3. ScCO₂ methodology

ScCO₂ synthesis was carried out in a high-pressure equipment involving a CO₂ bottle, cooling system, pump, pressure and temperature controllers and a stainless-steel reactor of 100 mL volume (figure 3). In a typical experiment, a Pyrex vial holding the solid reagents and a stirring bar and covered with a filter paper that allows the free entrance of the CO₂ but not the exit of the solids (zoom in figure 3), was first prepared. In some reactions, the addition of a small amount of EtOH as a co-solvent was necessary due to the low solubility of some of the reagent in the supercritical fluid. This vial was placed into the reactor and all the system was sealed. Then, the autoclave was filled with CO₂, heated until the desired temperature (40-60 °C) and pressurized (150-200 bar), thus reaching supercritical conditions. The reaction was kept this way and under stirring (150

rpm) during 24-72 h. After that, the CO₂ was evacuated in gas state by a slow depressurization, and the reactor was cooled down to room temperature, obtaining the product inside of the vial as a completely dry solid.

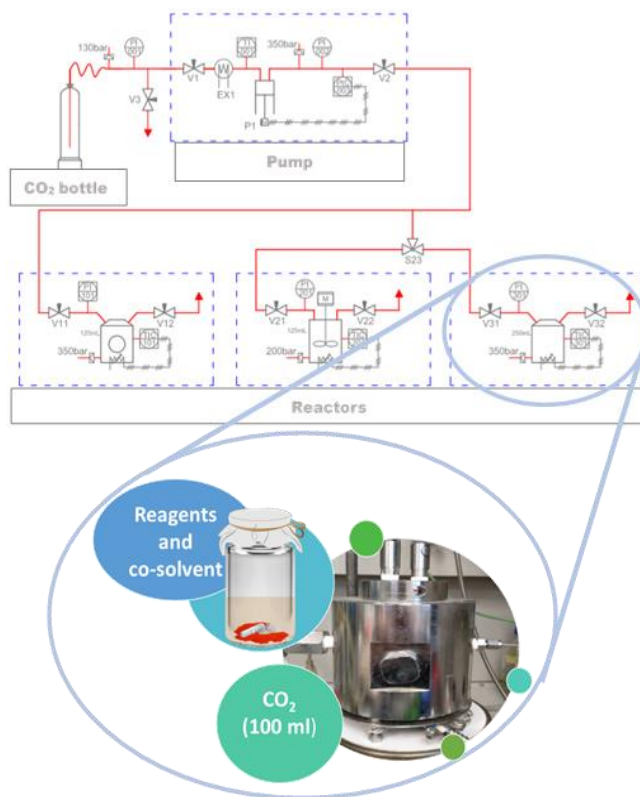


Figure 3. Schematic representation of the scCO₂ equipment, reactor, and sample montage.

The supercritical methodology has previously been used for the synthesis of CPs in the group,^{1,2} including one CP in which CCM was the organic linker³. In this doctoral thesis, the method was used with the same purpose and the results are presented in chapters II and III. Moreover, it was also used for the drying of some organic molecules to obtain the non-solvated forms (chapter I).

1.2. Liquid-assisted exfoliation

In this doctoral thesis, a *top-down* method was used to obtain nanosheets, starting with crystals of a bulk 2D material (Chapter III). Due to the small crystal size of this product, a liquid-assisted method was chosen, using ultrasounds as the mechanical force in the exfoliation process (figure 4). In a typical experiment, the 2D material and the solvent were added to a small vial and sonicated in an ultrasonic bath during 1h. After that, the vials were placed on a flat surface and left unaltered until the precipitation of the largest nanosheets (6h). Small nanosheets remained in the supernatant, as was checked by Tyndall effect. A drop of the supernatant, from the top of solution vial, was deposited on a TEM grid or a SiO₂ surface for its characterization.

The ultrasonic bath used was an ultrasonic Branson M3800-E.

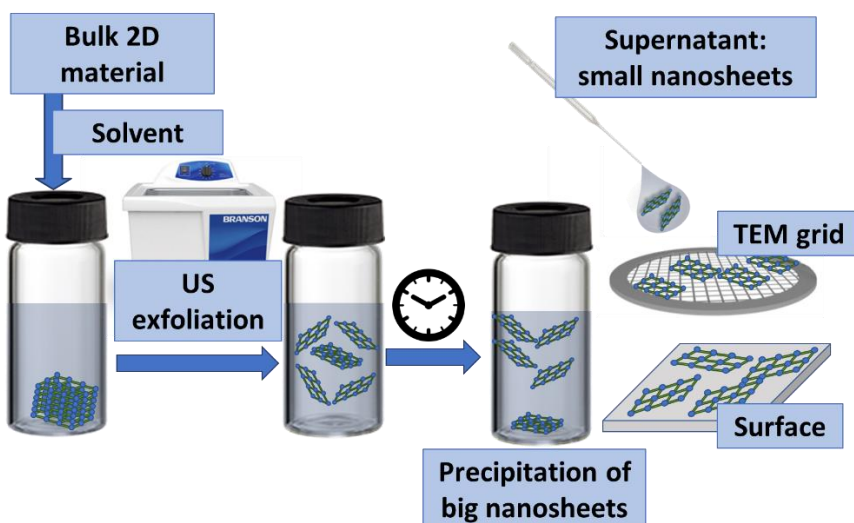


Figure 4. Schematic representations of the ultrasonic exfoliation methodology.

2. Characterization techniques.

The diversity of products obtained in this doctoral thesis implies the need of a variety of characterization techniques to attain the understanding of their molecular and supramolecular structure and related properties. In that way, this section aims to make a brief explanation of the techniques used, divided according to the information that we can extract from each of them.

2.1. Composition and structural information

First of all, new products must be characterized in regard of the composition and structure to determine if they are the desired ones. For that, it is mandatory to determine the composition of the sample and the way the atoms/molecules are interacting among them. For soluble organic compounds, the most used technique to ascertain product composition is nuclear magnetic resonance (NMR), which gives information on the number of different species, and therefore purity, and their local chemical environment. Mass spectroscopy (MS), elemental analysis (EA) and infrared spectroscopy (IR) are complementary techniques to extract information about the mass of the structural unit and its fragments, the molecular formula and functional groups, respectively. However, these techniques cannot give information of the molecular conformation in the solid state neither the atoms dispositions, being this aspect especially important for extended structures, much of them not soluble in organic solvents. Single crystal X-ray diffraction (XRD) is the most used technique to elucidate the structure of the new compounds; however, difficulties found sometimes to obtain high quality crystals reduce the applicability of this technique. In these cases, other solid state technique, such as powder XRD and solid state NMR, can provide additional clues on the structural composition. Following, the mentioned techniques are described briefly.

2.1.1. Nuclear magnetic resonance (NMR)

With NMR, signals from nuclei with magnetic moment different to zero are obtained, e.g., for ^1H , ^{13}C , ^{31}P , ^{19}F , ^{16}O , ^{11}B and ^{15}N , which make it a perfect technique to characterize organic samples. During measurement, the spin of these nuclei is aligned with an external magnetic field, some of them in the same direction and another in the opposite, producing a difference in energy between them that depends on the applied field. The frequency necessary for all the nuclei to go to the most energetic state (resonance) depends on the environment of the nucleus and therefore can be used to determine its nature. In this way, in a typical experiment, a constant frequency is applied, and the magnetic field is varied, detecting the moment in which this energetic jump occurs.⁴ In general, the samples are measured after solubilisation in a deuterated solvent, but it is also possible their measure as in solids.

In this doctoral thesis, solution ^1H and ^{13}C NMR techniques were applied as routine measurements to ascertain the molecular structure, composition and purity of soluble reagents and products. The spectra of all the synthesized CCMoids and non-commercial reagents are shown in chapter I. As well, the spectra of some soluble extended products are also shown in chapter IV.

Solid state ^{13}C NMR was utilised to prove different conformations, of some CCMoids, in the solid state (chapter I) and to delineate potential structures for some new CPs that could not be elucidated by other methods (chapter II), putting in value the great utility of this technique. The studies of solid NMR are focussed in the ^{13}C nucleus due to their

high abundance in all the studied molecules. Moreover, ^{13}C recorded spectra are, in general, of higher quality than the ones of NMR of protons. The ^{13}C NMR in solid state of CCM has been deeply studied, including theoretical calculations to facilitate the interpretation of the spectrum.⁵ For CCMoids, it has been demonstrated that changes in the solvent affect the molecular structure by establishing strong interactions, especially with polar solvents that interact with the proton of the enol form. First of all, the CCMoid/solvent complexes established with different solvents can be observed by changes in the solution colour. Moreover, due to the relative flexibility of CCMoid molecules, they can adopt different conformations that can be also affected by the presence of solvents. Solid state ^{13}C NMR can give much more information than the conformation of the molecule, since it is also sensible to the chemical environment of each atom.⁶ For this reason, better results are obtained for materials with a certain order in the structure, e.g., crystalline samples, than for amorphous powders. For the latter, the chemical environment of each atom is different, thus appearing very broad bands in the ^{13}C NMR spectra.⁷

Currently, solid state ^{13}C NMR is gaining attention as one of the best techniques for the characterization of highly ordered insoluble structures, such as MOFs and COFs, specially to analyse small changes in their structures.^{8,9} The establishment of solid state ^{13}C NMR as a routine technique for the characterization of this type of solids has been possible by the development of new data acquisition modes that greatly increase the quality of the spectra facilitating their interpretation. One of these approaches is to use cross polarization (CP) sequences to increase the intensity of the signals and spinning samples at the “magic angle” (MAS, magic angle spinning) to obtain sharper peaks, developing the solid-state CP MAS NMR technique.³

In this doctoral thesis, solution ^1H and ^{13}C NMR measurements were carried out in a spectrometer Bruker Avance-III of 400 MHz (9.4 T) and in a Bruker Avance DPX of 360 MHz (8.4 T). ^{13}C CPMAS NMR data was acquired in a Bruker Avance III (9.4 T) equipped with a double channel 4.0 mm MAS probe. Sample spinning was set to 10 kHz in all the experiments. Pure adamantane was used as external chemical shift reference (CH signal at 29.5 ppm).

2.1.2. Mass spectrometry (MS)

Mass spectrometry (MS) is a technique used to determine the mass to charge ratio (m/z) of the ions in vapour phase. First, it is necessary the ionization of the sample to obtain the charged molecule or charged fragments of it. In a matrix-assisted laser desorption/ionization (MALDI) measurement, the ionization is achieved by a laser pulse. In many cases, the sample is mixed with a matrix helping in the ionization and reducing the breakdown. After the ionization, the fragments are analysed in a time of fly (TOF) analyser, in which all the ions are accelerated with the same electric field and the time that they need to arrive to the detector, which is based on their m/z , is measured.¹⁰

In this doctoral thesis the mass spectrum of all the CCMoids (chapter I) was measured confirming the precipitation of the desired product in each case. The equipment used for this was a MALDI-TOF/TOF Bruker ultrafleXtreme with a laser power between 50-70 % and without the necessity of adding any matrix.

2.1.3. Elemental analysis (EA)

The composition of the samples can be determined through elemental analysis. Essentially, this technique is applied to obtain the weight percentages of C, N and H, although other elements, such as halogen atoms or S, can be also analysed. The analysis is performed by the combustion of the sample in the presence of oxygen and analysing the gas products (CO₂, H₂O, NO_x...).

In this doctoral thesis, EA measurements were performed in a Thermo Carlo Erba Flash 2000 apparatus. Experimental values measured for the CPs (chapters II and III) are compared with the calculated from the formula of the compounds. Moreover, when the structure of the compound is unknown, the elemental analysis can be taken as a guide to suggest a valid formula.

2.1.4. Fourier transformed infrared spectroscopy (FTIR)-attenuated total reflectance (ATR)

When a sample is irradiated with infrared light, part of the light is absorbed by the sample producing the vibration of specific bonds. The energy necessary for these vibrations is related with the type of bond and the atoms implicated- Hence, IR spectroscopy gives information about the functional groups present in the molecule. Nowadays, measurements are performed with fourier transform (FT) spectrophotometers, because of the enhance resolution and sensitivity obtained with them. Traditionally, the sample was mixed with dry KBr in a mortar and a pellet was made in a press. Regarding the measurement, the light goes through this ultrathin pellet and the not absorbed (transmitted) arrives to the detector.¹¹

Modern instruments include the ATR accessory due to the simplicity of sample preparation. In ATR, a few mg of the solid sample or a drop of the liquid species is placed on the surface of a zinc selenide (ZnSe), thallium bromide iodide (KRS-5) or Ge crystal, respectively, and hand-pressed against it. Crystals, in general, have a high index of refraction, so that when the IR radiation hits at the proper angle there is an effect called total internal reflection. This phenomenon produces in the boundary of the crystal and evanescence wave that interacts with the sample that is placed there. The attenuation of the radiation at specific wavelengths produced by the absorption of the sample is recorded by a detector, thus generating the spectrum of the compound. As the solid is placed directly on a crystal, a minimum or null sample preparation is necessary and the product can be recovered after the analysis, contrary to the classical method of FTIR. The principal drawback of the ATR-FTIR technique is the low penetration of the radiation at

short wavelengths, which discourages its use when the area of interest is below 600 cm^{-1} .^{1, 12}

In this doctoral thesis the IR spectrum was recorded for all the products, both CCMoids and extended structures. The ATR-FTIR spectra of the samples prepared were obtained in a FT-IR JASCO 4700LE in the range between 600 and 4000 cm^{-1} . For samples in which it was necessary to obtain data below 600 cm^{-1} , pellets with KBr were prepared and measured using the FTIR mode.

2.1.5. X-ray diffraction (XRD): powder and single-crystal. Synchrotron source

The X-ray diffraction is based on the capacity of X-rays of penetrating the matter and their dispersion produced when the incident beam collides with an atom. A single atom scatters the radiation in all directions, but when a certain number of atoms are ordered periodically, as in a crystalline compound, most scattered rays are eliminated by destructive interferences. In that way, diffraction is only produced in certain directions, related with the disposition of the atoms, and predicted by the Bragg's law.¹¹ Depending basically on the type of sample, two techniques are used, single-crystal XRD and powder XRD.¹¹

In single crystals, the X-ray radiation impacts the sample and when the Bragg's law is satisfied a constructive diffraction is produced and detected. Measuring the angles and intensities of this diffracted beams, the electron density of the structure can be determined, and thereby the atoms and the position of them in the structure. In that way, the XRD of a crystal can give the structure of the measured compound. The principal drawback of this technique is the experimental difficulty to obtain single crystals of many materials, which should have minimum sizes between 50 and $250\text{ }\mu\text{m}$. The use of synchrotron radiation as the source for X-ray allows to work with small crystals (few micrometres), because the incident beam is much smaller than in traditional sources. High collimation synchrotron radiation has other advantages that generally improves the measurement of any technique that requires radiation. These improvements are due to high brightness, high intensity, high level of polarization, low emittance, large tunability in wavelength by monochromatization and short pulse of the radiation. This last property, makes possible doing ultra-fast studies in minutes, which in routine instruments would take hours.¹³

In powder samples, the solid is irradiated and the angle of incidence of the beam (2θ) is modified continuously. The result is a series of peaks appearing at specific 2θ angles, which satisfy the Bragg equation. In amorphous samples, as there is no order in the atoms, destructive interference do not occur. Powder XRD can be used for determining the crystallinity of a solid and, by comparison with published files, the structure of the solid. It is also used for the determination of the purity and the identification of crystalline impurities denoted by extra peaks in the spectrum. This technique allows the

characterization of bulk material, but a high quantity of sample is necessary and the information about the structure, in general, is limited comparing with the achieved by single-crystal XRD.¹⁴

In this doctoral thesis, all the crystalline materials were routinely characterized by powder XRD on a Siemens D-5000 diffractometer with Cu K α radiation. For new compounds, in the cases where a single-crystal with the necessary quality and size could be obtained, structural data were collected on a Bruker APEXII Qazar CCD diffractometer equipped with a Mo-k wavelength using phi and omega scans at 100 K. For small single crystals, it becomes necessary the use of synchrotron facilities at the ALBA synchrotron collecting data at the XALOC beamline K with a 0.72931 Å wavelength using the Dectris Pilatus 6M detector at 100 K. The phi scan was repeated at three different κ angles (0, 45 and 90°), and merged afterwards to increase the completeness and redundancy, when possible.

Regardless of data source, the structures were solved by Dr. E. C. Sañudo at the University of Barcelona, using intrinsic phasing methods (SHELXT) and refined on F2 (SHELXL). Hydrogen atoms were included on calculated positions, riding on their carrier atoms. Data for the rest of characterized species were indexed, integrated and scaled using the XDS software. The corresponding CIF files of all the resolved structures have been deposited in the Cambridge Crystallographic Data Centre.

2.2. Morphology

The study of samples morphology, especially for the crystalline products, can give information about the crystal growth mechanism and, thus, in the pathway to achieve better crystals for structure determination. All the synthesized extended crystals have been studied by optical microscope and scanning electron microscope (SEM), and results are shown in chapters II and III. Moreover, nanosheets obtained of a 2D compound (chapter II) were characterized by transmission electronic microscopy (TEM) and atomic force microscopy (AFM).

2.2.1. Scanning electron microscopy (SEM)

SEM uses the interaction between electrons and matter to form images. The equipment uses an electron beam, instead of a light beam used in optical microscopes, being able to see much smaller structures.¹⁵ In this technique, the electrons are accelerated and hit the sample penetrating a few microns and producing secondary electrons, backscattered electrons, and characteristic X-rays that are recorded by different detectors. This electron bombardment can damage the samples, specially the not conducting ones, with higher content of organic compounds. For this reason, it is important to control the voltage used for the electron acceleration, which should be lower for non-conducting samples. Other option is to cover the sample with a thin layer of a metal, normally gold or platinum. This last approach allows the use of high voltages with organic samples while

reducing damage and obtaining a better resolution. In SEM, the morphology of the sample is observed through 3D images, then, allowing the analysis of textures and volumes.²⁰

2.3. Characterization techniques for nanosheets

Some additional techniques have been used for the analysis of 2D materials.

2.3.1. Energy Dispersive X-rays Spectroscopy (EDS)

As it was previously mentioned in the description of the SEM equipment, X-rays are also emitted by the sample when it interacts with the accelerated electrons. This radiation can be detected and used for determining the composition of the sample. This technique is called EDS and, nowadays, is usually coupled to most SEM microscopes.²⁰ The principal advantage is that the composition of the sample can be detected, while the SEM photos are acquired, chosen specific regions based on what the image show. In this doctoral thesis, it was used to determine if the nanosheets, attributed to the compound, have the same composition that the bulk 2D material.

A QUANTA FEI 200 FEG-ESEM was used to obtain the SEM images, while a FEI MAGELLAN 400L XHR was used for SEM/EDS.

2.3.2. Transmission electron microscopy (TEM)

TEM microscope is based in the same principles that SEM, but the detector is placed under the sample and only the electrons that go through it are measured. For this reason, only ultrathin samples (lower than 2000 Å) can be measured.¹⁶ Moreover, TEM can arrive to more magnification than SEM and organic compounds can be analysed with lower damage. However, images are displayed only in 2D, thus, not giving information on the sample texture or volume. Taken all this into account, the TEM technique is appropriate to analysed 2D nanosheets that meet the criteria of thickness.

For the preparation of the sample and in order to analyse the exfoliated 2D compound, a drop of an aqueous dispersion containing the nanosheets was deposited in a TEM grid and the liquid was allowed to evaporate. The TEM grid was covered with a carbon film with holes that allows to hold the sample.

For recording the TEM images a 120 KV JEOL 1210 was used.

2.3.3. Atomic force microscopy (AFM)

AFM does not use lenses or beam irradiation, but its resolution arrives to nanometre fractions. In the topography mode, a sharp conical tip is put in contact with the sample and it is moved scanning the surface of it. The different heights of the sample change the deflection of the cantilever that is connected to the tip, and these changes are plotted in a colour mapping image where each pixel represent a specific position of the sample, being the colour scale related with the different heights.¹⁷ In this doctoral thesis, to analyse the thickness of the layers in the exfoliated 2D material, topographic images of surfaces with nanosheets deposited by drop casting were obtained. The number of layers in the nanosheets can be estimated by knowing the 2D material structure and thus the distance between layers in the bulk material.

Here, for the AFM characterisation a Keysight 5100 AFM was used.

2.4. Optical spectroscopic properties

The optical properties of a material provide important information about its physical properties, such as texture and thickness obtained by electronic (SEM, TEM) and probe (AFM) microscopies. Moreover, valuable information about the electronic properties of a material can be also obtained through the use of optical spectroscopic strategies. It covers UV-Vis absorption and the fluorescence properties.¹⁸

2.4.1. Ultraviolet-visible (UV-Vis) absorption spectroscopy.

With this technique, the electronic transitions produced when light of the UV and visible region interact with the sample are measured. In a typical UV-Vis absorption experiment, the sample is irradiated with light of different wavelength, reaching the detector only the fraction that is not absorbed by the sample. An absorption band is observed at the specific wavelength in which the energy is enough to produce an electronic jump. This is a common technique used to characterized organic molecules, being particularly interesting in the case of CCMoids as they present high UV-Vis absorption due to their conjugated skeletons. In general, absorption spectra are recorded with the sample solubilised in an organic solvent. However, the absorption can be affected by interactions established between the solubilized molecules and the solvent. Then, absorption maxima at different wavelengths are observed in different solvents (solvatochromic species). In this doctoral thesis, CCMoids spectra were measured in different solvents to study the way in which they affect the spectra (chapter I).

The UV-Vis absorption was also measured in solid for the different samples to avoid solvent contribution to the wavelengths maxima. For solid samples, not all the light is transmitted linearly, as it occurs in solution. Depending on the nature of the sample, the light can be partially scattered (diffused transmittance) or reflected (specular reflectance and diffused reflectance), the latter occurring mainly in opaque samples where the light

cannot penetrate. In this case, the integrating sphere accessory must be used, in which a coating of BaSO₄ is used to allow the collection of the transmitted or reflected light concentrating it on the detector. With this methodology, powder samples can be measured.¹⁹ However, the measurement of pristine solids can be problematic in compounds displaying high absorbance, mainly due to problems related to saturation of the detector. To avoid that, a good option is to mix a small quantity of sample with KBr and to prepare a pellet, like it was done in the IR measurements. This procedure was used to prepare for analysis CCMoids pellets involving 0.1 mg of the compound and 100 mg of KBr and measuring it using the integration sphere. The absorption of a compound is specific of it and can be used for their identification and quantification, as well as to detect changes in the structure, such as the coordination mode. Moreover, UV-Vis solid spectroscopy can be used to estimate the bandgap energy from the absorption spectra in semiconductor molecules, such as CCMoids, as the absorption is related with the electronic jumps between HOMO and LUMO, not conditioned by solvent.²⁰ For this calculation, equation 1 is applied:

$$E_{\text{bandgap}} = h \cdot c / \lambda_{\text{onset}} \quad (\text{Equation 1})$$

where h is the Planck constant ($4.136 \cdot 10^{-15}$ eV/s), c is the speed of light ($3 \cdot 10^{17}$ nm/s) and λ_{onset} was obtained graphically from the crossing of the tangents, as it is explained in figure 5.

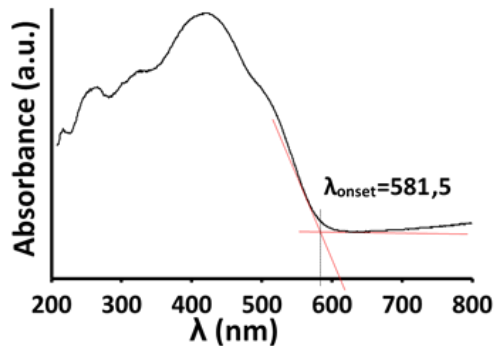


Figure 5. Example of the graphically determination of the λ_{onset} .

The instrument used for the measurement of all the UV-Vis spectra presented in chapter I was a Jasco V-780 UV-Visible/NIR spectrophotometer, with the liquid and the integrating sphere setups.

2.4.2. Fluorescence

Fluorescence is the process where a material absorbs light of high energy (short wavelength) and emits light at a lower energy, usually visible wavelength. After the absorption of light and the subsequent jump of the electrons from the ground state to an excited state, this energy is lost by different pathways. One of these paths is the fluorescence that is the loss of energy by the emission of a photon and that occurs nanoseconds after the excitation. The energy of this photon is lower than the energy absorbed, therefore of higher wavelength than the necessary for the absorption. This is because before this emission some energy is dissipated by internal conversion, e.g., radiationless transition between energy states of the same spin state.²⁰ CCMoids, and especially those that include BF_2 , are fluorophores and due to their conjugated nature, they emit in the visible region, and it is reported that some of them have been used as sensors and for photoelectronic applications.^{21,22}

In this doctoral thesis, a fluorometer Varian Cary Eclipse was used to measure the fluorescence of the different CCMoids (chapter I).

2.5. Electrochemistry

Electrochemistry links the flow of electrons with a chemical change, in other words, the transformation of electric energy in chemical energy.²³ The voltammetry techniques in electrochemistry are based on the intensity of current produced when an applied electric potential is measured. The most common equipment used for measurements is a potentiostat connected to three electrodes that are immersed in a solution of the analyte and the electrolyte in a solvent of high purity (figure 6).²⁴

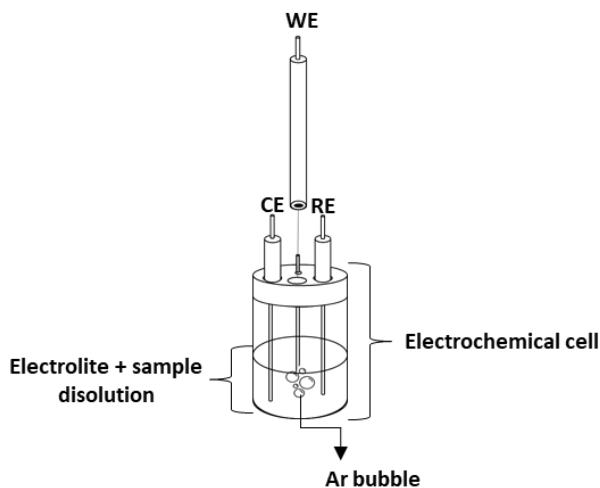


Figure 6. Setup of the electrochemical cell and electrodes used in this doctoral thesis.

Electrodes

The three electrodes are called reference (RE), counter (CE) and working (WE). A known potential is applied in the working electrode as a function of the reference one, producing a current (electron flow) between the WE and CE at the potential where the reduction or the oxidation of the specie of interest is produced. The reference electrode has a well-defined and stable potential, so that the potential of the others can be measured by taking this one as a standard. There are multiple reference electrodes, such as Ag/AgCl, calomel or hydrogen electrode, specially used in aqueous media. In organic solutions is more common the use of an internal reference compound, such as ferrocene, reporting the potentials vs. the couple Fc/Fc⁺, assigning to this redox proces the value of 0 V. The working electrode is commonly made of platinum or glassy carbon and the reference of platinum wire or disk.¹⁶

Electrolyte

During the voltammetry experiments, electron transfer processes are produced and the neutrality is maintained through ion migration in the solution. To reduce the solution resistance, a salt that migrates to balance the charges is added. A much higher concentration of electrolyte than the analyte is necessary to increase the probability of migration for the salt than for the rest of species. Typical salts that can be used are NaClO₄, Bu₂NBF₄ or Bu₄NPF₆ in concentrations of around 0.1 M.¹⁶

Purity, oxygen presence and other considerations

The solvent and the electrolyte must be both of high purity, avoiding the presence of any electroactive specie, and completely dry, since water suffers redox reactions easily. The same occurs with oxygen that must be removed before the process, by bubbling an inert gas such as Ar or N₂, being also recommendable to maintain a low flow of inert gas during measurements. This flow should not disturb the solution and, as well, any vibration or stirring must be avoided. Finally, the electroactive window should be also considered. This is the range of potentials where the experiment can be carried out and depends on the electrolyte, the electrodes and the solvent. It is very important to have this in mind, since the potential necessary for the reduction or oxidation of the specie of interest can be outside of this region and, therefore, not detectable.¹⁶

2.5.1. Cyclic voltammetry (CV)

There are different techniques that use the voltammetric principles. The most common, and the one used in this doctoral thesis is cyclic voltammetry (CV). In CV, the potential is linearly applied in a defined window of values, from an initial potential (E_i) until the first potential limit (E₁) and, then, it comes back until the second limit (E₂) and finishes in E_f. In figure 7, the applied potential vs. time is represented, as well as the resulting

voltammogram (current intensity vs. voltage) in an experiment from positive to negative potentials. At a specific positive potential (E_{pa}) the electroactive specie loses at least an electron (oxidation) generating a peak of anodic current (I_{pa}). The same occurs at negative potentials, in which the specie is reduced gaining electrons at a E_{pc} and generating a cathodic current (I_{pc}).²⁵

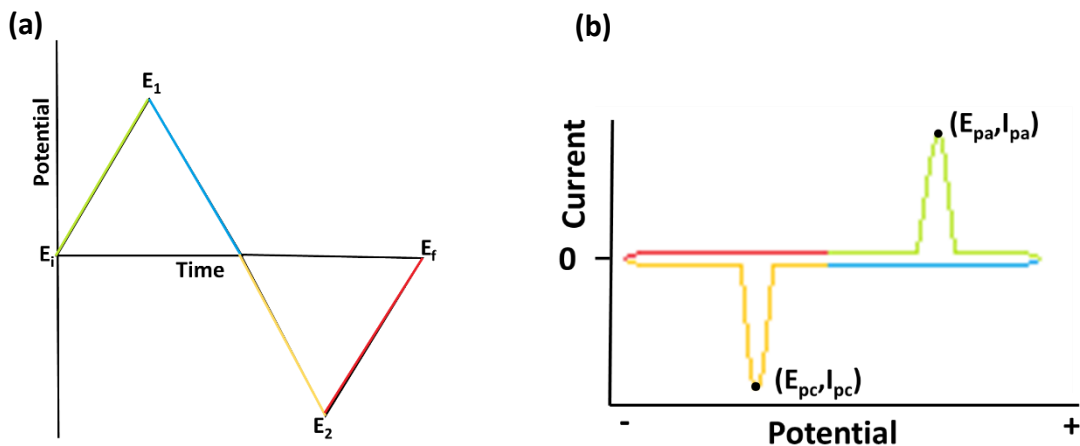


Figure 7. Diagrams of CV: (a) potential vs. time and (b) current vs. potential.

2.5.2. Reversibility

Total reversibility occurs when all the species come back to the initial state after a forward and reverse scan cycle in which they suffer an oxidation or reduction reaction. The voltammogram of a reversible process has the cyclic shape shown in figure 8.¹⁶

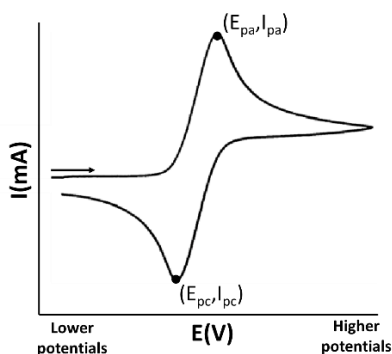


Figure 8. Diagram of cyclic voltammogram experiment displaying a reversible electron transfer process.

Experimentally, one way to analyse by CV the reversibility of a process consists of recording several voltammograms at different scan rates to determine the maxima values of the potential and the intensity in the oxidation and reduction peaks. To consider a process reversible, several requirements must be fulfilled:

- The coefficient between the maximum current intensity of the oxidation and the reduction bands (I_{pa} / I_{pc}) has to be to the closest to unity in value and independent of the scan speed.
- The difference of potentials ($\Delta E_p = E_{pa} - E_{pc}$) must be constant in all the scan speed range.
- The half-wave potential ($(E_0 = E_{pa} + E_{pc})/2$) must be constant in all the scan speed range.
- The representation of the maximum intensities (I_{pa} and I_{pc}) vs. the square root (v) of the scan rate must be a linear plot, Randles-Sevcik equation (equation 2):

$$i_p = 0.4463nFAC (nFvD/RT)^{1/2} \text{ (equation 2)}$$

In which i_p = current maximum [ampere, A]; n = number of electrons transferred in the redox event (usually 1); A = electrode area [cm^2]; F = Faraday constant [Cmol^{-1}]; D = diffusion coefficient [cm^2s^{-1}]; C = concentration [molcm^{-3}]; v = scan rate [Vs^{-1}]; R = gas constant [$\text{JK}^{-1}\text{mol}^{-1}$] and T = temperature [K].

2.5.3. Applications of the voltammetry technique

The principal application of the voltametric technique is the study of the oxidation and reduction processes in a substance. Kinetics of the redox reaction can be also studied by varying the scan rate. Acquired data can be related with other properties, such as the antioxidant capacity of the material, the lowest oxidation potential that indicates the facility to donate electrons, or, more interesting, the application in electronic devices, providing an idea of the HOMO and LUMO energies of the molecules under study.²⁶ The HOMO relates to the energy necessary for the extraction of an electron and therefore to, the potential of the first oxidation, observed in the CV diagram. In the same way, but related with the addition of an electron, the LUMO energy can be estimated with the first reduction potential. When using ferrocene as the reference, the HOMO and LUMO energies are calculated with equations 3-5, being Eoxonset and Eredonset the potential where the system is starting to be oxidised and reduced, respectively:

$$E(\text{HOMO}) = -e [E_{\text{oxonset}} + 4.8] \text{ (Equation 3)}$$

$$E(\text{LUMO}) = -e [E_{\text{redonset}} + 4.8] \text{ (Equation 4)}$$

$$E_{\text{Bandgap}} (\text{eV}) = E(\text{HOMO}) - E(\text{LUMO}) \text{ (Equation 5)}$$

The onset potentials are obtained graphically from the crossing of the tangents to the first oxidation and reduction peaks in the CV diagram, as it is exemplified in figure 9.

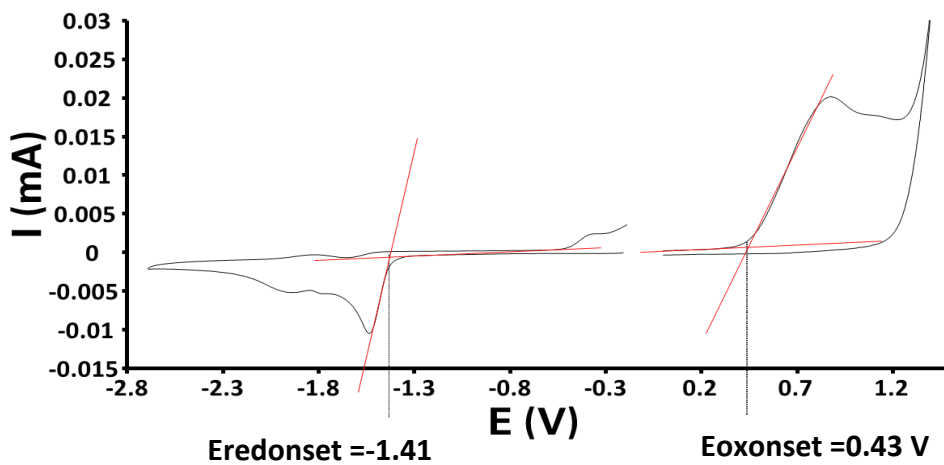
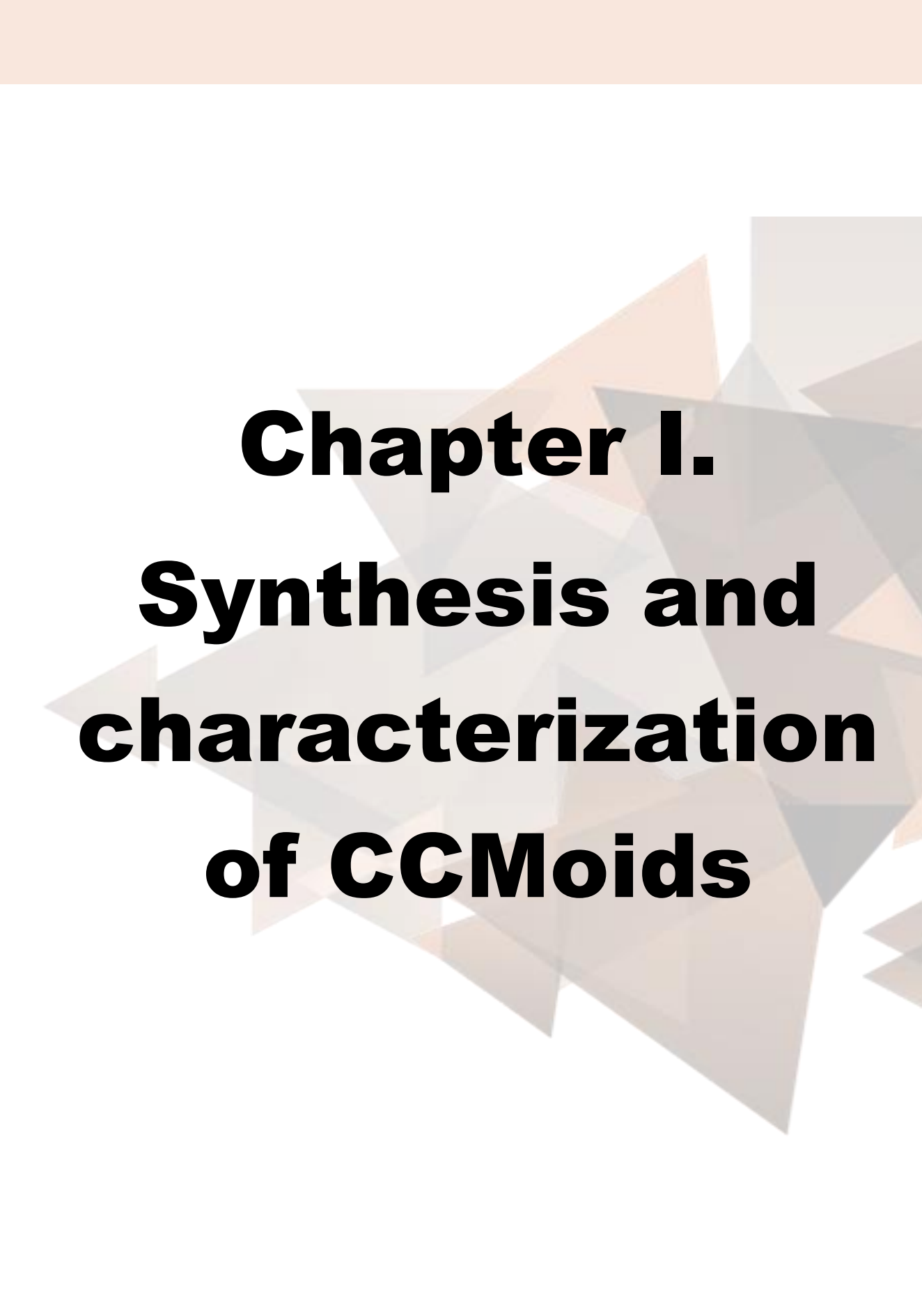


Figure 9. Example of the graphical determination of the onset potentials.

3. References

- (1) López-Periago, A. M., Portoles-Gil, N., López-Domínguez, P., Fraile, J., Saurina, J., Aliaga-Alcalde, N., ... & Domingo, C. (2017). Metal-organic frameworks precipitated by reactive crystallization in supercritical CO₂. *Crystal Growth & Design*, 17(5), 2864-2872.
- (2) Portoles-Gil, N. (2019). Green synthesis of coordination polymers using supercritical carbon dioxide (Doctoral dissertation, Universitat Autònoma de Barcelona).
- (3) Portoles-Gil, N., Lanza, A., Aliaga-Alcalde, N., Ayllon, J. A., Gemmi, M., Mugnaioli, E., ... & Domingo, C. (2018). Crystalline curcumin bioMOF obtained by precipitation in supercritical CO₂ and structural determination by electron diffraction tomography. *ACS Sustainable Chemistry & Engineering*, 6(9), 12309-12319.
- (4) Hore, P. J. (2015). Nuclear magnetic resonance. Oxford University Press, USA.
- (5) Nieto, C. I., Cabildo, P., Claramunt, R. M., Cornago, P., Sanz, D., Torralba, M. C., ... & Elguero, J. (2016). The structure of β -diketones related to curcumin determined by X-ray crystallography, NMR (solution and solid state) and theoretical calculations. *Structural Chemistry*, 27(2), 705-730.
- (6) Duer, M. J. (Ed.). (2008). Solid state NMR spectroscopy: principles and applications. John Wiley & Sons.
- (7) Bakhmutov, V. I. (2011). *Solid-State NMR in Materials Science: Principles and Applications*. CRC press.
- (8) Volklinger, C., Popov, D., Loiseau, T., Guillou, N., Ferey, G., Haouas, M., ... & Riekell, C. (2007). A microdiffraction set-up for nanoporous metal-organic-framework-type solids. *Nature materials*, 6(10), 760-764.
- (9) Stegbauer, L., Schwinghammer, K., & Lotsch, B. V. (2014). A hydrazone-based covalent organic framework for photocatalytic hydrogen production. *Chemical science*, 5(7), 2789-2793.
- (10) Hillenkamp, F., Karas, M., Beavis, R. C., & Chait, B. T. (1991). Matrix-assisted laser desorption/ionization mass spectrometry of biopolymers. *Analytical chemistry*, 63(24), 1193A-1203A.
- (11) Günzler, H., & Gremlich, H. U. (2002). IR spectroscopy. An introduction.
- (12) Chakrabarti, C. L., Gilmudinov, A., & Hutton, J. C. (1999). ATR and reflectance IR spectroscopy, applications. *Spectroc. Acta B*, 33, 193.
- (13) Ángeles, G., Martín-Sedeño, M. C., León-Reina, L., & José, M. Synchrotron X-ray Diffraction in Mineralogy and Materials Chemistry. Possibilities and Applications.
- (14) Klug, H. P., & Alexander, L. E. (1974). X-ray diffraction procedures: for polycrystalline and amorphous materials. *X-Ray Diffraction Procedures: For Polycrystalline and Amorphous Materials, 2nd Edition, by Harold P. Klug, Leroy E. Alexander, pp. 992. ISBN 0-471-49369-4. Wiley-VCH, May 1974., 992.*
- (15) Goldstein, J. I., Newbury, D. E., Michael, J. R., Ritchie, N. W., Scott, J. H. J., & Joy, D. C. (2017). Scanning electron microscopy and X-ray microanalysis. Springer.
- (16) Flegler, S. L., & Flegler, S. L. (1997). Scanning & Transmission Electron Microscopy. Oxford University Press.
- (17) Bennig, G. K. (1988). *U.S. Patent No. 4,724,318*. Washington, DC: U.S. Patent and Trademark Office.
- (18) Bhagyaraj, S. M., Oluwafemi, O. S., Kalarikkal, N., & Thomas, S. (Eds.). (2018). Characterization of Nanomaterials: Advances and Key Technologies.
- (19) Jacquez, J. A., & Kuppenheim, H. F. (1955). Theory of the integrating sphere. *JOSA*, 45(6), 460-470.
- (20) Costa, J. C., Taveira, R. J., Lima, C. F., Mendes, A., & Santos, L. M. (2016). Optical band gaps of organic semiconductor materials. *Optical Materials*, 58, 51-60.
- (21) Lichtman, J. W., & Conchello, J. A. (2005). Fluorescence microscopy. *Nature methods*, 2(12), 910-919.
- (22) D'Aléo, A., Felouat, A., & Fages, F. (2014). Boron difluoride complexes of 2'-hydroxychalcones and curcuminoids as fluorescent dyes for photonic applications. *Advances in Natural Sciences: Nanoscience and Nanotechnology*, 6(1), 015009.
- (23) Kamada, K., Namikawa, T., Senatore, S., Matthews, C., Lenne, P. F., Maury, O., ... & d'Aléo, A. (2016). Boron difluoride curcuminoid fluorophores with enhanced two-photon excited fluorescence emission and versatile living-cell imaging properties. *Chemistry—A European Journal*, 22(15), 5219-5232.
- (24) Bagotsky, V. S. (Ed.). (2005). *Fundamentals of electrochemistry* (Vol. 44). John Wiley & Sons.
- (25) Elgrishi, N., Rountree, K. J., McCarthy, B. D., Rountree, E. S., Eisenhart, T. T., & Dempsey, J. L. (2018). A practical beginner's guide to cyclic voltammetry. *Journal of chemical education*, 95(2), 197-206.
- (26) Scholz, F. (2010). *Electroanalytical methods* (Vol. 1). Berlin: Springer.
- (27) Li, Y. (Ed.). (2015). *Organic optoelectronic materials* (p. 26). Cham, Switzerland: Springer International Publishing.



Chapter I.
Synthesis and
characterization
of CCMoids

Chapter scope

The main goal of this chapter is to describe the synthesis and characterization of the CCMoids employed in this doctoral thesis. The comparison of their physicochemical properties is used to determine the influence of the different substituents at the sides of the molecules, including the presence of BF_2 species coordinated to the β -diketone moiety. Extracted information will be used to assist in future CCMoid research, by doing a more efficient design of new molecules towards specific applications. To have a better understanding of the monomeric organic molecules used in this doctoral thesis, toward the goal of building extended structures, a brief description of each one is given. Here, we report the materials (commercial precursors and synthesized reagents) and the synthetic methods used for the preparation of all the studied CCMoids. Moreover, an extensive characterization of all the compounds is provided as a crucial step towards potential applications.

1. Introduction

The CCMoid family has a remarkable chemical versatility, which makes possible to direct their design for further uses. During the development of this doctoral thesis, nine CCMoids were synthesized (figure 1), five of them were already described in the literature, while the rest have not been published before. Mainly, the new molecules were primarily synthesized and designed to create new CPs and OPs, as it is explained in the following chapters, but also with the idea of studying how the different functionalities of the structure affect their properties. CCMoids with BF_2 (CCMoid BF_2) were also prepared and are mentioned here because these compounds have shown differences in the optical,¹ electrochemical^{2,3} or even biomedical⁴ properties compared with pristine CCMoids.

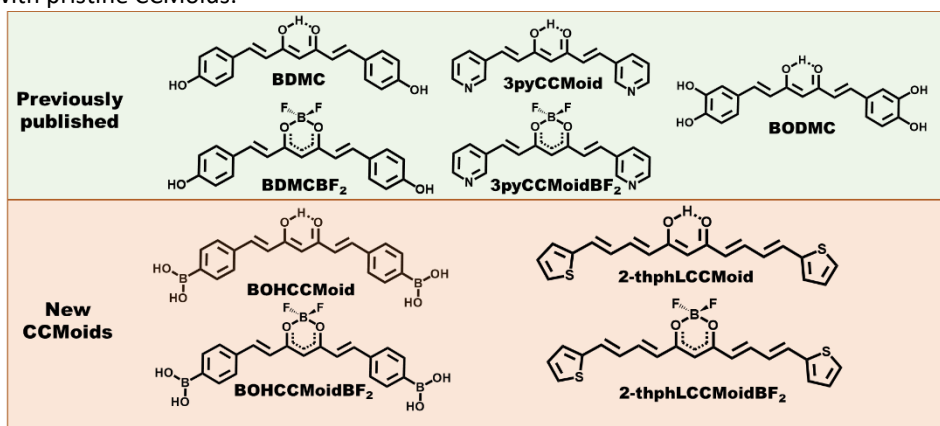


Figure 1. Structures and acronyms of the CCMoids synthesized in this doctoral thesis. The description of the acronyms is given below.

2. Materials and methods

2.1. Materials

The reagents used for the general synthesis of CCMoids: acetylacetone (acac), boric acid (B_2O_3), boron trifluoride ethyl etherate ($BF_3 \cdot OEt_2$), tributylborate and n-butylamine, as well as some different aldehydes: 4-hydroxybenzaldehyde, 4-hydroxy-3-methoxybenzaldehyde, 3-pyridinecarboxyaldehyde and 2-thiophenecarboxaldehyde, were purchased from Sigma Aldrich. Anhydrous aluminium chloride ($AlCl_3$) was supplied by TCI chemicals. 4-formylphenylboronic acid and triphenylphosphoranylidene acetaldehyde was supplied by Fluorochem Ltd. The solvents, ethyl acetate (EtOAc), toluene, acetone, acetonitrile (ACN), MeOH, hexane and diethyl ether (Et_2O) of synthesis grade and HCl 35 v% were provided by Carlo Erba Reagents S.A.S. Anhydrous pyridine was supplied by Sigma Aldrich and absolut EtOH by Scharlab S.L. Aqueous solutions were prepared using Milli-Q H_2O obtained from a purification system (Millipore).

2.2. Description and synthesis of CCMoids

For the preparation of pristine CCMoids, slight modifications from the synthetic method described by Pabon,⁵ already reported in the general introduction, were performed. In addition, BODMC was obtained by the demethylation of CCM and in the synthesis of CCMoids BF_2 two different approaches were used, starting from either the free CCMoid or acac coordinated with BF_2 (acac BF_2).

2.2.1. CCMoids using Pabon's method

2.2.1.1. BDMC

The (1E,6E)-1,7-bis(4-hydroxyphenyl)1,6-heptadiene-3,5-dione, known as bisdemethoxycurcumin or BDMC, is one of the three natural CCMoids present in the rhizomes of the plant *Curcuma Longa*. As it occurs with the rest of natural CCMoids, there are a big number of publications involving this molecule and covering different topics (figure 2). Being a natural CCMoid, the majority of articles are related to biological applications, such as medicine, pharmacology, microbiology and biology, but also to agriculture and environment. Moreover, a significant number of works deal with its synthesis, the study of its biological properties or its quantification in natural samples (chemical studies and characterization in figure 2). Even the works included in categories different than biomedicine are often related to medical applications, e.g., its used for the fabrication of nanoparticles or films for being therapeutic agents,⁶ patches⁷ or other composites with the objective of improving the low solubility of BDMC in biological media.⁸

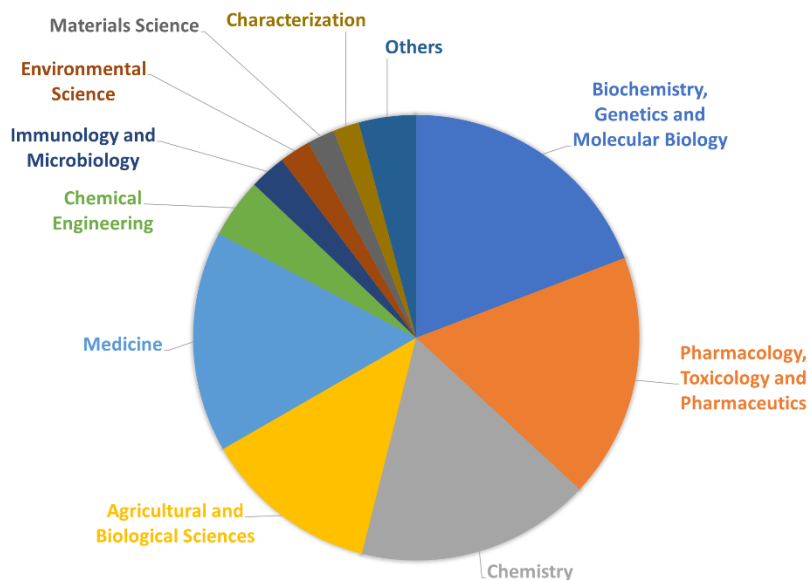
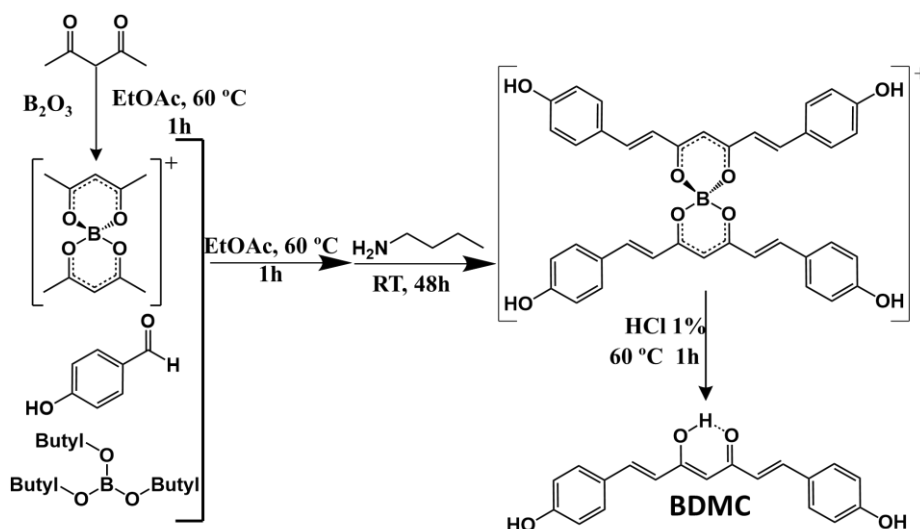


Figure 2. Application fields of BDMC.

In the synthesis of BDMC (scheme 1), acac (0.98 g, 9.7 mmol) and B_2O_3 (0.69 g, 10 mmol) were dissolved in 5 mL of EtOAc and heated at 60 °C during 1 h, resulting in a white paste. In parallel, a solution of 4-hydroxybenzaldehyde (2.39 g, 19.6 mmol) and tributyl borate (9.38 g, 72 mmol) was prepared in 20 mL of EtOAc and added to the first one. The mixture was stirred for 1 h at 60 °C and then it was allowed to cool down to room temperature. Afterwards, a solution of 0.5 mL of n-butylamine (5 mmol) in 10 mL of EtOAc was added dropwise to the stirred mixture. As a result, the solution colour evolves from pale yellow to a dark red precipitate, that was recovered after maintaining the mixture during two days under stirring at room temperature. The solid was filtered, washed with clean EtOAc and finally incorporated to 50 mL of a solution 1 % v/v of HCl (pH = 1) and heated at 60 °C during 1 h. An additional change of colour, from dark red to light orange, indicated the dissociation of the boron compound and, therefore, the release of the desired CCMoid, BDMC. 2.12 g, yield: 70 wt%, mp: 217-219 °C. 1H -RMN (360 MHz, DMSO- d_6) 16.39 (s, 1H), 10.06 (s, 2H), 7.58 (d, J= 7.2 Hz, 2H), 7.55 (d, J= 14,4 2H), 6.83 (d, J= 7.2 Hz, 2H), 6.71 (d, J= 18Hz, 2H), 6.05 (s, 1H). ^{13}C -RMN (100 MHz, $CDCl_3$) 183.2, 159.8, 140.3, 130.3, 125.8, 120.8, 115.9.⁹

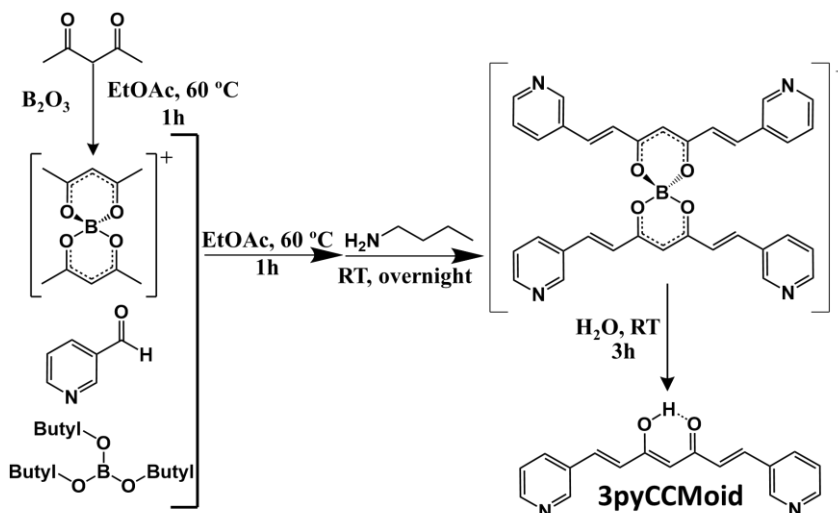


Scheme 1. Schematic synthetic route for BDMC.

In this doctoral thesis, the main focus for using BDMC was the formation of new materials not necessarily linked to its biological applications. In that sense, extended structures based on the coordination of BDMC molecules and metal salts (CPs) had been synthesized (chapter II) using the same approach that previously described for CCM (general Introduction).^{10,11}

2.2.1.2. 3pyCCMoid

The (1E,6E)-1,7-di(3-pyridinyl)1,6-heptadiene-3,5-dione, named here as 3pyCCMoid, is a synthetic CCMoid, with pyridine moieties as aromatic substituents in the corners (scheme 2). The N atom of the pyridine is located in one of the *meta*- positions in the rings of the CCMoid sides. The method used for the synthesis of the 3pyCCMoid was similar to the previously applied for BDMC, but using 3-pyridinecarboxyaldehyde (1.5 g, 14 mmol) as a reagent. In this case, the boron-3pyCCMoid intermedia precipitated in 24 h, instead of the 48 h required for the other CCMoids. The pristine 3pyCCMoid molecule was released by stirring the boron-3pyCCMoid in 30 mL of H₂O during 3 h at room temperature. After filtration, the CCMoid was obtained as a light-yellow solid, and further purification was not required. 1.56 g, yield: 80 wt%, mp: 172-176 °C. ¹H NMR (360 MHz, DMSO-d₆) δ 15.88 (s, 1H), 8.91 (s, 2H), 8.59 (dd, J = 4.8, 1.7Hz, 2H), 8.32 (d, J = 8.0 Hz, 2H), 7.70 (d, J = 16.1 Hz, 2H), 7.48 (dd, J = 7.9, 4.8 Hz, 2H), 7.13 (d, J = 16.1 Hz, 2H), 6.22 (s, 1H). ¹³C-RMN (101 MHz, CDCl₃) 182.9, 150.9, 149.8, 137., 134.4, 130.81, 126.0, 123.9, 102.3.²



Scheme 2. Schematic synthetic route for 3pyCCMoid.

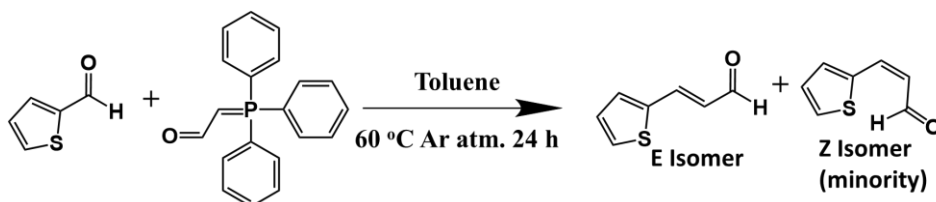
In the literature, this molecule has been proposed in the biomedical field for the treatment of Parkinson's illness¹² and inflammatory diseases.¹³ Although this compound was less effective than other CCMoids for this application, its low toxicity has triggered to proceed with its analysis in the biological field. As far as we know, the coordination of 3pyCCMoid with metals has not been published before. Going further in this unexplored topic, and encouraged by the interesting structure of this CCMoid, CPs based on 3pyCCMoid have been synthesized during this doctoral thesis and the results are presented in chapter III.

2.2.1.3. 2-thphLCCMoid

The named 2-thphLCCMoid, (1E,3E,8E,10E)-1,11-di(2-thiophenyl)-1,3,8,10-undecatetraene-5,7-dione, has eleven carbon atoms in the central chain, instead of the seven typically found for CCMoids, and thiophene moieties in the corners with the sulphur atoms located in position two. The first step in the preparation of 2-thphLCCMoid was the synthesis of the corresponding aldehyde (3-(2-thienyl)acrylaldehyde, scheme 3)¹⁴ followed by the use of Pabon's method (scheme 4).

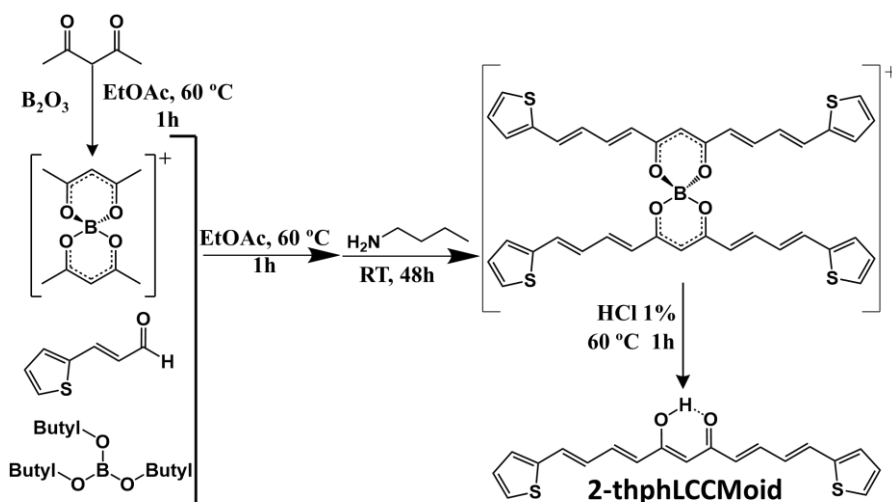
For the synthesis of 3-(2-thienyl)acrylaldehyde, 2-thiophenecarboxaldehyde (0.56 g, 5 mmol) and (triphenylphosphoranylidene)acetaldehyde (1.52 g, 5 mmol) were dissolved in toluene (10 mL) and then heated at 60 °C under Ar for 24 h. After cooling down the reaction mixture, the triphenylphosphine oxides was precipitated by the addition of hexane and removed by filtration. Finally, the solvents were evaporated using a rotatory-evaporator and the product was purified by column chromatography hexane/EtOAc (95:5 v/v%). In this step, it is possible the separation of a small quantity of the two isomers of the product (E and Z), although a portion of the sample remains

always with both mixed together. The utilization of only the isomer E improved the yield in the following step (2-thphLCCMoid formation). E-3-(2-thienyl)acrylaldehyde: 123 mg, yield: 16.37 wt%. ^1H NMR (360 MHz, DMSO-d_6) 9.62 (d, $J = 7.7$ Hz, 1H), 7.58 (d, $J = 15.6$ Hz, 1H), 7.50 (d, $J = 5.1$ Hz, 1H), 7.36 (d, $J = 3.6$ Hz, 1H), 7.11 (dd, $J = 5.0, 3.7$ Hz, 1H), 6.51 (dd, $J = 15.6, 7.7$ Hz, 1H). ^{13}C NMR (75 MHz, CDCl_3): $\delta = 193.0, 144.5, 139.4, 132.2, 130.5, 128.7, 127.5$.¹⁵ Mixture of E and Z isomers: 150 mg yield: 22 wt%.



Scheme 3. Schematic synthetic route for 3-(2-thienyl)acrylaldehyde (Wittig reaction).¹⁴

2-thphLCCMoid was obtained following the same methodology as in the rest of CCMoids, but using the previously synthesized E-3-(2-thienyl)acrylaldehyde (610 mg, 4 mmol) and maintaining the ratio of the reagents scaled to the aldehyde amount. The boron-intermediate species were dissociated using HCl 1 v% (pH= 1) and heating at 60 °C during 1 h. The pure CCMoid was obtained after recrystallization in hot ACN as a dark orange solid. 53 mg, yield: 82 wt%. mp: 190-210 °C ^1H NMR (360 MHz, DMSO-d_6) 16.15 (s, 1H), 7.63 (d, $J = 3.6$ Hz, 2H), 7.40 (dd, $J = 14.4, 10.8$ Hz, 2H), 7.33 (d, $J = 3.6$ Hz, 2H) 7.31 (d, $J = 10.8$ Hz, 2H), 7.13 (t, $J = 10.8$ Hz, 2H), 6.86 (dd, $J = 19.8, 14.4$ Hz), 6.37 (d, $J = 14.4$ Hz, 2H), 6.00 (s, 1H). ^{13}C -RMN (101 MHz, DMSO-d_6) 182.9, 141.8, 140.3, 132.7, 128.5, 128.1, 127.3, 126.7, 126.6, 102.0.

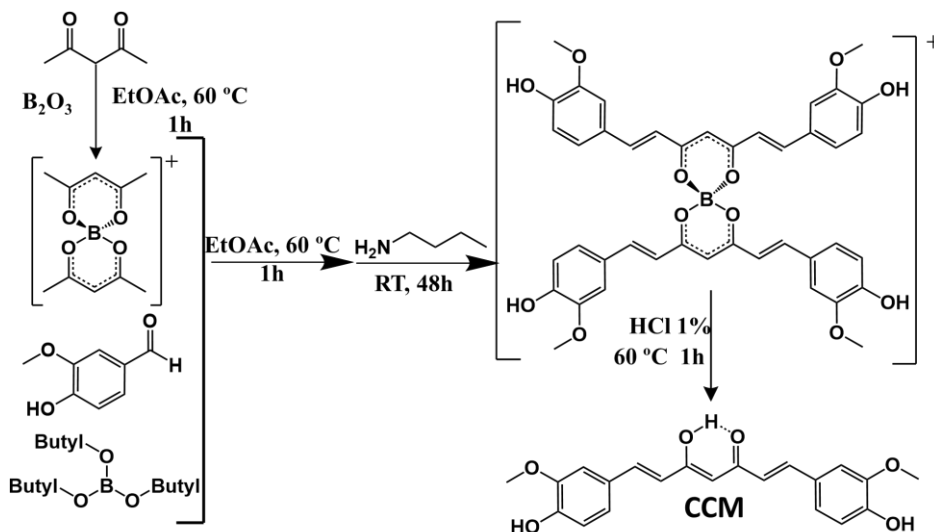


Scheme 4. Schematic synthetic route for 2-thphLCCMoid.

2-thphLCCMoid is a new compound, but the seven carbon-skeleton analogous, 2-thphCCMoid, was previously synthesized.¹⁶ As for the rest of CCMoids, some medical uses have been proposed for the latter in the treatment of antiinflammatory,¹⁷ anticancer^{18,19} and Parkinson diseases.¹⁹ In addition, applications for the 2-thphCCMoid have been studied taking advantage of the affinity of S atoms for gold, and, this way, the deposition of this molecule on Au surfaces.^{20,21} The HOMO-LUMO bandgap energies of 2-thphCCMoid and a related system (3-thphCCMoid) have been analysed in the bulk by using electrochemistry and solid state UV-VIS absorption techniques.²² 2-thphLCCMoid and its BF₂ analogous, 2-thphLCCMoidBF₂ (synthesis below) were here synthesized with the aim of going ahead with electronic studies on Au surfaces using Langmuir–Blodgett deposition in collaboration with the group of Prof. P. Cea at Department of Physical Chemistry, Faculty of Sciences (University of Zaragoza), work that is in progress.

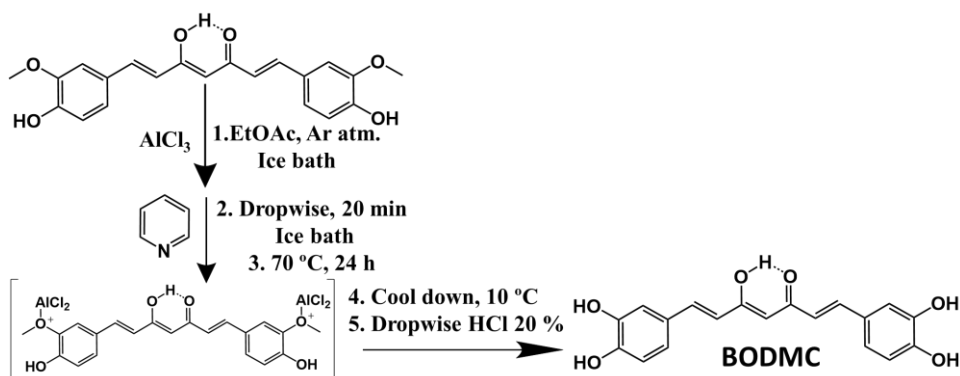
2.2.2. BODMC

The (1E,6E)-1,7-bis(3,4-dihydroxyphenyl)-1,6-heptadiene-3,5-dione is commonly named Bi-O-demethyl curcumin (BODMC). This compound has two hydroxyl groups in the positions three and four in the benzene ring (in *meta*- and *para*- positions). For the BODMC synthesis, the used methodology is based on the oxidation of the CCM's methoxy groups to obtain the diphenol CCMoid.²³ Hence, the first step was the synthesis of the CCM using the Pabon's method (scheme 5) and 4-hydroxy-3-methoxybenzaldehyde (2.9 g, 19.1 mmol). 2.2 g, yield: 62 wt%. mp: 223-225 °C RMN (360 MHz, DMSO-d₆) 16.43 (s, 1H), 9.68 (s, 2H), 7.54 (d, J = 14.4 Hz, 2H), 7.32 (s, 2H), 7.15 (d, J = 7.2 Hz, 2H), 6.82 (d, J = 7.2Hz, 2H), 6.75(d, J = 21.6Hz,2H), 6.05 (s, 1H). 3.84 (s, 6H).¹³C-RMN (75 MHz, DMSO-d₆) 183.2, 149.4, 148.0, 140.8, 126.3, 123.2, 121.1, 115.7, 111.3, 100.9, 55.7.²⁴



Scheme 5. Schematic synthetic route for CCM.

Next, 2.2 g (6.1 mmol) of CCM, were dissolved in 42 mL of EtOAc. The resulting solution was kept in an ice bath under Ar at low flow and 6 g (45 mmol) of AlCl_3 were slowly added. After that, 14 mL of pyridine were slowly added dropwise, lasting this process around 20 min. A dark precipitate was then observed, which vanished when the mixture was heated under reflux for 24 h at 70 °C. The system was cooled down at 10 °C, which caused the formation of a dense precipitate. Then, a solution of HCl 20 v% was slowly added until the dissolution of the solid was observed, which implied the dissociation of the aluminium complex. Finally, the mixture was stirred overnight, finding a precipitate afterwards. This solid was filtered, washed with fresh solvent, and dried with Et_2O , and the CCMoid was recovered as a brown product (scheme 6). 1.90 g, yield: 94 wt%. mp: 223-224 °C. ^1H -RMN (360 MHz, DMSO-d_6) 16.40 (s, 1H), 9.66 (s, 2H), 9.20 (s, 2H), 7.47 (d, $J = 14.4\text{Hz}$, 2H), 7.09 (s), 7.03 (d, $J = 7.2\text{Hz}$, 2H), 6.79 (d, $J = 7.2\text{Hz}$, 2H), 6.58 (d, $J = 18\text{Hz}$, 2H), 6.08 (s, 1H). ^{13}C -RMN (100 MHz, DMSO-d_6) 183.1, 147.8, 145.1, 140.8, 127.7, 126.5, 121.9, 115.9, 114.5, 100.9.²⁵



Scheme 6. Schematic synthetic route for BODMC.

BODMC is not present in nature, but it has been widely studied, since the phenol groups are the responsible of many of the interesting properties of CCMoids in the biological field. In that sense, BODMC has shown interesting results as antiapoptotic,²⁶ antineurotoxic,²⁷ antioxidant²⁸ and antiinflammatory,²⁹ and in the treatment of ophthalmologic diseases.³⁰ The two hydroxyl groups in the aromatic rings can be used for the synthesis of CPs as well as for OPs based on the formation of boronic esters. However, during the development of this doctoral thesis, the formation of extended structures based on this CCMoid has not been achieved, but some chemically interesting preliminary results related with the formation of boronic esters are introduced in chapter IV. In addition, in a collaboration with Prof. Maria Luisa Perez-Garcia at the Faculty of Pharmacy (University of Barcelona), the formation of anti-inflammatory gels with embedded BODMC CCMoid is currently under study.

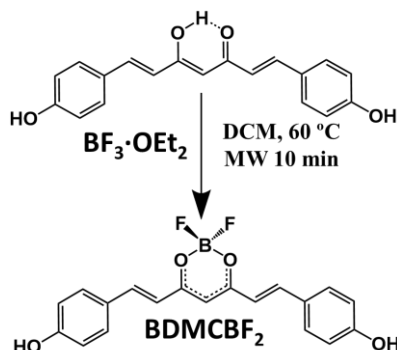
2.2.3. Synthesis of CCMoidBF₂

Two different strategies were used to obtain CCMoids coordinated to BF₂ moieties, either the free CCMoid was reacted with BF₃·OEt₂ or the acacBF₂ compound was synthesized followed by the condensation with the desired aldehyde.

2.2.3.1. CCMoidBF₂ from free CCMoid

BDMCBF₂

For the synthesis of BDMCBF₂ (scheme 7), 20 mg (6.4 mmol) of BDMC were dispersed in 3 mL of DCM and mixed with an excess of BF₃·OEt₂ (0.2 mL). After 10 min under stirring at 60 °C in a MW oven, the product was recovered as a dark red-purple solid, which was filtered and cleaned with a small amount of DCM. 0.23 mg, yield 99 wt%. ¹H-RMN (360 MHz, DMSO-d₆) 10.46 (s, 2H), 7.92 (d, J= 14.4 Hz, 2H), 7.74 (d, J= 12.6, 2H), 6.97 (d, J= 14.4Hz, 2H), 6.87 (d, J= 10.8Hz, 2H), 6.46 (s). ¹³C-RMN (MHz, CDCl₃) 179.3, 162.1, 147.1, 132.5, 125.9, 118.1, 116.7, 101.7.

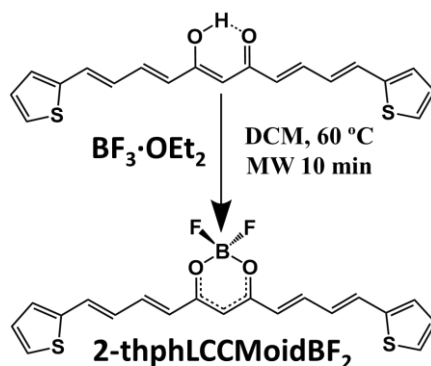


Scheme 7. Schematic synthetic route for BDMCBF₂.

The BDMCBF₂ has been synthesized previously as an intermediate for BDMC synthesis.^{31,32} However, BDMCBF₂ itself, as well as other CCMoidBF₂, have some interesting applications, for instance in the subject of sensors.^{33,34}

2-thphLCCMoidBF₂

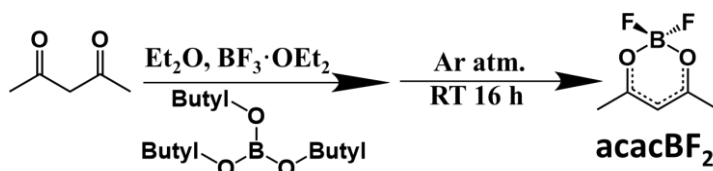
A similar methodology than for BDMCBF₂ was used, but using 2-thphLCCMoid (10 mg, 0.029 mmol) as a reagent. Therefore, after the MW assisted reaction and the removal of the solvent, 2-thphLCCMoidBF₂ was recovered as a dark purple solid (scheme 8). 11.20 mg, yield: 98 wt%. ¹H NMR (360 MHz, DMSO-d₆) 7.81 (d, J=10.8Hz, 2H), 7.77 (dd, J= 3.6, 9 Hz, 2H), 7.59 (d, J=10.8Hz, 2H), 7.45 (d, J=3.6Hz,2H) 7.18 (t, J=3.6Hz, 2H), 7.00 (t, J=10.8, 2H), 6.57 (d, J=14.4Hz, 2H), 6.48 (s, 1H). ¹³C-RMN (360 MHz, DMSO-d₆) 178.9, 147.5, 141.6, 138.1, 131.5, 130.6, 129.4, 126.9, 124.4, 102.4.



Scheme 8. Schematic synthetic route for 2-thphLCCMoidBF₂.

2.2.3.2. CCMoidBF₂ from acacBF₂

Pabon⁵ already proposed the use of boron oxide to coordinate with acac in order to avoid condensation processes of the aldehyde with the central carbon during the synthesis of CCMoids. For a similar objective, other boron species, such as BF₂, can be employed instead of B₂O₃, as it has been demonstrated in different works.³⁵ The first step implies the achievement of an acacBF₂ compound, which can be either formed *in situ*, or as in our case be isolated to ensure the purity of this compound (scheme 9).

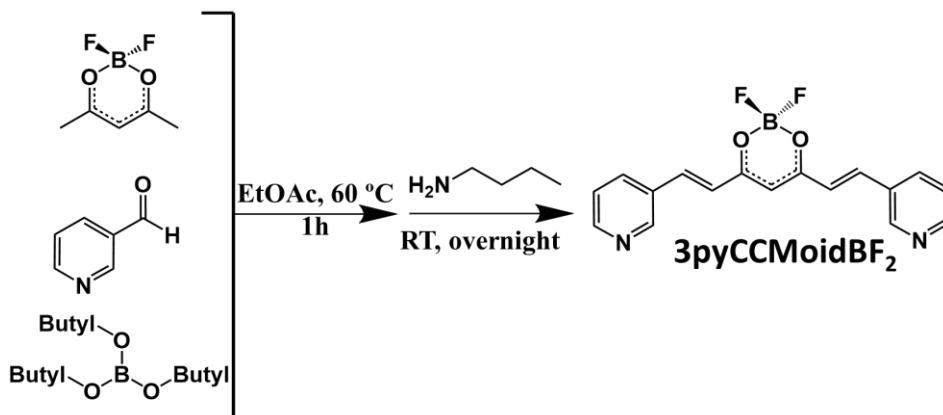


Scheme 9. Schematic synthetic route for acacBF₂.

For the synthesis of this compound, a method reported elsewhere was used.³⁶ In short, a solution of acac (15.4 mL, 0.15 mol) and tributyl borate (13.5 mL, 0.05 mol) in Et₂O (10 mL) was prepared and BF₃·OEt₂ (12.7 mL, 0.1 mol) was slowly added under Ar. The reaction mixture was then stirred at room temperature for 16 h. The solvent was removed using a rotatory-evaporator obtaining an oily residue that was placed in the freezer. After few hours, light pink crystals appeared. The crystalline material was cleaned with H₂O and filtered, giving as a result white crystals. 18.5 g, yield: 83 wt%. ¹H NMR (400 MHz, CDCl₃) δ 5.99 (s, 1H), 2.31 (s, 6H).

3pyCCMoidBF₂

The synthetic method of the BF₂ analogous of 3pyCCMoid (3pyCCMoidBF₂) has previously been described³¹ but in our case similar conditions than for the B₂O₃ synthesis were used. AcacBF₂ (1.43 g, 9.7 mmol) was dissolved in 3 mL of EtOAc and heated at 60 °C. Then, a solution of 3-pyridinecarboxyaldehyde (1.5 g, 14 mmol) and tributyl borate (9.38 g, 72 mmol) in 20 mL of EtOAc was added to the first one and the mixture was kept at 60 °C for 1 h. After that, the mixture was allowed to cool down to room temperature and a solution of 0.5 mL of n-butylamine (5 mmol) in 10 mL of EtOAc was added. The mixture was stirred for 24 h at room temperature, and an orange precipitate was formed. The pure CCMoid was obtained after recrystallization in hot ACN. 1.27 g, yield: 60 wt%. ¹H NMR (400 MHz, DMSO-d₆) 8.91 (s, 2H), 8.59 (dd, J= 4.8, 1.7Hz, 2H), 8.32 (d, J= 8.0 Hz, 2H), 7.13 (d, J= 14.4 Hz, 2H), 7.48 (dd, J= 8, 4 Hz, 2H), 7.43 (d, J= 12 Hz, 2H), 6.7 (s, 1H). ¹³C-RMN (400 MHz, DMSO-d₆) 180.8, 152.6, 151.5, 144., 136.1, 130.4, 124.7, 123.7, 103.2.

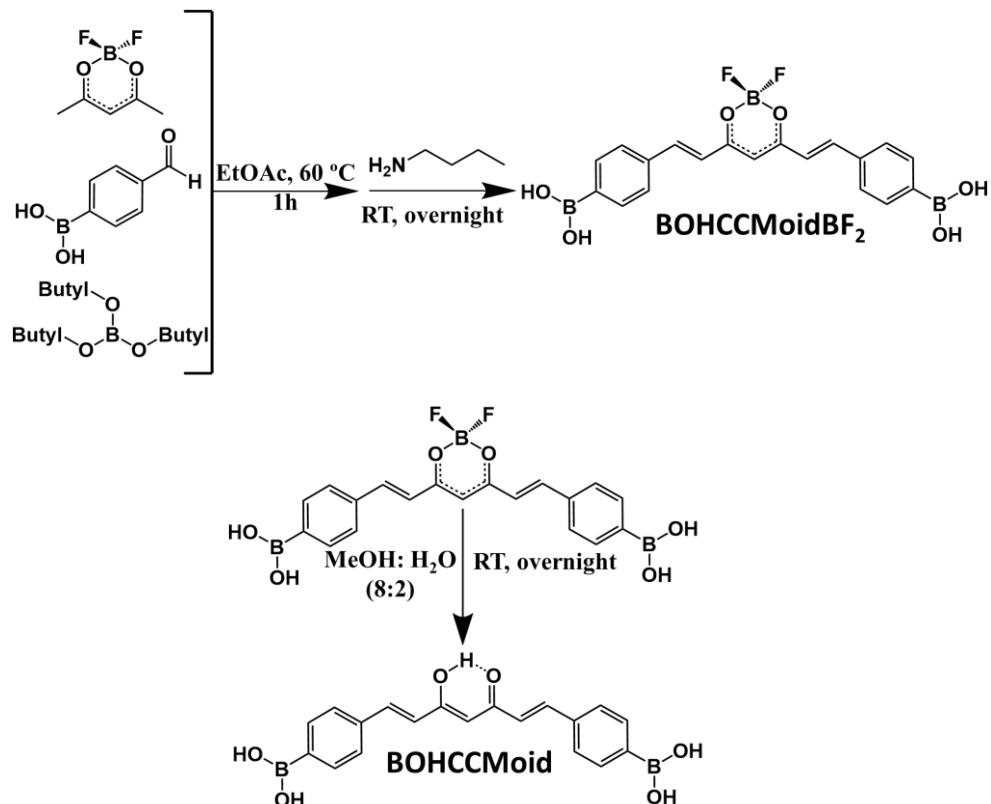


Scheme 9. Schematic synthetic route for 3pyCCMoidBF₂.

BOHCCMoidBF₂ and BOHCCMoid

BOHCCMoidBF₂ and BOHCCMoid ((((1E,6E)-3,5-dioxohepta-1,6-diene-1,7-diyl)bis(4,1-phenylene))diboronic acid) were synthesized for the first time during the development of this doctoral thesis. As it is depicted in schemes 10 and 11, these compounds have a boronic acid in the *para*- position in both phenyl rings. The same procedure than for 3pyCCMoidBF₂ was used to obtain BOHCCMoidBF₂ but using the aldehyde 4-formylphenylboronic acid. The pure CCMoid was precipitated as a light orange powder after stirring the mixture in a slightly basic aqueous solution (pH= 8). 1.96 g, yield: 47 wt%. ¹H NMR (360 MHz, DMSO-d₆) 8.25 (s, 4H), 8.15 (d, J= 14.4 Hz, 2H), 7.86 (m, 8H), 7.31 (d, J= 14.4 Hz, 2H), 6.69 (s, 1H). ¹³C-RMN (400 MHz, DMSO-d₆) 180.62, 147.38, 135.79, 135.20, 128.93, 122.32.

To obtain BOHCCMoid, the counterpart CCMoidBF₂ (100 mg, 0.24 mmol) was solubilised in MeOH (250 ml) precipitating the BOHCCMoid as an orange solid (scheme 11). 42.5 mg, yield: 48%. ¹H-RMN (360 MHz, DMSO-d₆) δ 8.17 (s, 4H), 7.74 (m, 10H), 7.01 (d, J = 14,4 Hz, 2H), 6.22 (s, 1H).



Scheme 10. Schematic synthetic route for BOHCCMoid.

In this doctoral thesis only BOHCCMoid have been obtained from the BF₂ analogous but it is also possible for the rest of CCMoids.

There are multiple methods to dissociate BF₂ from molecules with a β-diketone moiety, most of them implying the use of H₂O, MeOH or DMSO, even in some cases, the addition of bases has been also assayed.³⁷ In our group, a mixture MeOH:H₂O was used applying MW heating that dramatically reduced the reaction time, while maintaining high yield.³⁸ However, if this method is applied to BOHCCMoidBF₂ a variety of different products are obtained, likely due to additional reactions of the boronic acids but BOHCCMoid can be obtained easily in MeOH at RT.

In most cases, the CCMoidBF₂ compounds were obtained with similar yield and purity using both methods. The direct approach, which involves the formation of the CCMoidBF₂ starting from acacBF₂, could be also used to obtain BDMCF₂ and 2-

thphLCCMoidBF₂ with high yields. However, 3pyCCMoidBF₂ and BOHCCMoidBF₂ were not achieved from the reaction between free CCMoid and BF₃·OEt₂. For 3pyCCMoidBF₂, this fact can be explained by the probable protonation of the 3pyCCMoid system in acid media, due to the liberation of HF during complex formation. For BOHCCMoidBF₂, the low solubility of the free CCMoid in common organic solvents was the main drawback for such approach.

3. Characterization

All the studied CCMoids have been characterized using different techniques, some of them to corroborate the CCMoid nature, structure and purity and others to extract information on the optical and electronic properties. This way, ¹H and ¹³C NMR in solution, IR spectroscopy and mass spectrometry (MALDI-TOF) were used to identify the precipitated compounds and purity. X-ray diffraction (XRD) and ¹³C NMR in solid state (CPMAS¹³C) were applied to elucidate the disposition and conformation of the CCMoids in the solid state. Other techniques, such as UV-Vis absorption, fluorescence and electrochemistry, were used to study the optical and electronic properties of the bulk materials.

3.1. ¹H NMR

¹H NMR spectra were recorded after dissolving the studied CCMoids in deuterated DMSO. In figure 3, the ¹H NMR spectra of BDMC and BDMCBF₂ are displayed as representative examples of the description and distribution of proton shifts in CCMoids and related CCMoidBF₂ systems.

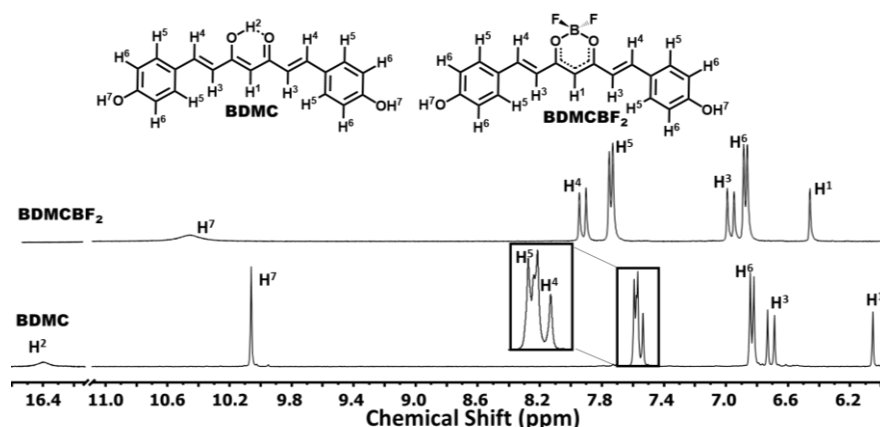


Figure 3. ¹H NMR spectra and signals assigned to BDMC (bottom) and BDMCBF₂ (top).

In general, the ¹H NMR spectrum of a CCMoid has series of common signals, used to identify the molecule as a member of this family. Two of them (H¹ and H² in figure 3 and table 1) are related to the enol form (figure 4), which is the exclusive tautomer present

in organic solvents. H^1 corresponds to the central proton, and it appears always as a sharp singlet around 6 ppm. This displacement is the expected for a proton bond to a sp^2 carbon and it would appear at higher fields (around 4 ppm) in the diketo form, as then the carbon has a sp^3 hybridization (figure 4). The existence of H^2 corroborates the permanence of the enol form in solution, appearing always at the lowest field region (15-16 ppm). Often, this proton is interacting with the solvent, especially with DMSO, resulting in a broad band. The rest of signals are related with the double bonds of the chain, the aromatic part and the substituents, respectively. The double bonds at the linear skeleton and the aromatic signals appear in the same region (6.5-8 ppm), but they are easy to differentiate through the analysis of the coupling constant (J) established between the protons. Hence, the double bonds of the CCMoids in solution are in E conformation (H^3 and H^4 , figure 3 and table 1) and appear as doublets with a high coupling constant ($J = 14-15$ Hz, isomer E), while the J values for the aromatic protons are between 1 and 7 Hz. The multiplicity of the aromatic protons also differs depending on the aromatic substituents (benzene, pyridine or thiophene, in our case).

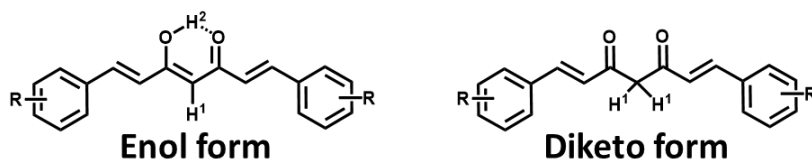
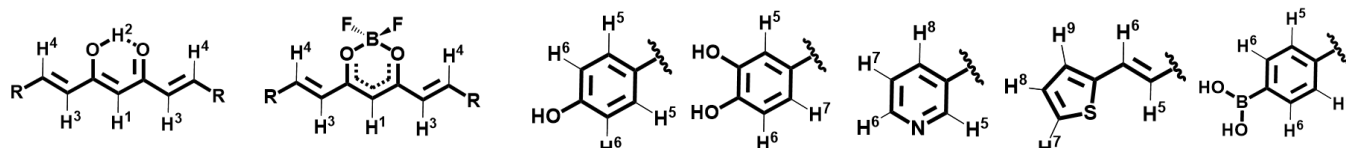


Figure 4. General structure of a CCMoid in the enol and diketo forms.

The coordination of CCMoids with the BF_2 group (exemplified by $BDMCBF_2$ in figure 3) produces shifts to lower fields in all the signals of the 1H NMR spectrum, being more remarkable for those protons that are closer to the β -diketone moiety. As expected, the H^2 is not present due to the loss of the enolic proton. For $BDMC$, the displacement and shape of the signals from the phenol groups (H^7 in figure 3) are very sensitive to the solvents and intermolecular interactions, giving as a result a smaller and broader signal for the $BDMCBF_2$ system than for $BDMC$.

Table 1. Assignment and multiplicity of the signals observed in the ^1H NMR spectra of the studied CCMoids.


	H ¹	H ²	H ³	H ⁴	H ⁵	H ⁶	H ⁷	H ⁸	H ⁹	Substituents
BDMC	6.05 (s)	16.39 (s)	6.70 (d)	7.55 (d)	7.58 (d)	6.83 (d)	-	-	-	10.06 (s) (HO-)
BDMCBF₂	6.46 (s)	-	6.97 (d)	7.92 (d)	7.74 (d)	6.87 (d)	-	-	-	10.46 (s) (HO-)
BODMC	6.08 (s)	16.40 (s)	6.58 (d)	7.47 (d)	7.09 (s)	7.03 (d)	6.79 (d)	-	-	9.66/9.20 (s)/(s) (HO-)
3pyCCMoid	6.22 (s)	15.88 (s)	7.13 (d)	7.70 (d)	8.91 (s)	8.59 (dd)	8.32 (d)	7.48 (dd)	-	-
3pyCCMoid BF₂	6.7 (s)	-	7.43 (d)	8.13 (d)	9.04 (s)	8.68 (dd)	8.2 (d)	7.56 (dd)	-	-
2-thpL CCMoid	6.00 (s)	16.15 (s)	6.37 (d)	6.86 (dd)	7.40 (dd)	7.63 (d)	7.31 (d)	7.13 (t)	7.33 (d)	-
2-thpL CCMoidBF₂	6.48 (s)	-	6.57 (d)	7.0 (dd)	7.59 (dd)	7.59 (d)	7.77 (d)	7.18 (t)	7.45 (d)	-
BOHCCMoid	6.22 (s)	16.4 (s)	7.0 (d)	7.65 (d)	7.69 (d)	7.84 (d)	-	-	-	8.17 (s) ((HO) ₂ -B)
BOHCCMoid BF₂	6.69 (s)	-	7.31 (d)	8.15 (d)	7.86 (m)	7.86 (m)	-	-	-	8.25 (s) ((HO) ₂ -B)

The signals of the rest of studied CCMoids were assigned taking into account tautomeric features and disposition of the skeleton, as well as functionality of the aromatic sides (table 1). The observed displacements matched with the values found in the literature, experimental and from simulations. The most complex spectra were those corresponding to the CCMoids with the longest skeletons, due to the accumulation of signals in the aromatic region (between 6-9 ppm). It is important to highlight the absence of impurities in all the studied species, especially considering the simple purification processes carried out for BDMC, BDMCBF₂, BODMC, 3pyCCMoid and BOHCCMoidBF₂, which were only washed with the used solvent for the synthesis and/or recrystallized using hot solvent.

As it is shown in figure 3 and mentioned above, for all the CCMoids studied in this doctoral thesis, the keto-enol form was the only one observed in the ¹H NMR spectra, with total absence of the diketo form. The chemical shifts observed for the aromatic groups at the terminal positions of the CCMoids agree well with the electron donating (phenol and thiophene groups)³⁸ or electron withdrawing (pyridine and neutral boronic acid)³⁹ nature of the different substituents.⁴⁰ This is obvious in the displacement of the protons within these aromatic groups, although differences can be observed in H¹, H², H³, H⁴ protons too, because of the CCMoids conjugated structure. Taking as an example the aromatic protons of the free CCMoids closer to the substituents, H⁶ (those in *ortho*-position, H⁷ for 2-thphLCCMoid), the CCMoids with the lowest displacements are those with electro-donating substituents, BDMC (6.83 ppm) and BODMC (7.03 ppm) followed by 2-thphLCCMoid (7.31 ppm). The electro-withdrawing groups promote signals at low field, being higher for 3pyCCMoid (8.59 ppm) than for BOHCCMoid (7.84 ppm). The same effect, but attenuated, can be observed in the displacement sequence for H¹: BDMC (6.05 ppm) < BODMC (6.08 ppm) < 2-thphLCCMoid (6.00 ppm) < 3pyCCMoid (6.22 ppm) = BOHCCMoid (6.22 ppm).

As for BDMCBF₂, the coordination of the boron specie produces a displacement to low fields of all the signals. In this case, the more affected signals are the closest to the β-diketone moiety, specially H¹ that is shifted in all the cases 0.3-0.5 ppm comparing with the free CCMoid. The coordination of BF₂ triggers the most remarkable shifts of the double bonds, as it can be seen in figure 3, where the signals of H⁴ (double bond proton) and H⁵ (aromatic proton) appear superimposed in BDMC and perfectly separated in BDMCBF₂.

Related to the double bonds, even in the CCMoids with the longest skeletons, 2-thphLCCMoid and 2-thphLCCMoidBF₂, in solution no traces of the Z isomers were observed as all the doublets present big J values.

3.2. ^{13}C -NMR

The spectra of 2-thphLCCMoid and 2-thphLCCMoidBF₂ are shown in figure 5 to exemplify the ^{13}C -NMR signals that can be found in the spectra of both families of compounds, under the absence of presence of coordination to BF₂ units.

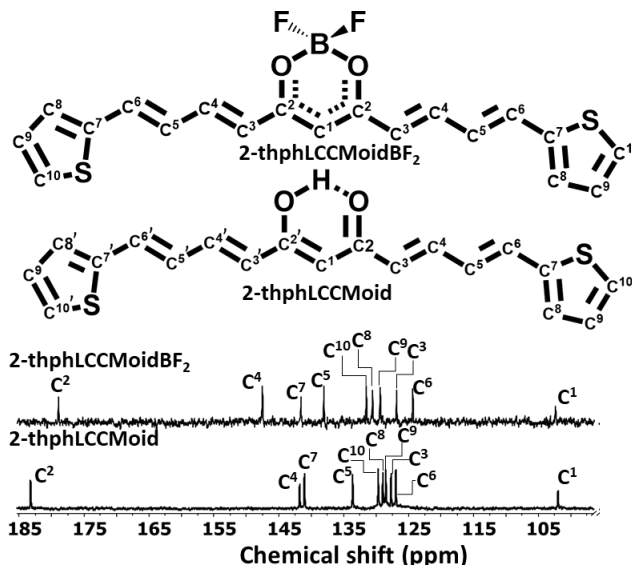


Figure 5. ^{13}C NMR spectra and signals assignment of 2-thphLCCMoid (bottom) and 2-thphLCCMoidBF₂ (top).

All the signals appear in the 100 to 200 ppm window. The signal that corresponds to the central carbon atom (C¹) appears at the highest field, around 100 ppm (102.0 ppm for 2-thphLCCMoid and 102.4 ppm for 2-thphLCCMoidBF₂). It is the less intense, comparing with the others because is the only signal that corresponds to only one C atom. This displacement is indicative of the enol form, as in the diketo form the central carbon should appear around 60 ppm. This is clearly different from the ^{13}C -NMR of the acac molecule, where keto and enol forms can be observed.⁴¹ In the 2-thphLCCMoid, the enol form makes the C atoms of both halves of the molecule no symmetric (name as C^x and C^{x'} in figure 5) but in the spectra only one signal for both C atoms is observed and are assigned in figure 5 as C^x. This way, the signals of C² are in the carbonyl region (180-200 ppm) being 182.9 ppm for the free CCMoid and 178.9 ppm for the coordinated one. The rest of signals corresponding to the double bonds in the chain and aromatic carbons from the arms of the 2-thphLCCMoid appear between 126 and 141 ppm. Here, the coordination of BF₂ produces a smaller effect than in the ^1H -NMR spectrum, with shifts of few ppm to lower fields. C₂ shows the highest displacements of approximately 4 ppm, less than for the CCMoidBF₂ (figure 5)

Table 2. Assignment of the signals observed in the ^{13}C NMR spectra of the CCMoids

	C^1	$\text{C}^2/\text{C}^{2'}$	$\text{C}^3/\text{C}^{3'}$	$\text{C}^4/\text{C}^{4'}$	$\text{C}^5/\text{C}^{5'}$	$\text{C}^6/\text{C}^{6'}$	$\text{C}^7/\text{C}^{7'}$	$\text{C}^8/\text{C}^{8'}$	$\text{C}^9/\text{C}^{9'}$	$\text{C}^{10}/\text{C}^{10'}$
BDMC	100.9	183.2	120.8	140.3	125.8	130.3	115.9	159.8	-	-
BDMCBF₂	101.7	179.29	118.06	147.09	125.9	132.5	116.7	162.1	-	-
BODMC	100.9	183.1	121.9	140.8	127.7	126.5	115.9	147.8	145.1	114.5
3pyCCMoid	102.3	182.9	125.98	134.4	130.8	149.8	150.9	123.9	137.3	-
3pyCCMoidBF₂	103.2	180.8	124.7	136.12	130.4	151.5	152.6	123.70	144.4	-
2-thpL CCMoid	102	182.93	126.7	141.85	132.7	126.6	140.3	128.5	127.3	128.1
2-thpL CCMoidBF₂	102.4	178.95	126.9	147.55	138.1	124.38	141.6	131.6	129.4	130.6
BOHCCMBF₂	101.2	180.62	128.9	139.02	135.2	135.8	122.2	147.38		

The rest of CCMoids (table 2, and spectra in appendix I) display similar displacements, although with different number of signals, depending on the substituents (structures of table 2). Lateral substituents do not have strong effects in the displacements of the C atoms, except the ones directly bonded to the heteroatoms, such as C⁸ in BDMC, BDMCBF₂, BODMC (together with C⁷) and BOHCCMoid or C⁶ and C⁷ in 3pyCCMoid and 3pyCCMoidBF₂ and C⁷ and C¹⁰ in 2-thphLCCMoid and 2-thphLCCMoidBF₂, respectively.

3.3. Infrared spectroscopy (FTIR-ATR)

The studied CCMoids display similar infrared features, presenting the highest variations upon coordination or due to the functional groups in the arms of the CCMoid structures. Figure 6 shows as examples the spectra of 3pyCCMoid and 3pyCCMoidBF₂, respectively. The intense band observed at 1626 cm⁻¹ for the carbonyl moiety (in blue figure 6; ν C=O in table 3) shifts few cm⁻¹ to higher wavenumbers for the 3pyCCMoidBF₂ (in orange figure 6). Moreover, in the free 3pyCCMoid two signals are assigned to the enol form, ν O-H in purple as a broad band between 3500-3200 cm⁻¹ and δ COH_{enol} as a sharp medium band at 1571 cm⁻¹ in green, correspondingly. These two vibrational bands disappear upon coordination of the 3pyCCMoid to the BF₂.

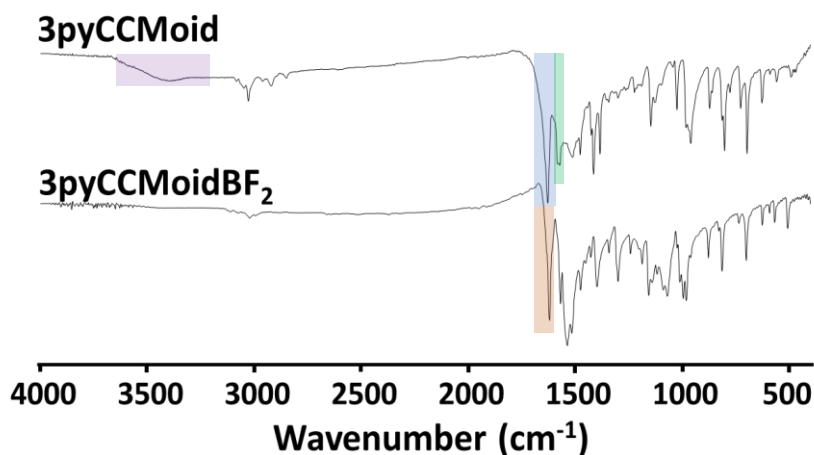


Figure 6. FTIR-ATR spectra of 3pyCCMoid and 3pyCCMoidBF₂.

Table 3. Principal IR bands of the CCMoids between 4000 and 1200 cm^{-1} .

BDMC cm^{-1}	BDMC BF ₂ cm^{-1}	BODMC cm^{-1}	3py CCMoid cm^{-1}	3py CCMoidBF ₂ cm^{-1}	2-thpL CCMoid cm^{-1}	2-thpL CCMoidBF ₂ cm^{-1}	BOH CCMoid cm^{-1}	BOH CCMoidBF ₂ cm^{-1}	Assignment
		3482							vO-H
3493-2890	3384	3374-2890	3500-3200	3020	3200	3125	3368	3500-3090	vO-H
1619	1598	1638/1628	1626	1619	1598	1589	1614	1622	vC=O vC=C
1598	1581	1597	1579	1567	1540		1555		vCC _{Ph}
1562		1571	1571		1526		1532	1556 1540	$\delta\text{COH}_{\text{enol}}$
1557	1543				1520				δCOH
1510	1495	1509	1509	1515		1499	1502	1506	vC=O, δCCC ,
1506	1469	1474	1476	1474		1489			$\delta\text{CC=O}$
1431	1444	1434	1418 1413	1451 1406	1415	1416	1405	1409	$\delta\text{CCC}_{\text{Ph}}$, $\delta\text{CCH}_{\text{Ph}}$, δCOH , $\delta\text{C=CH}$
1373	1374	1385	1383	1397	1363	1390	1373	1381	δCOH
1371		1351	1341	1342			1370	1363	$\delta\text{COH}_{\text{enol}}$
1338 1323	1331 1319	1306	1295	1298	1311	1315	1322	1327	vC=C, $\delta\text{CCH}_{\text{Ph}}$
1288	1275	1286			1277	1278	1299	1270	$\delta\text{C=CH}$
1268		1261					1265	1267	δCOH , δCCC , δCOH
1246	1238	1245		1240	1242	1244			δCOH
1234		1220	1221		1210				$\delta\text{COH}_{\text{enol}}$
1194	1222	1197 1184		1193 1186		1195	1212	1202	δCCH

Table 4. Principal IR bands of the CCMoids between 1200 and 400 cm^{-1} .

BDMC cm^{-1}	BDMC BF ₂ cm^{-1}	BODMC cm^{-1}	3py CCMoid cm^{-1}	3py CCMoidBF ₂ cm^{-1}	2-thphL CCMoid cm^{-1}	2-thphL CCMoidBF ₂ cm^{-1}	BOH CCMoid cm^{-1}	BOH CCMoidBF ₂ cm^{-1}	Assignment
1168	1171	1163		1156		1179	1156	1166/ 1157	$\delta\text{CCH}_{\text{Ph}}$
1138 1105	1143 1102	1140 1112	1145 1122	1138 1116	1119	1120 1095	1109	1125	δCCH
1009 985 976	1042 1006 970	988 974	973	1087 1068 1023 999 995 980	1041 981	1042 981	1036 1015 996 985 975	1058 1001 985 980	γCCH
954	951	952 941	958	960	958		954	957	vCO vCOH
933 922 877 867 828 792 734 706	931 871 823 819 788 742 706 682 639	930 870 840 819 808 779 768 736 606	870 858 810 801 774 726 695 624	876 877 812 733 700 624	880 846 779 754 690 632 600	930 910 881 798 748 730 710 635 619 600	908 891 875 848 827	884 830 751 715 624 506	$\delta\text{CCH}_{\text{Ph}}, \delta\text{CCC}_{\text{Ph}}$ $\gamma\text{CCH}_{\text{Ph}}, \gamma\text{CCH},$ $\gamma\text{CCC}, \gamma\text{COH}$

The same behaviour was observed for the rest of the studied CCMoids, observing intense bands for the ν O-H in BDMC, BDMCBF₂, BODMC, BOHCCMoid and BOHCCMoidBF₂, as they contain extra OH groups in the lateral substituents. The assignments given in tables 3 and 4 for the remainder bands of 3pyCCMoid and 3pyCCMoidBF₂ and the other CCMoids was performed by comparing them with the work from Kolev *et al.*⁴² The spectrum of BODMC displays a signal at 3483 cm⁻¹ related to the ν O-H vibration. Its sharp shape (appendix I) indicates a lack of interaction with other molecules.⁴³ The vibrations related to the lateral substituents of the rest of CCMoids, as pyridine, thiophene or boronic acid, are also visible in the spectra. Based on bibliography, C=N of pyridine appears between 1660 and 1480 cm⁻¹,⁴⁴ boronic acid in the region of 900 to 1000 cm⁻¹ has two signals corresponding to ν B-O and ρ O-H⁴⁵, and the ν C-S-C from thiophene appears at 594 cm⁻¹.⁴⁶ The number of signals that all the CCMoids present difficult proper assignments of the rest of signals.

3.4. Mass spectroscopy

The mass spectra of natural CCMoids have been extensively studied, mainly towards their identification in turmeric and in another plant extracts^{47,48} Of special relevance is the work carried out in 2006 by H. Jiang *et al.*,⁴⁹ presenting a full structural characterization of natural CCMoids that included fragments assignment for the different m/z , as well as the fragmentation routes. This information, together with the fragmentation route proposed by the authors, is shown in figure 7 and was used here for the identification of the fragments found in the rest of CCMoids spectra. For example, the authors of the above work established that the spectra of the natural CCMoid BDMC (MW 308.10) appears at 307.32 (m/z [M-1]), resulting from the loss of one proton with the corresponding isotopic distribution expected for this molecule. We observed the same fragmentation already described for BDMC.

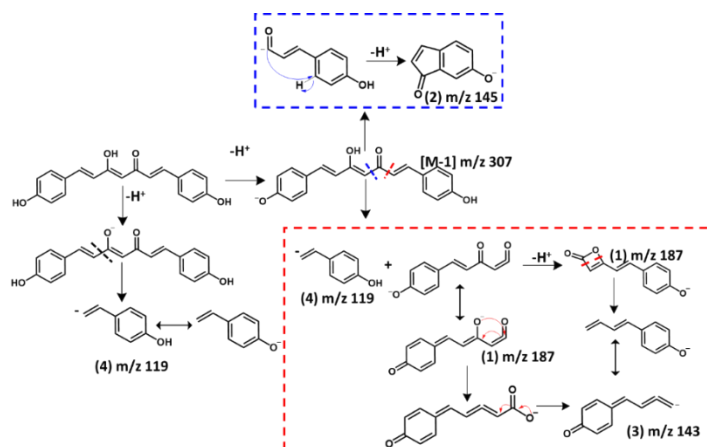
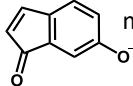
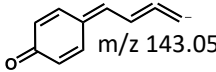
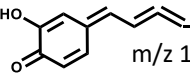
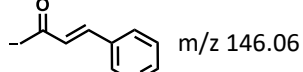
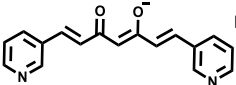
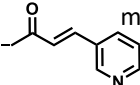
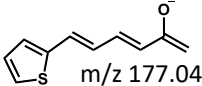
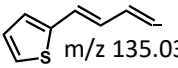
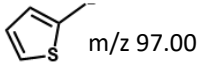
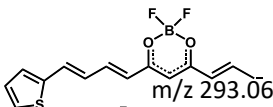
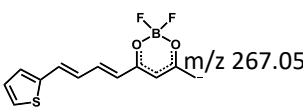
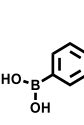
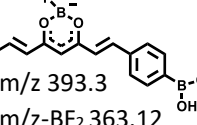
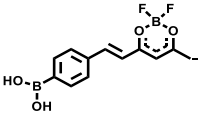
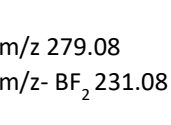


Figure 7. Fragmentation route of BDMC (adapted from the article of H. Jiang *et al.*).⁴⁹

Table 5. Molecular weight (MW), molecular peak ([M-1]), list of other m/z shown in each spectrum, structure, and theoretical m/z of some found fragments.

CCMOID	MW	[M-1]	PEAK LIST M/Z	POSSIBLE FRAGMENTS AND THEORETICAL M/Z
BDMCBF₂	356.10	354.85	402.96, 334.87, 302.13, 288.80, 196.95, 144.8, 143.06, 86.85	 m/z 145.03  m/z 143.05
BODMC	340.09	338.88	702.30, 549.52, 498.60, 294.87, 278.90, 210.89, 176.89, 167.79, 158.59,	 m/z 159.06
3PYCCMOID	278.11	277.1	555.17, 421.54, 380.25 318.62, 243.40, 223.46, 170.86, 146.42, 94.76	 m/z 146.06
3PYCCMOIDBF₂	326.10	325.9	648.83, 600.78, 393.82, 367.03, 340.38, 276.92, 242.94, 172.49, 63.73	 m/z 277.10  m/z 146.06
2-THPHLCCMOID	340.06	338.41	290.01, 240.04, 203.00, 176.78, 135.04, 96.7	 m/z 177.04  m/z 135.03  m/z 97.00
2-THPH LCCMOIDBF₂	388.06	387.78	420.82, 413.84, 338.69, 292.8, 266.86, 86.96	 m/z 293.06  m/z 267.05
BOHCCMOIDBF₂	411.72	411.82	392.62, 363.03, 278.91, 231.13	 m/z 393.3  m/z-BF ₂ 363.12  m/z 279.08  m/z- BF ₂ 231.08

In this doctoral thesis, the mass spectra of the different CCMoids were acquired in negative and positive modes, but only the negative ones are presented (appendix I), as better-quality signals were obtained. This was expected taking into account the straightforward deprotonation of the β -diketone group, as well as other functional groups present in the arms of the CCMoids (phenol, boronic acids, etc.), thus, facilitating the stabilization of negative charged fragments. In almost all the spectra, the characteristic m/z $[m-1]$ molecular peak was easy to allocate (table 5), showing the expected isotopic distribution (appendix I) as well. Moreover, some fragments were also identified (table 5), demonstrating again the formation of the desired molecule and similar fragmentation routes as the published one. An exception was the spectra of BOHCCMoidBF₂ where it was not possible to detect the expected molecular peak, although some fragments corresponding to this CCMoid could be identified (table 5). In the case of the BOHCCMoid spectrum, none of the signals could be assigned to the CCMoid or fragments of it, and the results could not be discussed further

3.5. Crystal structures: powder and single crystal X-ray diffraction (XRD)

The elucidation of the compounds structure by single-crystal XRD techniques allows to have insight on the conformation of the molecules in the solid state and to attain further information about supramolecular interactions among them. Moreover, powder XRD characterization is used to determine the crystallinity and purity of the bulk powder of known systems. The two types of analysis regarding the different structures obtained through the formation of different solvates (complex resulting from the combination of solvent molecules and the compound⁵⁰) is interesting for future applications, since depending on their packing and involved solvents they can have different properties, such as thermal stability, or different solubility. This is of special interest in the pharmaceutical industry, where these attributes are relevant in the processability and administration of drugs.⁵⁰

3.5.1. BDMC

The crystallographic data of BDMC has been extensively reported in the literature, with six entrances of different crystal structures in the Cambridge crystallographic data centre (CCDC). In the decade of 1980s, Tonnensen *et al.*⁵¹ published a series of articles called, "Structural studies of curcuminoids", in which crystals of BDMC were prepared in MeOH, being this the first structure published of a CCMoid aside of CCM. Later, Kasai *et al.*⁵² obtained crystals of this system interacting with molecules of H₂O. Having into account the possibility of precipitating different BDMC solvates, Yuan *et al.*⁵³ published in 2018 an extended study using nineteen solvents. In six of them, the solvate of the BDMC was observed, including in acetone, dioxane, DMSO and tetrahydrofuran (THF) molecules, joining the one of Tonnensen.⁵¹ The powder XRD patterns of all these solvates, and the one of the BDMC without solvate (figure 8), show how the same

molecule exhibits a variety of patterns that relate to different structural conformations due to the interactions of the molecules among themselves or with the used solvents. High quality crystals of three of these solvates (BDMC-MeOH, BDMC-IPA and BDMC-ACET, Figures 8 and 9) were obtained, allowing the determination of their structures (figure 9), which were extensively analysed in another work published in 2019 by the same authors.⁵⁴

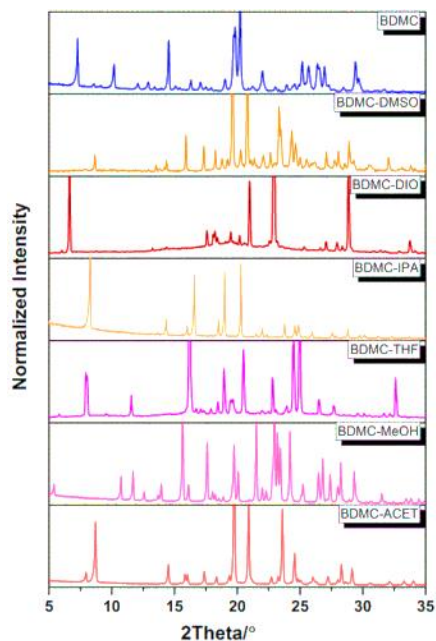


Figure 8. Powder XRD patterns of some BDMC solvates: BDMC-ACET (acetone), -MeOH, THF (tetrahydrofuran), IPA (isopropanol), DIO (1,4-dioxane), DMSO (dimethyl sulfoxide) and pattern of the non-solvated BDMC at the top.⁵³

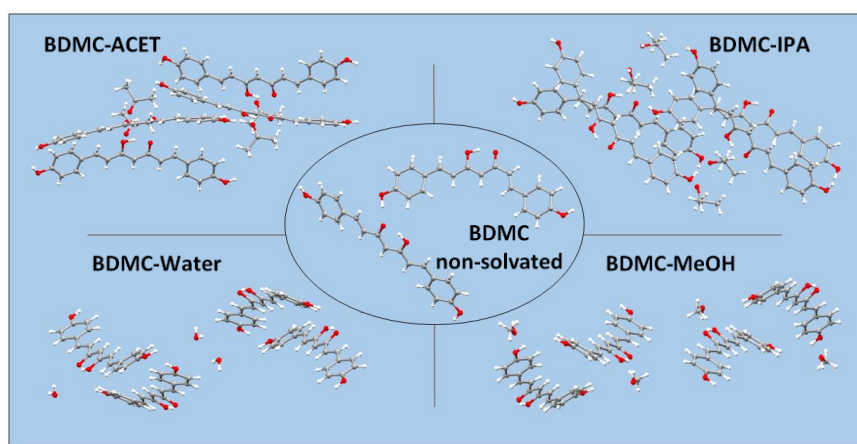


Figure 9. Structures published of the BDMC non solvated and solvated with MeOH, acetone, IPA⁵⁴ and H₂O.⁵²

In this doctoral thesis, a new crystalline solvate of the BDMC molecule was identified by powder XRD diffraction (figure 10, BDMC after synthesis). The solubilization of this phase in EtOH or EtOAc, followed by the complete elimination of the solvent using a rotatory-evaporator or supercritical CO₂, resulted in the non-solvated phase (figure 8 top and 10 top). Therefore, the used synthetic method provides a new reorganization of the BDMC molecules with the solvent (possibly, the employed in the synthesis, EtOAc and H₂O) different from those described before.

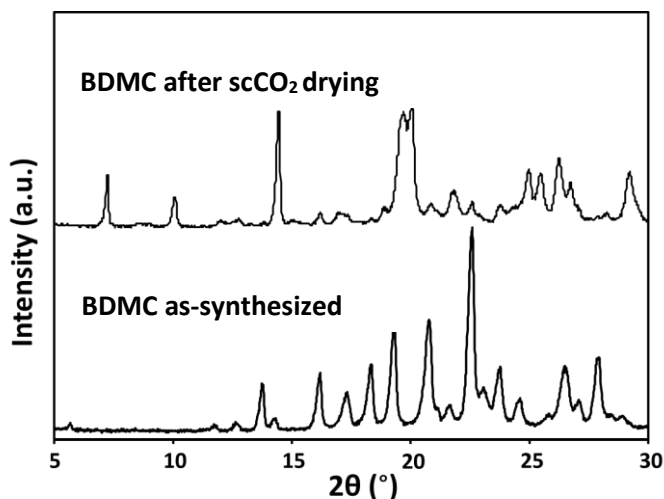


Figure 10. XRD patterns of the BDMC product as-synthesized compared with the same after solvent elimination in scCO₂.

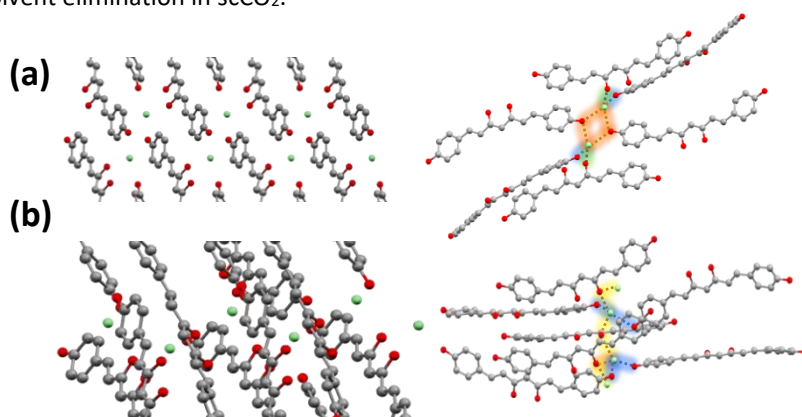


Figure 11. Structures of the BDMC-H₂O solvates obtained by layering crystallization in EtOH/H₂O: (a) cubic crystals, and (b) plates. The H-bonding interaction where a phenol group is forming a bridge are highlighted in orange or in yellow when it is a β-diketone unit. In the cases where these moieties are not forming bridges, the H-bonds are highlighted in blue when phenols are implicated and in green when it is a β-diketone moiety, respectively.

This new phase, obtained directly from the synthesis as a microcrystalline powder could not be resolved by single-crystal XRD, and further efforts to recrystallize the compound gave rise to other phases. In one of these attempts, the structure of the BDMC solvate with incorporated water molecules was obtained as the one published by Kasai *et al.*²⁴ The obtention of this phase is remarkable because Yuan *et al.*²⁵ pointed out the impossibility of replicate their result. In this doctoral thesis, this phase was crystallized by a layering method, solubilizing BDMC in a mixture of EtOH and H₂O. After several weeks, cubic crystals and orange thin plates were properly separated at the bottom of the vials. The cubic crystals corresponded to the BDMC-water structure previously published²⁴, presenting the thin plates a new powder XRD pattern and being possible to elucidate their structure by single-crystal XRD.

This new structure includes water molecules, but they interact with BDMC in a different way than the previous structure described by Kasai *et al.*²⁴, producing, therefore, a different packing, cell parameters and XRD pattern (figures 11 and 12). Kasai *et al.*²⁴ showed that, in the cubic crystals each water molecule (in green, figure 9a) is interacting with another water molecule by means of two phenol groups (orange lines, figure 11a) and to other two BDMC molecules through one β -diketone (green lines, figure 11a) and one phenol (blue lines, figure 11a) groups. Regarding the plate crystals, each water (in green, figure 11b) is connected to other two through bridges formed by β -diketone residues (yellow lines, figure 11b) and other two BDMC molecules by their phenol groups (blue lines, figure 11b).

	Orthohedral	Plates
Space group	P2 ₁ /c	Pbca
a(Å)	7	41
b(Å)	7	11
c(Å)	31	7
α°	90	90
β°	92	90
γ°	90	90
Cell volume (Å³)	1597.64	3201.3

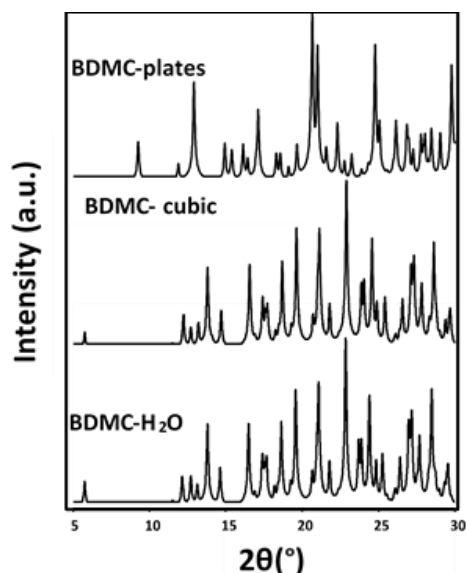


Figure 12. XRD patterns, simulated from single crystal structural data, of the BDMC structures precipitated in this doctoral thesis and of the H₂O solvates published by Kasai *et al.*²⁴ (BDMC-H₂O) together with the two obtained by us (BDMC-cubic and BDMC-plates).

3.5.2. 3pyCCMoid

Crystals of the 3pyCCMoid were previously resolved in our team by recrystallizing it in hot ACN (figure 13).⁵⁵ This structure does not incorporate solvent molecules, in contrast with what it happens in the structure of the BDMC. Only weak intermolecular interactions between the pyridine and β -diketone groups were observed.

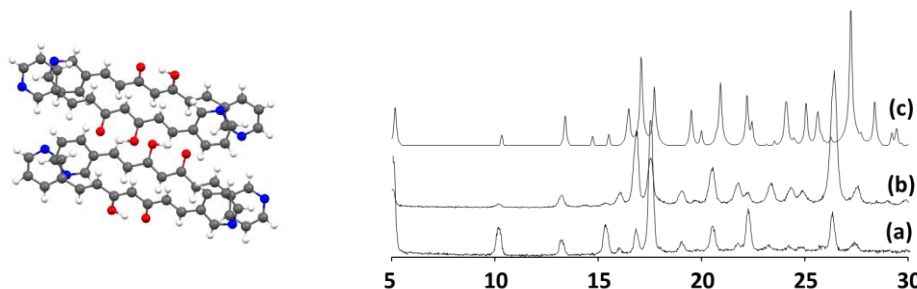


Figure 13. Structure and package of 3pyCCMoid crystals and XRD patterns of 3pyCCMoid: (a) after the synthesis, (b) after drying in $scCO_2$, and (c) simulated from the single-crystal structure.

The powder XRD patterns obtained for the as-synthesized sample and after $scCO_2$ treatment of the 3pyCCMoid were identical to the simulated diffractogram from the single-crystal structural data (figure 13), indicating that this CCMoid adopts always a disposition without any solvent in the structure. This seems to be an example of a CCMoid forming crystals by only establishing interactions between molecules of CCMoid, although to discard the possibility of forming solvates would require a more extensive study with different solvents.

3.5.3. BODMC

The crystallographic study of the BDMC system indicates the key role that the phenol group plays in the formation of solvates. Hence, the study of the solvation capacity of the BODMC molecules was carried out with the premise that the presence of two hydroxyl groups in each aromatic ring could make this compound to act in a similar way than the BDMC. Comparing to BDMC, studies with BODMC are scarce. To date, no information regarding its structure has been published in the CCDC. For the preparation of different solvates, the method of Yuan *et al.*²⁵ was here followed. Five organic solvents were chosen based on the solubility of BODMC: EtOAc, MeOH, EtOH, acetone and ACN. A saturated solution of the CCMoid in each one of these solvents (approx. 2 mL) was prepared and then heated, filtered while it was hot and placed in the fridge to allow the formation of crystals. Additionally, the powder XRD of the solid obtained directly from the synthesis, and the solid dry in $scCO_2$ (in an attempt to obtain the non-solvated specie) were compared with the solvates (figure 14).

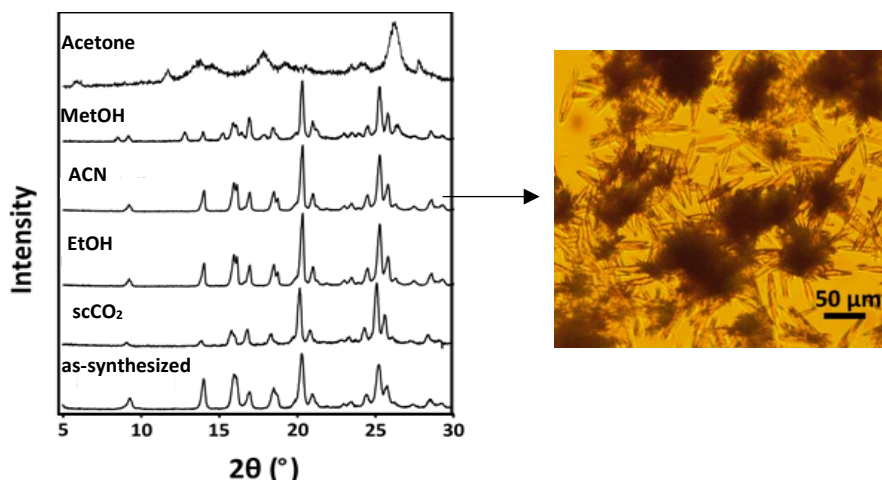


Figure 14. Powder XRD of as-synthesized BODMC and after $scCO_2$ treatment and recrystallized in different solvents and crystals of BODMC obtained in ACN.

All the solids were analysed by powder XRD, displaying the patterns shown in figure 14. The use of EtOAc, MeOH and EtOH solvents provided BODMC microcrystalline materials, while an amorphous powder was obtained in acetone. Relatively large crystals (figure 14 right) were only obtained in ACN but the resolution of the structure was not even possible in this case. The comparison of the XRD patterns shows that, despite of the phenol substituent present in BODMC, the interaction with the solvent molecules seems to be less relevant. This was extracted from the similarities among the powder XRD patterns of the as-synthesized powder, treated with $scCO_2$ and recrystallized in the different solvents. In all cases, the diffractograms show the same features (phase 1), implying that the presence of different solvents does not affect the packaging of the molecules. However, in MeOH, the pattern indicates the sum of more than one phase, including phase 1. Unfortunately, the further analysis of their structures remain unknown.

3.5.4. Other CCMoids

Crystals of the rest of CCMoids studied in this doctoral thesis were achieved by recrystallization in hot ACN (3pyCCMoidBF₂ and 2-thpCCMoidLBF₂, figures 15a and 15b, respectively), slow evaporation in DMSO-d₆ (2-thpCCMoidL, figure 13c) or layering in ACN/H₂O (2-thpCCMoidL, figure 13d). Unfortunately, crystals of not enough quality were accomplished.

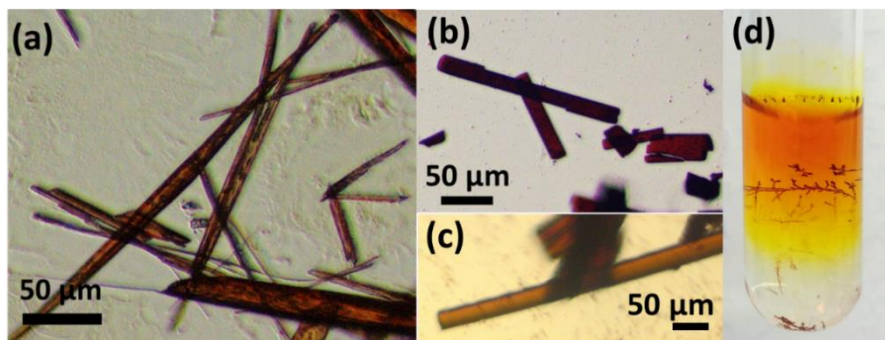


Figure 15. Crystals of: (a) 3pyCCMoidBF₂, (b) 2-thpCCMoidLBF₂ (c) and (d) 2-thpLCCMoid.

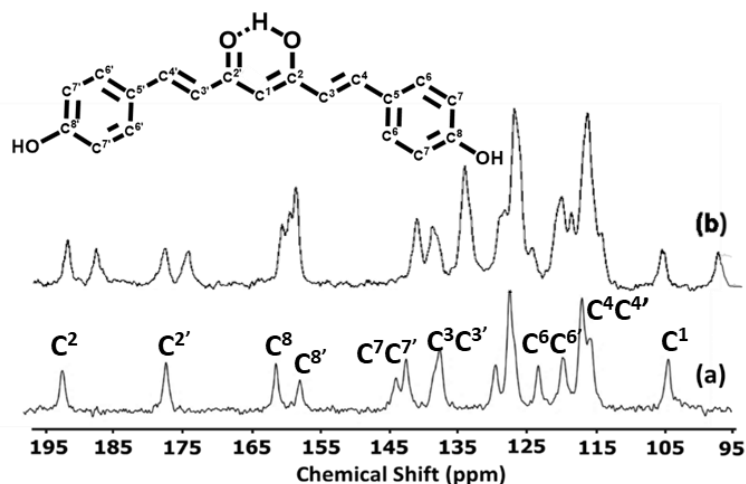
3.6. Solid state NMR (CPMAS¹³C)

CPMAS¹³C characterization was performed only for BDMC due to possibility of compare the results of this technique with the structures published and try to have more information about the new unknown structure obtained in our synthesis. Solid-state ¹³C NMR provides relevant information regarding conformations and intermolecular interactions, since it is very sensitive to changes in the environment that surround molecules. Moreover, this analysis can also give some clues about the number of conformations or different environments in the sample. The CPMAS¹³C spectra of the as-synthesized BDMC (figure 16a) was compared with the sample recovered after drying in scCO₂ (figure 16b) to study the influence of conformational features.

In the solid state ¹³C NMR, the signals appear in the same region than in solution (table 2), but as this technique is sensible to the different environments of each C atom the bands are much broader.

In solution ¹H NMR, both samples, the as-synthesized BDMC and the one dried with scCO₂, show identical features and purity. Instead, figure 16 shows that the CPMAS¹³C displays a duplication of the signals in the case of the scCO₂. The presence of this splitting only in the solid state proves the conformational nature of this phenomena. In the non-solvated BDMC structure published by Yuan *et al.*⁴⁹ (figure 9), two conformations of the BDMC molecule can be observed. In that case, one molecule adopts a complete extended structure, while the other presents half of the molecule rotated. The molecules adopt this disposition because in the absence of solvent the intermolecular interactions that stabilize the crystals are those from the BDMC themselves, showing that in the complete extended structures they cannot interact in an effective manner. This rotation produces the approximation of the phenol group of one molecule to the β-diketone of the other, thus creating a network of H-bonds between them. This type of interactions happens within pairs of molecules, so half of them adopt the rotated disposition, generating one group of shifts in the ¹³C spectrum, and the other half remain in their extended version, generating the other half of the set signals. In the as-synthesized solid, the presence of one group of signals indicates that only one

conformation is present, possibly the extended form, as it happens in the rest of published BDMC structures (figure 9).



	Chemical shift [ppm]					
	C ²	C ^{2'}	C ⁸	C ^{8'}	C ¹	Other C atoms
BDMC-S	191.89	176.80	160.79	157.32	103.69	At least 9 peaks 143.26-115.01
BDMC-scCO₂	192.49	178.29	161.27	160.14	105.96	At least 12 peaks 141.65-114.80
	188.35	174.90	160.14	159.28	97.80	

Figure 16. CPMAS¹³C of BDMC: (a) as-synthesized (BDMC-S), and (b) after scCO₂ drying (BDMC-scCO₂).

The assignment of the ¹³C NMR shifts in figure 16 was performed by comparison with the published data regarding CCM.⁵⁶ The displacements observed are the same than in solution, and the enol form is again the only one observed (signal of C¹ around 101 ppm). In the solid state, all the CCMoids display the enol-keto form that makes the molecule not completely symmetric, indicated as C^x and C^{x'} in the figure. However, in solution, the electronic distribution in the keto-enol moiety and the conjugated nature of the skeleton and arms shows a symmetric pattern for the two halves of the molecules, reducing the number of signals.

In the CPMAS¹³C spectra of the “as-synthesized” BDMC, the signal related to the methine carbon (C¹) is a singlet, around 100 ppm, like what it happens in solution. The differences observed due to the keto-enol form are clearly visible in the carbonyl region (176-192 ppm), with the two C² and C^{2'} now well-differentiated. In addition, the signals of the C⁸ and C^{8'} attached to the hydroxyl groups, appear repeated as well (157-160 ppm). As it has been explained above, in the case of the spectrum of the non-solvated BDMC (BDMC-scCO₂) the number of signals is even higher, due to the duplication of the signals

produced by the existence of two conformations of the molecule. In that way, for example, four signals are now observed in the carbonyl region: two for the C=O (C^2) and the OH-C=C ($C^{2'}$) of one conformer and of the same number for the other conformer. The same occurs with the C atoms related to the phenol groups (C^8 and $C^{8'}$) where also two signals are observed for the C^1 atom. The rest of the signals, from the diarylheptanoid skeleton and additional aromatic groups, fall in the 115-145 ppm region, where it is difficult to discriminate among them, because of their overlap and split. Considering the CCM literature and using the liquid spectrum, they may follow a $C^7/C^{7'}$ – $C^3/C^{3'}$ – $C^5/C^{5'}$ – $C^6/C^{6'}$ – $C^4/C^{4'}$ order, from highest to lowest field in the mentioned range.

3.7. Ultraviolet-visible absorption spectroscopy and fluorescence emission

Due to the intense colour of CCMoids and their use as dyes, the absorption features of these compounds have been extensively analysed by UV-Vis spectroscopy, as well as their fluorescence emissions.⁵⁷

In general, CCM and CCMoids display a typical and broad band centred approximately at 350-450 nm in the UV-visible region that relates to the CCMoid skeleton. In addition, several studies have shown the remarkable effect of solvent in the shift of such band; being all CCMoids solvochromic systems.⁵⁸ For example, the UV-Vis absorption and emission spectra of the BDMC were studied in a set of solvents and discussed by Tonnensen *et al.*,⁵⁹ in one of the articles of the series “Studies on Curcumin and Curcuminoids”. In this work, the authors observed a shift to the red region in the fingerprint absorption bands, while increasing the polarity of the solvents (figure 17). The same tendency was described for CCM.⁶⁰ In addition to the maximum wavelength, the spectrum of BDMC also shows an additional band of lower intensity in the region between 250 and 270 nm related to the phenol groups. The spectrum of the BOCMC in MeOH was measured by John *et al.*⁶¹ that attributed similar bands to those of BDMC in the $n \rightarrow \pi^*$ (358–445 nm) and $\pi \rightarrow \pi^*$ (258–265 nm) transitions. As far as we know, for the rest of CCMoids presented in this doctoral thesis no previous optical studies have been published.

Solvent	λ_{Abs} (nm)	λ_{Fl} (nm)
Cyclohexane	348, 362	531, 473, 447
CHCl_3	411	486
EtOAc	411	482
Acetone	413	486
ACN	411	490
DMF	424	506
DMSO	425	515
IPA	420	513
EtOH	418	525
MeOH	415	529
Ethylene glycol	423	541

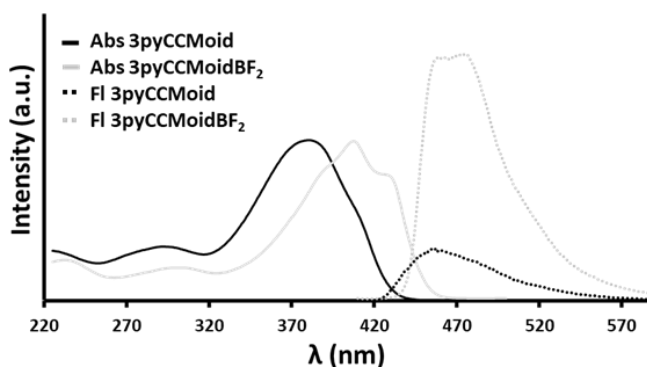


Figure 17. Maximum absorbance and fluorescent emission values of BDMC in different solvents⁵⁹ (top). Absorption spectra of 3pyCCMoid (black line) and 3pyCCMoidBF₂ (grey line) in MeOH and their corresponding fluorescence emission spectra (dotted black and grey lines, down).

Here, to perform a comparative study of the studied CCMoids, the UV-Vis spectra of these molecules were measured in three organic solvents, from low to high polarity: EtOAc < DMSO < MeOH. Moreover, the spectra of these compounds in solid state were also acquired to minimise the effects of the solvent in the absorption. For the latter, pellets with approximately 0.1 mg of the CCMoid and 100 mg of KBr were prepared and characterized using an integrating sphere accessory. The fluorescent spectra were measured exclusively in MeOH, using as excitation the wavelength of maximum absorption in this solvent. In figure 17 down, the absorption spectra of 3pyCCMoid

(black line) and 3pyCCMoidBF₂ (grey line) in MeOH are shown, as well as those of their corresponding fluorescence emissions (dotted lines).

In general, a similar tendency is observed for all the systems. Hence, the highest wavelength values are found in DMSO and the lowest in EtOAc; however the spectra show that the shifts of the bands do not follow the polarity trend, having in MeOH maxima values that were similar to those obtain in EtOAc or intermediate between EtOAc and DMSO. It is important to stress here that for 3pyCCMoid and BOHCCMBF₂ the use of different solvents had virtually no effect on the maximum of absorption bands (table 6). Finally, the absorption value for 2-thphLCCMoid was higher in MeOH than in DMSO, not following the general trend mentioned above. Related with the results in the solid state, all CCMoids present similar energy absorption values as their analogous in DMSO.

Table 6. Wavelength numbers, taken from the maximum absorption of the studied CCMoids, measured in different solvents and in the solid state. *Bibliographic data.⁵⁶

	λ_{\max}				
	Absorption				Fluorencence
	EtOAc	MeOH	DMSO	Solid	MeOH
BDMC	411	415	425	422	529*
BDMCBF₂	482	486	508	478	571
BODMC	416	428	439	422	530
3pyCCMoid	381	380	393	393	474
3pyCCMoidBF₂	411	420	423	420	478
2-thphLCCMoid	425	446	439	459	565
2-thphLCCMoidBF₂	508	518	540	476	620
BOHCCMoid	-	400	443	445.5	-
BOHCCMoidBF₂	431.5	426.5	426.5	437.5	498

In general, the coordination of BF₂ produced a shift to the red region, both, in absorption and fluorescence. This way, a bathochromic displacement is observed when BDMC coordinates to BF₂ units.^{2,3} Moreover, the CCMoidBF₂ systems usually have higher intensity fluorescent bands than the free CCMoids, and this is a common trend observed with other CCMoids in the literature when they coordinate to boron species.³⁶ The wavelength of maximum absorbance and fluorescence emissions of the rest of CCMoids are shown in table 6, and the complete spectra in appendix I.

Despite most CCMoids are soluble in polar solvents, their solubility in H₂O is negligible, being this one of the principal problems to use them in biological applications.⁶² The same behaviour was observed for the CCMoids studied in this doctoral thesis, except for 3pyCCMoid that was slightly soluble in H₂O (figure 18). For this, a saturated solution of 3pyCCMoid in water was sonicated and filtered before recording the spectrum (figure

18). Within the recording window, in this case, the typical absorption bands appear now at *ca.* 370 and 280 nm. Comparing with data from the other studied solvents, the use of H₂O promotes the hypsochromic shift of the CCMoid band, displaying again that the solvochromic behaviour of this molecule, as the rest, do not go in parallel with the polarity of the solvents. Regarding further studies of these materials, this result opens the possibility of using 3pyCCMoid towards biological applications.

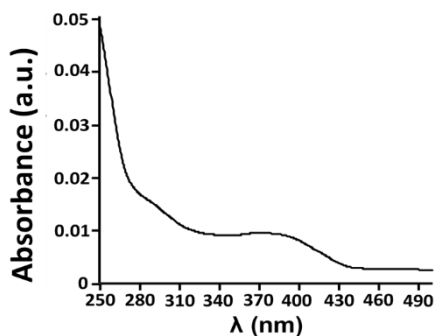


Figure 18. UV-Vis absorption spectrum of 3pyCCMoid in H₂O.

3.8. Electrochemistry

Electrochemistry measurements were performed for all the systems to analyse the redox behaviour of the synthesized CCMoids, as well as to provide information of their HOMO-LUMO energy gap. CCMoids are electroactive species that have been extensively studied with voltamperometric techniques. In that sense, some articles used cyclic voltammetry (CV) as an analytic technique for their detection,^{63,64} to study their oxidant capabilities^{65,66} or to get inside on their conductive properties.³⁷

In this work, the electrochemical experiments were carried out in dry extra-pure THF, solvent in which most of the studied CCMoids were soluble. For that, a solution 0.1 M of the electrolyte, tetrabutylammonium hexafluorophosphate (TBAPF₆), and solutions 10⁻³ M of each CCMoid were prepared. A glassy carbon electrode was chosen as the working electrode (WE), while two Pt wires were selected as the counter and reference electrodes (CE and RE), respectively. Ferrocene was used as the internal reference, which was added at the end of each measurement. The experiments were performed under Ar flow, to remove oxygen. A blank of the solution, with only the electrolyte, was also measured previously to any sample. The voltammograms of all the measured CCMoids were corrected establishing as zero the semipotential of ferrocene.

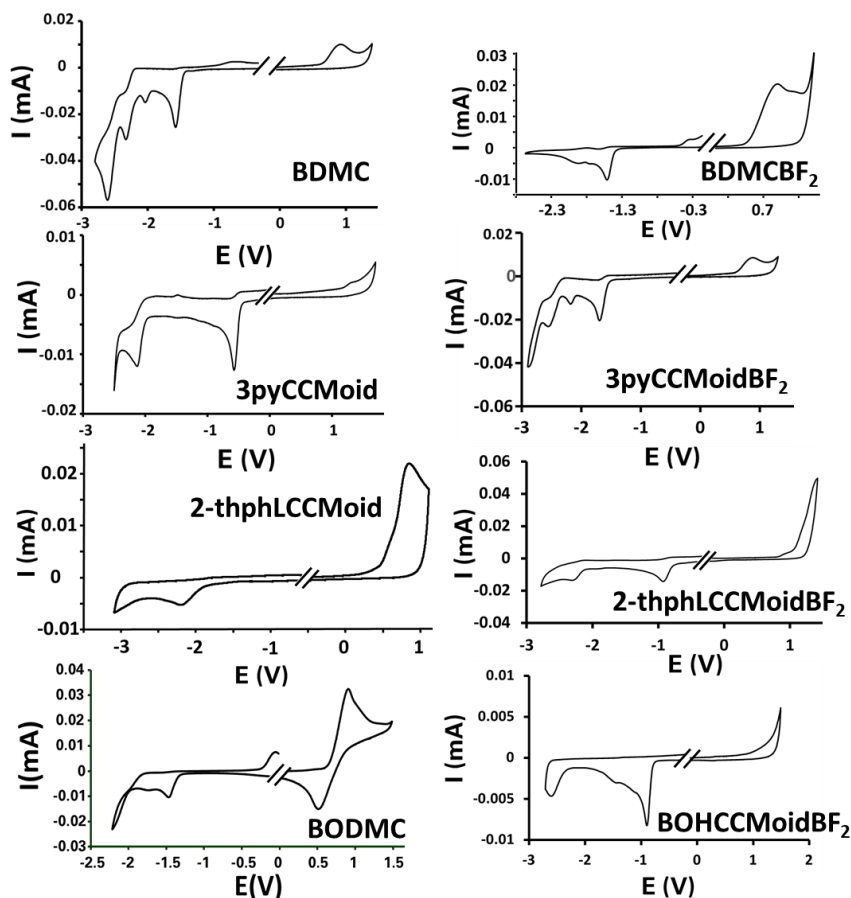


Figure 19. Cyclic voltammograms for all the CCMoids at scan rates of 100 mVs^{-1} .

In all the cases, it was possible to observe the redox activity that corresponds to the oxidation and the reduction processes for each CCMoid (figure 19), except for BOHCCMBF₂ where the oxidation was not visible, being possibly at high potentials outside of the analysed window. Moreover, BOHCCMoid could not be measured because of its low solubility. In general, the voltammograms displayed several reduction processes, all of them irreversible. This means, that under the conditions of the experiments (voltage, temperature, electrodes, and solvent used) the CCMoid give rise to new species in solution that are also electrochemically active. This was corroborated by the study of this first reduction process, being already irreversible.

A similar behaviour was observed for their oxidation processes in all the cases except for BODMC which displayed a different pattern (figure 20). Then, to analyse the nature (e.g., reversible, quasi-reversible or irreversible) of this oxidation wave, a set of voltammograms were performed at different scan rates, from 20 to 2000 mVs^{-1} , for this CCMoid. The results are presented in table 7 and figure 20. The oxidative wave obtained

at different rates was analysed by: (i) attaining the coefficient between the anodic and cathodic currents (maxima of the waves in both cases), (ii) calculating the voltage difference between the cationic/anodic processes, and (iii) using the Randles-Sevcik equation (RS).⁶⁷ For a reversible behaviour it is expected to achieve values close to one and smaller than 200 mV in the (i) and (ii) analyses, respectively. In the case of the RS equation (characterization techniques chapter) the achievement of a linear regression is indicative of reversibility. Despite of the first impression, only the requirements of the Randles-Sevcik equation were fulfilled, displaying values far from the ideal in the first two approaches (table 7). Therefore, it cannot be considered that the first oxidation process of the BODMC has a pure reversible nature and should better be described as a quasi-reversible process in these conditions.

From the data achieved, in general CCMoids present irreversible behaviour, although the nature of their arms, in combination with the solvents and solvated species created by the applied voltage, may provide different outcomes. In this regard, there are also studies where the modification of the working electrode can allow reversible processes for CCM, therefore, having the stabilisation of the corresponding redox species in the conditions of the experiments.⁶⁸

Table 7. Current intensity and potential values for the oxidation and reduction processes at different scan rates for BODMC.

v (mVs ⁻¹)	E_{pa} (V)	I_{pa} (mA)	E_{pc} (V)	I_{pc} (mA)	I_{pa}/I_{pc}	ΔE_p (V)	E_0 (V)
20	0.698	0.028	0.395	-0.010	2.851	0.304	0.896
50	0.753	0.041	0.355	-0.020	2.075	0.398	0.931
100	0.798	0.054	0.318	-0.027	1.999	0.480	0.957
200	0.872	0.081	0.314	-0.044	1.827	0.557	1.029
500	0.946	0.120	0.248	-0,067	1.798	0.697	1.070
1000	1.072	0.162	0.225	-0,084	1.914	0.848	1.185
2000	1.149	-0.218	0.167	-0.106	2.055	0.982	1.233

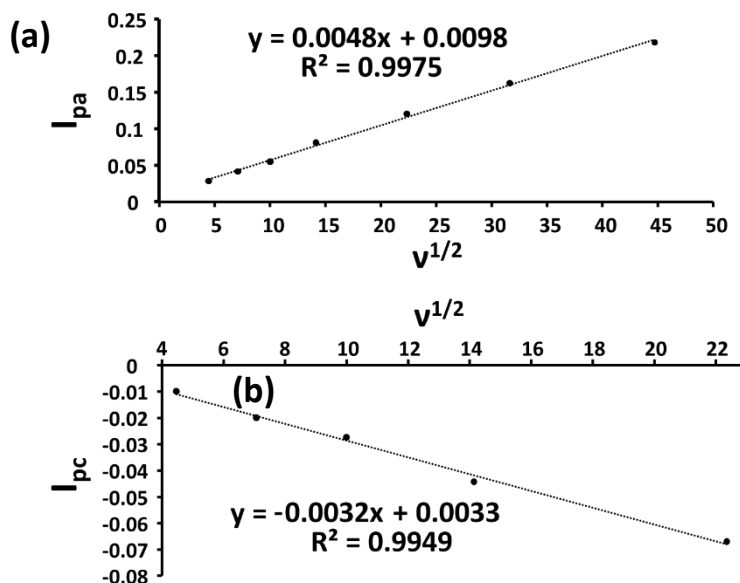


Figure 20. Plot of the maximum intensity vs. the square root of V: (a) oxidation, and (b) reduction.

3.8.1. HOMO-LUMO energy bandgap estimation

Electrochemistry is a technique used for the estimation of the bandgap energy as well, since the oxidation and reduction processes can be related with the HOMO and LUMO energies, respectively. This way, the semiconductor nature of the CCMoids has been proved in different works^{69,70} including our team,^{2,3} with bandgap values between 1.5 and 2.5 eVs. It has been also described the use of UV-Vis absorption spectra for the analysis of the gap. Here, we compared the values achieved using both techniques. Regarding the electronic behaviour of CCMoids, the study of the single electron transport properties of a family of CCMoids have also been described by our group using break junction and mechanically controlled break-junctions techniques.^{71,72}

From the point of view of the CCMoids, in this doctoral thesis the interest was on the analysis of the effect in the energy gap due to the existence of different arms, lengths of the skeleton and coordination. This way, 2-thphLCCMoidBF₂ was compared with a previous synthesised system, 2-thphCCMoidBF₂, both depicted in figure 21.²

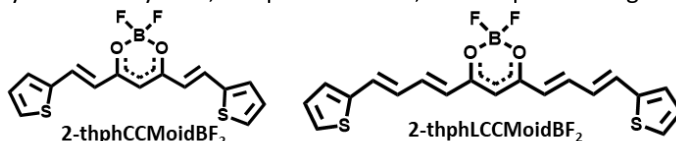


Figure 21. Structure of 2-thphCCMoidBF₂ and 2-thphLCCMoidBF₂.

A schematic representation of the HOMO and LUMO obtained for each CCMoid using electrochemistry is presented in figure 22 helping in the comparison and visualization of the changes observed.

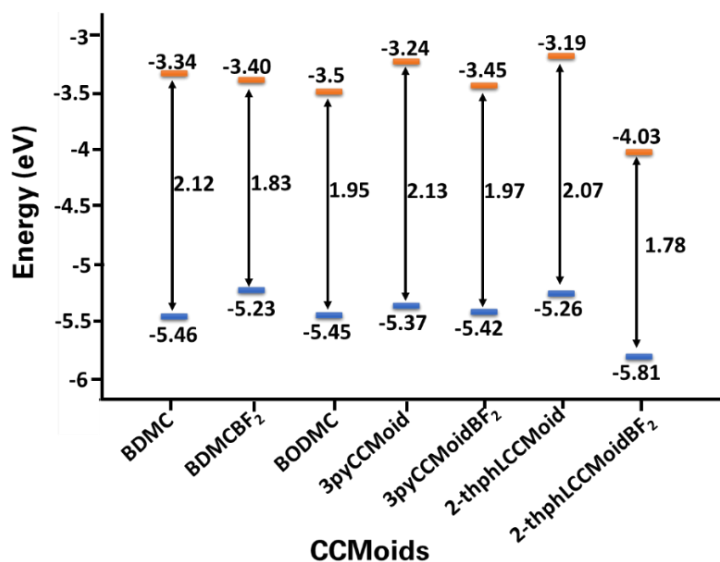


Figure 22. Representation of the HOMO and LUMO values of the CCMoids studied in this doctoral thesis

The energy of the HOMO and LUMO and the bandgap using electrochemistry was calculated for most of the studied CCMoids, except for BOHCCMoid, 2-thphCCMoidBF₂ and BOHCCMoidBF₂. In the case of the BOHCCMoid, its low solubility made impossible the measurement. For the other two, the oxidation bands were not evident, thus the estimation of the HOMO was not achieved. For these three compounds the bandgap estimation could only be performed by using UV-Vis absorption data.

The estimated values of the bandgaps using electrochemistry and UV-Vis are shown in table 8.

Table 8. Data extracted from the CV referenced to Fc/Fc⁺ and UV-vis in solid state.

	1 st oxidation (V)	1 st reduction (V)	E HOMO (eV)	E LUMO (eV)	Bandgap EC (eV)	Bandgap UV-Vis (eV)
BDMC	0.95	-1.88	-5.46	-3.34	2.12	2.13
BDMCBF₂	0.88	-1.53	-5.23	-3.4	1.83	2.00
BODMC	0.92	-1.46	-5.45	-3.5	1.95	1.94
3pyCCMoid	0.94	-1.68	-5.37	-3.24	2.13	2.41
3pyCCMoidBF₂	0.80	-1.10	-5.42	-3.45	1.97	2.14
BOHCCMoid	-	-	-	-	-	2.02
BOHCCmoidBF₂	-	-0.86	-	4.09	-	2.16
2-thphLCCMoid	0.66	-1.72	-5.26	-3.19	2.07	1.86
2-thphLCCMoidBF₂	1.19	-0.81	-5.81	-4.03	1.78	1.65
2-thphCCMoidBF₂	-	-1.29	-	-3.63	-	1.92

In general, all the measured values are in the range of published data (1.5 and 2.5 eVs), displaying all a semiconductor behaviour.^{2,3,37,38} Overall, the coordination of the BF₂ unit seems to reduce the HOMO and LUMO gap, affecting particularly the LUMO values. This change is especially noticeable for the 2-thphLCCMoidBF₂ in comparison to 2-thphLCCMoid with LUMO values of 3.19 and -4.03, respectively. Moreover, this CCMoid, with an extended framework (11 carbon atoms instead of the 7 found in the rest of CCMoids) shows the smallest bandgap when coordinates to BF₂ (figure 21). Comparing the CCMoids structures, it was seen that the lateral substituents do not significantly affect the bandgaps of the molecules (table 8). However, the results obtained with BODMC deserve special attention, since this CCMoid presents similar values to other CCMoids when coordinated with BF₂ and/or have long carbon skeletons. Unfortunately, attempts of preparing this compound coordinated to BF₂ were unsuccessful. Considering these results, it can be concluded that all the CCMoids of this doctoral thesis have a semiconductor behaviour, and to achieved small bandgap values the trend is the coordination of the β -diketone moiety to BF₂ and the extension of the CCMoid framework.

4. Conclusions

The synthesis of all the CCMoids studied in this doctoral thesis was carried out with remarkable yields and straightforward purification processes. We have demonstrated the efficiency of the modification of the Pabon's method to prepare a new CCMoid, the 2-thphLCCMoid, with an extended CCMoid skeleton, hence, additional double bonds in the chain. Also related with the synthesis of this CCMoid, we have proposed an effective synthetic route that can be hypothetically used for the preparation of long versions of CCMoids, starting with the commercially available aldehydes. Finally, we remark the

interesting perspectives of the synthesis of CCMoids by using acacBF_2 . This procedure was used as a convenient solution due to the impossibility of coordinating the BF_2 to the free 3pyCCMoid, and to overcome difficulties found when working with a highly insoluble compound, as it is BOHCCMoid.

The CCMoids have been characterized by several techniques, including NMR, IR mass spectroscopy, UV-Vis absorption, and electrochemistry. All these characterization methods have been useful for determining the composition and purity of the desired compounds giving also valuable information about the molecules. The set of characterization techniques also gives information about how the lateral substituents and the central carbon chain affect to different properties. Having a better understanding of this influence is considered advantageous for the design of new molecules inside of the CCMoid family. The established analytical protocols would be useful for the characterization of the extended structures and to find new applications for these molecular platforms.

5. References

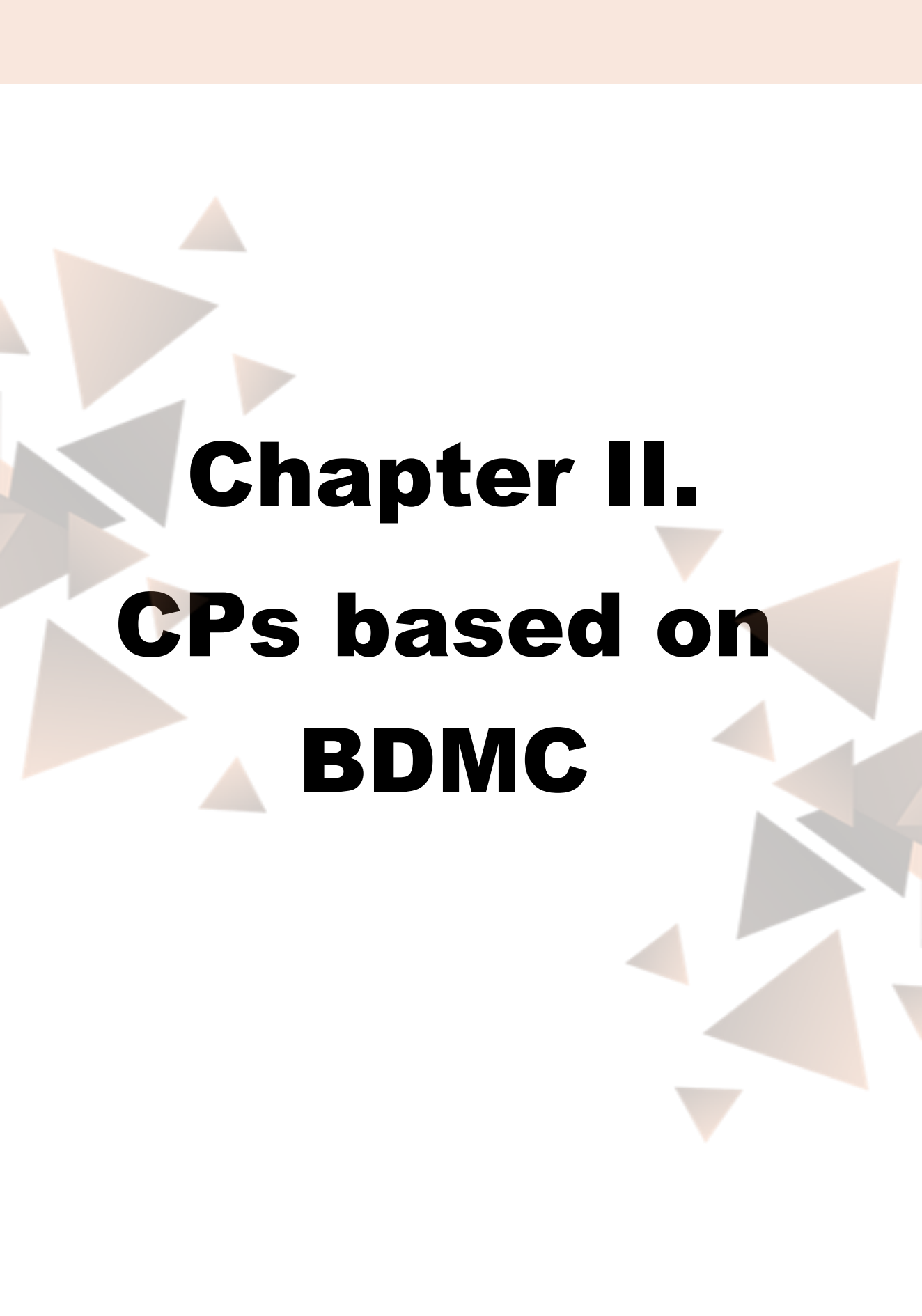
- (1) Bai, G., Yu, C., Cheng, C., Hao, E., Wei, Y., Mu, X., & Jiao, L. (2014). Syntheses and photophysical properties of BF₂ complexes of curcumin analogues. *Organic & biomolecular chemistry*, 12(10), 1618-1626.
- (2) Etcheverry Berríos, Á. F. (2018). Diseño y síntesis de sistemas curcuminoides para aplicaciones en electrónica molecular. Doctoral dissertation, Universidad de Chile.
- (3) Díaz Torres, R. (2018). *Synthesis, characterization and deposition on surfaces of curcuminoid-based systems*. Doctoral dissertation, Universitat de Barcelona.
- (4) Abonia, R., Laali, K. K., Raja Somu, D., Bunge, S. D., & Wang, E. C. (2020). A Flexible Strategy for Modular Synthesis of Curcuminoid-BF₂/Curcuminoid Pairs and Their Comparative Antiproliferative Activity in Human Cancer Cell Lines. *ChemMedChem*, 15(4), 354-362.
- (5) Pabon, H. J. J. (1964). A synthesis of curcumin and related compounds. *Recueil des Travaux Chimiques des Pays-Bas*, 83(4), 379-386.
- (6) Dhanya, C. S., Paul, W., Victor, S. P., & Joseph, R. (2021). On improving the physiological stability of curcuminoids: Curcuminoid-silver nanoparticle complex as a better and efficient therapeutic agent. *Nano-Structures & Nano-Objects*, 25, 100661.
- (7) Cocean, A., Cocean, I., Cimpoesu, N., Cocean, G., Cimpoesu, R., Postolachi, C., ... & Gurlui, S. (2021). Laser Induced Method to Produce Curcuminoid-Silanol Thin Films for Transdermal Patches Using Irradiation of Turmeric Target. *Applied Sciences*, 11(9), 4030.
- (8) Liu, Y., Liu, M., Yan, H., Liu, H., Liu, J., Zhao, Y., ... & Han, J. (2021). Enhanced solubility of bisdemethoxycurcumin by interaction with Tween surfactants: Spectroscopic and coarse-grained molecular dynamics simulation studies. *Journal of Molecular Liquids*, 323, 115073.
- (9) Yaprakasha, G. K., Jagan Mohan Rao, L., & Sakariah, K. K. (2002). Improved HPLC method for the determination of curcumin, demethoxycurcumin, and bisdemethoxycurcumin. *Journal of agricultural and food chemistry*, 50(13), 3668-3672.
- (10) Su, H., Sun, F., Jia, J., He, H., Wang, A., & Zhu, G. (2015). A highly porous medical metal-organic framework constructed from bioactive curcumin. *Chemical Communications*, 51(26), 5774-5777.
- (11) Portolés-Gil, N., Lanza, A., Aliaga-Alcalde, N., Ayllón, J. A., Gemmi, M., Mugnaioli, E., ... & Domingo, C. (2018). Crystalline curcumin bioMOF obtained by precipitation in supercritical CO₂ and structural determination by electron diffraction tomography. *ACS Sustainable Chemistry & Engineering*, 6(9), 12309-12319.
- (12) Jha, N. N., Ghosh, D., Das, S., Anoop, A., Jacob, R. S., Singh, P. K., ... & Maji, S. K. (2016). Effect of curcumin analogs on α -synuclein aggregation and cytotoxicity. *Scientific reports*, 6(1), 1-15.
- (13) Anto, R. J., Kuttan, G., Babu, K. D., Rajasekharan, K. N., & Kuttan, R. (1998). Anti-inflammatory activity of natural and synthetic curcuminoids. *Pharmacy and Pharmacology Communications*, 4(2), 103-106.
- (14) Herranz, M. A., Martín, N., Sánchez, L., Seoane, C., & Guldi, D. M. (2000). New π -extended tetrathiafulvalene-containing fulleropyrrolidine dyads endowed with vinyl spacers. *Journal of Organometallic Chemistry*, 599(1), 2-7.
- (15) Schmidt, A., & Hilt, G. (2013). Scope and Limitations of 1, 3, 5-Hexatriene Derivatives in Regioselective Cobalt-Catalyzed Reactions. *Organic letters*, 15(11), 2708-2711.
- (16) Khan, M. A., El-Khatib, R., Rainsford, K. D., & Whitehouse, M. W. (2012). Synthesis and anti-inflammatory properties of some aromatic and heterocyclic aromatic curcuminoids. *Bioorganic chemistry*, 40, 30-38.

- (17) Khan, M. A., El-Khatib, R., Rainsford, K. D., & Whitehouse, M. W. (2012). Synthesis and anti-inflammatory properties of some aromatic and heterocyclic aromatic curcuminoids. *Bioorganic chemistry*, *40*, 30-38.
- (18) Ahmed, M. M., Khan, M. A., & Rainsford, K. D. (2013). Synthesis of thiophene and NO-curcuminoids for antiinflammatory and anti-cancer activities. *Molecules*, *18*(2), 1483-1501.
- (19) Lei, X., Su, W., Li, P., Xiao, Q., Huang, S., Qian, Q., ... & Lan, H. (2014). Ruthenium (II) arene complexes of curcuminoids: synthesis, X-ray diffraction structure and cytotoxicity. *Polyhedron*, *81*, 614-618.
- (20) Flores, M., Cisternas, E., Mella, A., Jullian, D., Nunez, A. S., & Soler, M. (2018). Adsorption of 2-thiophene curcuminoid molecules on a Au (111) surface. *Applied Surface Science*, *427*, 620-625.
- (21) Berlanga, I., Etcheverry-Berrios, A., Mella, A., Jullian, D., Gómez, V. A., Aliaga-Alcalde, N., ... & Soler, M. (2017). Formation of self-assembled monolayer of curcuminoid molecules on gold surfaces. *Applied Surface Science*, *392*, 834-840.
- (22) Etcheverry Berríos, Á., Olavarría, I., Perrin, M. L., Díaz Torres, R., Jullian, D., Ponce, I., ... & Soler Jauma, M. (2016). Multiscale Approach to the Study of the Electronic Properties of Two Thiophene Curcuminoid Molecules.
- (23) Gokaraju GR, Gokaraju RR, Golakoti T, et al., Inventors; Laila Pharmaceuticals Pvt. Ltd., India. assignee. Method of inhibition of beta-secretase by using bis-O-demethylcurcumin for the prevention, management and treatment of neurodegenerative diseases patent. WO2015186144A2. 2015.
- (24) Feng, J. Y., & Liu, Z. Q. (2009). Phenolic and enolic hydroxyl groups in curcumin: which plays the major role in scavenging radicals?. *Journal of agricultural and food chemistry*, *57*(22), 11041-11046.
- (25) Venkateswarlu, S., Ramachandra, M. S., & Subbaraju, G. V. (2005). Synthesis and biological evaluation of polyhydroxycucurminoids. *Bioorganic & medicinal chemistry*, *13*(23), 6374-6380.
- (26) Pinkaew, D., Changtam, C., Tocharus, C., Thummayot, S., Suksamrarn, A., & Tocharus, J. (2015). Di-O-demethylcurcumin protects SK-N-SH cells against mitochondrial and endoplasmic reticulum-mediated apoptotic cell death induced by A β 25-35. *Neurochemistry international*, *80*, 110-119.
- (27) Pinkaew, D., Changtam, C., Tocharus, C., Govitrapong, P., Jumnonprakhon, P., Suksamrarn, A., & Tocharus, J. (2016). Association of Neuroprotective Effect of Di-O-Demethylcurcumin on A β 25–35-Induced Neurotoxicity with Suppression of NF- κ B and Activation of Nrf2. *Neurotoxicity research*, *29*(1), 80-91.
- (28) Portes, E., Gardrat, C., & Castellan, A. (2007). A comparative study on the antioxidant properties of tetrahydrocurcuminoids and curcuminoids. *Tetrahedron*, *63*(37), 9092-9099.
- (29) Ravindran, J., Subbaraju, G. V., Ramani, M. V., Sung, B., & Aggarwal, B. B. (2010). Bisdemethylcurcumin and structurally related hispolon analogues of curcumin exhibit enhanced prooxidant, anti-proliferative and anti-inflammatory activities in vitro. *Biochemical pharmacology*, *79*(11), 1658-1666.
- (30) Chaniyilparampu, R. N., Nair, A. K., Kapoor, A., Parthasarathy, K., Bhupathiraju, K., Gokaraju, R. R., ... & Golakoti, T. (2011). *U.S. Patent Application No. 13/127,590*.
- (31) Liu, K., Chen, J., Chojnacki, J., & Zhang, S. (2013). BF₃-OEt₂-promoted concise synthesis of difluoroboron-derivatized curcumins from aldehydes and 2, 4-pentanedione. *Tetrahedron letters*, *54*(16), 2070-2073.
- (32) Rao, E. V., & Sudheer, P. (2011). Revisiting curcumin chemistry part I: A new strategy for the synthesis of curcuminoids. *Indian journal of pharmaceutical sciences*, *73*(3), 262.

- (33) Sherin, D. R., Thomas, S. G., & Rajasekharan, K. N. (2015). Mechanochemical synthesis of 2, 2-difluoro-4, 6-bis (β -styryl)-1, 3, 2-dioxaborines and their use in cyanide ion sensing. *Heterocyclic Communications*, 21(6), 381-385.
- (34) Tang, B.; Wang, X.; Wang, C.; Sun, J.; Qi, W., Faming Z. S. (2012) Difluoro-boron dye fluorescent probes, the synthesis method and application in the detection of intracellular hydrogen ion. Chinese patent CN 102603782.
- (35) Laali, K. K., Rathman, B. M., Bunge, S. D., Qi, X., & Borosky, G. L. (2016). Fluoro-curcuminoids and curcuminoid-BF₂ adducts: Synthesis, X-ray structures, bioassay, and computational/docking study. *Journal of Fluorine Chemistry*, 191, 29-41.
- (36) Liu, W., Wu, S., Su, Q., Guo, B., Ju, P., Li, G., & Wu, Q. (2019). Difluoroborate-based conjugated organic polymer: a high-performance heterogeneous photocatalyst for oxidative coupling reactions. *Journal of Materials Science*, 54(2), 1205-1212.
- (37) Weiss, H., Reichel, J., Görls, H., Schneider, K. R. A., Micheel, M., Pröhl, M., ... & Weigand, W. (2017). Curcuminoid-BF₂ complexes: Synthesis, fluorescence and optimization of BF₂ group cleavage. *Beilstein journal of organic chemistry*, 13(1), 2264-2272.
- (38) Szajda, M., & Lam, J. N. (1996). Thiophenes and their Benzo Derivatives: Structure. *Comprehensive Heterocyclic Chemistry II*, 2, 491-605.
- (39) DiCesare, N., & Lakowicz, J. R. (2002). New sensitive and selective fluorescent probes for fluoride using boronic acids. *Analytical biochemistry*, 301(1), 111-116.
- (40) Abraham, R. J., & Reid, M. (2002). ¹H chemical shifts in NMR. Part 18. ¹H Ring currents and π -electron effects in hetero-aromatics. *Journal of the Chemical Society, Perkin Transactions 2*, (6), 1081-1091.
- (41) https://sdbs.db.aist.go.jp/sdbs/cgi-bin/direct_frame_top.cgi. Integrated Spectral Database System of Organic Compounds. National Institute of Advanced Industrial Science and Technology (AIST)
- (42) Kolev, T. M., Velcheva, E. A., Stamboliyska, B. A., & Spiteller, M. (2005). DFT and experimental studies of the structure and vibrational spectra of curcumin. *International Journal of Quantum Chemistry*, 102(6), 1069-1079.
- (43) Pretsch, E. (2002). Determinación estructural de compuestos orgánicos (No. Sirsi) i9788445812150).
- (44) Ibrahim, I., Yunus, S., & Hashim, M. (2013). Relative performance of isopropylamine, pyrrole and pyridine as corrosion inhibitors for carbon steels in saline water at mildly elevated temperatures. *International Journal of Scientific & Engineering Research*, 4(2), 1-12.
- (45) Smith, M. K., & Northrop, B. H. (2014). Vibrational properties of boroxine anhydride and boronate ester materials: model systems for the diagnostic characterization of covalent organic frameworks. *Chemistry of Materials*, 26(12), 3781-3795.
- (46) Rassie, C., Olowu, R. A., Waryo, T. T., Wilson, L., Williams, A., Baker, P. G., & Iwuoha, E. I. (2011). Dendritic 7T-polythiophene electro-catalytic sensor system for the determination of polycyclic aromatic hydrocarbons. *Int. J. Electrochem. Sci*, 6, 1949-1967.
- (47) He, X. G., Lin, L. Z., Lian, L. Z., & Lindenmaier, M. (1998). Liquid chromatography-electrospray mass spectrometric analysis of curcuminoids and sesquiterpenoids in turmeric (*Curcuma longa*). *Journal of Chromatography A*, 818(1), 127-132.
- (48) Jia, S., Du, Z., Song, C., Jin, S., Zhang, Y., Feng, Y., ... & Jiang, H. (2017). Identification and characterization of curcuminoids in turmeric using ultra-high performance liquid chromatography-quadrupole time of flight tandem mass spectrometry. *Journal of Chromatography A*, 1521, 110-122.

- (49) Jiang, H., Somogyi, Á., Jacobsen, N. E., Timmermann, B. N., & Gang, D. R. (2006). Analysis of curcuminoids by positive and negative electrospray ionization and tandem mass spectrometry. *Rapid Communications in Mass Spectrometry: An International Journal Devoted to the Rapid Dissemination of Up-to-the-Minute Research in Mass Spectrometry*, 20(6), 1001-1012.
- (50) Griesser, U. J. (2006). The importance of solvates. *Polymorphism in the pharmaceutical industry*, 211-233.
- (51) Tønnesen, H.H.; Karlsen, J.; Mostad, A.; Pedersen, U.; Rasmussen, P.B.; Lawesson, S.-O. Structural studies of curcuminoids. II. Crystal structure of 1,7-bis(4-hydroxyphenyl)-1,6-heptadiene-3,5-dione methanol complex. *Acta Chem. Scand. B* 1983, 37, 179–185.
- (52) Kasai, K.; Saito, A.; Sato, S. Crystal structure and pseudopolymorphism of bisdemethoxycurcumin-alcohol solvates. *Bull. Miyagi Univ. Educ.* 2017, 51, 83–88.
- (53) Yuan, L., & Lorenz, H. (2018). Solvate formation of bis (demethoxy) curcumin: Screening and characterization. *Crystals*, 8(11), 407.
- (54) L. Yuan, E. Horosanskaia, F. Engelhardt, F. T. Edelmann, N. Couvrat, M. Sanselme, Y. Cartigny, G. Coquerel, A. Seidel-Morgenstern, H. Lorenz, *Crystal Growth & Design*, **2019**
- (55) Rodríguez-Cid, L., Qian, W., Iribarra-Araya, J., Etcheverry-Berrios, A., Martínez-Olmos, E., Choquesillo-Lazarte, D., ... & Aliaga-Alcalde, N. (2021). Broadening the scope of high structural dimensionality nanomaterials using pyridine-based curcuminoids. *Dalton Transactions*.
- (56) Matlinska, M. A., Wasylshen, R. E., Bernard, G. M., Terskikh, V. V., Brinkmann, A., & Michaelis, V. K. (2018). Capturing elusive polymorphs of curcumin: A structural characterization and computational study. *Crystal Growth & Design*, 18(9), 5556-5563.
- (57) Péret-Almeida, L., Cherubino, A. P. F., Alves, R. J., Dufossé, L., & Glória, M. B. A. (2005). Separation and determination of the physico-chemical characteristics of curcumin, demethoxycurcumin and bisdemethoxycurcumin. *Food Research International*, 38(8-9), 1039-1044.
- (58) Marini, A., Muñoz-Losa, A., Biancardi, A., & Mennucci, B. (2010). What is solvatochromism?. *The Journal of Physical Chemistry B*, 114(51), 17128-17135.
- (59) Nardo, L., Andreoni, A., Masson, M., Haukvik, T., & Tønnesen, H. H. (2011). Studies on curcumin and curcuminoids. XXXIX. Photophysical properties of bisdemethoxycurcumin. *Journal of fluorescence*, 21(2), 627-635.
- (60) Mondal, S., Ghosh, S., & Moulik, S. P. (2016). Stability of curcumin in different solvent and solution media: UV-visible and steady-state fluorescence spectral study. *Journal of Photochemistry and Photobiology B: biology*, 158, 212-218.
- (61) John, V. D., & Krishnankutty, K. (2005). Synthesis, characterization and antitumour activities of some synthetic curcuminoid analogues and their copper complexes. *Transition Metal Chemistry*, 30(2), 229-233.
- (62) Nguyen, T. T. H., Si, J., Kang, C., Chung, B., Chung, D., & Kim, D. (2017). Facile preparation of water soluble curcuminoids extracted from turmeric (*Curcuma longa* L.) powder by using steviol glucosides. *Food chemistry*, 214, 366-373.
- (63) Ziyatdinova, G. K., Nizamova, A. M., & Budnikov, H. C. (2012). Voltammetric determination of curcumin in spices. *Journal of Analytical Chemistry*, 67(6), 591-594.
- (64) Burç, M., Güngör, Ö., & TİTRETİR DURAN, S. (2020). Voltammetric determination of curcumin in spices using platinum electrode electrochemically modified with poly (vanillin-co-caffeic acid). *Analytical and Bioanalytical Electrochemistry*, 12(5), 625-643.
- (65) Arrue, L., Barra, T., Camarada, M. B., Zarate, X., & Schott, E. (2017). Electrochemical and theoretical characterization of the electro-oxidation of dimethoxycurcumin. *Chemical Physics Letters*, 677, 35-40.

- (66) Priyadarsini, K. I., Maity, D. K., Naik, G. H., Kumar, M. S., Unnikrishnan, M. K., Satav, J. G., & Mohan, H. (2003). Role of phenolic OH and methylene hydrogen on the free radical reactions and antioxidant activity of curcumin. *Free Radical Biology and Medicine*, 35(5), 475-484.
- (67) Bard, A. J., & Faulkner, L. R. (2001). Fundamentals and applications. *Electrochemical methods*, 2(482), 580-632.
- (68) Zokhtareh, R., & Rahimnejad, M. (2018). A novel sensitive electrochemical sensor based on nickel chloride solution modified glassy carbon electrode for curcumin determination. *Electroanalysis*, 30(5), 921-927.
- (69) Ivoal, M., Zaborova, E., Canard, G., D'Aléo, A., & Fages, F. (2016). Synthesis, electrochemical and photophysical studies of the borondifluoride complex of a meta-linked biscurcuminoid. *New Journal of Chemistry*, 40(2), 1297-1305.
- (70) Canard, G., Ponce-Vargas, M., Jacquemin, D., Le Guennic, B., Felouat, A., Rivoal, M., ... & Fages, F. (2017). Influence of the electron donor groups on the optical and electrochemical properties of borondifluoride complexes of curcuminoid derivatives: a joint theoretical and experimental study. *RSC advances*, 7(17), 10132-10142.
- (71) Burzurí, E., Island, J. O., Díaz-Torres, R., Fursina, A., González-Campo, A., Roubeau, O., ... & van der Zant, H. S. (2016). Sequential electron transport and vibrational excitations in an organic molecule coupled to few-layer graphene electrodes. *ACS nano*, 10(2), 2521-2527.
- (72) Prins, F., Barreiro, A., Ruitenbergh, J. W., Seldenthuis, J. S., Aliaga-Alcalde, N., Vandersypen, L. M., & van der Zant, H. S. (2011). Room-temperature gating of molecular junctions using few-layer graphene nanogap electrodes. *Nano letters*, 11(11), 4607-4611.



Chapter II.
CPs based on
BDMC

1. Introduction

Previous to this doctoral thesis, only two CPs, by Su *et al.*¹ and Domingo *et al.*², have been published having a CCMoid as the linker in charge of the expansion of the structures. In both cases, CCM was the chosen molecule, where the CPs show Zn(II) ions coordinated to the central β -diketone moiety and to the lateral phenol/methoxy groups of this molecule. Despite of the structural similarities with the rest of natural CCMoids, no other coordination-based extended systems have been published until now.

Based on this idea, BDMC (figure 1) was chosen as the organic linker to screen for new CPs based on CCMoids. Moreover, since it is a natural molecule that have shown some health benefits as antioxidant, anti-inflammatory or antitumoral,³⁻⁶ their CPs are also expected to have some therapeutical properties. It is worth to mention that BDMC has been described to improve some CCM properties and presents higher stability at physiological pHs.^{7,8}

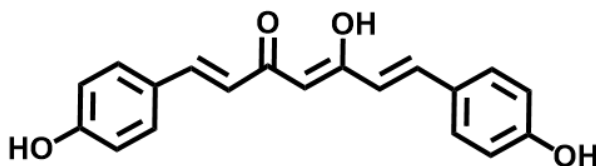


Figure 1. Representation of the structure of the BDMC.

From a bibliographic point of view, and comparing with CCM, there is a limited literature that examine the coordination of BDMC with metals. Even so, there are already works regarding coordination compounds that display two BDMC molecules bonded to Zn(II), Ni(II), Cu(II), Pd(II)⁹, U(II)¹⁰ and La(III)¹¹ ions (figure 2), respectively, and additional publications with only one molecule of BDMC in the coordination sphere of the metallic centre in addition to other ligands (figure 2). The latter have been synthesized with the same metallic units named above and also using Ru(II)¹², Pd(II)¹³, Ir(II) and Rh(II),¹⁴ correspondingly. However, as far as we know, all the previous systems are coordination compounds (OD structures), and therefore, the CPs introduced in this chapters are the first ones synthesized with a natural CCMoid, BDMC, outside CCM.¹⁵

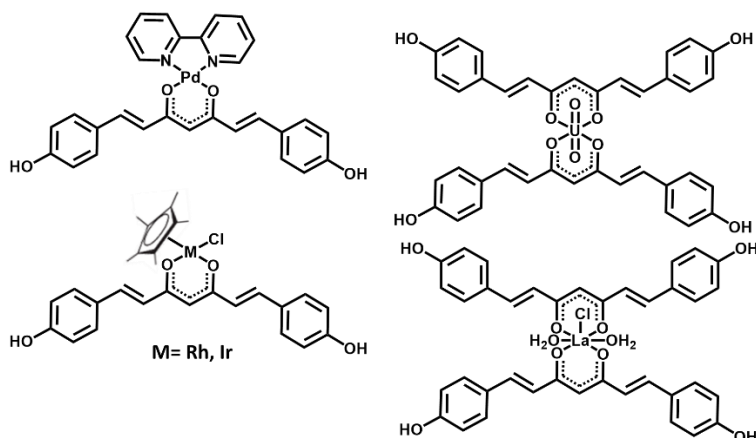


Figure 2. Examples of BDMC-metal compounds.

Moreover, in this work the use of co-linkers together with BDMC was examined too. Because of the charged nature of this phenolic CCMoid, neutral co-linkers of the bipyridine family were used. Three representative molecules of this family with different spacer lengths and nature were chosen: (1,2-bis(4-pyridyl)ethylene (bpe), 1,3-bis(4-pyridyl)propane (bpp) and 4,4'-bipyridine (bpy)) (figure 3). Here, one of our goals was to analyse how the different spacers could affect the structure and properties of the final mixed-linker CPs. Hence, bpy is chosen as a very rigid and short molecule, while bpp is longer and relatively flexible. Finally, the presence of the unsaturated chain in bpe makes this molecule the longest and most flexible one of the chosen set, missing the conjugation features that the other two have.

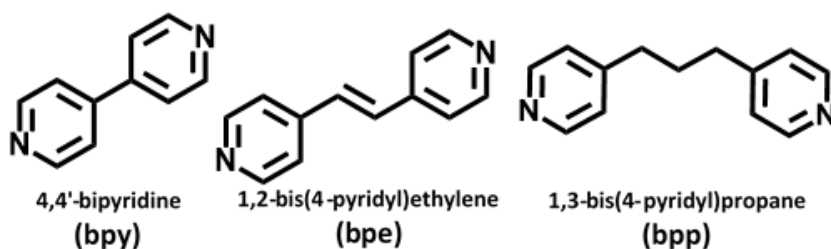


Figure 3. Scheme, name, and abbreviation of the molecules used as co-ligands in this chapter.

Here, using solvothermal methods, seven new CPs have been obtained with BDMC as the principal linker together with the above co-linkers and Zn(II) ions as the metallic centres. They are named: **BDMCzn-1**, **BDMCzn-2a**, **BDMCzn-2b**, **BDMCzn-3**, **BDMCzn-4a**, **BDMCzn-4b** and **BDMCzn-4c**, respectively. Moreover, the synthesis of CPs using scCO₂ methodology was explored as well, due to the expertise of the group in this technique and the synthesis of a previous MOF based on CCM using this methodology.²

2. Objectives

The principal objective of the work described in this chapter is the synthesis and physicochemical characterization of new CPs based on BDMC. Together with this general purpose, two secondary aims were also proposed:

- The achievement of mixed-linkers CPs using BDMC and a family of bipyridine derivatives.
- The attainment of BDMC-CPs by $scCO_2$ methodology, to compare with the results achieved using traditional methods, and as an alternative green technique for the synthesis of CCMoid-CPs.

3. Materials and methods

3.1. Materials

The BDMC was synthesized following a modification of the Pabon's methodology¹⁶ as was explained in chapter I. The co-ligands (4,4'-Bipyridine, 1,2-Bis(4-pyridyl)ethylene and 1,3-Bis(4-pyridyl)propane) and all the metal salts precursors for the CP synthesis (zinc acetate, $Zn(OAc)_2$; zinc acetylacetonate, $Zn(AcAc)_2 \cdot xH_2O$); were purchased in Sigma Aldrich (Merck KGaA). MeOH was provided by CARLO ERBA Reagents S.A., absolute EtOH by Scharlab and the compressed CO_2 by Carbueros Metálicos S.A.

3.2. Methods. CPs synthesis

3.2.1. Solvothermal method

The crystallisation of the accomplished BDMC-CPs, in the presence or absence of co-linkers, was achieved using the methodology described in the methodology chapter, using EtOH as solvent at 80 °C for three days, working at solvothermal conditions. Here, autogenous pressure is produced inside of the vial, but due to the low filling volume (2 mL), we can describe it as soft solvothermal conditions.

BDMCZn-1. 30.00 mg (0.097 mmol) of BDMC and 21.36 mg (0.097 mmol) of $Zn(OAc)_2 \cdot 2H_2O$ were mixed in 2 mL of EtOH. Yield 56-60 wt.%.

BDMCZn-2a and **BDMCZn-2b.** Both were synthesized as **BDMCZn-1** but adding as an extra reagent bpe, in the quantities of 8.86 mg (0.048 mmol) or 17.73 mg (0.097 mmol), respectively. Yields 52-70 wt.%.

BDMCZn-3. The system was synthesized as **BDMCZn-1** but adding bpp, either 19.29 mg (0.048 mmol) or 38.58 mg (0.097 mmol) were used, obtaining the same product independently of the BDMC:bpp ratio.

BDMCZn-4a, BDMCZn-4b and BDMCZn-4c. The three systems were synthesized as **BDMCZn-1** but adding bpy, either 15.19 mg (0.048 mmol) or 30.30 mg (0.097 mmol), showing identical results with the two different BDMC:bpy ratios. A crystalline mixture was obtained, from which **BDMCZn-4c** was the only compound obtained in significant quantities, with a yield of 38-54 wt.%. Some crystals of **BDMCZn-4a** and **BDMCZn-4b** were obtained together with **BDMCZn-4c** but it was not possible to isolate them neither to vary/increase their yields.

3.2.2. scCO₂ method

In most of the cases the reactor was set at 60 °C, pressurized to 200 bar and the mixture was stirred during 72 h, only **BDMCZn-3sc** was carried out following the same procedure but at 40 °C.

BDMCZn-1sc. 156 mg (0.50 mmol) of BDMC and 200 mg (0.76 mmol) of Zn (acac)₂·xH₂O were mixed in 2 mL of EtOH in a vial.

BDMCZn-2sc. This compound was synthesized as **BDMCZn-1sc** but adding bpe as an extra reagent (76.8 mg, 0.42 mmol).

BDMCZn-3sc. This product was achieved as **BDMCZn-1sc** but adding bpp as an additional reagent (83.6 mg, 0.42 mmol). Moreover, *tert*-butylpyridine was added to increase the crystallinity of the products. In this approach, previously published by Domingo *et al.*,¹⁷ *tert*-butyl pyridine was used as ancillary ligand that forms an intermediate with the metal salts helping the completion of the reaction.

BDMCZn-4sc. This product was synthesized as **BDMCZn-1sc** but adding as an extra reagent 65.8 mg (0.42 mmol) of bpy.

4. Result and Discussion

4.1. Solvothermal synthesis

Six new CPs, based on BDMC, have been obtained in this doctoral thesis (table 1) following the solvothermal approach. One of them with the exclusive use of BDMC and a Zn(II) salt (**BDMCZn-1**). For the rest, two CPs present BDMC and bpe (**BDMCZn-2a** and **BDMCZn-2b**), one shows BDMC and bpp (**BDMCZn-3**) and three different systems were isolated containing BDMC and bpy (**BDMCZn-4a**, **BDMCZn-4b** and **BDMCZn-4c**).

Table 1: Co-linkers and stoichiometry of the CPs obtained

CPs	Co-linker	Ratio metal: BDMC:Co-linker
BDMCZn-1	-	1:1:-
BDMCZn-2a	bpe	1:1:1
BDMCZn-2b	bpe	1:1:0.5
BDMCZn-3	bpp	1:1:1
BDMCZn-4a, 4b, 4c	bpy	1:1:1

4.1.1. Crystallographic description

The reaction of BDMC and $\text{Zn}(\text{OAc})_2$ in EtOH under solvothermal conditions resulted in a 1D structure called here **BDMCZn-1**, with $[\text{Zn}(\text{BDMC})(\text{EtOH})]_n$ stoichiometry.

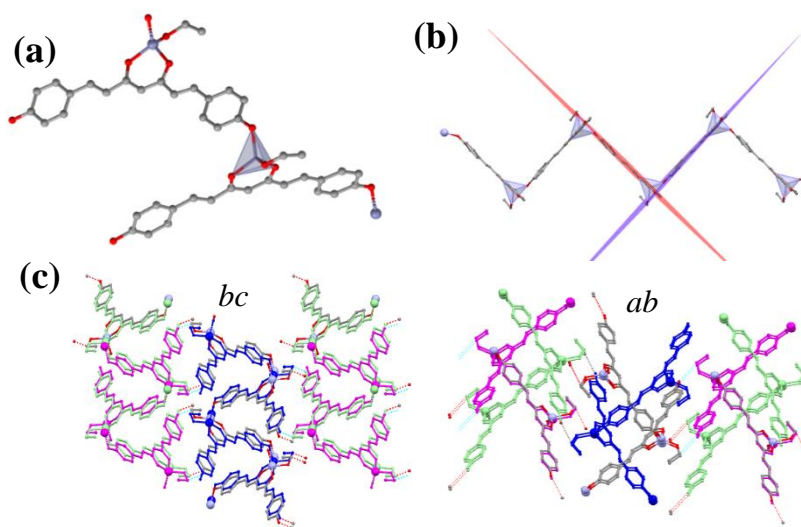


Figure 4. Schematic representation of the crystal structure of compound **BDMCZn-1**: (a) repeating unit showing the coordination mode of Zn(II) and BDMC, (b) zig-zag chain in the 1D structure, and (c) extended 3D framework through H-bonding projected in the *a* and *c* directions. Colour legend: Zn, light blue; C, grey; O, red; N, dark blue; H atoms are omitted for clarity.

BDMCZn-1 crystallizes in the monoclinic $P2_1/c$ space group. In the asymmetric unit, one Zn(II) atom appears tetracoordinated, having the basal plane occupied by the β -diketone of one BDMC linker and one EtOH molecule; meanwhile, in the apical position the metallic centre coordinates to the phenolic ring of a neighbouring BDMC linker (figure 4a). The chelate formed with the two oxygens in the β -diketone distorts in great manner the geometry, presenting smaller O-Zn-O angle (99°) than the rest (105 - 120°).

The pseudo-tetrahedral geometry of the Zn(II) is imposed by the coordination with the two oxygen atoms in the β -diketone (angles O-Zn-O between 99° and 120°). Each BDMC is coordinated to two different Zn(II) atoms by the β -diketone and one phenolic ring, while the second phenol remains protonated. As a consequence, the system presents a 1D zigzag chain where successive BDMC molecules form angles of 85.50° (Figure 4b). The chains are held together in a 3D structure by hydrogen bonds established through the coordinated EtOH molecules (figure 4c). The result is a compact packing with negligible structural porosity (calculated using Mercury).

As previously mentioned, bpe, bpp and bpy were used in the synthesis to promote higher dimensional systems and to analyse the effect of the co-linkers. In our experiments, the co-linkers were always added in the mixture after the solvothermal reactions were carried out.

In the experiments with bpe, two different structures, called **BDMCZn-2a** and **BDMCZn-2b**, were obtained changing the ratio linker:co-linker.

Using a ratio 1:1:1 (metal:BDMC:bpe), a 1D structure named **BDMCZn-2a** was obtained with formula $[Zn(BDMC)(bpe)(OAc)]_n \cdot 2nH_2O$. **BDMCZn-2a** crystallizes in the monoclinic $P2_1/c$ space group. The asymmetric unit contains a single pentacoordinated Zn(II) atom bonded to the β -diketone of one BDMC, two pyridine N atoms of two additional bpe co-linkers, and one oxygen from the acetate ligand. The Zn(II) ion adopts a square-based pyramidal geometry with the β -diketone, the acetate, and one of the bpe co-linkers on the basal plane and the second bpe at the apical position (figure 5a). Overall, the geometry is slightly distorted ($\tau = 0.43$), with angles smaller than 90° in the bonds that implicate the oxygen atoms of the β -diketone (between 85.4° and 88.1°) and larger in the angle between the two N-donor linkers (94.88°). A similar coordination number has been observed in the past in CPs and MOFs^{18,19}, as well as when Zn(II) coordinate to a synthetic CCMoid.²⁰ In this structure, both phenol groups of the BDMC molecule remain protonated and do not participate in the coordination to the metal, which is exclusively established through the β -diketone. Therefore, a new 1D zigzag array is formed by coordinative bonds established entirely between the Zn(II) metal centres and the ditopic bpe molecules (with an angle of 64.58° , figure 5b). In the supramolecular structure, the chains are held together by hydrogen bonds established between the remaining protonated phenol groups in the BDMC molecules and the acetate groups of different

chains, with half of those through water bridges (figure 5c). Again, the result is a dense structure with a negligible porosity (calculated using Mercury). Although the general disposition of Zn(BDMC)(OAc) units attached through the bpe is similar to other CCMoid-CPs published with Co(II) and Ni(II) using bpy,²¹ the molecular blocks of **BDMCZn-2a** are unique in the sense that each Zn unit coordinates to BDMC and acetate ligands instead of coordinating only to CCMoid molecules.

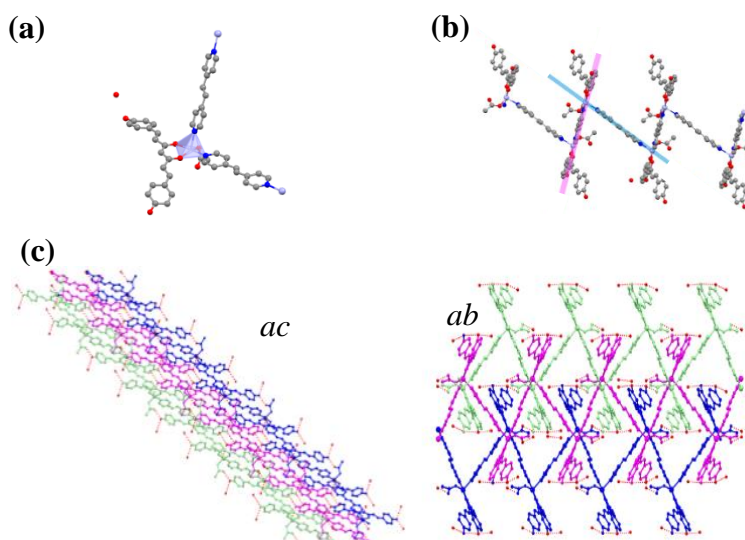


Figure 5. Schematic representation of the crystal structure of compound **BDMCZn-2a**: (a) repeating unit showing the coordination mode of Zn(II) and BDMC, (b) zig-zag chain in the 1D structure, and (c) extended 3D framework through H-bonding in the *b* and *c* projections. Colour legend: Zn, light blue; C, grey; O, red; N, dark blue; H atoms are omitted for clarity.

The reduction of the molar ratio of bpe, from 1 to 0.5, provided a new compound named here **BDMCZn-2b**, displaying a different PXRD pattern than **BDMCZn-2a** (see powder XRD section). However, its structural analysis was not possible due to the poor quality of the crystals. Its composition was estimated using EA data and further analysed by CPMAS¹³C.

In a different way than before, all the experiments performed varying the ratios with bpp provided the same crystalline product, called **BDMCZn-3**, with formula $[\text{Zn}(\text{BDMC})(\text{bpp})_{0.5}]_n \cdot n/2\text{EtOH}$. **BDMCZn-3** crystallizes in the orthorhombic $P2_1$ space group. The repeating unit has a similar composition as **BDMCZn-1**, but now the EtOH groups are replaced by bpp co-linkers. As a result, a new 3D architecture is found in contrast to the 1D observed for **BDMCZn-1**. The structure of **BDMCZn-3** is highly complex, with four crystallographically different Zn(II) atoms, all of them

tetracoordinated (figure 6), and four independent BDMC units. Each pseudo-tetrahedral Zn(II) is bonded on the basal plane to the β -diketone of one BDMC linker and to one phenolic ring of a neighbour. The apical position is occupied by the pyridinic moiety of a bpp co-linker. Hence, as described in **BDMCZn-1**, each BDMC is coordinated to two different Zn(II) atoms, through the β -diketone and one phenol ring, while the second phenol group remains protonated.

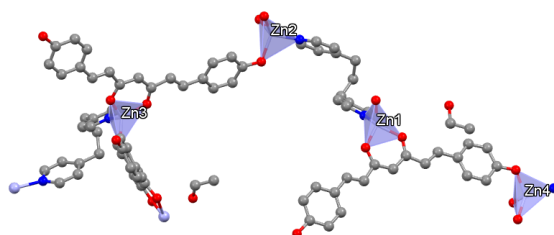


Figure 6. Repeating unit in the crystals of **BDMCZn-3**. Colour legend: Zn, light blue; C, grey; O, red; N, dark blue; H atoms are omitted for clarity.

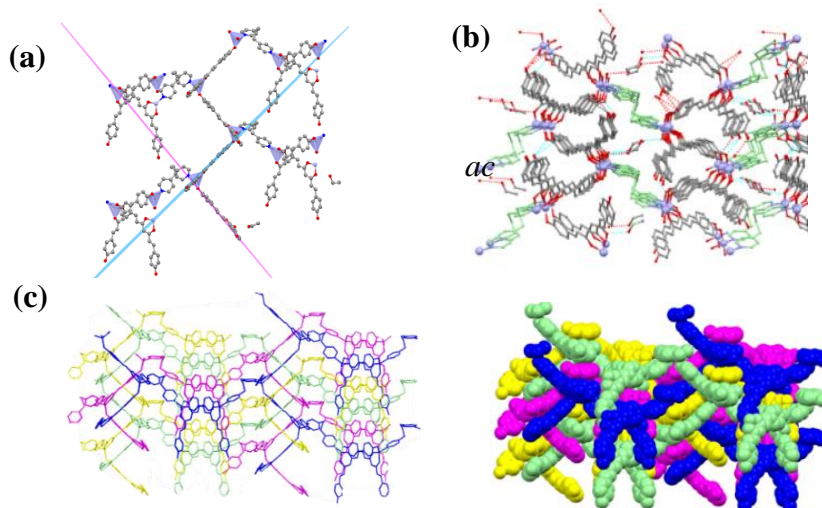


Figure 7. Extended structure of **BDMCZn-3**. (a) Projections of the zig-zag basic unit chain, (b) projection of the 3D and (c) views of the interpenetrated structure, without and with space filling function in Mercury.

The basic unit is constituted by zigzag $[\text{Zn}(\text{BDMC})]_n$ chains extended in two perpendicular directions with an angle of 86.81° (figure 7a). These units are attached by the co-linker bpp (figure 7b) that adopts an L-shaped conformation, reducing in a great manner its length. The dense packing of this basic construction leads to interpenetration of the elements within the 3D structure (figure 7c), giving place to a dense material with null porosity (calculated by Mercury).

Finally, three different products precipitate together after the reaction with bpy, called **BDMCZn-4a**, **BDMCZn-4b** and **BDMCZn-4c**, respectively. In all the experiments, most of the isolated product was formed by **BDMCZn-4c** crystals, which does not present high crystallinity and its structure was not resolved. However, some crystals from the other two systems could be separated by hand and measured using single crystal XRD.

Both compounds (**BDMCZn-4a** and **BDMCZn-4b**) are rather similar and have alike stoichiometry, with formulae $[\text{Zn}_2(\text{BDMC})_2(\text{bpy})]_n \cdot n\text{H}_2\text{O} \cdot n\text{EtOH}$ and $[\text{Zn}_2(\text{BDMC})_2(\text{bpy})]_n \cdot 2n\text{EtOH}$, in that order, differentiating themselves in the nature and number of adsorbed solvent molecules. Even though these two systems present similarities, they crystallize in different space groups, $C2/c$ and $P2_1/n$, for **BDMCZn-4a** and **BDMCZn-4b**, correspondingly. Both structures are formed by dinuclear units connected through the ligands. Each dimer displays a Zn_2O_6 core formed by two pentacoordinated and crystallographically equivalent $\text{Zn}(\text{II})$ atoms (figures 8a,b), coordinated each to one β -diketone moiety from one BDMC unit and one pyridinic group (from the 4,4'-bpy) in addition to two phenolate groups from neighbouring CCMoid molecules; the latter act as the bridging ligands within the dimeric cluster. Therefore, the coordination sphere of the metallic centres in **BDMCZn-4a** and **BDMCZn-4b** is the same; however, the geometry of the $\text{Zn}(\text{II})$ ions differ between structures. In **BDMCZn-4a**, each $\text{Zn}(\text{II})$ centre adopts a square based pyramidal geometry ($\tau = 0.28$) with four oxygen atoms from three different BDMC linkers on the basal plane (depicted in figure 8a; β -diketone is shown in red and phenolate in black) and one N atom from a pyridine moiety in the apical position (figure 8a displayed in green). In **BDMCZn-4a**, the angles O–Zn–N are between 96.1° and 108.2° and the angles O–Zn–O are in the range 76.8 – 93.4° . In contrast, the $\text{Zn}(\text{II})$ centres in **BDMCZn-4b** display a bipyramidal trigonal geometry ($\tau = 0.79$) having at the apical positions a phenolate group (figure 8b, in black) from a CCMoids and a half-coordinated β -diketone moiety from another (figure 8b, in red). The equatorial positions contain similar fragments and include a pyridinic moiety (figure 8b, in green). In **BDMCZn-4b**, the angles are rather smaller for O–Zn–N (86.8 – 129.3°) and larger for O–Zn–O (79.1 – 98.1°).

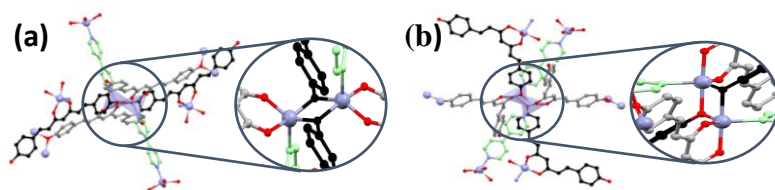


Figure 8. Repeating unit showing the coordination modes of $\text{Zn}(\text{II})$ and BDMC for **BDMCZn-4a** and **-4b**, respectively.

Again, **BDMCZn-4a** and **BDMCZn-4b** present similar trends in the way of expanding and connecting the dimers through the phenolate bridges and the bpy. Both structures display all the BDMC units coordinated through the β -diketone moiety to one Zn(II) ion and one phenolate ring to another centre, remaining protonated the second phenolate in the CCMoid unit and giving an overall 3D structure (figures 9a,b). Another important difference between these two products resides in the incorporated solvents: H₂O and EtOH in **BDMCZn-4a**, and only EtOH in **BDMCZn-4b**, which intermolecular interactions add discrepancies between the two 3D structures (figures 9a, b).

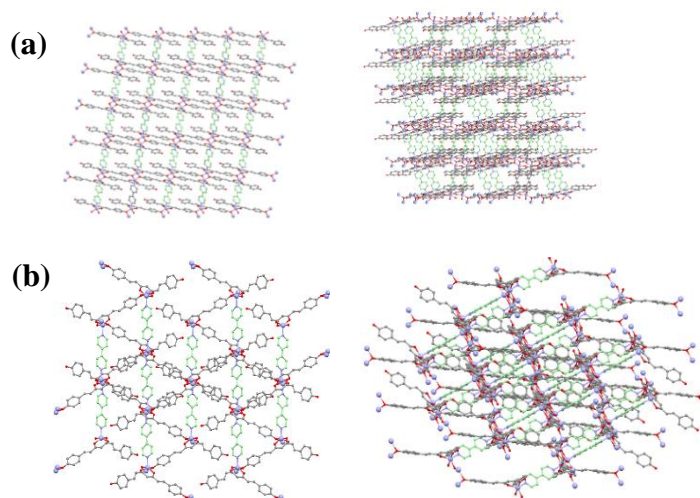


Figure 9. Projections of the tridimensional structures of (a) **BDMCZn-4a** and (b) **-4b**.

The void space in **BDMCZn-4a** take up 20.2 vol% of the unit cell volume. The porosity is organized in 1D channels extended in the b axis (figure 10a). The EtOH/H₂O molecules fill up such porous and are distributed in pairs, relating through an inversion centre, having strong hydrogen bonds between one EtOH and one H₂O molecule within the sets (with a O_{H₂O}...H-O_{EtOH} distance of 2.630 Å and angle of 164.9°). In addition, each one of these molecules presents several interactions with the surroundings, displaying O _{β -diketone}-O_{H₂O}, C-H_{py}...O_{H₂O}, and C-H_{CCMoid}...O_{EtOH} distances of 2.793, 2.874, and 3.636 Å, in that order (showing in the last an angle of 169.64°). This crowded supramolecular network allows the interrelation of separated BDMC linkers through the solvent molecules (figure 10c).

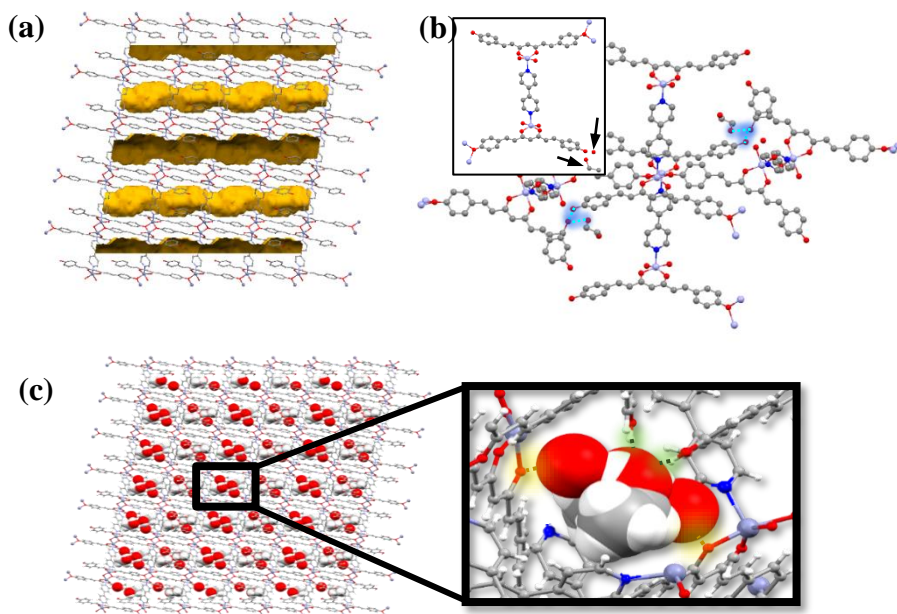


Figure 10. Structure of **BDMCzn-4a**: (a) void maps of the channels (generated by Mercury), (b) established H bonding (arrows indicate the solvent molecules) (c) filling of the voids with solvent molecules, H-bonds highlighted in green and yellow. Colour legend: Zn, light blue; C, grey; O, red; N, dark blue; H atoms are omitted for clarity.

For **BDMCzn-4b**, the structural porosity is reduced to 12.6 vol%, constituted by isolated non-connected pores (figure 11a) where the EtOH molecules are placed. The adsorbed EtOH units are disordered, displaying, in the structure, the same probability for two opposite positions at the same location (green and blue in figure 11b). Now, the EtOH is confined in a smaller void, surrounded by pyridinic and CCMoid segments, with not as effective hydrogen bonding as in the former, presenting short $O_{\text{Phenol}} \cdots H-O_{\text{EtOH}}$ distances (2.941 Å) but small angles; such poor interactions allow the dual disposition of the molecule in the crystal.

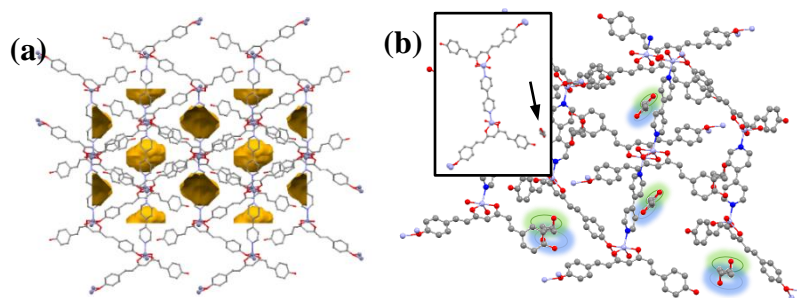


Figure 11. Structure of **BDMCZn-4b**, (a) H-bonding established between the BDMC residues, solvent molecules mark with arrows. (b) void maps of the isolated voids (generated by Mercury). Colour legend: Zn, light blue; C, grey; O, red; N, dark blue; H atoms are omitted for clarity.

In **BDMCZn-4b** the softer interaction with the solvent is compensated with additional contacts between the neighbouring BDMC molecules. They are basically H-bonding interactions between one oxygen from the β -diketone of one molecule and the proton of the non-coordinated phenol of another. To do so, in the same way that occurs for the structure of the non-solvated pristine ligand (chapter I), one of the sides of the CCMoid molecule in **BDMCZn-4b** rotate allowing the interaction between them (figure 12).

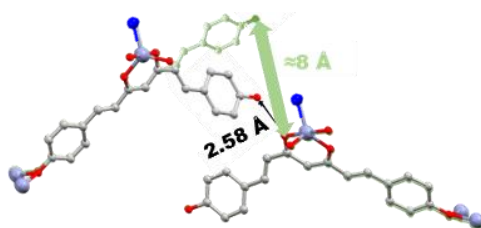


Figure 12. Disposition of two BDMC molecules in the **BDMCZn-4b** structure. Superimposed in green, the hypothetical disposition and distance of the extended conformation is shown. Colour legend: Zn, light blue; C, grey; O, red; N, dark blue; H atoms are omitted for clarity.

In the case of **BDMCZn-4c**, its structure could not be resolved even though it was the major phase obtained in the solvothermal treatment of the Zn:BDMC:bpy mixtures. For this compound, knowledge of the composition and formulas was acquired using EA and TGA (SI) data together with solid-state ^{13}C NMR studies and ATR-FTIR spectrum.

The lack of a single-crystal structure for **BDMCZn-4c** has been compensated with the knowledge acquired by EA and CPMA ^{13}C (see corresponding sections).

4.1.2. CPMAS¹³C. Structural correlation studies

As it has been explained in the characterization technique chapter and shown as well in chapter I, the ¹³C NMR in solid state give us information about the disposition and environment of each C atom. The CPMAS¹³C of all the CCMoid-CPs were measured as well as the spectrum of the pristine ligand. All the CPs with a resolved structure provides relevant information regarding the coordination and conformation of the BDMC molecules in each case. Particularly, this study was applied to the spectra of the unknown structures to have further insight in their composition. The spectra of the different CCMoid-CPs compared with the pristine BDMC are shown in figure 13 and the displacements in table 2.

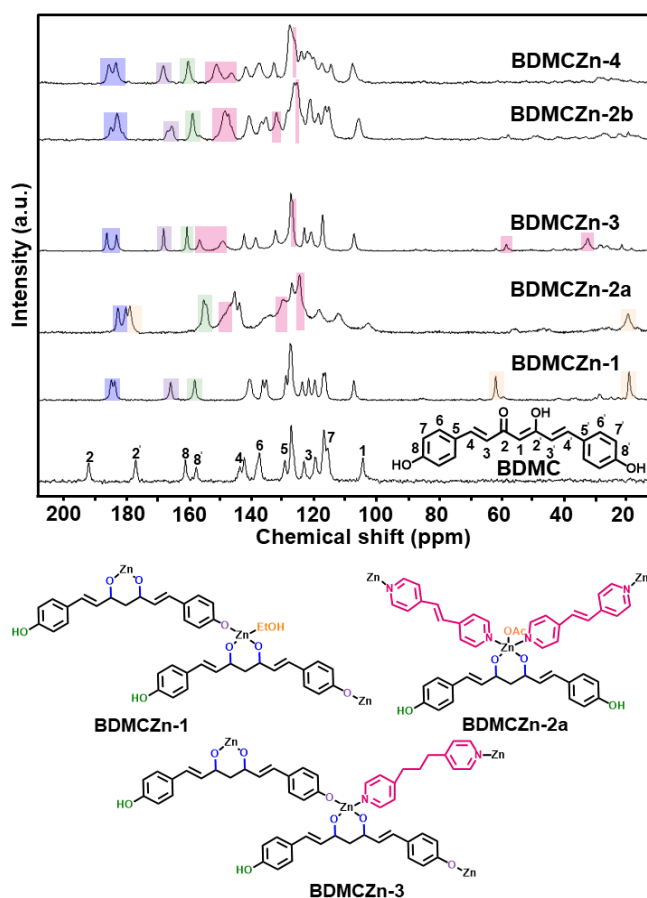


Figure 13. CPMAS¹³C spectra of the pristine BDMC and CPs. Assignment of the peaks in the pristine ligand and highlighted peaks in the CP following a colour code (signals from co-linkers in pink, β-diketone in blue, coordinated phenol in purple, free ones in green and additional coordinated molecules in orange).

Table 2. Carbon displacement values of BDMC and CPs.

	Chemical shift [ppm]							
	BDMC signals				Co-linker signals			
	C2	C2'	C8	C8'	C1	Ring	C-chain	Other
BDMC	191.89	176.80	160.79	157.32	103.69	---	---	---
BDMC Zn-1	184.64	183.51	165.55	157.77	106.59	---	---	EtOH 18.10 (CH ₃ -) 60.96 (-CH ₂ -OH)
BDMC Zn-2a	179.86	182.46	154.90	153.95	102.03	150.90 146.96 126.58	135.52 132.96	AcOH 18.42 (-CH ₃) 179.86 (-C=O)
BDMC Zn-2b	184.77	180.83	165.15	158.39	104.92	148.05 146.93 124.82	131.47	182.72 (unknown)
BDMC Zn-3	186.09	182.91	167.79	160.29	106.52	156.22 148.82 126.39	31.34 25.19	---
BDMC Zn-4c	185.40	183.14	167.88	159.91	106.97	150.87 145.79 121.64	---	---

This way, comparing **BDMCZn-1** and **BDMCZn-3**, the chemical shifts of C2 and C2' appear closer now and at lower fields than pristine BDMC (184.64 and 183.51 ppm for **BDMCZn-1** and 179.96 and 178.61 ppm for **BDMCZn-3**, respectively). This alignment is a consequence of the coordination of the β -diketone moiety with Zn(II) ions, making C2 and C2' alike. For **BDMCZn-2a**, a similar behaviour is observed (appearing at 182.46 and 179.86 ppm, respectively), although here the spectrum displays an additional signal from the C=O group of the acetate ligand coordinated to the metallic centre (at 179.86 ppm). In addition, the C8' chemical displacement for **BDMCZn-1** and **BDMCZn-3** remains similar to the pristine BDMC, as the moieties that contain this carbon atom remain uncoordinated in these structures. Nevertheless, the analogous in each system displays shifts to lower fields (than BDMC) due to the coordination of this phenol group to a Zn (II) centre. However, when the two phenol groups in the phenyl rings remain free, as it happens in **BDMCZn-2a**, the displacement of C8 and C8' are close in value among them and similar to pristine those of BDMC as well. Additional features for **BDMCZn-1** were

observed, such as the shifts for the coordinated EtOH (18.10 and 60.96 ppm corresponding to the CH₃- and the -CH₂-OH, respectively) that are well-differentiated, as well as the signals of the coordinated acetate moiety in **BDMCZn-2a** (179.86 and 18.42 ppm, corresponding to the -C=O and the -CH₃, in that order). In a similar manner, chemical shifts of the pyridinic co-linkers for **BDMCZn-2a** and **BDMCZn-3** appear in the range of 120 to 160 ppm (aromatic groups of bpe and bpy together with the double bond from the bpe system) and between 30 to 60 ppm in the case of the aliphatic groups of **BDMCZn-3**. Their assignment was possible by comparing with the CPMAS¹³C spectra of the free co-linkers.

The correlation attained by analysing the displacement and the structures of **BDMCZn-1**, **BDMCZn-2a** and **BDMCZn-3** was used towards the analysis of the spectra of the unresolved systems: **BDMCZn-2b** and **BDMCZn-4c**. The necessity of a significant amount of sample (approx. 100 mg) limited the use of the technique towards the analysis of the minor phases, such as **BDMCZn-4a** and **BDMCZn-4b**. Nevertheless, general trends from the co-linkers observed in **BDMCZn-2a** and **BDMCZn-3** were also applicable for the bpy bridges in **BDMCZn-4c** (table 3). In addition, the displacements in the CPMAS¹³C NMR spectra of **BDMCZn-2b** and **BDMCZn-4c** indicate the coordination of their respective BDMC linkers through the keto/enol moiety and one phenolic ring. In both cases, the displacements of C2 - C2' and C8 - C8' were similar to those found for **BDMCZn-1** and **BDMCZn-3**. Furthermore, both spectra suggest exclusive coordination of the Zn(II) centres with BDMC and bpe or bpy, excluding the possibility of extra coordinated with EtOH or acetate molecules. Having into account all the above and the information gathered through EA, it is expected a higher dimensional structure for **BDMCZn-2b** than for **BDMCZn-2a**. We base our hypothesis on the double coordination of the BDMC linker and displacements of the bpe C atoms, together with the estimated stoichiometry found by EA ([Zn(BDMC)(bpe)_{0.5}]). Here, the CPMAS¹³C spectrum strongly suggests the formation of a similar structure to that found for **BDMCZn-3** (figure 7), including the possibility of a different coordination number for the Zn(II) within the structure comparing with **BDMCZn-4a** and **BDMCZn-4b** (four instead of five in both cases).

4.1.3. Elemental analysis.

In general, an excellent correlation between the values of the elemental analysis obtaining experimentally and the calculated one is observed for the resolved structures, proving once more the purity of the species (table 4). Especially important were the results for the not resolved structures, **BDMCZn-2b** and **BDMCZn-4c**. In that way, the formulae [Zn(BDMC)(bpe)_{0.5}] and [Zn(BDMC)(bpy)_{0.5}]_n·2nH₂O were proposed, in that order, based on the previous characterization techniques and the good fitting of the EA data (table 3).

Table 3. Experimental (Exp.) values obtained in the elemental analysis of the CPs and values calculated (cal.) from the formula presented in the second column.

Name	Formula	%C		%H		%N	
		Cal.	Exp.	Cal.	Exp.	Cal.	Exp.
BDMCZn-1	ZnC ₂₁ H ₁₉ O ₅	60.52	57.99	4,60	5.30	---	---
BDMCZn-2a	ZnC ₃₃ H ₂₈ O ₆ N ₂ ·2H ₂ O	60.98	61.05	4.96	4.76	4.31	4.54
BDMCZn-3	Zn ₂ C ₅₁ H ₄₂ O ₈ N ₂ ·C ₂ H ₆ O	64.45	64.03	4.9	5.21	2.84	2.91
BDMCZn-2b	ZnC ₂₅ H ₁₉ O ₄ N	64.88	64.41	4.14	4.42	2.9	3.03
BDMCZn-4c	ZnC ₂₄ H ₁₈ O ₄ N·2H ₂ O	59.33	58.71	4,56	4.07	2,88	3.4

EA data for **BDMCZn-4a** and **BDMCZn-4b** were not possible due to the small quantity obtained of both samples.

4.1.4. Powder XRD

The homogeneity and purity of the precipitated samples is relevant for their final characterization and application, as it happens in general for other CPs. For this purpose, powder XRD is of great assistance and it is used as a routine method to evaluate these features by analysing the experimental pattern in comparison to that of reagents, secondary phases or simulated patterns obtained from single crystallographic data. In our case, the comparison of the different BDMC-CPs is depicted in figure 14, where the simulations are in grey and the experimental data in different colours.

Figure 14 shows a good match between the simulated and the experimental patterns of **BDMCZn-1** (blue) and **BDMCZn-3** (purple), respectively. In the case of **BDMCZn-2a** (green) differences (mainly peaks at $2\theta = 5.96$ and 8.62°) are attributed to the low stability of the crystals in the absence of solvent (figure 15). Moreover, no crystalline material was achieved for **BDMCZn-2b** (yellow) and **BDMCZn-4c** (red), so there are not simulated PXRD for them. In the same way, **BDMCZn-4a** and **BDMCZn-4b** were isolated in small quantities, not having the proper amount to perform powder XRD characterization. For these two, the simulated patterns were obtained from the single-crystal XRD studies. The comparison between the two simulated spectra from **BDMCZn-4a** and **BDMCZn-4b** with that of **BDMCZn-4c** (red), shows that the structure obtained for the last one is different.

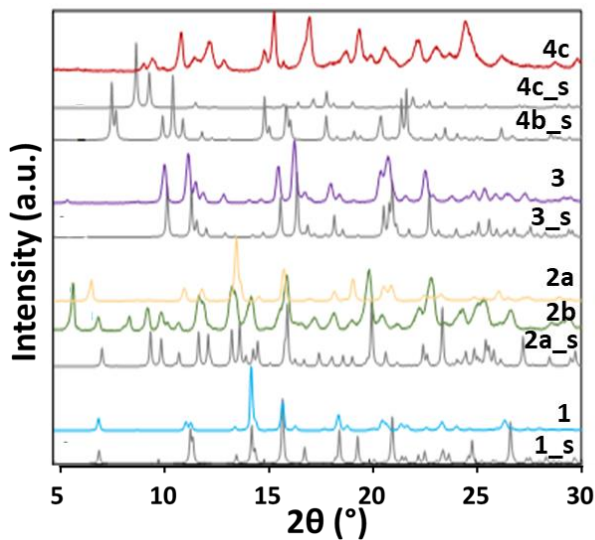


Figure 14. PXRD patterns of the different BDMC-CPs species, in which the coloured lines correspond to measurements performed for the bulk powder of the different samples (blue for **BDMCZn-1**, green for **BDMCZn-2a**, yellow for **BDMCZn-2b**, purple for **BDMCZn-3**, and red for **BDMCZn-4c**) whereas the grey lines represent the simulated profiles from single crystal structures (CuK α wavelength).

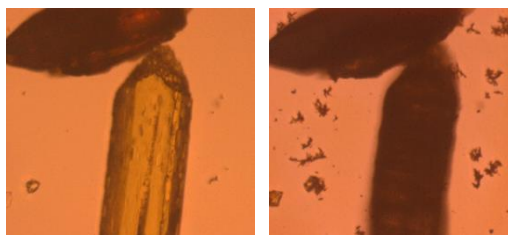


Figure 15. Pictures of a crystal of **BDMCZn-2a** using an optical microscopy: (a) just after solvent removal, and (b) after the complete drying.

Some small shifts in 2θ , observed between the simulated and the experimental patterns, are associated with low temperature measurements (at 100 K) in single XRD versus the room temperature in PXRD experiments.

4.1.5. General trends in BDMC-CPs

From the point of view of the CCMoid ligand, BDMC has three potential positions for the coordination to metal centres: one from the β -diketone moiety and two for each phenol group on the sides of the molecule. However, full coordination of BDMC has not been observed in this work, with or without the use of co-linkers.

Total coordination has been only described for CPs based on Zn(II)/CCM that have been precipitated in mixtures of alcohol and a rather basic solvent, such as dimethylacetamide (DMA) or dimethylformamide (DMF).²² The basic solvent can help in the deprotonation of the phenol lateral groups. The coordination of only one corner of CCM was previously observed in our group using $scCO_2$ as solvent and EtOH as co-solvent.^{iError! Marcador no definido.} The work of this doctoral thesis involves several trials using basic solvents as well, however, no crystals were achieved in this way with BDMC, regardless of the use or absence of co-ligands. In fact, from all the solvents tested (DMA, DMF, DEF, ACN and acetone), only MeOH and EtOH provided crystalline or semicrystalline materials. Particularly, with EtOH, the number of coordinated positions of the BDMC molecules never reached a maximum, displaying only one binding position in **BDMCZn-2a** and two sites in **BDMCZn-1**, **BDMCZn-3** and the **BDMCZn-4** series. As expected, in all cases, the most reactive group is the central β -diketone moiety which always appears coordinated.

All the systems studied in this chapter can be categorized by two factors: (i) the dipyridinic co-linker used (considering equal attachment although different lengths and flexibility) and (ii) the adsorbed/coordinated solvent molecules. Both factors affect in great manner the coordination and conformation adopted by the main linker, BDMC.

4.1.5.1. Dipyridinic co-linkers

Our analyses indicate that the addition of a dipyridine based co-linkers increases the dimensionality of the systems with respect to **BDMCZn-1**, going from 1D to 3D, independently of the quantity of co-linker used. Only **BDMCZn-2a**, that involves the addition of bpe molecules, displays a 1D network. The difference with the rest of co-linkers may relates with its length (distance N1-N2 of 9.37 Å) and limited degree of flexibility. Bpe confers the possibility of locate the Zn(II) metal centres far away from each other (distance Zn-Zn of 13.49 Å) thus, restricting potential interactions between BDMC molecules and the Zn(II) atoms, preventing further coordination of the ligand through its additional sites. Certainly, in **BDMCZn-2a**, the BDMC did not act as a linker extending the network of the CP, but rather it is essentially a ligand that completes the coordination of Zn(II) centre. However, in the presence of low amounts of bpe, as it happens in **BDMCZn-2b**, and taking into account the information supplied by ¹³C NMR

and EA, coordination modes through two positions are interpreted, participating the BDMC in the extension of the chain.

In the cases of **BDMCZn-3** and the **BDMCZn-4** series, involving bpp (with an L-shape due to its flexible aliphatic skeleton) and bpy, respectively, the N1-N2 distances are shorter than that of bpe (6.87 and 7.06 Å, in that order). The length of both co-linkers is adequate to allow the coordination of the BDMC molecules through two points (the β -diketone and one phenolate group) to Zn(II) atoms. These CPs are extended simultaneously by means of the BDMC and respective dipyridinic co-linkers, resulting in 3D structures with variable complexity.

4.1.5.2. Adsorbed/coordinated solvent molecules

For the analysis of the crystal structures based on the BDMC linker, it should be considered the different disposition of the phenolic rings promoted by the conformations originated within the CCMoids skeleton (figure 16). For that, it is worthwhile to pay attention to the networks described for the pristine and solvated BDMC ligand.

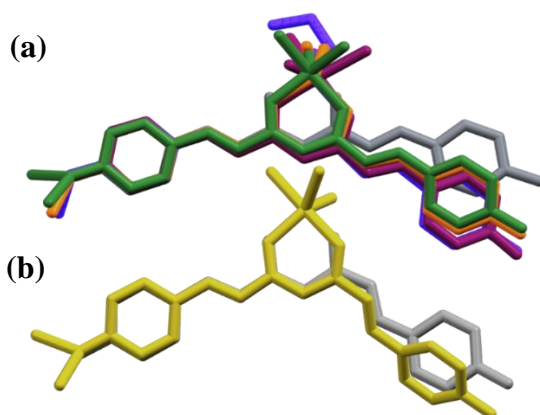


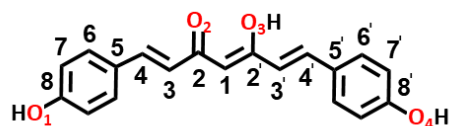
Figure 16. Superimposition of the BDMC moieties in the asymmetric units of the different precipitated compounds, compared to pristine BDMC conformations: (a) BDMC-H₂O (grey), **BDMCZn-1** (blue), **BDMCZn-2a** (purple), **BDMCZn-3** (orange), **BDMCZn-4a** (green), and (b) BDMC (grey), **BDMCZn-4b** (yellow).

In figure 16, the structures of the **BDMCZn-1**, **BDMCZn-2a**, **BDMCZn-3**, **BDMCZn-4a** and **BDMCZn-4b** systems are compared with the conformation of pristine BDMC in either the solvated (involving H₂O, figure 16a) or unsolvated crystal (figure 16b). Superimposition of the BDMC molecules taken from the asymmetric unit of each system shows the flexibility of the CCMoid molecule which adopts different conformations. The BDMC disposition in **BDMCZn-1**, **BDMCZn-2a**, **BDMCZn-3** and **BDMCZn-4b** is similar to

that found in solvated BDMC (figure 16a), while **BDMCZn-4c** has a conformation similar to that of the non-solvated BDMC (figure 16b).

As it was explained in chapter I, BDMC prefers to crystallise together with solvent molecules forming solvated systems. This fact decreases the crystal free energy, the solvent species fill voids and/or bind efficiently molecules from the structure, providing a multipoint hydrogen bonding network. Typically, adsorbed protic solvents are involved in the formation of this type of supramolecular networks, by acting as bridges between consecutive BDMC molecules. Therefore, BDMC molecules appear separate enough to adopt a non-tensioned, near-flat conformation. Previous works had shown that the asymmetric units of BDMC·H₂O and BDMC·MeOH are composed by one molecule of BDMC with O1-O4 distances (numeration of BDMC molecule in table 2) of 17.79 Å and to 17.73 Å, respectively.^{23,24} On the contrary, non-solvated BDMC structures display packing arrangements in which the molecules present strong and direct interactions among them. To achieve this, the BDMC adopts distorted conformations presenting curvy forms or parts of their molecular backbone not fully extended, presenting both cases shorter O1-O4 phenolate distances (numeration of BDMC molecule in table 2) between 16.41 and 17.06 Å. Similarly, the BDMC conformations found in this work can be classified analysing the established short interactions and hydrogen bonding created with the solvent or even additional molecules. These interactions affect the overall BDMC architecture, with one side of the molecule remaining fully extended and planar (typically the one containing the phenolic ring coordinated to the metal) defined in all the cases here as plane P1 (determined by C3 to C8, numbers shown in table 4). The other side of the CCMoid molecule is contained in plane P2 (determined by C3' to C8', numeration of BDMC molecule in table 4). Significant atomic distances between O1-O4 for the coordinated BDMC linkers and P1-P2 angles are shown in table 4 for each resolved CP.

Table 4. BDMC distances O1-O4 and angles P1-P2 in the different compounds. The schematic draw shows the linker conformation in each compound.



	O1-O4 [Å]	P1-P2 [°]	Schematic draw
BDMCZn-1	17.32	10.32	
BDMCZn-2a	16.57	38.26	
BDMCZn-3	17.05-17.30	8.76-11.19	
BDMCZn-4a	15.98	17.75	
BDMCZn-4b	15.98	44.10	

Taking into account the defined P1 and P2 planes, we can extrapolate that, in **BDMCZn-1**, the CCMoid linker has a quasi-flat conformation with a P1-P2 angle of 10.32° and one of the longest O1-O4 lengths (17.32 Å). Here, the BDMC molecules interact through the coordinated EtOH molecule. The context for **BDMCZn-2a** is quite different, since the BDMC coordinates the Zn(II) centre through the β -diketone moiety and the network is exclusively extended by the bpe co-linker. Hence, the co-linker establishes the 3D structure, allowing extra structural degrees of freedom for the BDMC ligand. Therefore, the latter can fully interact with the surroundings, creating hydrogen bonding through

both phenol groups and restraining the ligand. As a result, the BDMC displayed a curved geometry with a marked P1-P2 angle of 38.26°, which bring together the O1-O4 atoms to a distance of 16.57 Å. On the other hand, compound **BDMCZn-3** has an elaborated 3D structure with four differentiated BDMC conformations that interact through bridges of EtOH and H₂O. The result is a low distorted and almost flat conformation for all the BDMC molecules, with O1-O4 distances and P1-P2 angles between 17.05-17.30 Å and 8.76-11.9°, respectively. Finally, the **BDMCZn-4x** series (**BDMCZn-4a**, **BDMCZn-4b** and **BDMCZn-4c**), involving the bpy co-linker, exhibit the strongest influence of the adsorbed solvent in the resulting structures. Note that **BDMCZn-4a** and **BDMCZn-4b** had the same network stoichiometry, [Zn₂(BDMC)₂(bpy)]_n, differing in the composition only in the adsorbed solvent molecules (H₂O or EtOH). In **BDMCZn-4a**, strong hydrogen bonds are established through H₂O and EtOH bridges and here the BDMC adopts a near planar geometry with a O1-O4 distance of 17.42 Å and a P1-P2 angle of 17.75°. In a different scenario, the adsorbed EtOH molecules in **BDMCZn-4b** interact weakly with the crystal network. In this case, the lack of interaction of the BDMC linkers through solvent bridges results in a highly tensioned molecule with a distorted conformation. As a result, the O1-O4 distance is of 15.98 Å and the P1-P2 angle of 44.10°. Again, larger stretching promotes the approximation between BDMC molecules, allowing short interactions that stabilize the structure with the corresponding higher distortion of the CCMoid skeleton, through the site that remains uncoordinated (figure 15).

4.1.6. Supplementary structural analysis of CCMoid-CPs

4.1.6.1. Infrared spectroscopy (FTIR-ATR)

In figure 17, the FTIR-ATR spectra obtained for the pristine ligand and the CPs are compared. As expected, a reduction of the band related with the O-H stretching is observed in the CPs due to the coordination of the β-diketone and part of the phenol groups as well (in blue, figure 17a). Taking into consideration the window between 1600 and 550 cm⁻¹ (figure 17b), unambiguous changes related to the C=O vibrational modes are observed (from 1600 to 1550). In general, there are slight shifts of the peaks of 1619 and 1598 cm⁻¹ (in green figure 17) with the most relevant changes for the bands of 1598 and 1562 cm⁻¹ (in yellow, figure 17b), almost vanished. Since these bands are related to the bending of the C-OH of the enol moiety of the β-diketone and the hydroxyl groups of the aromatic ring²⁵, is logical to assume that coordination promotes such changes. As well as it is also reasonable to still observed part of the bands when there are hydroxy groups that remain protonated. In the case of **BDMCZn-2a**, the existence of a carboxylic group may provide the superposition of different vibrational modes at 1608 cm⁻¹. In addition, there is a band in the 1550-1650 cm⁻¹ region that may relate to the δC-OH (in blue, figure 18b) from two uncoordinated phenyl groups.

Regarding the rest of the spectra, some differences are observed that can be also associated with the coordination and the presence in the structures of bipyridine units. This relates to the duplicity in the pristine CCMoid of some peaks due to the lack of symmetry in the keto-enol form. Kolev *et al.*^{!Error! Marcador no definido.} already described this effect assigning peaks at approximately 933 and 922 cm^{-1} to the bending of CCH and CCC in the enol and keto sides, respectively.

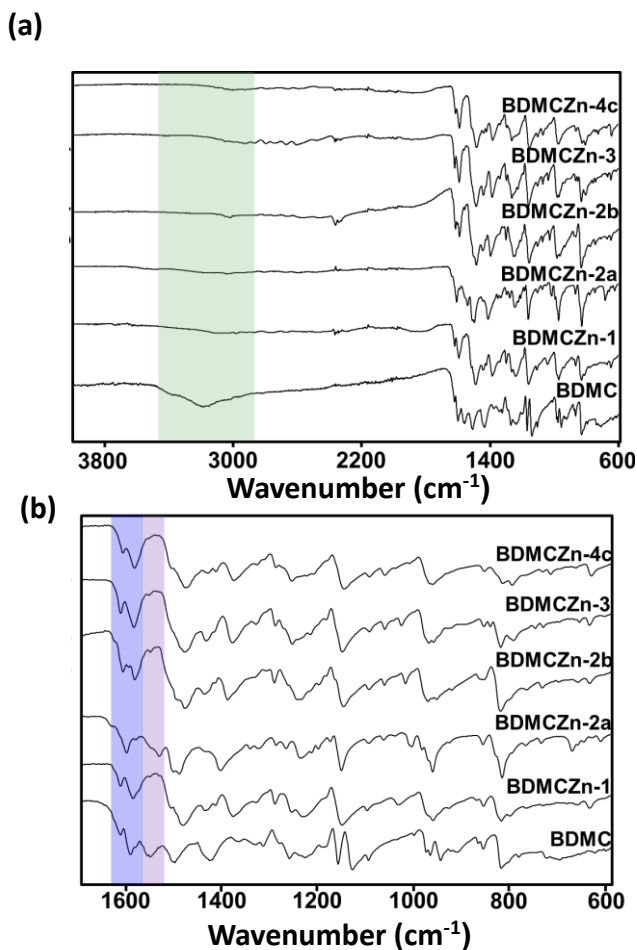


Figure 17. FTIR-ATR spectra of BDMC and the CPs. (a) Entire spectra from 3800 to 550 cm^{-1} and (b) zoom in the 1700-550 cm^{-1} region.

4.1.6.2. Morphology of the crystals. Optical microscope and SEM images

The observation of the **BDMCZn-1** crystals under the SEM allows the differentiation of twinning formed by the agglomeration of plates (figure 18). Their breaking allowed the separation of suitable single crystals for their analysis using a conventional single crystal diffractometer.

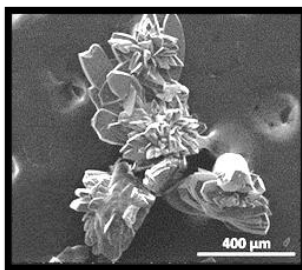


Figure 18. SEM image of some crystals of **BDMCZn-1**.

The rest of CPs appear as spherulites (figure 19). Defined as “radially polycrystalline aggregates with an outer spherical envelope” by Shtukenberg *et al.*²⁶, some of the crystallised spherulites in this work were found in millimetre sizes, but there was a lack of homogeneity between different batches. In general, the spherulites are formed from single crystal nuclei that grow radially. In some cases, controlling the experimental conditions, such as the concentration or the temperature, it becomes possible to achieve single crystal nuclei with high quality for XRD analysis. Unfortunately, trials performed in this doctoral thesis toward this objective were unsuccessful. As a second option, the spherulites were broken with the aim of finding reasonable single crystals suitable for single crystal XRD. However, having into account the size of this subunits (figure 20), this was a challenge in conventional diffractometers and in all the cases the use of a synchrotron source was necessary.

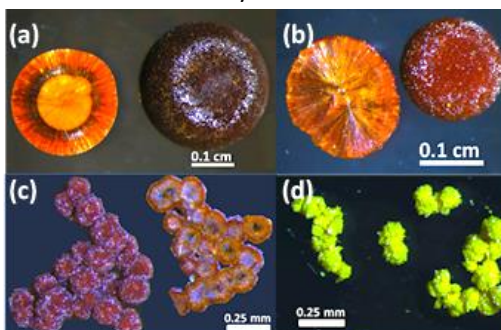


Figure 19. Images of the spherulite crystals of (a) **BDMCZn-3** synthesized in MeOH, (b) **BDMCZn-3**, (c) **BDMCZn-4c** (d) **BDMCZn-2a**.

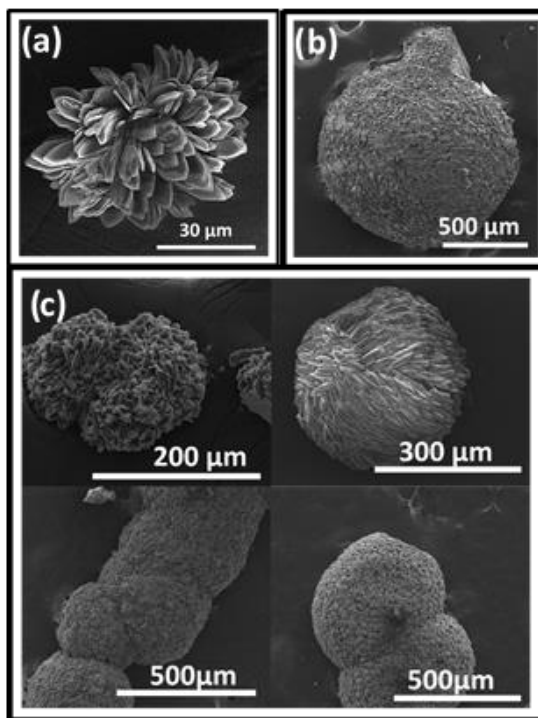


Figure 20. SEM images of (a) **BDMCZn-2a**, (b) **BDMCZn-3**, (c) different spherulites found in **BDMCZn-4**.

4.2. Synthesis in scCO_2 .

In general, scCO_2 synthesis provide powdered products involving small particle sizes, hindering the structural analysis by single crystal XRD. In addition, the small domains of these crystalline powders are randomly oriented producing a huge variety of environments that translate in broad signals in $\text{CPMAS}^{13}\text{C}$ NMR making their interpretation also difficult. The products prepared in this doctoral thesis by scCO_2 synthesis show this morphological characteristic, although, despite of the drawbacks, some conclusions could be extracted and are presented below.

4.2.1. Powder XRD

BDMCZn-1sc

The reaction between $\text{Zn}(\text{acac})_2$ and BDMC in scCO_2 (**BDMCZn-1sc**) gave a dark red solid. The powder XRD diffractogram showed an amorphous product (figure 21).

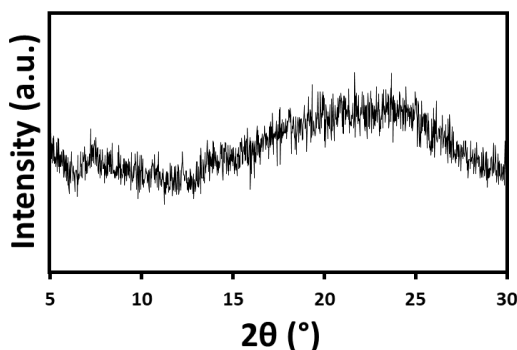


Figure 21. XRD patterns of **BDMCZn-1sc**.

This, together with the high solubility of the product in organic solvents (EtOH, DMSO...), indicated that most likely it corresponded to a mononuclear coordination compound instead of a CP. Nevertheless, the product was further characterized by FTIR and compared with the rest of structure below.

BDMCZn-2sc, BDMCZn-3sc and BDMCZn-4sc

By using as a co-linker any of the three bipyridinic molecules described above, yellow crystalline powders of different tonalities were attained.

In the reactions with co-linkers, crystalline products were obtained with the patterns depicted in figure 22. None of them match with those from the CPs obtained with the solvothermal method, indicating the presence of new structures.

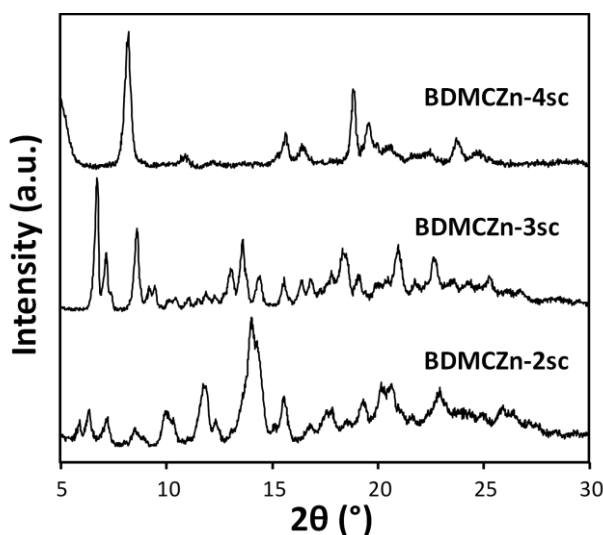


Figure 22. XRD patterns of **BDMCZn-2sc**, **BDMCZn-3sc** and **BDMCZn-4sc**.

4.2.2. Infrared spectroscopy (FTIR-ATR)

As it has been shown for the CCMoid-CPs obtained using the solvothermal method, the FTIR-ATR spectra can provide some insight of structural features for the CCMoid-CPs in scCO_2 . The FTIR-ATR spectra of the scCO_2 products are shown in figure 23.

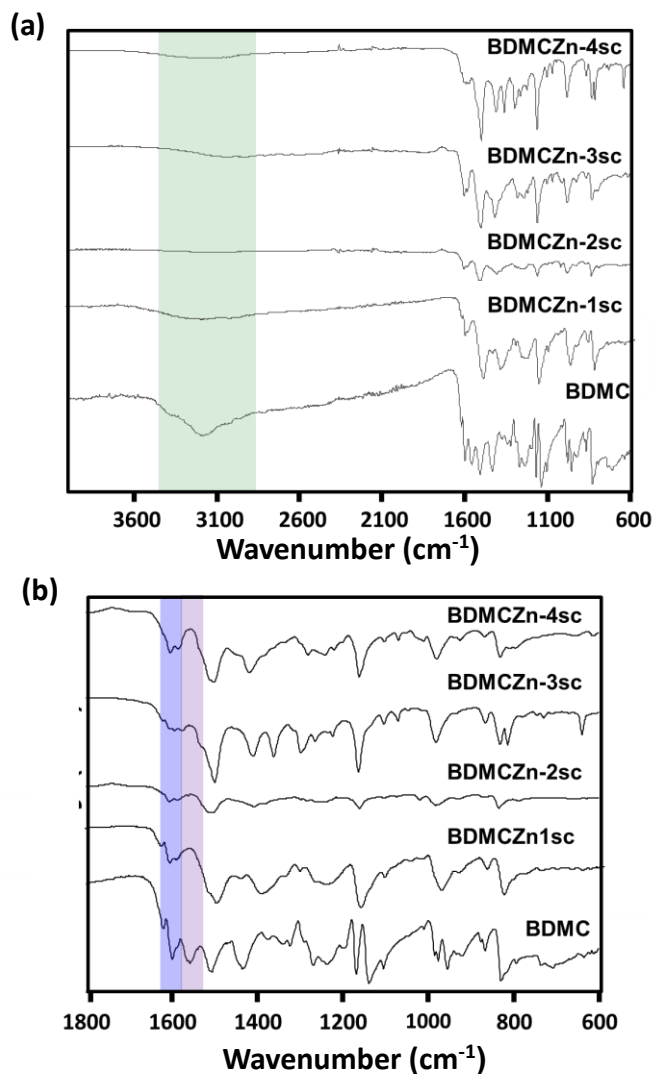


Figure 23. FTIR-ATR spectra of the products obtained in scCO_2 . (a) Entire spectra from 3800 to 550 cm^{-1} and (b) zoom in the 1700-550 cm^{-1} region.

Figure 23 shows some vibrational features already observed in the CCMoid-CPs obtained with the first method. For instance, reduction of the vibrational peaks related with the

O-H stretching in all the CPs, with respect to the pristine ligand (in green, figure 23a). However, in the region between 1600 and 550 cm^{-1} (figure 23b), the three supercritical systems display different trademarks than solvothermal products. Multiple signals were observed related to the C=O stretching (in blue, figure 23b) for **BDMCZn-1sc**, **BDMCZn-2sc** and **BDMCZn-3sc**, correspondingly, suggesting that the CCMoid and also the acac ligand could be still coordinated to the Zn(II) centres. The spectrum of **BDMCZn-4sc** was similar to the pristine CCMoid ligand, suggesting that the system is only coordinated by the β -diketone moiety to the Zn(II) ions.

The solubility of the three solids was tested in typical organic solvents (EtOH, MeOH, acetone and DMSO). The three solids have low solubility in the studied solvents, except for DMSO in which a considerable solubilisation was achieved.

4.2.3. Elemental analysis

EA was measured to determine the composition of the samples, but different fittings could be extracted from the data (table 5) suggesting that not pure products were obtained.

Table 5. Experimental (Exp.) values obtained in the elemental analysis of the results in scCO_2 .

	%C	%H	%N
Name	Exp.	Exp.	Exp.
BDMCZn-1sc	51.09	4.41	----
BDMCZn-2sc	58.22	4.22	3.80
BDMCZn-3sc	62.85	4.38	4.37
BDMCZn-4sc	55.84	3.90	3.44

4.2.4. Morphology

Related with the morphology, the ones that precipitate as microcrystalline powders (**BDMCZn-2sc**, **BDMCZn-3sc** and **BDMCZn-4sc**) present flake shapes in the SEM images but the samples show low homogeneity as well (figure 24).

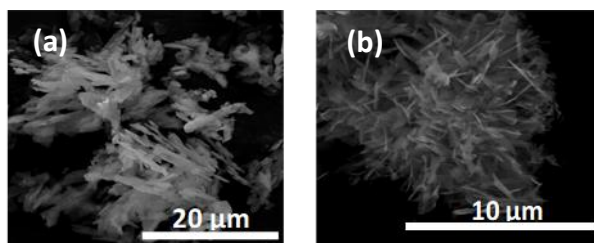


Figure 24. SEM images of: (a) **BDMCZn-2sc** and (b) **BDMCZn-4sc**.

Despite of the limitations to attain the molecular composition for these systems, from the characterization some trends could be extracted. This way, through our analysis we can conclude that in all the cases, at least one CCMoid is coordinated to the metal centre, as can be seen in the IR spectra. Also, in the experiments with the co-linkers, they seem to be included in the structures, because they produce clear changes in the XRD patterns.

4.3. Reactions of BDMC with other metals.

Reactions of the BDMC with other transitional metals (Cu(II) Mn(II), Fe(III), Co(II) and Ni(II)) were pursued as well using the solvothermal method and also introducing here layering methods, different salts of the same metals and solvents. Most of the reactions did not provide solids, only those with Fe(III) and Cu(II) ions provided powder materials.

Concerning the reactions with Fe(III) ions, crystals were obtained by layering processes, solubilizing BDMC in EtOH and Fe(OAc)₃ in water and setting between the two solutions a layer of EtOH. After the complete mixing of the reagents by slow diffusion, hexagonal crystals were obtained and resolved by single crystal XRD using a synchrotron source. However, the acquired data was not proper for publication (R factor 11 %), although, provides a clear idea of the system achieved. Hence, a mononuclear compound with three molecules of BDMC coordinated to a Fe(III) ion was accomplished (figure 25). An octahedral geometry is obtained where only the β-diketone of the three molecules are participating in the coordination leaving free the phenolic part.

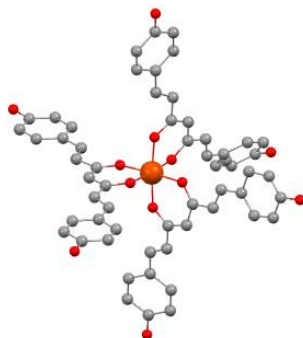


Figure 25. Structure obtained by the reaction of BDMC and iron acetate by slow diffusion. Colour legend: Fe, orange; C, grey; O, red; H atoms are omitted for clarity.

For copper, a fast precipitation of solids was always observed. In that way, different powders were isolated using solvothermal, $scCO_2$ and layering methodologies. The solubility in common organic solvents indicates that probably the β -diketone from the BDMC is the only coordinated ligand. However, this could not be confirmed due to the impossibility of obtaining crystals, even by layering, and the difficulties of using NMR techniques due to the paramagnetic nature of copper.

5. Conclusions

In this chapter, the capability of BDMC as organic linker for the creation of new CPs has been tested as well as the effects of the use of co-linkers and different methodologies. Having into account the results obtained, BDMC can be considered as a promising heteroditopic ligand in the field of CPs. Also, it has been proved that the possibility of adopting different conformations make plausible the formation of different structures. This can be extended to the rest of members of the CCMoid family that present the same skeleton and therefore gives these molecules an advantage over more rigid linkers. In addition, the experimental conditions determine if one or two coordinative positions are bonded to metallic centres. This is interesting since the presence of free phenol groups in the structures opens the possibility of post-synthetic reactions that can modify the properties of the CPs. The used of co-linkers have been an effective solution to increase the dimensionality and the different results obtained highlights the importance in the chosen spacers. All of this emphasizes the rich chemistry that is possible to attain with CCMoids and encouraged us with this study as it is showed in the next chapter.

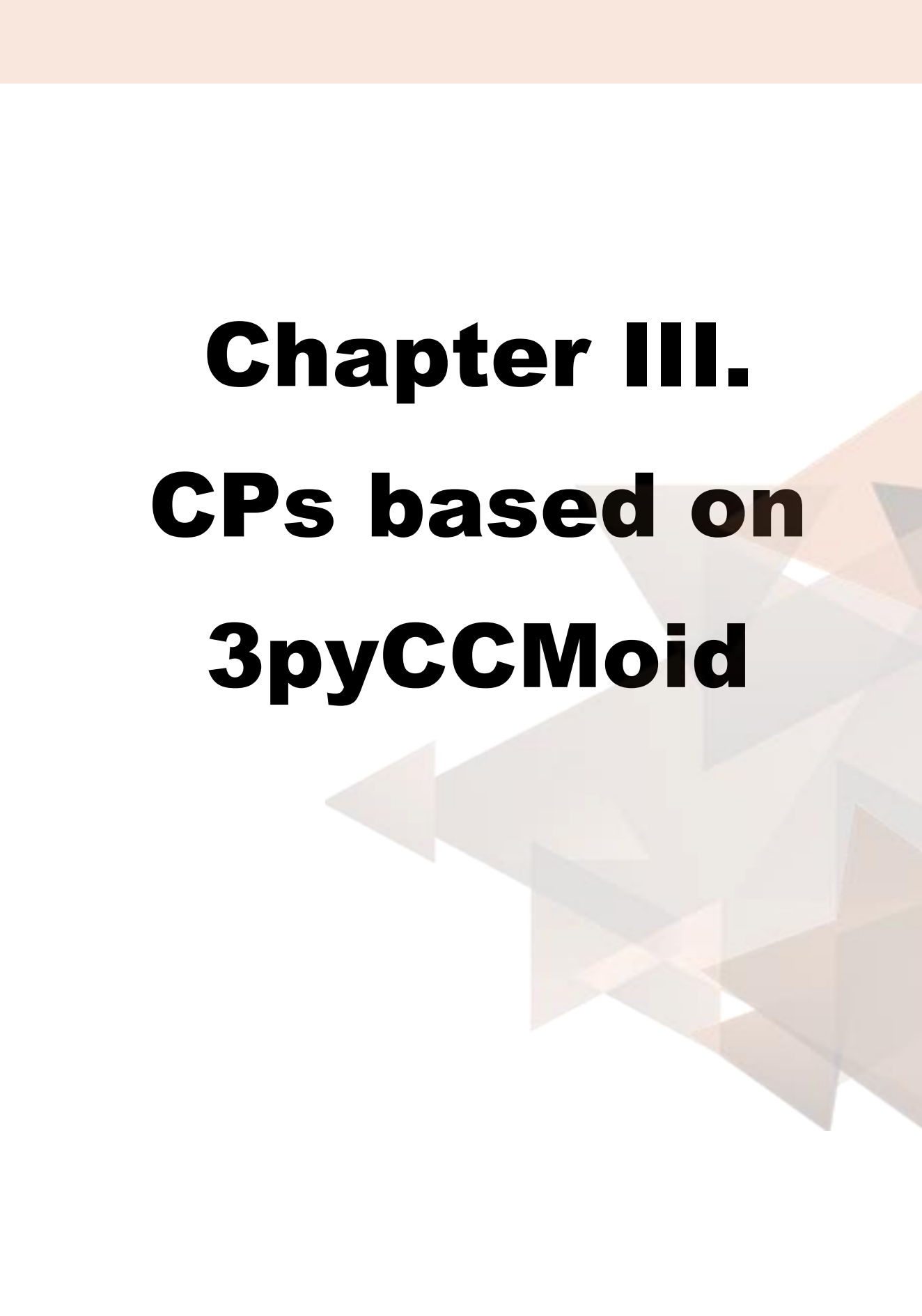
Related to the methodologies, the solvothermal approach is the one that has reported the best results with this type of molecules. The synthesis in $scCO_2$, that had been

proposed as a green alternative and that had given good results with CCM cannot be considered a good strategy to obtain CPs with BDMC. However, it cannot be discarded for future experiments in CPs chemistry, since it has shown interesting results with many molecules (general introduction) and in this chapter the coordination of some parts of the CCMoid in this media has been proved.

6. References

- (1) Su, H., Sun, F., Jia, J., He, H., Wang, A., & Zhu, G. (2015). A highly porous medical metal–organic framework constructed from bioactive curcumin. *Chemical Communications*, 51(26), 5774-5777.
- (2) Portolés-Gil, N., Lanza, A., Aliaga-Alcalde, N., Ayllón, J. A., Gemmi, M., Mugnaioli, E., ... & Domingo, C. (2018). Crystalline curcumin bioMOF obtained by precipitation in supercritical CO₂ and structural determination by electron diffraction tomography. *ACS Sustainable Chemistry & Engineering*, 6(9), 12309-12319
- (3) Jayaprakasha, G. K., Rao, L. J., & Sakariah, K. K. (2006). Antioxidant activities of curcumin, demethoxycurcumin and bisdemethoxycurcumin. *Food chemistry*, 98(4), 720-724.
- (4) Ramezani, M., Hatamipour, M., & Sahebkar, A. (2018). Promising anti-tumor properties of bisdemethoxycurcumin: A naturally occurring curcumin analogue. *Journal of cellular physiology*, 233(2), 880-887..
- (5) Sandur, S. K., Pandey, M. K., Sung, B., Ahn, K. S., Murakami, A., Sethi, G., ... & Aggarwal, B. B. (2007). Curcumin, demethoxycurcumin, bisdemethoxycurcumin, tetrahydrocurcumin and turmerones differentially regulate anti-inflammatory and anti-proliferative responses through a ROS-independent mechanism. *Carcinogenesis*, 28(8), 1765-1773.
- (6) Anand, P., Thomas, S. G., Kunnumakkara, A. B., Sundaram, C., Harikumar, K. B., Sung, B., ... & Aggarwal, B. B. (2008). Biological activities of curcumin and its analogues (Congeners) made by man and Mother Nature. *Biochemical pharmacology*, 76(11), 1590-1611.
- (7) Price, L. C., & Buescher, R. W. (1997). Kinetics of alkaline degradation of the food pigments curcumin and curcuminoids. *Journal of food science*, 62(2), 267-269.
- (8) Basile, V., Ferrari, E., Lazzari, S., Belluti, S., Pignedoli, F., & Imbriano, C. (2009). Curcumin derivatives: molecular basis of their anti-cancer activity. *Biochemical pharmacology*, 78(10), 1305-1315.
- (9) Krishnankutty, K., & Venugopalan, P. (1998). Metal chelates of curcuminoids. Synthesis and reactivity in inorganic and metal-organic chemistry, 28(8), 1313-1325.
- (10) Ummathur, M., Malini, P., & Krishnankutty, K. (2013). Dioxouranium (VI) complexes of some unsaturated β -diketones. *International Journal of Chem Tech Research*, 5, 1-5.
- (11) Krishnankutty, K., Malini, P. T., & Ummathur, M. B. (2011). La (III) complexes of some 1, 7-diaryl-1, 6-heptadiene-3, 5-diones.
- (12) Pettinari, R., Marchetti, F., Condello, F., Pettinari, C., Lupidi, G., Scopelliti, R., ... & Dyson, P. J. (2014). Ruthenium (II)–arene RAPTA type complexes containing curcumin and bisdemethoxycurcumin display potent and selective anticancer activity. *Organometallics*, 33(14), 3709-3715.
- (13) Li, Y., Gu, Z., Zhang, C., Li, S., Zhang, L., Zhou, G., ... & Zhang, J. (2018). Synthesis, characterization and ROS-mediated antitumor effects of palladium (II) complexes of curcuminoids. *European journal of medicinal chemistry*, 144, 662-671.
- (14) Pettinari, R., Marchetti, F., Pettinari, C., Condello, F., Petrini, A., Scopelliti, R., ... & Dyson, P. J. (2015). Organometallic rhodium (III) and iridium (III) cyclopentadienyl complexes with curcumin and bisdemethoxycurcumin co-ligands. *Dalton Transactions*, 44(47), 20523-20531.
- (15) Rodríguez-Cid, L., Sañudo, E. C., López-Periago, A. M., González-Campo, A., Aliaga-Alcalde, N., & Domingo, C. (2020). Novel Zn (II) Coordination Polymers Based on the Natural Molecule Bisdemethoxycurcumin. *Crystal Growth & Design*, 20(10), 6555-6564.
- (16) Pabon, H. J. J. (1964). A synthesis of curcumin and related compounds. *Recueil des Travaux Chimiques des Pays-Bas*, 83(4), 379-386.
- (17) Portolés-Gil, N., Gowing, S., Vallcorba, O., Domingo, C., López-Periago, A. M., & Ayllón, J. A. (2018). Supercritical CO₂ utilization for the crystallization of 2D metal-organic frameworks using tert-butylpyridine additive. *Journal of CO₂ Utilization*, 24, 444-453.

- (18) Dong, L., Chu, W., Zhu, Q., & Huang, R. (2011). Three Novel Homochiral Helical Metal–Organic Frameworks Based on Amino Acid Ligand: Syntheses, Crystal Structures, and Properties. *Crystal growth & design*, 11(1), 93-99.
- (19) Singh, W. M., & Baruah, J. B. (2008). Nickel, copper and zinc complexes of (2-methoxycarbonylmethylimino-5-methyl-thiazol-3-yl)-acetic acid. *Polyhedron*, 27(13), 2968-2972.
- (20) Aliaga-Alcalde, N.; Rodríguez, L.; Ferbinteanu, M.; Höfer, P.; Weyhermüller, T. Crystal structure, fluorescence, and nanostructuration studies of the first ZnII anthracene-based curcuminoid. *Inorg. Chem.* 2012, 51, 864–873
- (21) Díaz-Torres, R., Menelaou, M., González-Campo, A., Teat, S. J., Sañudo, E., Soler, M., & Aliaga-Alcalde, N. (2016). Comparative Magnetic Studies in the Solid State and Solution of Two Isostructural 1D Coordination Polymers Containing Coll/Nill-Curcuminoid Moieties. *Magnetochemistry*, 2(3), 29.
- (22) Kaljurand, I., Lilleorg, R., Murumaa, A., Mishima, M., Burk, P., Koppel, I., ... & Leito, I. (2013). The basicity of substituted N, N-dimethylanilines in solution and in the gas phase. *Journal of Physical Organic Chemistry*, 26(2), 171-181.
- (23) Yuan, L., Horosanskaia, E., Engelhardt, F., Edelmann, F. T., Couvrat, N., Sanselme, M., ... & Lorenz, H. (2018). Solvate formation of bis (demethoxy) curcumin: Crystal structure analyses and stability investigations. *Crystal Growth & Design*, 19(2), 854-867.
- (24) Karlsen, J., Mostad, A., Tønnesen, H. H., Hörnfeldt, A. B., Lönnberg, H., Berg, J. E., ... & Dombi, G. (1988). Structural studies of curcuminoids. VI. Crystal structure of 1, 7-bis (4-hydroxyphenyl)-1, 6-heptadiene-3, 5-dione hydrate. *Acta Chem. Scand*, 42, 23-27.
- (25) Kolev, T. M., Velcheva, E. A., Stamboliyska, B. A., & Spiteller, M. (2005). DFT and experimental studies of the structure and vibrational spectra of curcumin. *International Journal of Quantum Chemistry*, 102(6), 1069-1079.
- (26) Wu, Q. Y., Wan, L. S., & Xu, Z. K. (2013). Centimeter-scale giant spherulites in mixtures of polar polymers and crystallizable diluents: morphology, structure, formation and application. *RSC advances*, 3(38), 17105-17112



Chapter III.
CPs based on
3pyCCMoid

1. Introduction

Synthetic CCMoids, with the proper design, appear as an almost endless group to be explored in the field of CPs. Particularly, this chapter concentrates in a CCMoid with pyridine moieties at the lateral sites. On one side, it is well-known the relevance of pyridinic linkers in the creation of CPs¹⁻⁷ and, on the other hand, a CCMoid with this moiety, named as 3pyCCMoid (figure 1), is proposed as a linker for the creation of diverse CPs taking into account the tuneable nature of these molecules. Initial results using this linker were presented in a previous doctoral thesis of the research group,⁸ and during the development of this doctoral thesis, the studies have been continued designing new CPs and finalising other studies with the previous, using the below CCMoid.

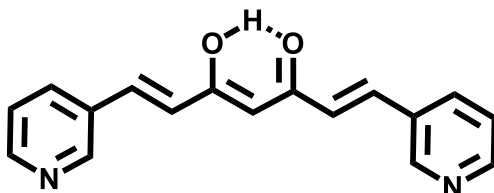


Figure 1. Scheme of the 3pyCCMoid.

3pyCCMoid presents the typical CCMoid skeleton, having in the centre of the conjugated chain a β -diketone moiety that easily deprotonates and therefore can satisfy the charge required by metallic centres with different oxidation states. On the contrary, the pyridines at the corners are neutral and through the N in the aromatic groups can provide electronic density to the cations, completing their coordination sphere. Hence, in the same molecule, 3pyCCMoid combines functions seen before in the linker (BDMC) and co-linkers (bipyridine moieties) in chapter II.

Few articles describe the use of this CCMoid for biomedical proposes as antioxidant⁹ or anticancer¹⁰. However, as far as we know, before our work, none of these publications show the coordination potential of 3pyCCMoid with transition metals. Also, prior to this doctoral thesis, two structures, called here **3pyCCMoidZn-1** and **-2**, were synthesized by the coordination of 3pyCCMoid with Zn(II) atoms⁸. The former is a 1D structure, meanwhile the second corresponds to a 2D system. Here, new studies were carried out with these two CPs, emphasizing the exfoliation of the 2D compound, **3pyCCMoidZn-2**. In addition, experiments using 3pyCCMoid and different metallic centres were continued, obtaining two new structures called **3pyCCMoidZn-3** and **3pyCCMoidCo-1**, respectively. As can be extracted from the name, the first is again a CP with Zn ions and the second one is the first CP obtained with a CCMoid and a different metallic ion, Co(II), instead of Zn(II).

In this chapter, the three structures of the **3pyCCMoidZn-x** family are compared proving how simple changes in the synthetic methods (solvents, temperature, and reaction time), keeping the same reagents, produce a variety of structures, this triggered in part by the huge versatility of this CCMoid. Moreover, the new structure with Co(II) is presenting as well as the results obtained using scCO_2 .

2. Objectives

The principal objective in this chapter is the synthesis of new CPs based on 3pyCCMoid. Within this general goal, specific aims have been also established:

- Exploration of new structures based on metal centres other than Zn (II) ions, been the latter the only transition metal used and published in the creation of CCMoid-CPs.
- Investigation of additional methodologies, different from the solvothermal technique, e.g.: layering and scCO_2 .
- Evaluation of reproducible nanosheets from a 2D CCMoid-CP obtained previously in the group with this CCMoid.

3. Materials and methods

3.1. Materials

3pyCCMoid was synthesized using the methodology described in chapter I. All the metal precursors for the CP synthesis (zinc acetate, $\text{Zn}(\text{OAc})_2$; zinc nitrate ($\text{Zn}(\text{NO}_3)_2$); zinc acetylacetonate, $\text{Zn}(\text{acac})_2 \cdot x\text{H}_2\text{O}$; zinc hexafluoroacetylacetonate, $\text{Zn}(\text{hfacac})_2 \cdot x\text{H}_2\text{O}$; Copper acetylacetonate $\text{Cu}(\text{acac})_2 \cdot x\text{H}_2\text{O}$; Copper hexafluoroacetylacetonate, $\text{Cu}(\text{hfacac})_2 \cdot x\text{H}_2\text{O}$; nickel acetylacetonate, $\text{Ni}(\text{acac})_2 \cdot x\text{H}_2\text{O}$, nickel hexafluoroacetylacetonate, $\text{Ni}(\text{hfacac})_2 \cdot x\text{H}_2\text{O}$ and cobalt acetate, $\text{Co}(\text{OAc})_2 \cdot x\text{H}_2\text{O}$) were purchased in Sigma Aldrich (Merck KGaA, Darmstadt, Germany and/or its affiliates), as well as the dimethylacetamida (DMA) used as solvent in some of the CP syntheses. For the rest, MeOH and dimethylformamide (DMF) were provided by CARLO ERBA Reagents S.A., EtOH by Scharlab and the compressed CO_2 by Carbueros Metálicos S.A.

3.2. Methods

As it has been mentioned above, before this doctoral thesis two 3pyCCMoid CPs were synthesized, **3pyCCMoidZn-1** and **3pyCCMoidZn-2**, using solvothermal methods.⁸ In this doctoral thesis, a new structure called **3pyCCMoidCo-1** has been successfully achieved by the use of a Co(II) salt applying the same synthetic technique as before. Moreover, a new structure of the **3pyCCMoidZn-x** family, **3pyCCMoidZn-3**, was also synthesized but using a layering method. Finally, as it was performed in chapter II, scCO₂ was used toward the attainment of CPs in a greener way.

3.2.1. Solvothermal synthesis

3PyCCMoidZn-1 and **3PyCCMoidZn-2**. The same methodology, reagents and concentrations were used in the synthesis of both systems: 5 mg (0.017 mmol) of 3pyCCMoid and 16 mg (0.085 mmol) of Zn(NO₃)₂·xH₂O, respectively. In both cases, the starting materials were dissolved in mixtures of solvents, and each system was achieved using different sets of them. This way, **3PyCCMoidZn-1** was attained using DMF:MeOH (0.5:1.5 mL) and **3PyCCMoidZn-2** by means of a DMA:EtOH mixture (0.5:1.5 mL). Crystallization was accomplished after setting the loaded vials in an oven at 80 °C for three days, therefore, working at soft solvothermal conditions of temperature and pressure, attained by the use of a high boiling point solvent and working with low filling vials (2 mL in 10 mL vials).

3PyCCMoidCo-1. 1.25 mg (0.004 mmol) of 3pyCCMoid and 4.25 mg (0.02 mmol) of Co(NO₃)₂·xH₂O were added to 2 mL of EtOH. The mixture was sonicated until the complete dissolution of the reagents from where few minutes after a dark orange precipitate appeared. This was redissolved with the addition of few drops of acetic acid. After 72 h at 80 °C in the oven, dark orange crystals appeared.

3.2.2. scCO₂ method

In parallel with the experiments performed with BDMC in the previous chapter, the scCO₂ approach was also tested for the creation of 3PyCCMoid-CPs maintaining the reactor at 200 bar for 72 h under stirring. In all the cases the amount of 3pyCCMoid was fixed and different metal salts utilized, always using identical molar ratio among the two reagents. The addition of a co-solvent (EtOH) before the introduction of the vial in the reactor depended on the solubility of the reagents in scCO₂. In the case of the BDMC experiments (chapter II), the low solubility of the BDMC made compulsory the use of a small quantity of EtOH as a co-solvent in all the cases. However, 3pyCCMoid presents a relatively good solubility in this media and the use of a co-solvent was only mandatory in the cases where the metal salt was not very soluble. In addition, the reaction with Zn(acac)₂·xH₂O was carried out with and without co-solvent, and different results were obtained in both cases.

This way:

3Py-CCMoidZn-sc: 80 mg (0.29 mmol) of 3pyCCMoid and 118 mg (0.45 mmol) of $\text{Zn}(\text{acac})_2 \cdot x\text{H}_2\text{O}$ were mixed in 2 mL of EtOH.

3Py-CCMoidZn-sc-ns: 80 mg (0.29 mmol) of 3pyCCMoid and 118 mg (0.45 mmol) of $\text{Zn}(\text{acac})_2 \cdot x\text{H}_2\text{O}$ were mixed without the addition of a co-solvent.

3Py-CCMoidZn-sc-hf: as in the previous reaction, 80 mg (0.29 mmol) of 3pyCCMoid and 226 mg (0.45 mmol) of $\text{Zn}(\text{hfacac})_2 \cdot x\text{H}_2\text{O}$ were mixed.

3Py-CCMoidCu-sc: 80 mg (0.29 mmol) of 3pyCCMoid and 116 mg (0.45 mmol) of $\text{Cu}(\text{acac})_2 \cdot x\text{H}_2\text{O}$ were mixed.

3Py-CCMoidCu-sc-hf. In this case, 80 mg (0.29 mmol) of 3pyCCMoid and 210 mg (0.45 mmol) of $\text{Cu}(\text{hfacac})_2 \cdot x\text{H}_2\text{O}$ were used.

3Py-CCMoidNi-sc. Like with the other metal salts, 80 mg (0.29 mmol) of 3pyCCMoid and 114 mg (0.45 mmol) of $\text{Ni}(\text{acac})_2 \cdot x\text{H}_2\text{O}$ were mixed.

3Py-CCMoidNi-sc-hf. 80 mg (0.29 mmol) of 3pyCCMoid and 208 mg (0.45 mmol) of $\text{Ni}(\text{hfacac})_2 \cdot x\text{H}_2\text{O}$ were used.

3Py-CCMoidCo-sc. Here, 80 mg (0.29 mmol) of 3pyCCMoid and 110.66 mg (0.45 mmol) of $\text{Co}(\text{OAc})_2 \cdot x\text{H}_2\text{O}$ were mixed.

3.2.3. Layering method

3PyCCMoidZn-3. 3PyCCMoid (30 mg, 0.108 mmol) was solubilised in 1.5 ml of DMF and placed in a recrystallization tube. Then, 2 mL of EtOH were placed on top of the initial solution, forming a clear and visible layer. Finally, a solution of $\text{Zn}(\text{NO}_3)_2 \cdot x\text{H}_2\text{O}$ (64 mg, 0.35 mmol) in 2 mL of EtOH was deposited on the top of the second layer. This vial was closed and kept unaltered for three weeks until the appearance of few small crystals in the walls of the tube.

3.2.4. Exfoliation method

Due to the 2D nature of **3PyCCMoidZn-2**, studies to exfoliate this sample were carried out with the protocol described in the methodology and characterization techniques chapter. Summarising the process, 1 mg of **3pyCCMoidZn-2** crystals was placed in a 2 mL vial, and 1 mL of Milli-Q H_2O was added. The mixture was sonicated during 1 h in an ultrasonic bath. After this, the vial was kept unaltered for 6 h. Meanwhile, the heaviest nanosheets precipitated and the lighter, presumably constituted by less aggregated layers, remained suspended in the solvent. The presence of nanosheets within the supernatant was corroborated using a conventional laser, observing the Tyndall effect.

Finally, 10 μL of the top part of the vial were placed on a TEM grid or on a silicon oxide surface for their characterization.

To analyse the origin of the degradation process of the nanosheets in H_2O that could be related with the solvent, the sonication process or resting time, experiments were performed by diluting 10 μL of the supernatant (obtained after the exfoliation process) with 50 μL of fresh Milli-Q water, which were properly mixed using a vortex.

4. Results and discussion

4.1. CPs based on 3pyCCMoid. Solvothermal and layering method

4.1.1. Crystallographic description

3pyCCMoidZn-1 crystallizes in the monoclinic space group $C2/c$ with stoichiometry $[\text{Zn}_{0.5}(\text{3pyCCMoid})]_n$. The asymmetric unit includes one 3pyCCMoid molecule and one-half of the Zn ion. The Zn(II) centres are hexacoordinated, where each unit binds to two 3pyCCMoids through their β -diketone moieties (Zn–O distances between 2.026 and 2.132 Å) and two pyridine groups (Zn–N distances of 2.211 Å) from neighbouring CCMoids (figure 2a). In this arrangement, the β -diketone groups are contained in crossed planes, disposing in a Z conformation the two pyridine moieties (figure 2b). Regarding each 3pyCCMoid ligand, one of the pyridine moieties remains always free (figure 2a).

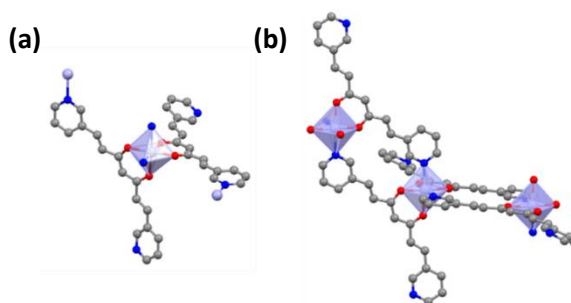


Figure 2. Crystal structure of **3pyCCMoidZn-1**: (a) Representation of the coordination sphere of a Zn(II) ion and the coordination modes of 3pyCCMoid molecules; (b) representation of two loops connected through the intermediate Zn(II) centre. Colour legend: Zn, light blue; C, grey; O, red; N, dark blue; H atoms are omitted for clarity.

The CCMoid skeletons are slightly bent (23.16° , figure 3) with the pyridine groups facing in opposite directions as seen before.

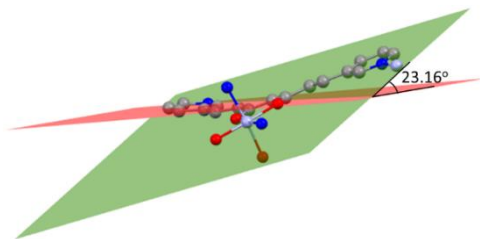


Figure 3. Planes formed by the N and C atoms in *meta*- positions of the pyridinic rings and the central C atom of the studied 3pyCCMoid. Example of the measurement of the angle between planes to determine the planarity of the CCMoid molecule in **3pyCCMoidZn-1**.

The framework spreads forming loops through the coordination of the adjacent unit, figure 2b, by pyridine endings ($\text{Zn}\cdots\text{Zn}$ distance 9.271 Å, figure 2a-b). In addition, the Zn (II) centres act as nodes among the loops, displaying them in a nearly perpendicular way (angles of 87.52° and 93.77°) and as a result, the system evolves into a staircase shaped 1D net (figure 4a). The chains are aligned and efficiently packed (figure 4b), with $\text{Zn}\cdots\text{Zn}$ distances of 14.5 Å and 12.5 Å among the closest neighbours.

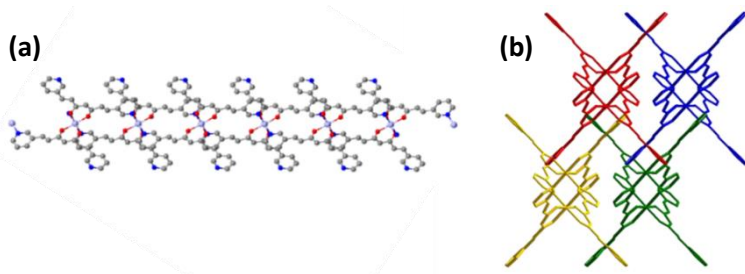


Figure 4. Crystal structure of **3pyCCMoidZn-1**: (a) extended view of one chain; (d) arrangement of four chains in the crystal. Colour legend: Zn, light blue; C, grey; O, red; N, dark blue; H atoms are omitted for clarity.

3pyCCMoidZn-2 crystallizes in the monoclinic space group $P2_1/n$ with the stoichiometry $[\text{Zn}_2(3\text{pyCCMoid})_2(\text{NO}_3)_2]_n$. The asymmetric unit cell contains two $[\text{Zn}(3\text{pyCCMoid})(\text{NO}_3)]$ fragments, each presenting 3pyCCMoid molecules with slightly different distances and conformations. As in **3pyCCMoidZn-1**, the Zn(II) ions adopt a pseudo-octahedral geometry, but now there is only one 3pyCCMoid chelating the metal centre together with one NO_3^- anion. The two remaining sites, within the Zn(II) unit, are occupied by pyridine moieties from nearby CCMoids. Here again, the disposition of the chelating groups, CCMoid and NO_3^- , is in the Z conformation (figure 5a). The 3pyCCMoid ligand is now fully coordinated, bringing into play its three coordinative sites. Each 3pyCCMoid

coordinates through the β -diketone moiety to one of the Zn(II) ions in the fragment, binding the pyridine groups to two neighbouring Zn(II) centres (figure 5a). The assembly of two asymmetric units forms loops too (Zn \cdots Zn distance of 9.028 Å, figure 5b). Within such dimers, everything relates by an inversion centre, making the NO₃⁻ groups point out in opposite directions. The connection of four of these loops through the remaining pyridine groups creates a bigger cavity (figure 5c).

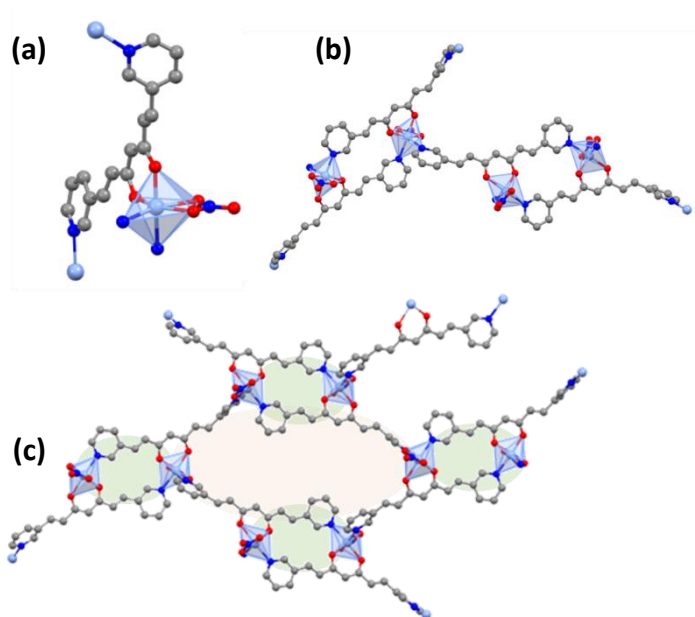


Figure 5. Crystal structure of **3pyCCMoidZn-2**: (a) Representation of the coordination sphere of a Zn(II) centre and the coordination mode of 3pyCCMoid; (b) picture of the smallest loops in the layer; (c) picture of the small (in green) and big (in orange) loops of the layer. Colour legend: Zn, light blue; C, grey; O, red; N, dark blue; H atoms are omitted for clarity.

Now the void displays a rhomboid shape, being the longest Zn \cdots Zn distance of 22.060 Å. This implies a greater twist of the skeletons of the CCMoids (60.42° and 75.52°, figure 6).

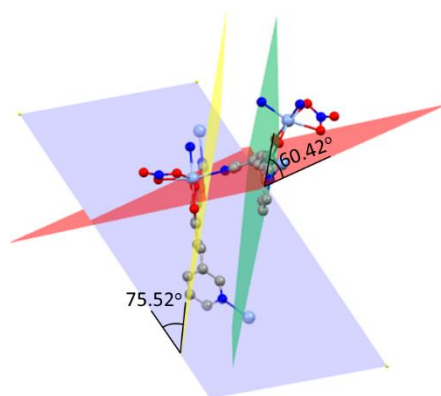


Figure 6. Planes formed by the N and C atoms in *meta*- positions of the pyridinic rings and the central C atom of the studied 3pyCCMoid. Representation of the measurement of the angles between planes to determine the planarity of the CCMoid molecules in structure the **3pyCCMoidZn-2**. Colour legend: Zn, light blue; C, grey; O, red; N, dark blue; H atoms are omitted for clarity.

The pyridine moieties face almost perpendicularly allowing the extension in two dimensions and forming infinite 2D layers (figure 7a and b) stacked among them by weak interactions (figure 7c). Despite the presence of several cavities in each single layer, the material presents a dense arrangement, where two NO_3^- groups, from adjacent layers, are inserted in the bigger voids resulting in a compact material (figure 7d).

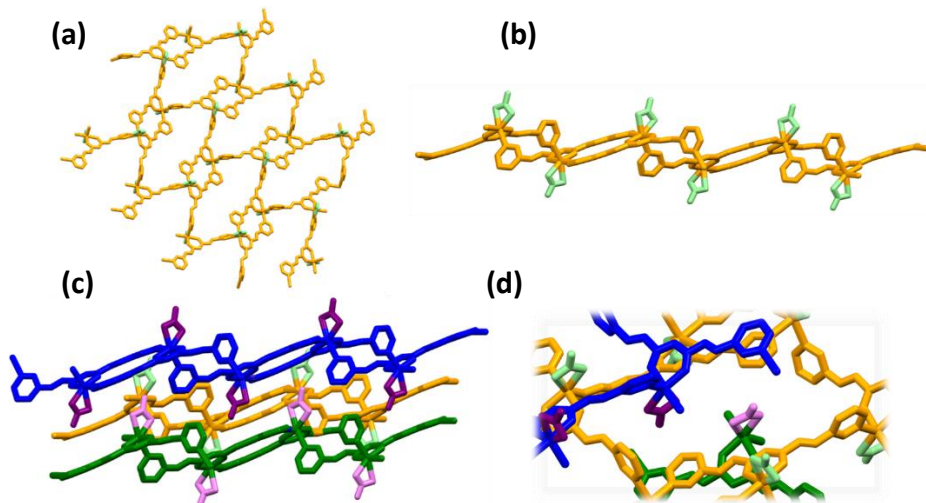


Figure 7. Extended structure of **3pyCCMoidZn-2**: (a) structure of a 2D layer (bc plane); (b) structure of a 2D layer (ac plane); (c) three 2D layers stacked on top of each other; (d) big loop of a layer with the NO_3^- groups of the lower and upper layer inserted into it.

In figure 7 three consecutive layers are represented in blue, orange and green, respectively, with the NO_3^- groups depicted also in different colours for all of them (purple, light green and pink, in that order). The alternating disposition of the latter (up and down) restrict the growth of the system, confining the structure as a 2D system (figure 7b). As an example, figure 7d shows the inclusion of NO_3^- groups from the blue and green layers, downward and upward directions, respectively, within a big loop of the orange one providing a final compact system.

3pyCCMoidZn-3 crystallizes in the orthorhombic $P2_12_12_1$ space group with $[\text{Zn}(\text{3pyCCMoid})(\text{NO}_3)(\text{EtOH})_2]_n$ stoichiometry. The asymmetric unit is formed by one $[\text{Zn}(\text{3pyCCMoid})(\text{EtOH})] \cdot \text{NO}_3 \cdot \text{EtOH}$ fragment. Here, the Zn(II) ions are pentacoordinated adopting a trigonal bipyramidal geometry ($\tau = 0.85$). Their coordination sphere chemically resembles the previous one, with every metallic centre coordinated to one β -diketone group from one CCMoid and two pyridine moieties from two other neighbours. However, the remaining position is now occupied by an EtOH molecule leaving uncoordinated the NO_3^- ion (figure 8a). In the structure, the CCMoid shows deviations from planarity (39.25° , figure 8b) but less pronounced than for compound **3pyCCMoidZn-2**, having here the pyridine groups oriented in opposite directions as in all the structures.

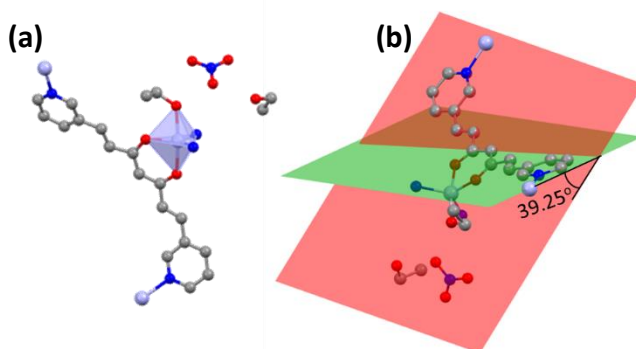


Figure 8. Crystal structure of **3pyCCMoidZn-3**: (a) Representation of the coordination sphere of a Zn(II) centre and coordination mode of 3pyCCMoid; (b) Planes formed by the N and C atoms in *meta*- positions of the pyridinic rings and the central C atom of the studied 3pyCCMoid. Representation of the measurement of the angle between planes to determine the planarity of the CCMoid molecule in structure **3pyCCMoidZn-3**. Colour legend: Zn, light blue; C, grey; O, red; N, dark blue; H atoms are omitted for clarity.

A remarkable difference with previous **3pyCCMoidZn** structures is the absence of loops (figure 9). The shortest Zn \cdots Zn distance is now 9.31 Å.

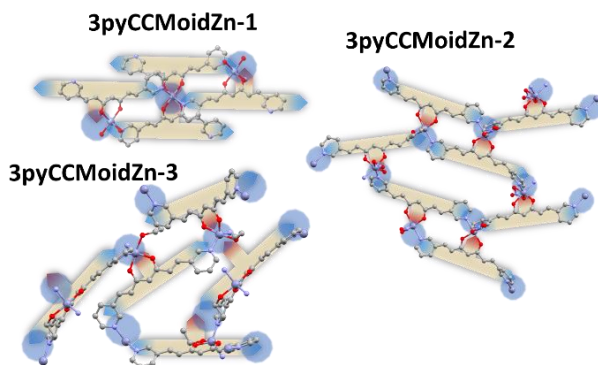


Figure 9. Crystallographic and overlapped schematic representation of the extended structures of **3pyCCMoidZn-1,-2** and **-3**, respectively.

In this case, the pyridine groups of the neighbouring CCMoids do not promote the formation of dimers, exhibiting their rotational freedom and spreading of the net (figure 10a) assisted by the Zn(II) centres. This, together with the fact that all the active sites of the 3pyCCMoid ligands are coordinated, favours the formation of a compact 3D structure (figure 10b). The new CP displays small voids occupied by one extra molecule of EtOH and the NO_3^- ion (in dark and light green respectively, figure 10c), both promoting supramolecular interactions with adjacent CCMoid residues.

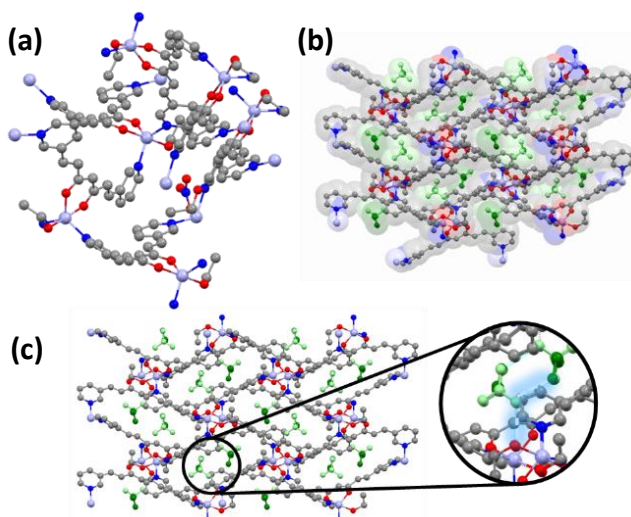


Figure 10. Extended structure of **3pyCCMoidZn-3**: (a) short fragment; (b) extension in the three directions with superposed spacefill; (c). extension in the three directions and zoom of one void. Colour legend: Zn, light blue; C, grey; O, red; N, dark blue; H atoms are omitted for clarity. In figures (b) and (c) NO_3^- ions are depicted in light green and free EtOH molecules in dark green highlighting their interactions in light blue.

3pyCCMoidCo-1. The system crystallizes in the monoclinic space group $P2_1/n$ with $[\text{Co}_2(\text{3pyCCMoid})_2(\text{NO}_3)_2(\text{H}_2\text{O})_{0.5}]_n$ stoichiometry. It presents the same structural organization than **3pyCCMoidZn-2**, but replacing the Zn(II) centres by Co(II) and including H_2O molecules in the structure (figure 11).

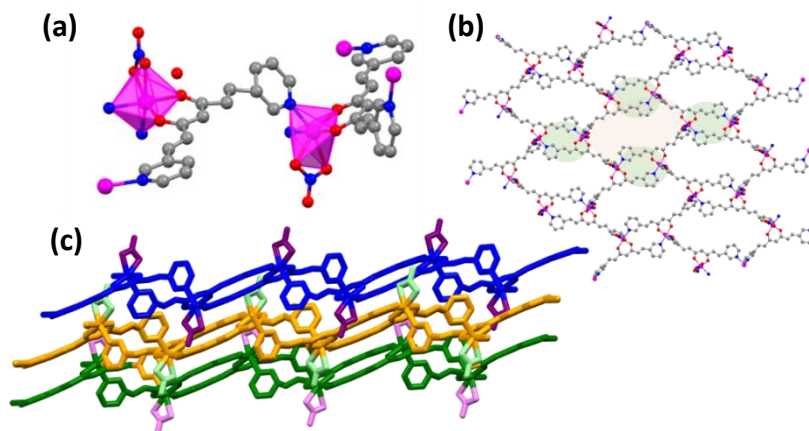


Figure 11. Crystal structure of **3pyCCMoidCo-1**: (a) Representation of the coordination sphere of a Zn(II) centre and the coordination mode of 3pyCCMoid; (b) picture of a single layer, in green four small loops and in orange the big loop formed among them; (c) three 2D layers stacked in blue, orange and green, respectively, with the nitrates in purple, light green and light pink, in that order. Colour legend: Co, pink; C, grey; O, red; N, dark blue; H atoms are omitted for clarity.

Comparing with the Zn analogous, the cation change introduces small differences in the Metal...Metal distances within the loops (Co...Co distances of 9.041 Å and 21.699 Å in the small and big loops, in that order, vs Zn...Zn distances of 9.028 and 22.060 Å, observed in **3pyCCMoidZn-2**). In addition, there are small variations in the twist of the CCMoid skeletons (63.29° and 73.51° for **3pyCCMoidCo-1** and 60.42° and 75.52° for **3pyCCMoidZn-2**, calculated as in the crystal description of this compound).

Intermolecular distances among the layers show variations as well, being this specially interested in the exfoliation studies of these materials. In both systems, the asymmetric unit is formed by two crystallographically different metal centres, despite of having the same coordination sphere, called here Co1 and Co2 in the case of **3pyCCMoidCo-1** and Zn1 and Zn2 for **3pyCCMoidZn-2** (figure 12a). Taking as a reference the ac plane in both systems, we can draw planes using the metal centres as nodes (figures 12b-c). The stacking among the layers occurs in such way that the metal centres of one type in one layer are always close to the metals of the same type in the neighbouring layers. In each layer, the Metal1 atoms are arranged downwards and the Metal2 upwards, while the next layer the placement is the opposite (figure 12c). Measuring the distances between

the created planes, we obtained distances of planeCo1-planeCo1 of 0.429 Å and planeCo2-planeCo2 of 1.205 Å, for **3pyCCMoidCo-1**. For **3pyCCMoidZn-2** two different distances (0.645 and 1.419 Å) were obtained in the same way, being the shortest from the Zn1 centres (figure 12c).

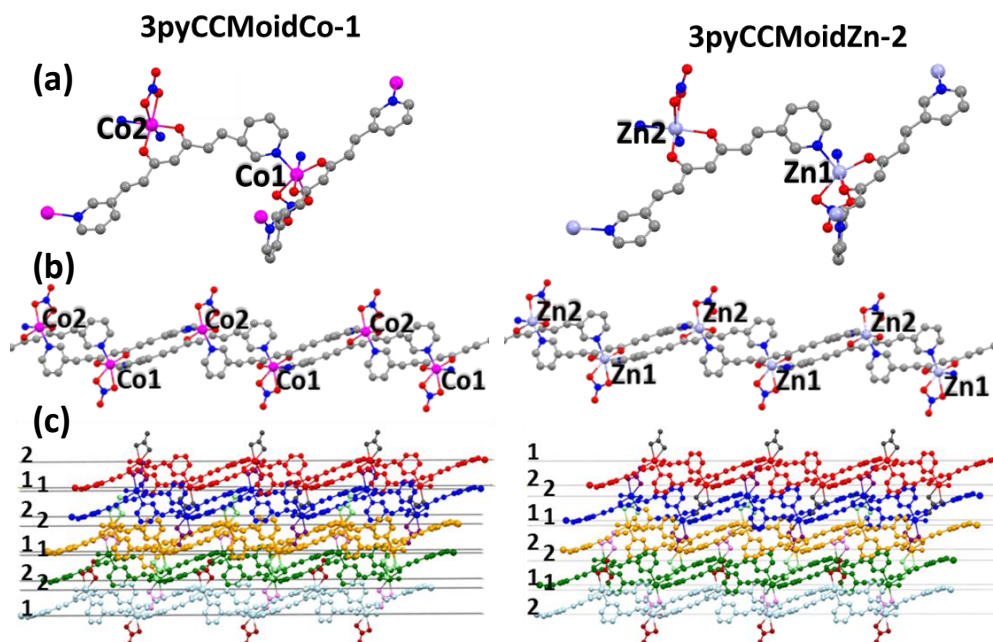


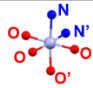
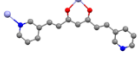
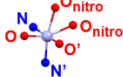
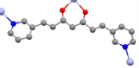
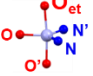
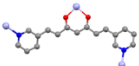
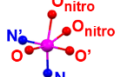
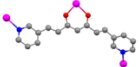
Figure 12. Structural comparison between **3pyCCMoidCo-1** and **3pyCCMoidZn-2** structures: (a) asymmetric units; (b) representation of a single layer; (c) five stacked layers and highlighted planes.

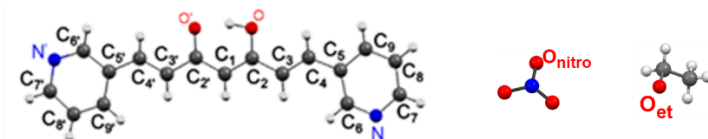
As it has been mentioned in the objectives, a robust methodology for the exfoliation of **3pyCCMoidZn-2** has been developed during this doctoral thesis with results presented latter in this chapter. However, due to the lack of time, these studies have not been evaluated for **3pyCCMoidCo-1**. Equivalent results may be expected as both CPs have the same structure and similar distances between layers, however, further studies regarding the stability of the Co(II) ions vs. the Zn(II) ions, in the presence of H₂O, should be taken under account and carefully review it.

4.1.2. Comparative studies of the 3pyCCMoidM-x structures

Several structures have been obtained with 3pyCCMoid presenting different metal geometries, coordination environments as well as coordination modes of this CCMoid (summarised in table 1).

Table 1. Geometry, coordination environment of the metal and CCMoid coordination modes in the CP structures.

CPs	Metal coordination	Metal geometry	Metal coordination environment	CCMoid coordination mode
3pyCCMoidZn-1	Hexacoordinate	Pseudo-octahedral		
3pyCCMoidZn-2	Hexacoordinate	Pseudo-octahedral		
3pyCCMoidZn-3	Pentacoordinate	Pseudo-trigonal bipyramid		
3pyCCMoidCo-1	Hexacoordinate	Pseudo-octahedral		



Although the coordination number and geometry adopted by the metal centres are crucial for the extension of the coordination and therefore dimensionality, curiously the metal centres of the 3D CP (**3pyCCMoidZn-3**) are pentacoordinated while the rest are hexacoordinated. In this regard, the 3pyCCMoid linker plays a more relevant role. On one hand, the coordination through only two positions in the **3pyCCMoidZn-1** reduced its dimensionality (1D system), despite of being the only one that coordinates exclusively to CCMoids (**3pyCCMoidCo-1**, **3pyCCMoidZn-2** and **-3** have NO_3^- ions and EtOH molecules as stoppers, respectively). On the other hand, the 3pyCCMoid presents certain flexibility, accommodating the shape to improve coordination and/or packing. This feature is general in most CCMoids, and here observed by the disposition of the double bonds in the skeleton, the presence of linear/curvy chains and the orientation of the pyridine groups. Figure 13 shows the superimposition of all the conformations observed for 3pyCCMoid within the three Zn structures; those from **3pyCCMoidCo-1** are not display because they exhibit similar CCMoid arrangement than **3pyCCMoidZn-2**.

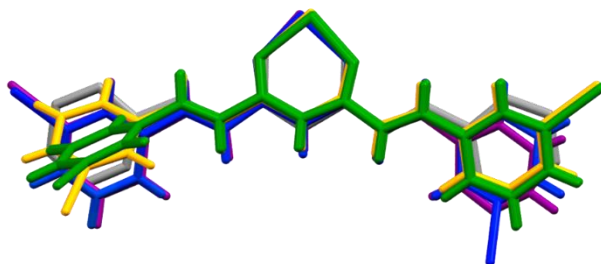


Figure 13. Overlap of the 3pyCCMoid units that appear in the three **3pyCCMoidZn-x** compounds -1 (purple), -2 (yellow and green) and -3 (blue), compared to the pristine ligand (grey).

A common trait for all the systems is that one of the N atoms, from the pyridine groups, is always oriented in the same way than the β -diketone moiety and the other in the opposite direction, facilitating in **3pyCCMoidZn-1,-2** and **3pyCCMoidCo-1** the formation of loops and the extension of the structures in the case of **3pyCCMoidZn-3**. This behaviour is observed even in the structure of **3pyCCMoidZn-1**, where one of the pyridinic units does not participate in the coordination.

Related with the disposition of the chain and aromatic rings, the presence of double bonds allows small degrees of rearrangement within the molecule that, together with the free rotation of the pyridine moieties, favoured the correct disposition of the N atoms to bond with the metal centres. This rotation is clearly seen in the pristine CCMoid (figure 14) that presents a small deviation (6.68°), in contrasts with the angles found in the CPs (23.16° in **3pyCCMoidZn-1**, 60.42° and 75.52° for **3pyCCMoidZn-2**, 39.25° for **3pyCCMoidZn-3** and finally, 63.29° and 73.51° in the case of **3pyCCMoidCo-1**). These values have been described previously in the crystallographic section (figures 3,6 and 8).

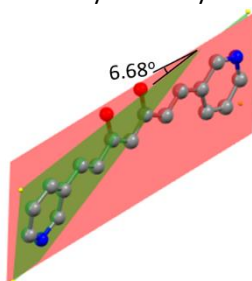


Figure 14. Planes formed by the N and C atoms in *meta*- positions of the aromatic rings together with the central C atom of the pristine 3pyCCMoid. Example of the measurement of the angle between planes to determine the planarity of the CCMoid molecule in structure **3pyCCMoidZn-1**. Colour legend: Zn, light blue; C, grey; O, red; N, dark blue; H atoms are omitted for clarity.

The highest distortion is observed for the **3pyCCMoidZn-2** and **3pyCCMoidCo-1** systems, showing, in the same structure, two conformations adopted by 3pyCCMoid. This allows the formation of the two types of loops and therefore the 2D dimensionality. Figure 13 shows how that for **3pyCCMoidZn-2** one half of the CCMoid molecule is almost planar for both conformations, the one involved in the creation of the small loops, while the other half rotates to join the following metal centre and forms part of the big loops (figure 15a). In **3pyCCMoidZn-1**, the more linear part participates in the creation of the loops, however, the distortion in the rest of the CCMoid molecule is not as pronounced as before and this part remains uncoordinated. In the absence of loops, **3pyCCMoidZn-3** presents small differences between the two halves of the CCMoid molecule, but all the molecule adopts an arched shape (figure 15c).

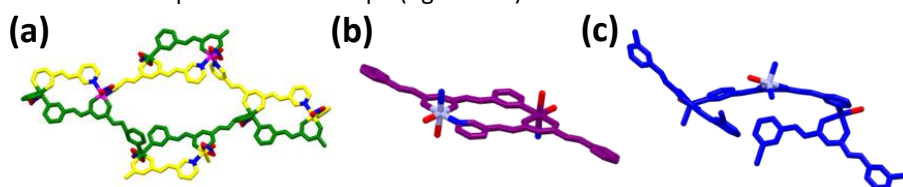


Figure 15. Details of the structures of: (a) **3pyCCMoidCo-1** (equivalent to **3pyCCMoidZn-2**); (b) **3pyCCMoidZn-1** and (c) **3pyCCMoidZn-3**.

Overall, variations in the linearity of the conjugated chain of 3pyCCMoid, due to small rotations or bending, facilitates the formation of the loops and packing allowing organized units and therefore crystalline materials.

4.1.3. Additional characterizations

In this section information regarding the bulk materials and morphology of the crystals is described, with the aim of using the extracted information in the creation of new CPs. The low yield, small crystal size and reproducibility difficulties encountered in the synthesis of **3pyCCMoidZn-3** hampered additional analyses outside the single-crystal structure, therefore it is not going to be included in most of the section.

4.1.3.1. Powder XRD

In general, a good agreement between the experimental powder XRD of the bulk material and the simulated patterns was obtained for all the structures (figure 16) emphasising the isomorphism and absence of impurities of the samples.

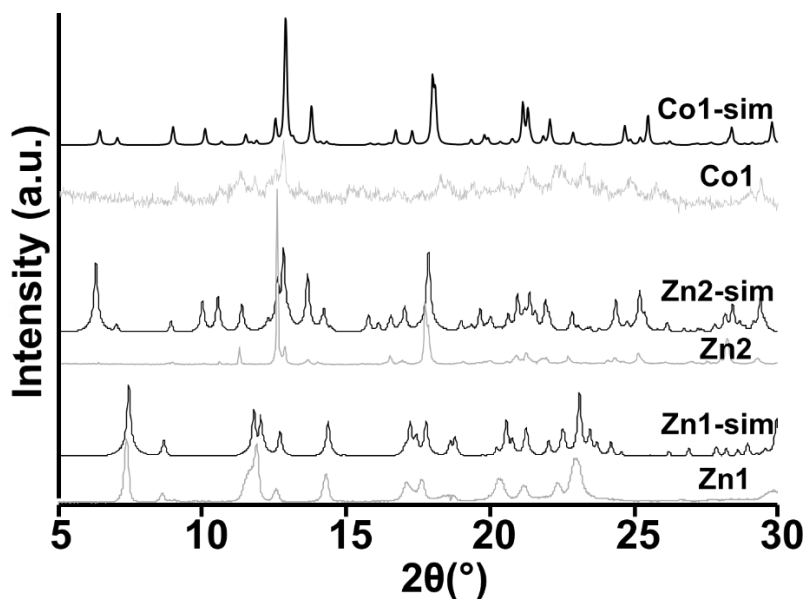


Figure 16. Comparison between the experimental powder XRD of **3pyCCMoidZn-1** (Zn1), **3pyCCMoidZn-2** (Zn2) and **3pyCCMoidCo-1** (Co1) and the simulated using mercury (Zn1-sim, Zn2-sim and Co1-sim).

As expected, **3pyCCMoidZn-2** and **3pyCCMoidCo-1** display similar powder XRDs and differences can be attributed to the water molecules in the Co structure, the different metal ratios and the additional intermolecular variations described previously.

4.1.3.2. Crystal morphology

In chapter II, most of the CPs grow as spherulites. However, the systems that contain **3pyCCMoid** display a completely different behaviour (figure 17). **3pyCCMoidZn-1** and **3pyCCMoidZn-2** grow in an almost amorphous way, where the biggest crystalline samples are formed by the agglomeration of small crystals. Instead, **3pyCCMoidZn-3** forms yellow plates and in the case of **3pyCCMoidCo-1** bladed orange crystals were observed; the different crystal growth of the latter is particularly interesting taking into account that was created with the same methodology than **3pyCCMoidZn-2** and shares structural features but the appearance is completely different.

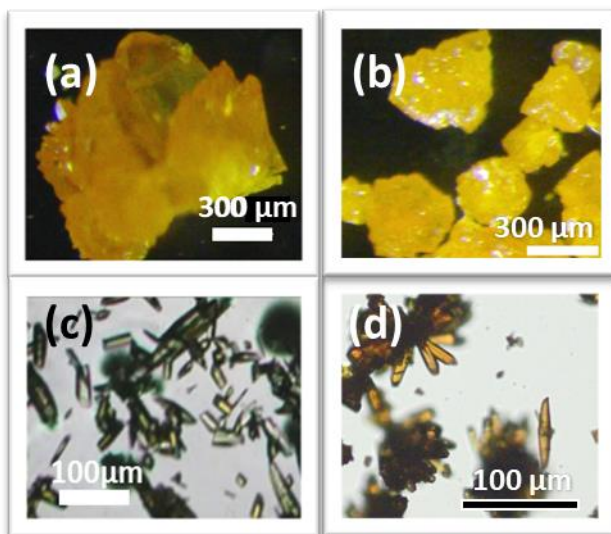


Figure 17. Optical images of the crystals of: (a) **3pyCCMoidZn-1**, (b) **3pyCCMoidZn-2**, (c) **3pyCCMoidZn-3** and (d) **3pyCCMoidCo-1**, respectively.

For the single crystal XRD measurements, segmentation of the bigger crystals into small units was always necessary except for **3pyCCMoidZn-3**. In this case, the crystals grew far apart from each other, being easy their isolation. This could relate, among other factors, to the slow growth of the crystals by diffusion taking three weeks to appear.

4.1.3.3. CPMAS ^{13}C NMR

As it has been highlighted in other chapters of this doctoral thesis, this technique allows us to evaluate CCMoid systems in the solid state and, even in the absence of crystallographic information, to extract information regarding coordination and ligand environment. Here, the systems under study were the pristine ligand (3pyCCMoid), **3pyCCMoidZn-1** and **3pyCCMoidZn-2**, respectively. The small amount attained for **3pyCCMoidZn-3** and the creation of **3pyCCMoidCo-1** in the last stage of this doctoral thesis limited the additional information for these two systems. The assignment of the signals in the case of 3pyCCMoid has been accomplished by comparison with BDMC, CCMoid bibliographic data and simulation of the ^{13}C NMR in solution of the same ligand. As described in the past, the free ligand presents two sets of characteristic signals, at the regions of 100-110 ppm and 180-190 ppm, corresponding to the methine C atom and the C-OH/C=O atoms, respectively. The rest of signals remain in the area of 120-160 ppm and comprise the pyridinic units and the rest of C atoms of the CCMoid chain. In comparison to the pristine molecule, **3pyCCMoidZn-1** presents less number of signals and broader bands. Unlike the information gathered in chapter II, now the coordination of the lateral parts, as well as the presence of a free pyridine, in **3pyCCMoidZn-1**, are

not so evident in the overall form of the spectra, being difficult to extrapolate further information.

The main feature that can be extracted comes from the spectra of the **3pyCCMoidZn-2** system, where the duplicity of the methine C signal (100-105 ppm) as well as others in the aromatic area clearly indicates the existence of the two conformations adopted by the 3pyCCMoid in the crystal.

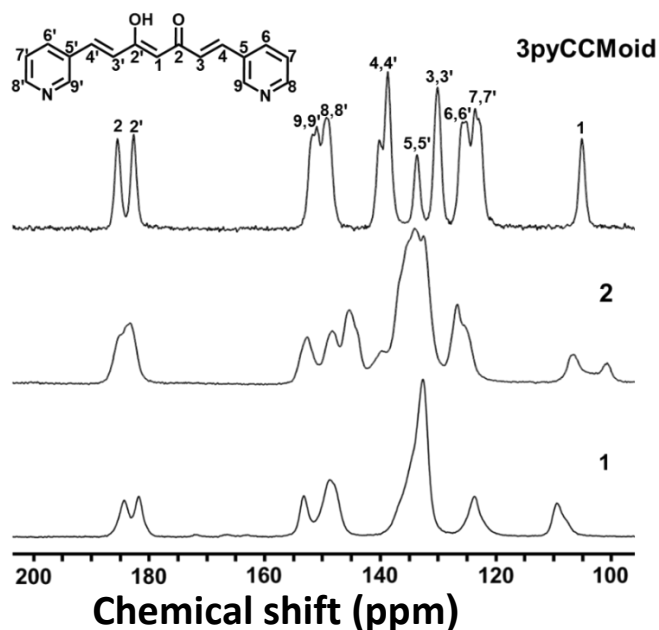


Figure 18. CPMAS¹³C NMR of the free CCMoid (3pyCCMoid), **3pyCCMoidZn-1** (1) and **3pyCCMoidZn-2** (2).

4.1.4. Infrared spectroscopy (FTIR-ATR)

In the following section, the FTIR-ATR spectra of **3pyCCMoidZn-1**, **3pyCCMoidZn-2** and **3pyCCMoidCo-1** together with the pristine ligand (figure 19) are discussed.

Characteristic bands for the mentioned systems are in the region between 1700 and 600 cm^{-1} (figure 19b). As expected, in the case of the three CPs, shifts to higher frequencies are observed in the C=O zone (1600 to 1550 cm^{-1}) due to the coordination of the Zn(II) ions with the β -diketone. In the case of the CPs, a wide band at 1630 cm^{-1} appears (in blue, figure 19b) always with a shoulder around 1640 cm^{-1} , together with the absence of the bands related with the bending of the enol groups (1570 cm^{-1} , in purple figure 19b).

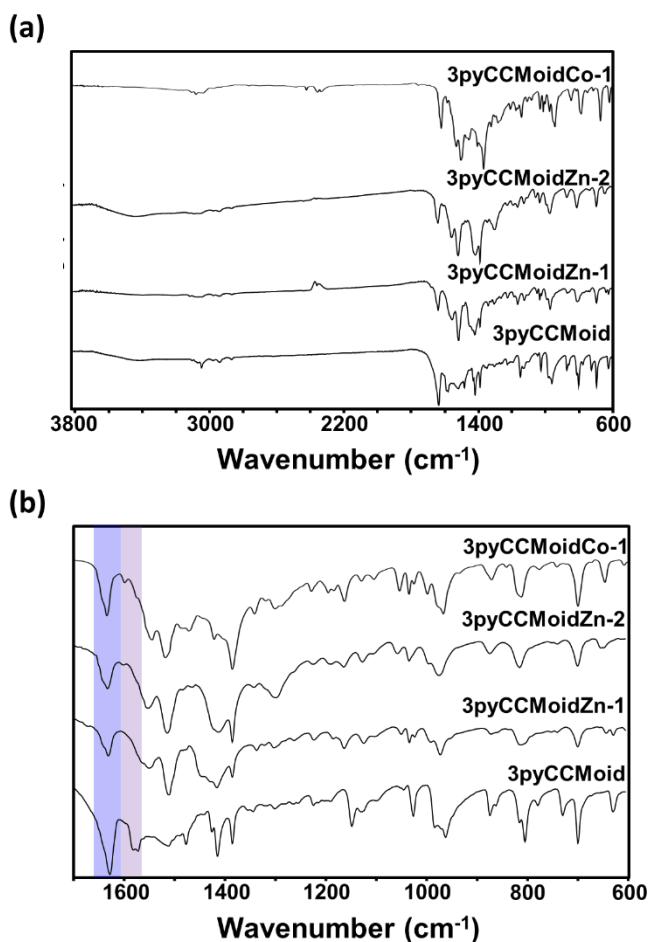


Figure 19. FTIR-ATR spectra of 3pyCCMoid, 3pyCCMoidZn-1, 3pyCCMoidZn-2 and 3pyCCMoidCo-1, from bottom to top.

As expected, the spectra of 3pyCCMoidZn-2 and 3pyCCMoidCo-1 are very similar but overall, as in previous cases, the multiple signals in the rest of the regions complicate the observation of additional changes.

4.1.5. Elemental analysis

A good correlation between the calculated formula from the resolved structure and the experimental values have been achieved with the use of EA technique for **3pyCCMoidZn-1**, **3pyCCMoidZn-2**. In the case of **3pyCCMoidCo-1**, the lack of time made impossible having these results before the deposition of this doctoral thesis.

This, together with XRD, confirms that in all the cases, the bulk material has the composition of the resolved structure.

Table 2. Calculated (Cal.) and experimental (Exp.) values of the elemental analysis of **3pyCCMoidZn-1 (1)** and **3pyCCMoidZn-2 (2)**.

CP	Formula	%C		%H		%N	
		Cal.	Exp.	Cal.	Exp.	Cal.	Exp.
1	$[\text{Zn}(\text{C}_{17}\text{H}_{14}\text{N}_2\text{O}_2)_2]_n \cdot n / 2\text{ZnO}$	61.8	61.56	3.96	4.06	8.48	8.60
2	$[\text{Zn}(\text{C}_{17}\text{H}_{14}\text{N}_2\text{O}_2)]_n \cdot 1 / 2n\text{H}_2\text{O}$	49.35	49.33	3.41	3.33	10.15	9.80

4.2. CPs based on 3pyCCMoid. scCO₂ procedure

The reaction of 3pyCCMoid with different metal ions (M=Zn(II), Cu(II), Co(II) and Ni(II)) in scCO₂ provided powdered samples. In contrast with BDMC, 3pyCCMoid displayed enough solubility in scCO₂ to be able to react without the use of a co-solvent. This section describes the characterization of the attained products.

4.2.1. Powder XRD

The XRD analysis of the different powders shows that the systems achieved by the scCO₂ method (figure 20) are different from those attained with the solvothermal synthesis (figure 16).

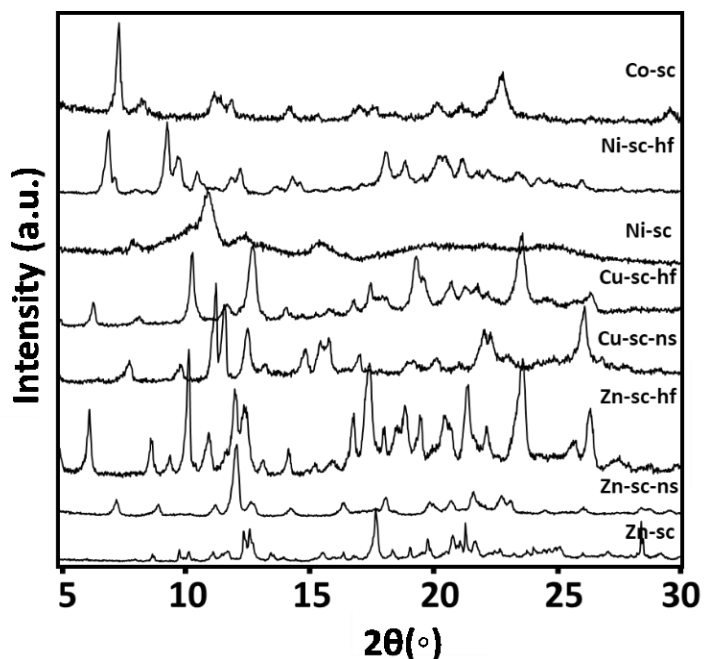


Figure 20. Powder XRD patterns of the products obtained in scCO_2 .

All the reactions, except the one between $\text{Ni}(\text{acac})_2$ and 3pyCCMoid (figure 20, Ni-sc), provided crystalline powders displaying a variety of patterns, without presenting common trends among them (figure 20). This was also applicable for the reactions where the same metal centre was introduced but using different metallic counterions (e.g., $3\text{pyCCMoid-Cu-sc-hf}$ and $3\text{pyCCMoid-Cu-sc-ns}$). Different results were also obtained by performing the reaction with the same metal centre, with and without co-solvent (e.g., $3\text{pyCCMoid-Zn-sc-ns}$ and 3pyCCMoid-Zn-sc). These results prove the complexity and great variability of structures that can be obtained with 3pyCCMoid where the metal counterions play a key role too. The small size of the crystalline powders hampered the possibility of structural resolution by single-crystal XRD and as before, additional techniques were used to assist in the characterization of the solids.

4.2.2. Infrared spectroscopy (FTIR-ATR)

The FTIR-ATR spectra of the CPs were compared among them and with the pristine ligand. Figure 21 depicts the complete and expanded spectra of all these systems. Again, differences were specially observed in the carboxylic region (in blue, figure 21b) because of the coordination of the β -diketone moiety. As it happens with the CPs achieved with the solvothermal synthesis, the reaction of 3pyCCMoid with the metals produced the appearance of a shoulder and even a distinct new peak around 1650 cm^{-1} in all the products. Also, in this region (1700-1600 units), some products (3pyCCMoid-Ni-sc , 3pyCCMoid-Cu-sc)

sc-hf, -Cu-sc, -Zn-sc-hf) present extra peaks that may relate with the coordination of other species with carbonyl groups, as for example acetate, acetylacetonate or hexafluoroacetylacetonate groups.

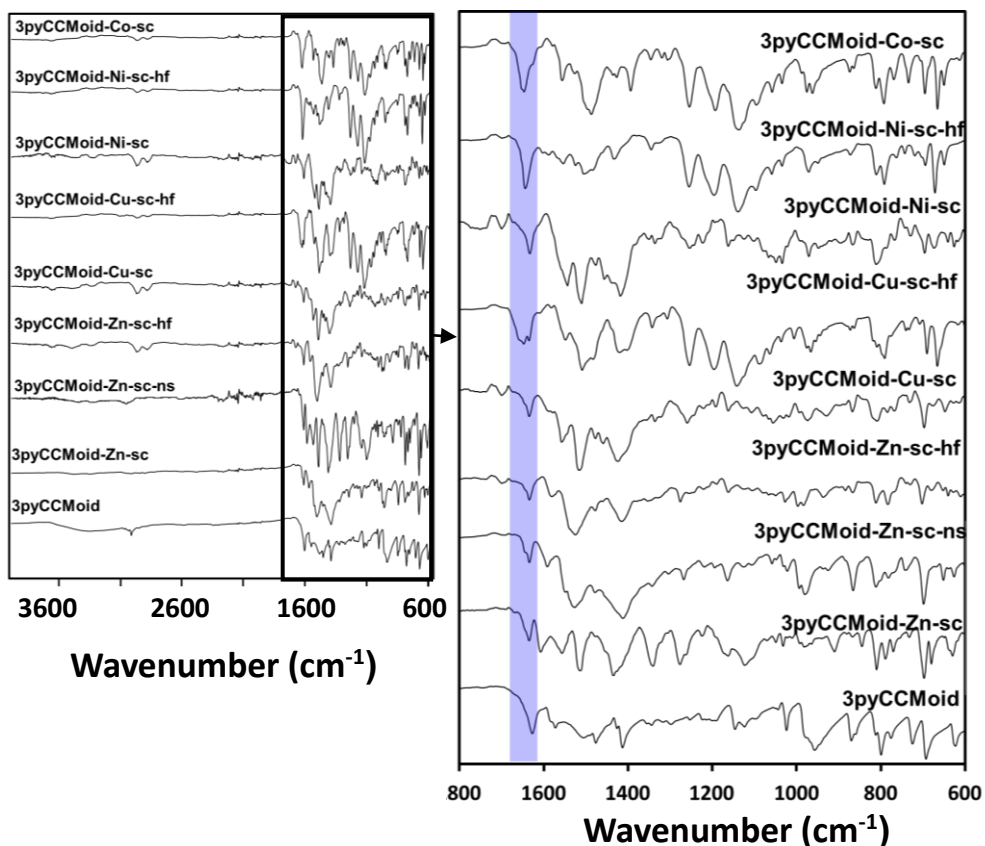


Figure 21. FTIR ATR of the products obtained with 3pyCCMoid and different metals in $s\text{CCO}_2$.

4.2.3. Solubility test

All the products were partially soluble in conventional organic solvents (EtOH, MeOH, ACN, acetone...) being always higher soluble in DMSO (approx. 0.4 mg in 9 mL). **3pyCCMoid-Co-sc** is the most insoluble among all the systems. The total or partial solubility of the compounds could be an indication of the low dimensionality and therefore coordination compound nature of the achieved systems.

Based on all the studies above, we can conclude that the coordination of the ligand to the different metal centres, through the β -diketone, was achieved; meanwhile, the coordination of the pyridinic units could not be confirmed either denied.

4.3. Exfoliation studies of 3pyCCMoidZn-2

The supramolecular structure of **3pyCCMoidZn-2** is formed by the piling of 2D layers, stacked together by weak interactions (figure 22). In addition, SEM images corroborate the vision of a layered material (figure 22).

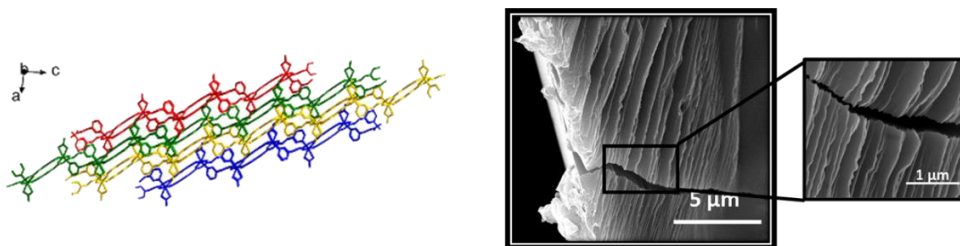


Figure 22. Layers of **3pyCCMoidZn-2**, (a) structure of four layers in different colours each one and (b) SEM images of the layers.

The exfoliation of **3pyCCMoidZn-2** was studied to find out, in a first stage, an efficient and reproducible methodology to achieve few-layers of the system and, in a further step, the study of the electronic capabilities of the exfoliated material. Such analysis is pursued at the moment by some of the members of the group.

The nanosheets obtained were characterized using TEM, AFM and EDX, respectively. After the sonication process in H_2O and resting the samples for 6 h (methodology section), the non-exfoliated crystals and the highest nanosheets precipitated. However, small nanosheets remain in suspension, their presence was confirmed by the existence of Tyndall effect (figure 23).

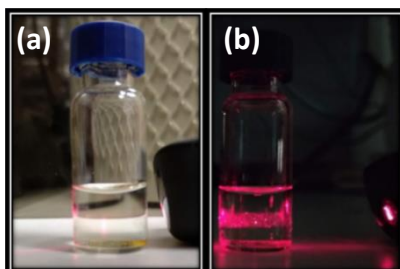


Figure 23. Vial of an exfoliation experiment irradiated with a laser: (a) big material deposited in the bottom part of the vial and (b) nanosheets of small size in suspension, visible thanks to Tyndall effect.

The average thickness of the nanosheets was determined by AFM measuring the height profile of 100 nanosheets (figures 23 a-c) and carrying out a statistical analysis of the results (figure 23d). Although the analysis shows a considerable diversity of heights, half of the nanosheets population present heights below 40 nm. From the rest approximately a 15 % of the samples were under 10 nm.

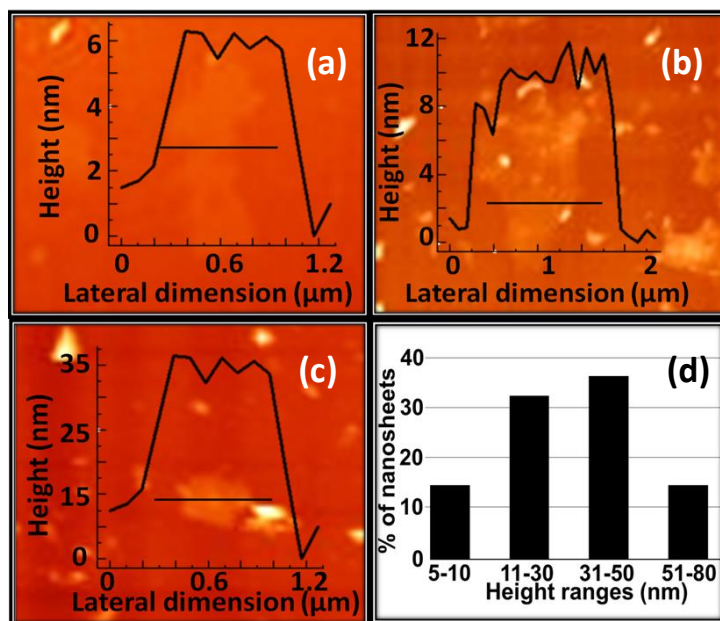


Figure 23. (a)(b)(c) AFM height profile of three different nanosheets; (d) statistical analysis of the nanosheets thickness.

Apart from the thickness, an interesting observation about the exfoliated system was the extension of the nanosheets, in the range of 40-100 μm (figure 24a) presenting all continuous surfaces. Regarding their stability, the samples were measured in the TEM grids after 72 h, observing breaks of the edges and folding on themselves but any further degradation was appreciated (figures 24d and e).

Having into account that the heights related to several layers, longer resting times were tested. However, to appreciate changes in the samples more than 12 h were required and then, a big degradation of the material was observed. Taking into account the structure of **3pyCCMoidZn-2**, we postulate that the labile nature of the NO_3^- groups that coordinate the Zn(II) atoms, are the cause of this degradation. After sonication and having long periods of contact with water the layered material may react and decompose. In fact, similar degradation processes were observed (figure 24f) when we

took a portion of the samples left for 6 h and add more water, without more sonication time or leaving the samples resting longer times. In addition, other solvents were also tested (e.g.: ACN, EtOH and MeOH), showing always higher degradation of the material than in water.

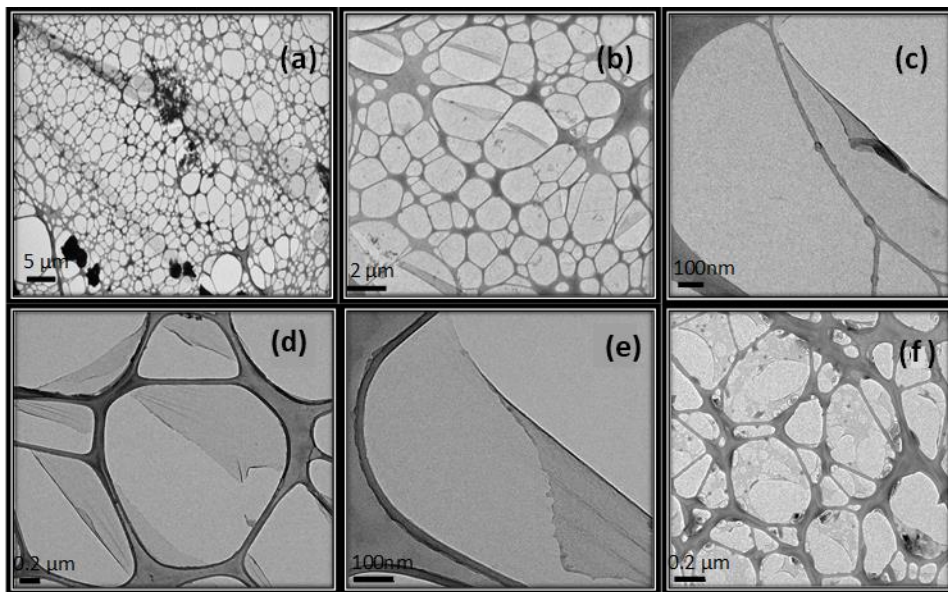


Figure 24. TEM images of nanosheets: (a) after the evaporation of a sample drop on the TEM grid; (b) magnification of (a); (c) magnification of (b); (d) after 72 h in the TEM grid. (e) Magnification of (d). (f) After the addition of extra water.

In order to further study the layers from **3pyCCMoidZn-2**, EDX analysis of the same sample used for the TEM images was performed (figure 25), observing the expected elements (C, O, N and Zn) from the CP system, apart of the microscope and grid materials (Al, Si and Cu).

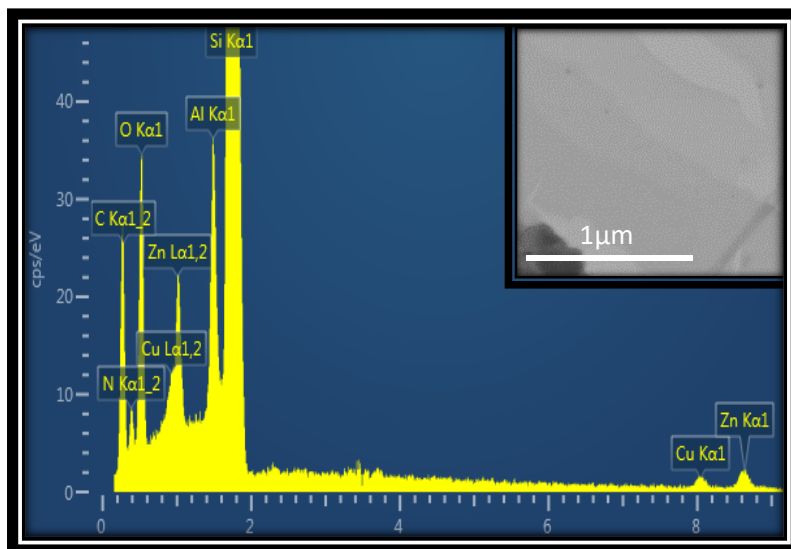


Figure 25. EDX spectrum and SEM image of the analysed area.

5. Conclusions

Here, studies of the 3pyCCMoid as organic linker have been extended, achieving a new highly dimensional structure (3D, **3pyCCMoidZn-3**) and a structure with a metal different from Zn (**3pyCCMoidCo-1**). In addition, comparative studies between the new systems and two previous ones reported in the group have been carried out to show the versatility of the ligand regarding coordination (partial or total) and different conformations. This, together with the versatile coordination nature of the Zn(II) salts, the use of different synthetic methods (solvothermal and $scCO_2$) and limiting the number of variables in the reactions (e.g.: reagents and solvents), provided a clear map of different crystallographic structures that could be achieved.

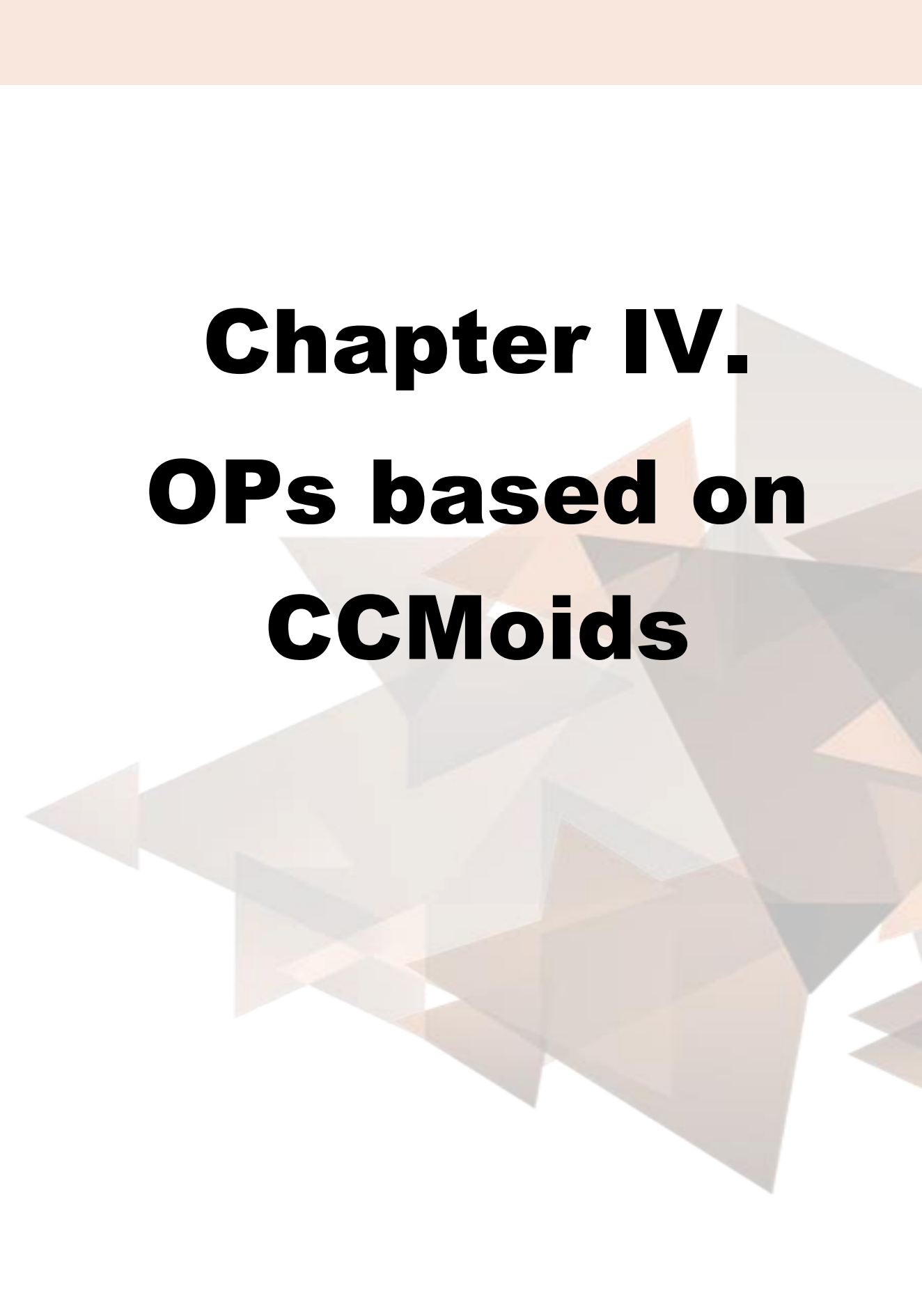
The three **3pyCCMoidZn-x** structures, that present different dimensionalities and coordination modes, probe how crucial are the synthetic conditions but also the huge versatility that this CCMoid brings to the field of coordination polymers. Comparing with the structures of the previous chapter, it seems that the combination of charged and neutral moieties present in 3pyCCMoid favours the full coordination of the linker, while in BDMC always at least one phenol remained protonated. Moreover, the synthesis of **3pyCCMoidZn-3** has proved that an effective coordination of all the coordinative positions of the CCMoid is possible without temperature and using low/mild boiling point solvents, as EtOH, in the case of **3pyCCMoidCo-1**. Another important achievement in this doctoral thesis was the synthesis of the first CP based on a CCMoids coordinated to Co(II) ions. The system is a 2D structure almost identical to that of **3pyCCMoidZn-2**.

Again, as in the previous chapter, $scCO_2$ methodology allows the reaction of the ligand but our studies suggest that coordination compounds are created instead of CPs. Nevertheless, 3pyCCMoid have shown good solubility in $scCO_2$, which implies that it is possible the completely elimination of organic solvents in future reactions with this molecule and possibly with other similar CCMoids.

Finally, as general conclusions, the results presented in this and the previous chapter add value to BDMC, 3pyCCMoid and in general to the CCMoid family in CP chemistry as interesting linkers, evidence which so far was limited to curcumin.

6. References

- (1) Hou, H., Meng, X., Song, Y., Fan, Y., Zhu, Y., Lu, H., ... & Shao, W. (2002). Two-Dimensional Rhombohedral Grid Coordination Polymers [M (bbbt) 2 (NCS) 2] n (M= Co, Mn, or Cd; bbbt= 1, 1'-(1, 4-butanediyl) bis-1 H-benzotriazole): Synthesis, Crystal Structures, and Third-Order Nonlinear Optical Properties. *Inorganic chemistry*, 41(15), 4068-4075.
- (2) Stang, P. J., & Olenyuk, B. (1997). Self-assembly, symmetry, and molecular architecture: Coordination as the motif in the rational design of supramolecular metallacyclic polygons and polyhedra. *Accounts of chemical research*, 30(12), 502-518.
- (3) anack, M., Hirsch, A., & Lehmann, H. (1990). Soluble, oligomeric bridged phthalocyaninatoiron (II) complexes. *Angewandte Chemie International Edition in English*, 29(12), 1467-1468.
- (4) Blake, A. J., Champness, N. R., Hubberstey, P., Li, W. S., Withersby, M. A., & Schröder, M. (1999). Inorganic crystal engineering using self-assembly of tailored building-blocks. *Coordination Chemistry Reviews*, 183(1), 117-138.
- (5) Janiak, C., Uehlin, L., Wu, H. P., Klüfers, P., Piotrowski, H., & Scharmann, T. G. (1999). DALTONFULL PAPER. *J. Chem. Soc., Dalton Trans*, 3121, 3131.
- (6) Wu, B., Zhang, W. J., Yu, S. Y., & Wu, X. T. (1997). Synthesis and structure of a helical polymer [Ag (R, R-DIOP)(NO₃)] n {DIOP=(4R, 5R)-trans-4, 5-bis [(diphenylphosphino) methyl]-2, 2-dimethyl-1, 3-dioxalane}. *Journal of the Chemical Society, Dalton Transactions*, (11), 1795-1796.
- (7) Konno, T., Tokuda, K., Okamoto, K. I., & Hirotsu, M. (2000). Enantioselective Aggregation of Cobalt (III) Octahedrons in a One-Dimensional S-Bridged CoIII AgI Array That Leads to Spontaneous Resolution. *Chemistry letters*, 29(11), 1258-1259.
- (8) Qian, W. (2018). Preparation and processing of molecular materials with optoelectronic properties.
- (9) Li-min, C. H. E. N., Jian-jun, K. A. N. G., Yang, L. I. U., & You-wen, L. I. N. (2011). Synthesis and in vitro Antioxidant Activity of Curcumin Analogs. *Natural Product Research & Development*, 23(4).
- (10) Theppawong, A., Van de Walle, T., Van Hecke, K., Grootaert, C., Van Camp, J., & D'hooghe, M. (2019). Synthesis of 1, 4-Thiazepane-Based Curcuminoids with Promising Anticancer Activity. *Chemistry—A European Journal*, 25(54), 12583-12600



Chapter IV.

OPs based on CCMoids

1. Introduction

As it was summarized in the general introduction of this doctoral thesis, the number of published organic polymers (OPs) based on CCMoids is scarce. Hence, with the aim of exploring OPs based in this family of molecules, in the progress of this doctoral thesis, two synthetic approaches were followed: (i) the use of designed CCMoid as the building units of the OPs; such CCMoids repeat in the polymeric structures through reactions with themselves or compatible monomers (figure 3) and (ii) the synthesis of CCMoid-OPs through the reaction of monomers which generate “in situ” an extended structure with a CCMoid skeletons.

In the first case, a set of CCMoids displaying boronic acids in the lateral substituents has been synthesized and already introduced in chapter I. Now, the idea was to examine their reactivity with polyalcohols, creating boronic ester bonds toward the achievement of new CCMoid-OPs. On the other hand, using the second method, CCMoid-CPs have been attempted by the use of acacBF_2 and aromatic polyaldehydes, where the condensation reaction between these two types of molecules generate CCMoid segments that, at the same time, promote the extension of the final systems.

1.1. CCMoids as monomeric units

1.1.1. Boronic acid: definition and reactivity

Boronic acids are trivalent boron containing molecules that present two hydroxyl groups and an alkyl substituent (figure 1).¹ They are used as organic reagents in many reactions, being probably the most famous the Suzuki-Miyaura coupling reaction, where aromatic boronic acids can react with organohalides forming C-C bonds with the assistance of a Pd (0) complex as a catalyst.² Moreover, boronic acids are used with multiple biomedical purposes, such as enzyme inhibitors, sensors and lectin mimics. Some are known as boron neutron capture therapy agents, transmembrane transporters and bioconjugators, used as well for protein immobilization.³ Many of these applications are based in their strong binding capacity with diols, thus acting as saccharide sensors, glucose controller, cell protein markers, and so on. The general reaction, among a diol and a boronic acid, produces the formation of a boronic ester (figure 1), with the loss of water molecules, as it occurs with carboxylic acids. The polyols can be aliphatic but also aromatic, as for catechol, giving rise to cyclic catechol boronic esters (figure 1).⁴

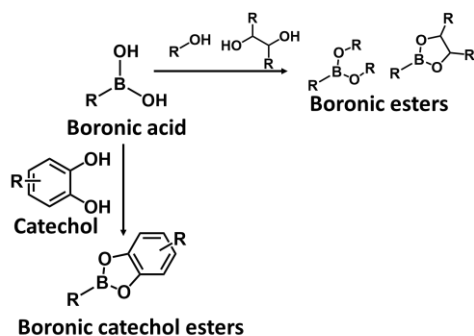


Figure 1. Boronic acids and boronic esters.

The creation of the covalent bond with diols have been exploited for the formation of macrocycles, cages, and polymers. For the latter, it is necessary to have more than one boronic acid and one diol units (figure 2).⁴

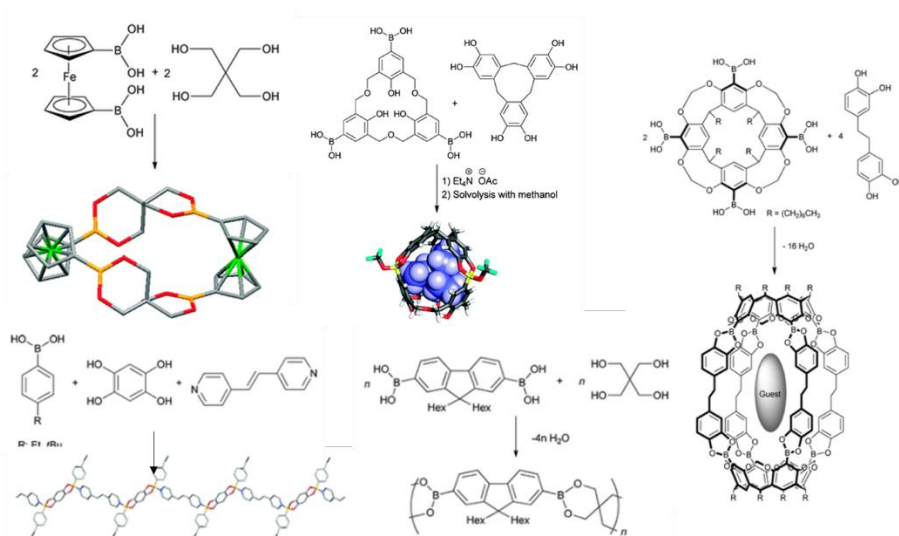


Figure 2. Examples of macrocycles and polymers based on the formation of boronic esters.⁴

To date, a number of examples of COFs (organic porous polymers, general introduction) involving different boronic acids has been published.⁵ Some of them are formed by the self-condensation of poly-boronic acids (figure 3), but primarily they are used in reactions with polyols forming boronic esters (figure 3). Since COFs are systems with a high degree of order, commonly, aromatic reagents are used in their formation because of their high rigidity and π - π stacking interactions.

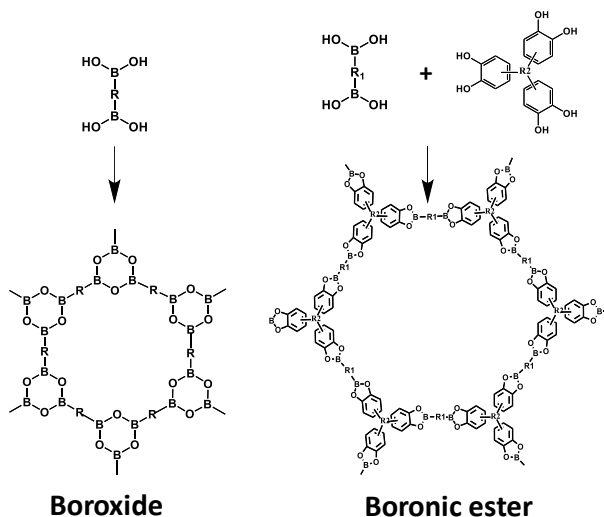


Figure 3. Schematic representation of COF structures based on the formation of boroxides and boronic esters.

1.1.2. Molecules used in this approach.

A CCMoid with boronic acid as substituent in the *para*- position of the aromatic rings (arms) and its analogous with BF_2 (coordinated to the β -diketone, figure 4) have been synthesized in this doctoral thesis (chapter I).

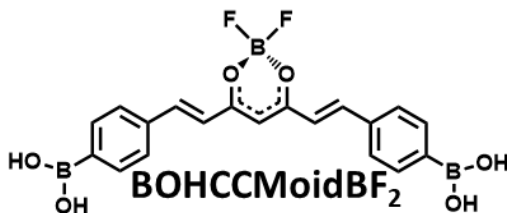


Figure 4. Scheme representing the structure of the BOHCCMoidBF₂ system with boronic acids as lateral substituents.

Here, the reactivity of this new boronic CCMoid was explored. Taking into account that boronic systems react with diols for the formation of extended structures and having as a goal the formation of new polymers, in an initial step, we have chosen two diol species: one aliphatic (pinacol) and another aromatic (catechol, figure 5), to analyse the reactivity of our CCMoids by studying the formation of boronic esters-based CCMoids.

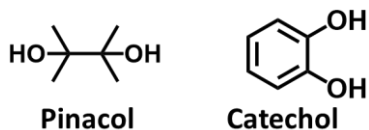


Figure 5. Schematic representation of the chosen diols.

In a second step, the formation of extended structures using more complex polyols has been also carried out. As before, two types of molecules were chosen: one aromatic and one aliphatic as before, 2,3,6,7,10,11-hexahydroxytriphenylene (HHTP) and 2,2-bis(hydroxymethyl)-1,3-propanediol (pentaerythritol), respectively (figure 6).

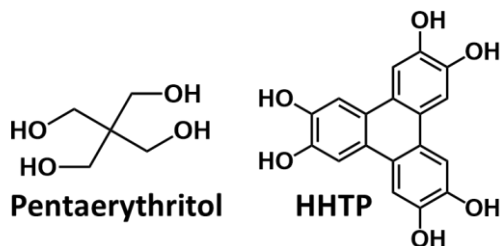


Figure 6. Schematic representation of the chosen polyols.

These molecules have already been used in the literature for the synthesis of extended structures. Due to the number of diols in the molecule, the pentaerythritol forms 1D polymers,^{6,7} while the HHTP produces structures with more dimensionality, as for example 2D COFs (figure 7).⁸⁻¹⁰

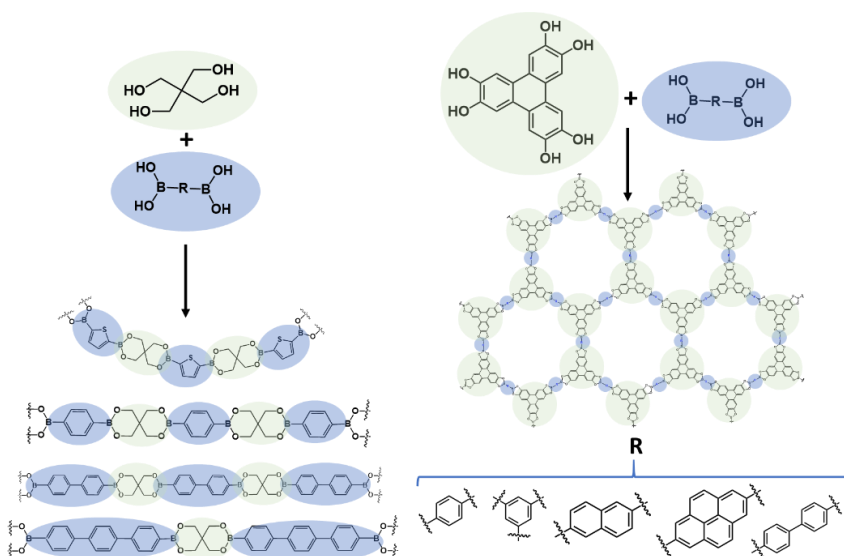


Figure 7. Examples of polymers obtained with HHTP and pentaerythritol.

The above ideas depict the creation of boronic esters by the reaction of a boronic acid-based CCMoid and commercial diols. Moreover, the opposite situation: the creation of a diol-based CCMoid (BODMC) and reactions with a diboronic molecule (benzene-1,4-diboronic acid, BDDBA) was also tested in this doctoral thesis.

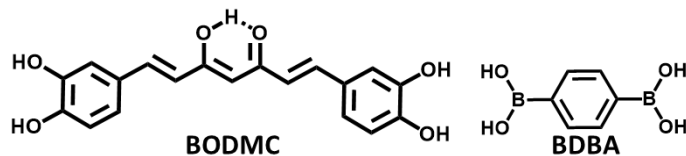


Figure 8. Schemes of the BODMC and BDDBA molecules.

1.2. Polymers with CCMoid-like structure

The condensation reaction between a benzaldehyde and boron-acac derivative is involved in the synthesis of CCMoids, generating the characteristic double bonds of the CCMoid skeleton. Since the acac has two reactive positions, the use of di- or tri-benzaldehydes often leads to extended structures, that can be considered as CCMoid-OPs. These new systems have seven carbon conjugated chains with β -diketone moieties connected among them through aromatic rings. During the development of this doctoral thesis, Liu *et al.*¹¹ published the first example of these species (figure 9) using tris(4-formylphenyl)amine and acacBF_2 .

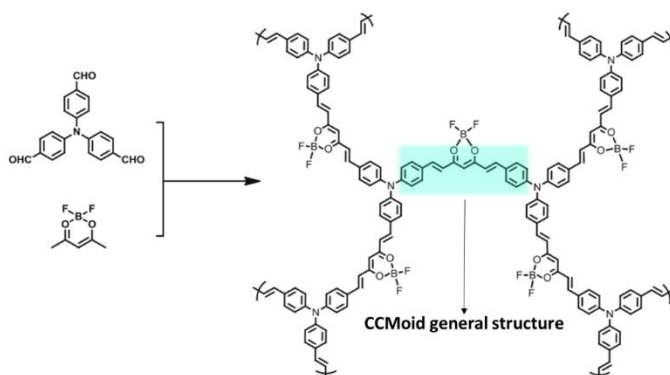


Figure 9. Organic polymer synthesized by Liu *et al.*¹⁰

In this doctoral thesis, two dibenzaldehydes (figure 9), benzene-1,4-dicarboxaldehyde (terephthalaldehyde) and benzene-1,3-dicarboxaldehyde (isoterephthalaldehyde), have been proposed for the condensation with acacBF_2 , as well as a planar tribenzaldehyde, benzene-1,3,5-tricarbaldehyde (figure 10).

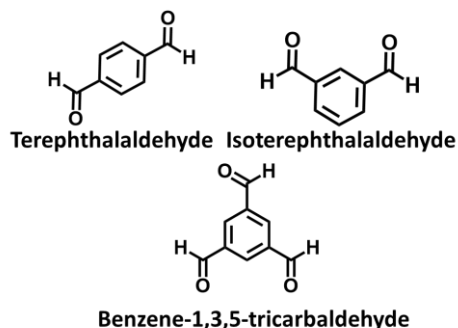


Figure 10. Benzaldehydes used in these studies.

Using these molecules, 1D (terephthalaldehyde and isoterephthalaldehyde) and 2D (benzene-1,3,5-tricarbaldehyde) structures could be obtained by making *in situ* the CCMoid segments (figure 9).

Here, we have applied both approaches, with the aim of creating systems with optoelectronic properties, as some of them are completely conjugated compounds and involve the coordination to BF_2 units.^{12,13} In this chapter, the preliminary results obtained in the reactions between BOHCCMoidBF_2 and the diols and acacBF_2 with polybenzenealdehydes are presented, as well as future work and perspectives. The insoluble behavior of the BOHCCMoid molecule limited its uses, being preferred the BF_2 coordinated version of it.

2. Objectives

The principal aim of this chapter is to obtain CCMoid-OPs by using a pre-synthesized CCMoid (BOHCCMoidBF_2) as a monomeric unit or by synthesizing *in situ* the CCMoid-like polymer. In this sense, using BOHCCMoidBF_2 and a set of diols, 1D or 2D species were expected to be obtained and have been initially characterized. To get insight on relevant factors, and possible drawbacks, in the formation of boronic esters is one of the main objectives addressed in this chapter. In the same way, using the approach of synthesizing *in situ* the polymer with a CCMoid-like structure, the principal goal was to obtain as well 1D/2D structures but having, in this case, as an exclusive repeating unit the CCMoids, with the use of no further molecules.

3. Materials and methods

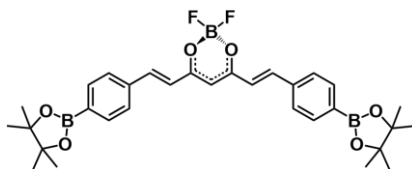
3.1. Materials

The syntheses of the BOHCCMoidBF₂, BODMC and acacBF₂ were described in chapter I. BOHCCMoidBF₂ was reacted with different commercial diols purchased in Fluorochem Ltd. (2,2-pentaerythritol and catechol), TCI EUROPE N.V. (pinacol) and Across Organics (HHTP). BDBA, used for the reaction with BODMC, was purchased in Sigma Aldrich, Merck KGaA. For the condensation with the acacBF₂, the used aldehydes were provided by Sigma Aldrich, Merck KGaA (benzene-1,3,5-tricarbaldehyde) and ABCR (terephthalaldehyde and isoterephthalaldehyde). THF, MeOH and EtOAc solvents used in the different synthesis were provided by CARLO ERBA Reagents S.A.S., while dioxane was acquired in Sigma Aldrich, Merck KGaA and the mesitylene in Fluorochem Ltd.

3.2. Synthetic methods

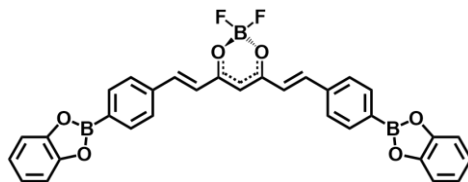
3.2.1. Boronic esters based on BOHCCMoidBF₂

3.2.1.1. BOHCCMoidBF₂-Pin (**Bpin**)



Scheme 1. Scheme representing the structure of **Bpin**.

For this synthesis, the method used was reported elsewhere.¹⁴ In short, BOHCCMoidBF₂ (100 mg, 0.24 mmol) and pinacol (86.5 mg, 0.73 mmol) were dissolved in 20 ml of THF. The mixture was stirred at room temperature for 24 h having molecular sieves 4A in the solution. Then, the solvent was evaporated under vacuum and the solid was rinsed with water to finally obtain a red solid (38.1 mg, yield 34 wt%). ¹H-RMN (360 MHz, DMSO-d₆) δ 8.07 (d, J = 14.4 Hz, 2H), 7.82 (m, 8H), 7.76 (d, J = 18 Hz, 2H), 6.73 (s, 1H), 1.32 (s, 24H) ppm. FTIR (cm⁻¹): 2978, 1618, 1556, 1509, 1359, 1270, 1141, 1089, 1059, 1005, 857, 651. MALDI-TOF m/z: 575.83 ([M-H]).

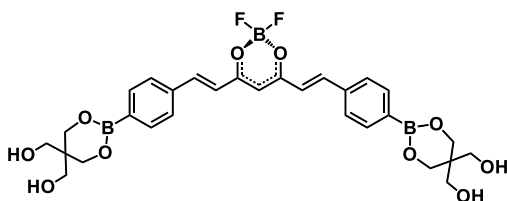
3.2.1.2. BOHCCMoidBF₂-cate (Bcate)**Scheme 2.** Schematic representation of the possible structure of **Bcate**.

Different conditions, including the one used for **Bpin** and modifications of it (higher temperature, times, different solvents...), were tested to achieve the **Bcate** as it is depicted above. However, the creation of the desired compound was not as straightforward as the previous, containing always mixtures with the reagents and uncoordinated version of the system (hence, some BF₂ units no longer coordinated to the β-diketone moieties). This was concluded by ¹H NMR. Even though it is a mixture, **Bcate** is described so we can follow the discussion later in regarding the creation of OPs.

The best results in the synthesis of **Bcate** were attained following a reported for the synthesis of COFs,¹⁵ which bases in the use of a microwave reactor. This way, in a microwave vial of 30 mL, BOHCCMoidBF₂ (21 mg, 0.05 mmol) and catechol (11 mg, 0.10 mmol) were dissolved in 2.5 mL de mesitylene and 2.5 mL of dioxane. The mixture was placed in a microwave at 150 °C for 1 h achieving a solid that was filtered and washed.¹⁶

3.2.1.3. BOHCCMoidBF₂-pol

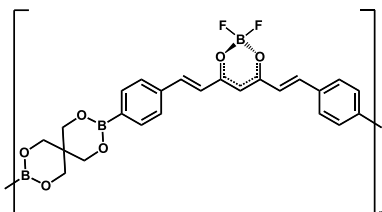
The methodology used is based on a previous work reported by Matsushima *et al.*⁵ In this case, the length and terminations of the polymer could be controlled by changing the stoichiometry of the two reagents involved: BOHCCMoidBF₂ (C) and pentaerythritol (D).

BOHCCMoidBF₂-pol-DCD (**Bpol-DCD**)**Scheme 3.** Structure of **Bpol-DCD**.

For the synthesis of the smallest segment, that only involves a molecule of the CCMoid and two of pentaerythritol (pol-DCD), one mol of C (67.5 mg, 0.16 mol)

and 2 mol of D (44.6 mg, 0.32 mol) were dissolved in THF and stirred at room temperature for 72 h. Afterward a solid was formed and then filtered and washed with fresh THF.

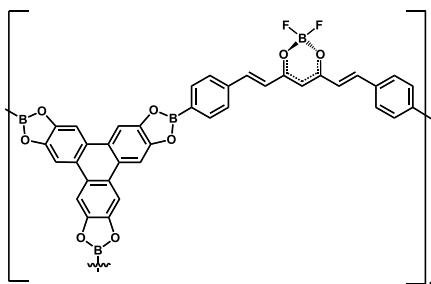
BOHCCMoidBF₂-pol-n (**Bpol-n**)



Scheme 4. Structure of **Bpol-n**.

By following the same procedure but using equimolecular quantities of both reagents (100 mg, 0.24 mol of C and 33.1 mg, 0.24 mol of D, respectively), a new system was synthesized. In these conditions, a solid precipitated and it was filtered and washed with THF. The system was found insoluble in most common organic solvents.

3.2.1.4. BOHCCMoidBF₂-HHTP (**BHHTP**)



Scheme 5. Structure of **BHHTP**.

With the aim of obtaining 2D systems, three different syntheses^{7,12,17} were tested, achieving three products:

(i) BOHCCMoidBF₂-HHTP1 (**BHHTP-1**). BOHCCMoidBF₂ (30 mg, 0.07 mmol) and HHTP (15.8 mg, 0.05 mmol) were dissolved in a solution of mesitylene and dioxane 1:1 (2 mL) and EtOH (0.1 mL). Then, the solution was left in an oven at 90 °C for 48 h. As a result, a black solid was isolated by filtration and washed with fresh solvents (dioxane/EtOH).

(ii) BOHCCMoidBF₂-HHTP2 (**BHHTP-2**). In this case, the procedure pursued was similar to that of **BHHTP-1**. BOHCCMoidBF₂ (20 mg, 0.048 mmol) and HHTP (10.4 mg, 0.032

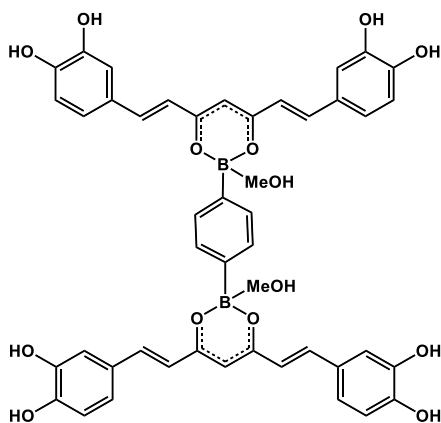
mmol) were dissolved in mesitylene /dioxane 1:1 (4 mL), placed in an oven for 72 h at 120 °C and washed with fresh solvent (mesitylene/dioxane 1:1).

(iii) BOHCCMoidBF₂-HHTP3 (**BHHTP-3**). Here, a synthetic protocol based in the one developed by Smith *et al.*¹⁶ was used. Briefly, BOHCCMoidBF₂ (30 mg, 0.072 mmol) and HHTP (15.8 mg, 0.049 mmol) were dissolved in a mixture of THF (10 mL) and EtOH (1 mL) and heated under reflux for 72 h 90 °C, having washed the solid accomplished with fresh solvent (THF).

3.2.2. Boronic esters based on BODMC

Different synthetic paths were attempted to form a polymer based on boronic ester using BODMC and BDBA. However, the lateral reaction was never achieved. Instead, an unexpected compound, BODMCBDBA-1, was precipitated with the use of solvothermal methods.

3.2.2.1. BODMCBDBA-1.



Scheme 6. Structure of **BODMCBDBA-1**

BODMC (30 mg, 0.088 mmol) and BDBA (21 mg 0.13 mmol) were solubilized in 4 mL of MeOH and placed in a 10 mL vial with hermetic closure. After 72 h in an oven at 80 °C, purple crystals appear in the walls and the bottom part of the vial, which were recovered and washed with fresh MeOH.

3.2.3. Polymers with CCMoid-like structures

The general synthesis involves the use of acacBF₂ (1.43 mg, 9.7 mmol) dissolved in 3 mL of EtOAc and heated at 60 °C. Then, a solution of the specific aldehyde (9.7 mmol) and tributyl borate (9.38 mg, 72 mmol) in 20 mL of EtOAc was added to the first one and the mixture was kept at 60 °C for 1 h. After that, the mixture was allowed to cool down to

4. Results and discussion

4.1. Boronic esters based on BOHCCMoidBF₂

Some of the species achieved using the first approach were partially soluble and it was possible to perform their ¹H-NMR spectra in DMSO-d₆. Figure 11 compares the spectra of **Bpin** and **Bpol-DCD** with the free CCMoid (BOHCCMoidBF₂).

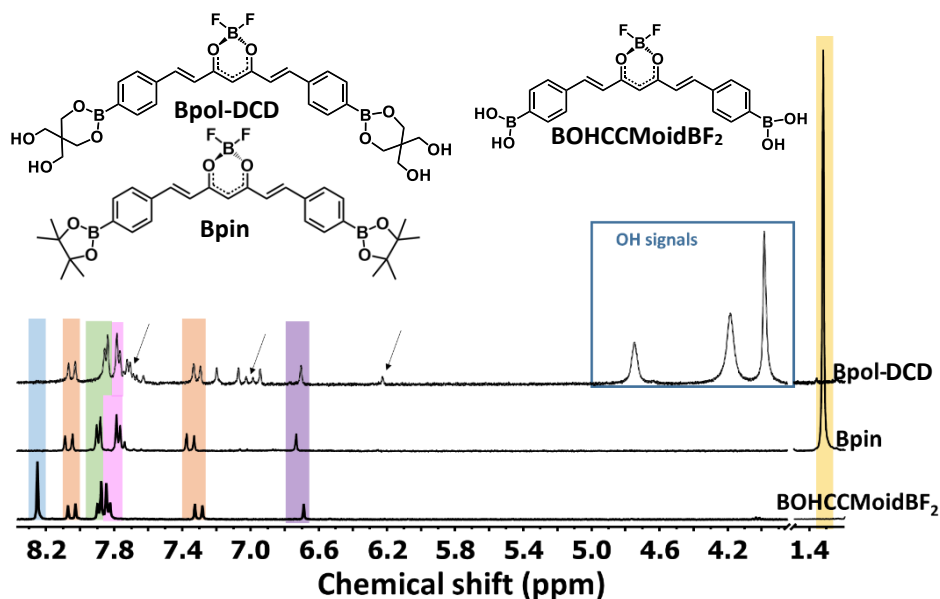


Figure 11. ¹H-NMR of **Bpin**, **Bpol-DCD** and BOHCCMoidBF₂.

The spectrum of the pristine BOHCCMoidBF₂ (figure 11) presents the typical signals of a CCMoidBF₂ with the central proton at 6.7 ppm (in purple, figure 11), the doublets of the double bond protons around 7.3 and 8 ppm (in orange, figure 11) and the aromatic signals around 7.9 ppm (in green and pink, figure 11). Moreover, the protons of the boronic acid are located at 8.3 ppm as a singlet (in blue, figure 11).

The formation of the boronic esters is evidenced by the disappearance of the acid boronic protons (8.3 ppm, figure 10) and in the case of the **Bpin**, also by the appearance of the pinacol methyl protons (1.3 ppm, in yellow figure 11). Moreover, the formation of the new species produced a shift of the aromatic protons, displacing the closest to the boron (in green, figure 11) to lower fields and the remaining two (in pink in figure 11) to higher fields. The rest of signals (doublets of the E protons in orange and the central proton, from the methine, in purple colour). The coordination of the BF₂ in the β-diketone is retained in the case of **Bpin**, proved by the displacement of the signals that is similar to the ones of BOHCCMoidBF₂ (at lower field than in the case of the non-coordinated compounds, chapter I).

The spectrum **Bpol-DCD** shows a similar set of shifts, including those corresponding to the remaining –OH groups from the pentaerythritol units at the sites of the molecule (approximately from 4 to 5 ppm). However, it can be observed partial deprotection of this CCMoid too, missing part of BF₂ units. This is supported by the presence of the signals pointed out with arrows in figure 11, e.g., at 6.3 ppm (central proton), the doublets at 7.0 ppm (E proton) and those appearing between 7.6 and 7.7 ppm (aromatic region and E protons).

The absence of the boronic acid protons (8.2-8.3 ppm) suggest that both, BOHCCMoidBF₂ and its unprotected version, form boronic ester bonds. Nevertheless, this has further implications in the creation of polymers, where it can be possible that in the polymer **Bpol-n** mixtures of protonated and deprotonated chains are present. Moreover, as the β-diketone can also interact with boronic acids when it remains free (e.g.: BODMCBDBA-1) we cannot discard additional coordination through this moiety as well. Further analyses using, solid state NMR techniques, should be performed with all the samples to provide further insight.

In the spectrum of **Bcate**, a more complicated sets of signals are observed (figure 12) with the appearance of a total of 4 species, the reagents (catechol in blue and BOHCCMoidBF₂ in orange colours), unprotected CCMoid (in red colours) and the desired product (in green colour). Here, the necessity of more intense conditions than those applied for **Bpin**, does not favours the formation of the boronic esters with aromatic molecules. Nevertheless, to generalize this idea, additions reagents and synthetic methods should be tested. In our case, the use of MW assisted reactions has an additional drawback, triggering the loss of the BF₂ units and therefore, providing extra undesired products. It is important to stress that the coordination of BOHCCMoid to BF₂ improves solubility (BOHCCMoidBF₂) of the starting materials and protects the β-diketone for the possibility of further reactions; however, the idea of having the non-coordinated systems is highly desired as well, due to the possibility of using the extended version of **Bcate** (hence, BHHTP-x) to capture/sensor different metal/metalloid centres.

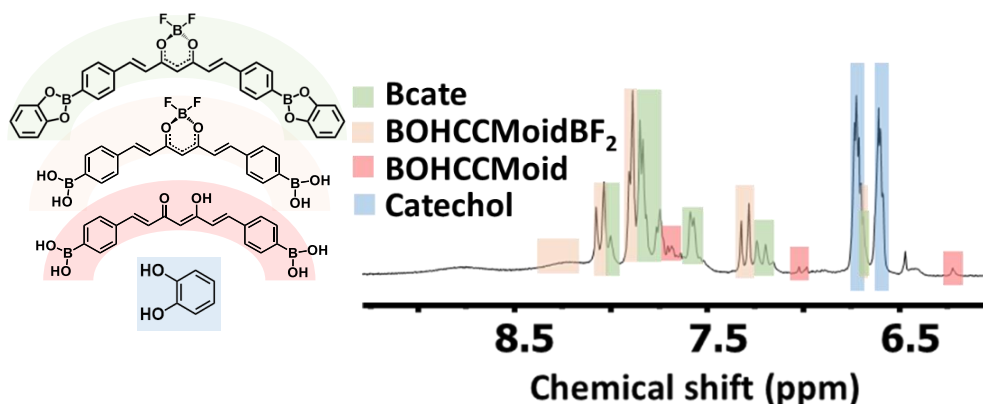


Figure 12. ^1H -NMR spectra of the solid obtained in the reaction between BOHCCMoidBF₂ and catechol.

For **Bpol-n** and **BHHTP-x**, characterization by ^1H NMR in DMSO- d_6 was not possible due to their low solubility of the systems. The formation of the boronic ester was identified by FTIR, being assisted by the work of Smith *et al.*¹⁸ that performed a complete experimental study of the bands observed in the spectra of boronic acids, boroxines, and boronic esters, combined also with computational modelling. The authors determined that the boronic esters have two characteristic signals around 1250 and 650 cm^{-1} , which are not observed for boronic acids neither for boroxides. For **Bpol-n** and **BHHTP-x**, the first signal was difficult to identify due to the overlap of bands in that region, while the region between 600 and 400 cm^{-1} was more useful due to the absence of band from the net CCMoid (figures 13 and 14).

A signal around 650 cm^{-1} (in green, figure 13) appears in all the species in which boronic acid esters were formed, confirmed in the soluble molecules, **Bpin** and **Bpol-DCD**, by ^1H NMR and in extended systems as **Bpol-n**, being this the proof of polymer formation. The infrared spectra of **Bpol-CDC** and **Bpol-n** present identical bands, except for the broad band between 3500 and 3200 cm^{-1} displayed by **Bpol-CDC** and also a sharp one around 1000 cm^{-1} . Both signals are related to the presence of primary alcohols corresponding to the O-H stretching and the C-C-O asymmetric stretching, respectively. Many of the other bands are related with the CCMoid skeleton and, therefore, the spectra show similarities among all the species, being remarkable the carbonyl region (orange area in figure 13) that remains unaltered. This may indicate that the β -diketone region was preserved during the different reactions although in some cases, as discussed in the NMR section, we cannot discard partial release of the BF₂ units.

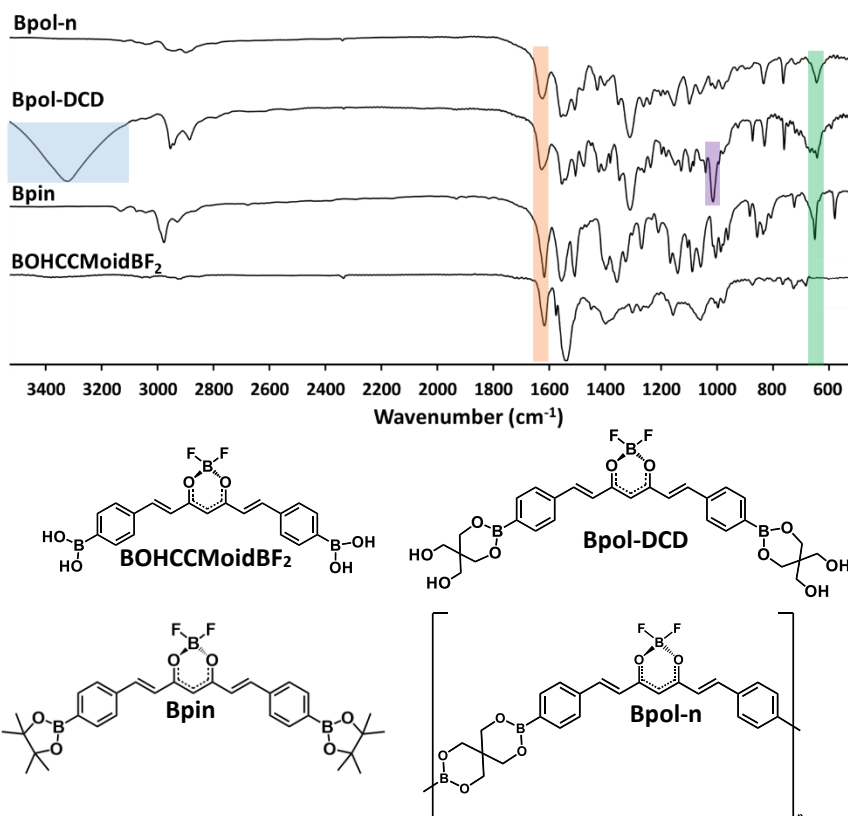


Figure 13. FTIR spectra of **Bpin**, **Bpol-CDC**, **Bpol-n** and net CCMoid together with representations of the desired systems.

Changes in the FTIR spectra were also observed for the compounds obtained by the reaction of the CCMoid with aromatic molecules, either catechol, **Bcate**, or **HHTP-x** systems, figure 14). For instance, the absence of signals at 650 cm^{-1} for **BHHTP-x** requires further investigation to assess the possible formation of the boronic ester, however, the precipitation of an insoluble solid indicated that some reactivity took indeed place. Moreover, the same spectra were observed for the three studied reaction conditions indicating a similar product in all the cases. In addition, the presence of signals in the carbonyl region (in orange in figure 13) indicated that the CCMoid is forming part of the new structure. Again, further studies in the solid state, as for example ^{13}C NMR, may provide insight on the remaining queries.

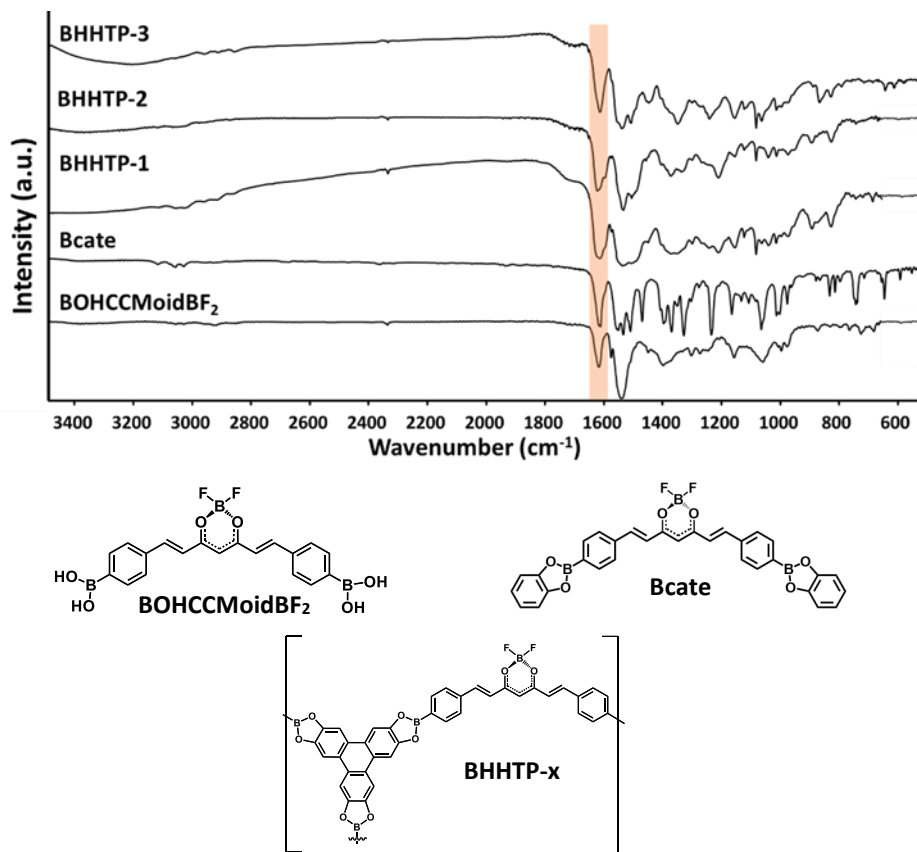


Figure 14. FTIR spectra of **Bcate**, **BHHTP-1**, **-2** and **-3**, and **BOHCCMoidBF₂**.

The crystallinity of **Bpol-n** and **BHHTP-1** was studied by XRD (figure 15), showing that both solids are amorphous. For **BHHTP-1**, the broad bands observed at 6°, 17° and 26° may indicate some order in the structure. However, the synthesis should be further investigated to improve the crystallinity factor in these materials. The rest of the solids of BHHTP series have totally amorphous patterns.

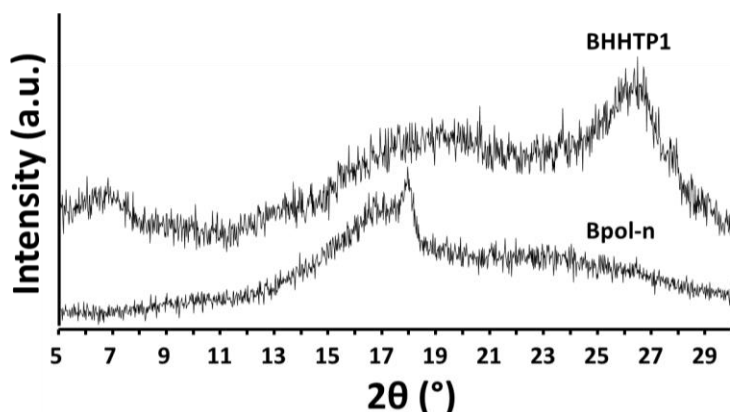


Figure 15. XRD spectra of **BHHTP1** and **Bpol-n**.

4.2. Boronic esters based on BODMC

By using BODMC and BDBA, a boronic ester system was achieved. This way, **BODMCBDBA-1** was obtained as purple cubic crystals from the mother solution (figure 16).

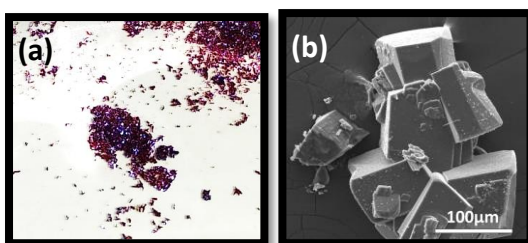


Figure 16. Crystals of **BODMCBDBA-1**: (a) optical microscope image and (b) SEM image (right).

The compound was analysed by single crystal XRD using a synchrotron source. **BODMCBDBA-1** crystallizes in the space group $P2_1/n$. It is a 0D structure consisting of a dimer of BODMC molecules connected through their β -diketone moieties by the BDBA unit. Thus, forming boronic ester bonds. Two MeOH molecules, from the solvent, complete the tetracoordination geometry (angles between 104.3° and 111.08°) of the boron atoms (figure 17a). The BDBA adopts a planar disposition with an angle of 95° between the boron, the carbon atom connected to it and the central atom of the CCMoid. The CCMoids are disposed one above the BDBA plane and the other below, being the MeOH molecule in the opposite direction (figure 17a). Apart from the coordinated solvent molecules, one MeOH molecule is present close to each dimer. The dimers are disposed stacked on top of each other, forming a supramolecular stairs-like

structure (figure 17b). All of the “stairs” interact among them and through the extra solvent molecules, forming a compact structure (figure 17c).

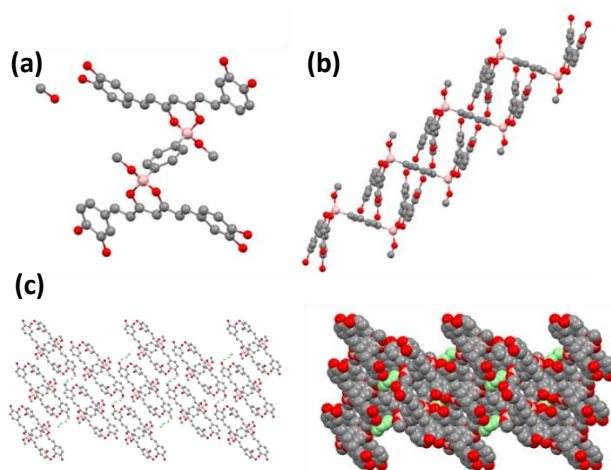


Figure 17. BODMCBDBA-1. (a) 0D structure, (b) organization of the 0D structure, (c) extension in the 3D space and space filling (solvent molecules in green).

The FTIR spectrum of **BODMCBDMA-1** does not have the characteristic band observed for the other systems at 650 cm^{-1} , instead a new band around 1200 cm^{-1} was observed. Changes in the carbonyl region are observed due to the reaction of the β -diketone with the boronic acid (orange range, in figure 18). The band corresponding to the O-H stretching was still observed (purple area in figure 17) at $3000\text{--}3500\text{ cm}^{-1}$, as the phenols remained free. Differences in the shape of this band with respect to BODCM could be due to the interactions that these protons establish in the supramolecular net and the absence of the enol proton from the β -diketone moieties.

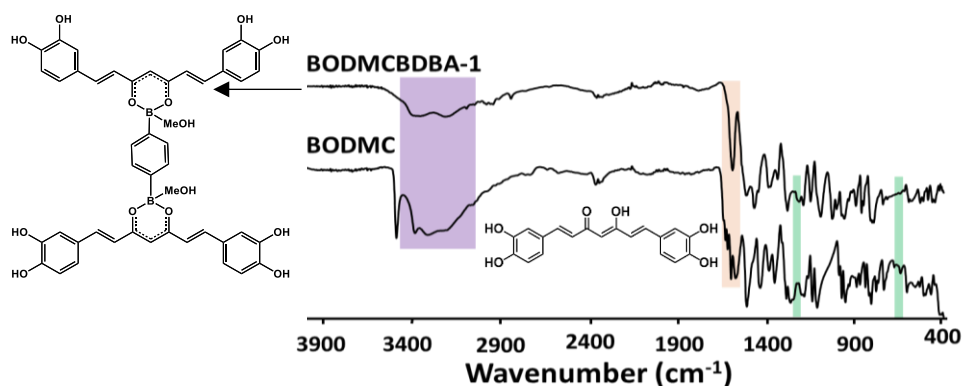


Figure 18. FTIR spectrum of the BODMCBDBA-1 compared with the pristine CCMoid.

4.3. CCMoid like polymeric structure.

Obtained polymers were highly insoluble and did not present crystallinity, therefore they could only be exclusively characterized by FTIR. An extra technique that can give us information of this compounds is solid state ^{13}C NMR but some technical problems difficult their use during the last stage of this doctoral thesis.

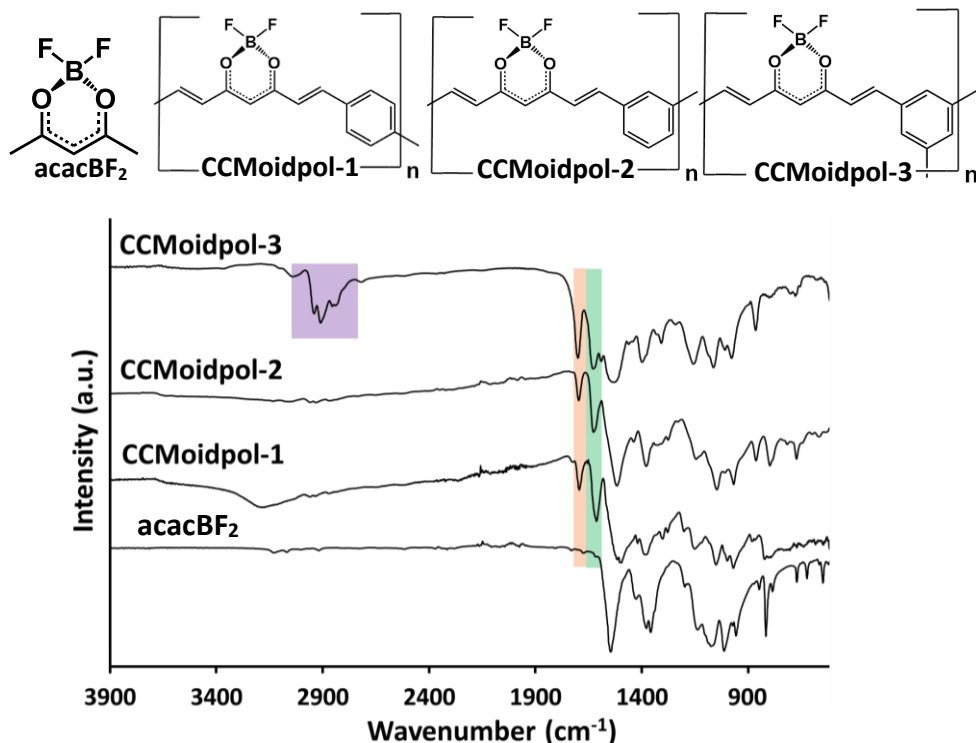


Figure 19. FTIR spectra of the **CCMoidpol-x** series compared with acacBF_2 .

In figure 19, the FTIR spectra of the products are compared with the β -diketone precursor, acacBF_2 . The three **CCMoidpol-x** systems, being $x=1, 2$ and 3 , present the expected bands originated by the formation of the condensation products: the band in the carbonil region corresponded to the β -diketone (orange band in figure 19) and the bands of the $\nu\text{C}=\text{C}$ and νC_{Ph} (green band in figure 19). These bands are comparable to those expected in CCMoid spectra, because of their conjugated skeletons (chapter I).

Here, similar signals are observed for the three polymers, except the bands around 2900 cm^{-1} that only appear in **CCMoidpol-3**. Regarding the nature of the latter, typically the C-H stretching of aldehydes appears in this region. In the case of **CCMoidpol-3**, the aldehyde used (benzene-1,3,5-tricarbaldehyde) has several signals in the same area

(appendix I). Our results indicate that likely, in the polymer structure, a considerable amount of aldehyde moiety remains free giving place to this band. This may reduce the dimensionality of the final structure, but can also be a point for further post-synthetic modifications.

In the rest of of polymers, **CCMoidpol-1** and **-2**, the aldehyde signals were not observed, indicating that all the aldehyde moieties may participate in the condensation process.

5. Conclusions

In this chapter the possibility of precipitating organic polymers based on boronic esters with CCMoids has been initially explored, being the obtained polymers, the first ones involving a CCMoid different of CCM or its derivatives. In addition, it can be concluded that the reaction of BOHCCMoidBF₂ to form boronic esters is more favourable with aliphatic molecules than with their aromatic analogous. Despite of this, some results were obtained with catechol and HHTP that encourage further research in this topic.

The production of polymers with CCMoid-like structure created in-situ has been also found plausible although requires of further investigation. Extended conjugated planar structures could be obtained, expanding the CCMoid features to polymeric architectures.

In this way, this thesis has expanded the number of extended organic structures based on CCMoids, improving the family of CCMoid-polymers.

6. Future work and perspectives

This chapter shows preliminary results, but the promising findings encourage to continue with the two presented approaches.

In this sense, additional characterizations of the 1D polymers based on CCMoid are necessary as the determination of their size using techniques as gel permeation chromatography (GPC), ss ¹³C NMR and MALDI. These studies were not included in this thesis due to the lack of time or impossibility of using some of the techniques in the same framework of time. We must take into account that the application of some of the techniques is hampered by the lack of solubility of some of the systems, as for example, **Bpol-n**, that makes unfeasible the application of GPC, being therefore more useful for this system MALDI experiments. However, considering the latter, some optimizations should be also done finding a matrix and a laser intensity that achieve the ionization of the polymer with a low fragmentation. In addition, the stability and possible reassemble,

biocompatibility and optical properties of this polymer should be analysed, among others.

Despite of being an interesting material by itself, the presence of the β -diketone coordinated to a labile group (BF_2) open the possibility of form new more extended materials using diboronic molecules (as in the case of **BODMCBDBA-1**) or metal centres.

In the reaction of BOHCCMoidBF_2 with aromatic molecules, an optimization of the conditions is necessary, both with catechol and HHTP, with the objective of having a pure compound in the first case and a crystalline ordered system in the second. Moreover, in the extended structures, to determine if the boronic ester bonds are being formed and having into account the lack of solubility, solid state NMR can be performed, studying ^{13}C and ^{11}B nucleus. As it was demonstrated in previous chapters, CPMAAS ^{13}C NMR can be a useful technique for determining the structure of the CCMoid-like polymers structures and analyse their purity. Once the structures were known, and the synthetic conditions optimized, additional studies related to their biocompatibility, electronic transport and luminescence properties should be analysed to promote further uses and applications (e.g.: I-V experiments with probe station of the team).

Finally, an although polymers with BODMC could not be obtained, **BODMCBDBA-1** can be an interesting building block for the creation of more complex structures. It has four reaction points (the four diols of the two curcuminoid molecules) and its stair shape may promote extended structures with a variety of shapes.

7. References

- (1) Hall, D. G. (Ed.). (2006). *Boronic acids: preparation, applications in organic synthesis and medicine*. John Wiley & Sons.
- (2) Lennox, A. J., & Lloyd-Jones, G. C. (2014). Selection of boron reagents for Suzuki–Miyaura coupling. *Chemical Society Reviews*, 43(1), 412-443.
- (3) Yang, W., Gao, X., & Wang, B. (2005). Biological and medicinal applications of boronic acids. *Boronic Acids*, 481-512.
- (4) Nishiyabu, R., Kubo, Y., James, T. D., & Fossey, J. S. (2011). Boronic acid building blocks: tools for self assembly. *Chemical Communications*, 47(4), 1124-1150.
- (5) Li, H., Li, H., Dai, Q., Li, H., & Brédas, J. L. (2018). Hydrolytic Stability of Boronate Ester-Linked Covalent Organic Frameworks. *Advanced Theory and Simulations*, 1(2), 1700015.
- (6) Matsushima, Y., Nishiyabu, R., Takanashi, N., Haruta, M., Kimura, H., & Kubo, Y. (2012). Boronate self-assemblies with embedded Au nanoparticles: preparation, characterization and their catalytic activities for the reduction of nitroaromatic compounds. *Journal of Materials Chemistry*, 22(45), 24124-24131.
- (7) Yuji, K., Ryuhei, N., Yasuhiro, M., (2016). Catalyst using boronic acid ester type polymer as carrier and preparing of γ -valerolactone, JP 2016159247, Japan.
- (8) Cote, A. P., Benin, A. I., Ockwig, N. W., O'Keeffe, M., Matzger, A. J., & Yaghi, O. M. (2005). Porous, crystalline, covalent organic frameworks. *science*, 310(5751), 1166-1170.
- (9) Wan, S., Guo, J., Kim, J., Ihee, H., & Jiang, D. (2008). A belt-shaped, blue luminescent, and semiconducting covalent organic framework. *Angewandte Chemie International Edition*, 47(46), 8826-8830.
- (10) Cote, A. P., El-Kaderi, H. M., Furukawa, H., Hunt, J. R., & Yaghi, O. M. (2007). Reticular synthesis of microporous and mesoporous 2D covalent organic frameworks. *Journal of the American Chemical Society*, 129(43), 12914-12915.
- (11) Liu, W., Wu, S., Su, Q., Guo, B., Ju, P., Li, G., & Wu, Q. (2019). Difluoroborate-based conjugated organic polymer: a high-performance heterogeneous photocatalyst for oxidative coupling reactions. *Journal of Materials Science*, 54(2), 1205-1212.
- (12) Etchevery Berríos, Á. F. (2018). Diseño y síntesis de sistemas curcuminoides para aplicaciones en electrónica molecular.
- (13) Weiss, H., Reichel, J., Görls, H., Schneider, K. R. A., Micheel, M., Pröhl, M., ... & Weigand, W. (2017). Curcuminoid–BF₂ complexes: Synthesis, fluorescence and optimization of BF₂ group cleavage. *Beilstein journal of organic chemistry*, 13(1), 2264-2272.
- (14) Iwamoto, T., Okuzono, C., Adak, L., Jin, M., & Nakamura, M. (2019). Iron-catalysed enantioselective Suzuki–Miyaura coupling of racemic alkyl bromides. *Chemical Communications*, 55(8), 1128-1131.
- (15) Tilford, R. W., Gemmill, W. R., zur Loye, H. C., & Lavigne, J. J. (2006). Facile synthesis of a highly crystalline, covalently linked porous boronate network. *Chemistry of materials*, 18(22), 5296-5301.
- (16) Hall, D. G. (2005). Structure, properties, and preparation of boronic acid derivatives. Overview of their reactions and applications. *Boronic Acids*, 1.
- (17) Smith, B. J., & Dichtel, W. R. (2014). Mechanistic studies of two-dimensional covalent organic frameworks rapidly polymerized from initially homogenous conditions. *Journal of the American Chemical Society*, 136(24), 8783-8789.
- (18) Smith, M. K., & Northrop, B. H. (2014). Vibrational properties of boroxine anhydride and boronate ester materials: model systems for the diagnostic characterization of covalent organic frameworks. *Chemistry of Materials*, 26(12), 3781-3795.



General Conclusions

The main objective of this doctoral thesis was the synthesis of CCMoids and the evaluation of a set of these molecules as building blocks for the formation of extended metal-organic (CPs) and organic structures (OPs).

In the synthesis of CCMoids, nine molecules have been obtained including four new ones. Regarding their synthesis, the straightforward methodologies and high yields accomplished prove the versatile possibilities on the design and creation of new CCMoids, being this an attractive tool toward the achievement of functional molecular-based materials. Our thorough characterization allows among others (identification, purity, etc.) assessments on the conformation adopted by the molecules in solid state using ^{13}C CPMAS NMR, and therefore, assisting in great manner the analysis of polycrystalline materials in the absence of single XRD. At the same time, the estimation of the bandgap energy of the studied CCMoid molecules (electrochemical analyses and absorption spectroscopy studies) indicated the semiconductor nature of CCMoids, being able to conclude that the shortest HOMO-LUMO distances and better acceptor capabilities are observed for long CCMoidBF₂.

In the formation of extended structures (CPs and OPs), the great ability of the chosen CCMoids to create expanded systems has been probed, accomplishing materials with a variety of dimensions and indicating the necessity of their further analysis regarding their use in electronics and/or biomedical topics.

In the use of CCMoids as organic linkers for the formation of CPs, only two structures were described in the literature before this doctoral thesis and both using CCM. Our work shows the capability of another natural CCMoid but the great potential that synthetic CCMoids has in the creation of CPs. Moreover, the published works have used exclusively Zn as a metallic source, and here we present the first CCMoid-CP that contains Co(II) centres. This new 2D system will be exfoliated in a similar manner than the Zn(II) analogue studied in this doctoral thesis toward the study of their electron transport behaviour.

In addition, from the different synthetic approaches tested here in the creation of CPs, we can state that, in most of the structures, where the three CCMoid sides require deprotonation (e.g.: BDMC), at least one corner remains uncoordinated (partial coordination). Instead, if the system contains neutral coordination groups (e.g.: 3pyCCMoid) seems easier to accomplish full coordination of the CCMoid linker. Nevertheless, this conclusion depends in great manner on the reaction parameters used (solvents, metal salts, method, etc.), being they of great relevance in the creation of CPs. In our studies, partial coordination of the ligand reduces the dimensionality of the structures (1D) and the combination of the CCMoids with additional co-linkers has been proved successful toward the goal of increasing the dimensionality of final systems.

Within the CPs, the studies of the different conformations of the CCMoid units (sometimes in the same structure), highlights the flexibility of these molecules and the

great advantage that this means in the achievement of crystalline materials (solvated or non-solvated).

The work of this doctoral thesis shows the difficulties encountered in the characterization of the final CCMoid systems using $scCO_2$, where in all the cases the micro-sized crystalline materials could not be analysed by single XRD and, sometimes, additional analyses could not assert the creation of polymeric structures.

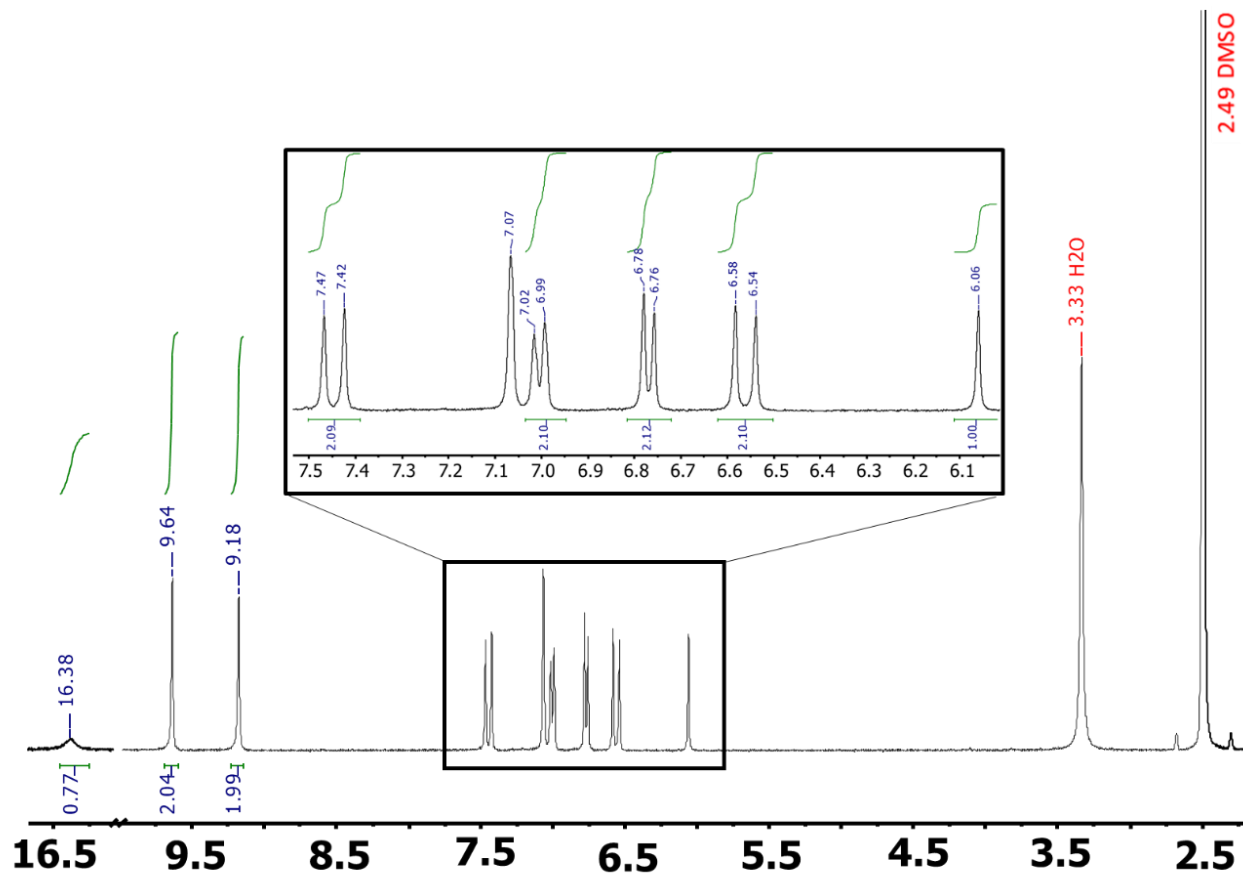
In the formation of OPs, the limited time hampered the possibility of further analyses, but some encouraging preliminary results have been obtained that will be pursued in future studies in the group. In that sense, we have proved the possibility of forming polymeric structures based on the creation of boronic ester bonds between the designed CCMoid and polydiol molecules. This way, it has been corroborated the reaction between the boronic acid terminal groups in the CCMoid with commercial diols, especially when the latter are aliphatic in nature, maintaining the β -diketone moiety from the CCMoid unaltered. However, the opposite occurs when trying to carry out the reverse approach, hence, reacting a CCMoid with diol endings, as substituents, with commercial diboronic molecules, where the reaction happens through the β -diketone moieties.

Finally, the possibility of reacting $acacBF_2$ with di- or trialdehydes was proved obtaining product solid from their condensation. Having into account the complete conjugated nature of the final system and the electrochemical results obtained from the CCMoid BF_2 molecules, our results encourage the optimization of the method to achieve materials with interesting optoelectronic properties.

As a general conclusion, the main objectives of this doctoral thesis have been fulfilled as we have accomplished effective syntheses of the desired CCMoids as well as extended structures of different nature (CPs and OPs) and dimensionality (1D-3D). From these results, the capacity of CCMoids to be used as building blocks have been proved. This, together with the huge number of CCMoids synthesized in the past and that may be synthesized in the future open almost infinite and new possibilities in the field of CPs and OPs.

The page features a light beige header bar at the top. The background is white with several semi-transparent, light beige triangles of various sizes scattered across it. The text is centered and reads:

Appendix I.
Supplementary
figures

Figure A.1. ^1H NMR spectrum of BODMC

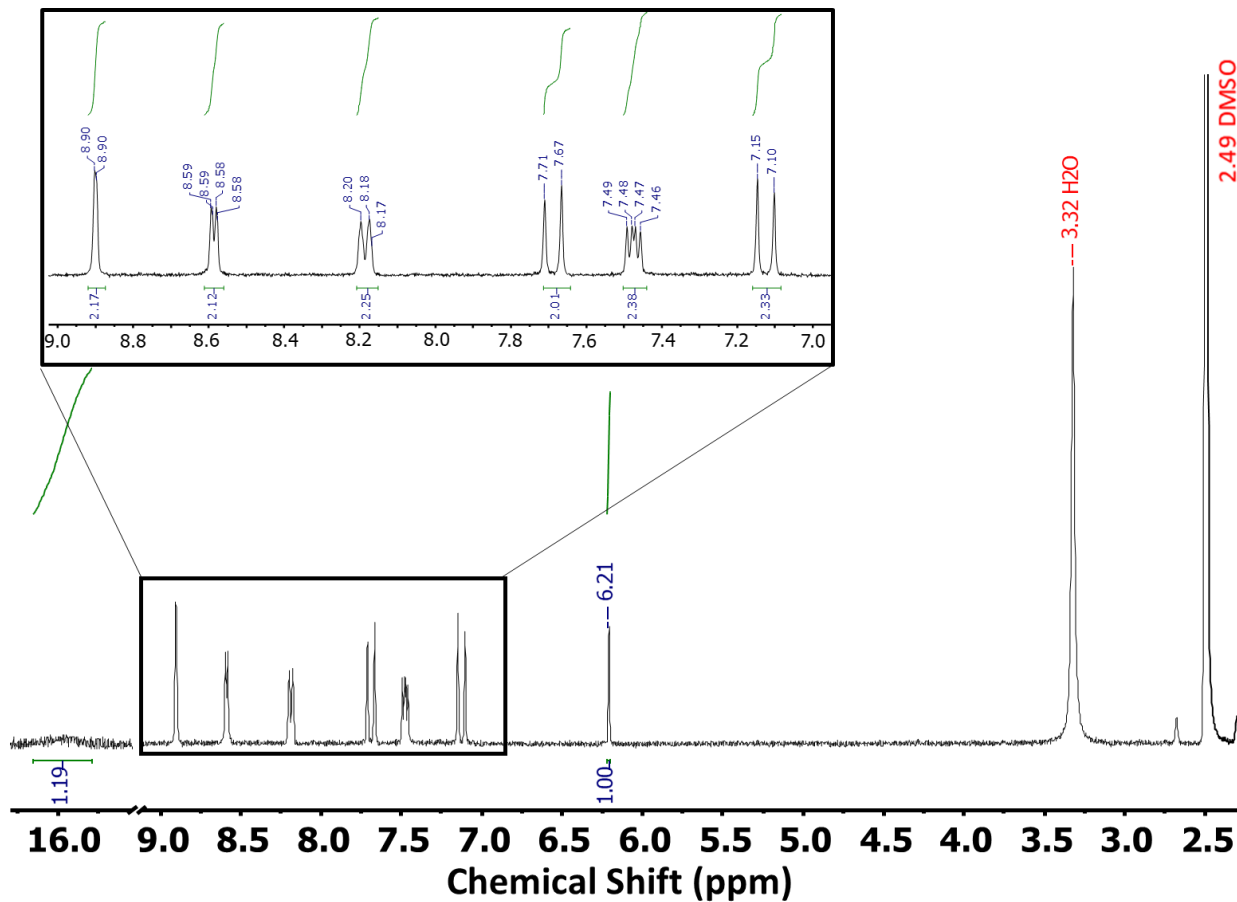
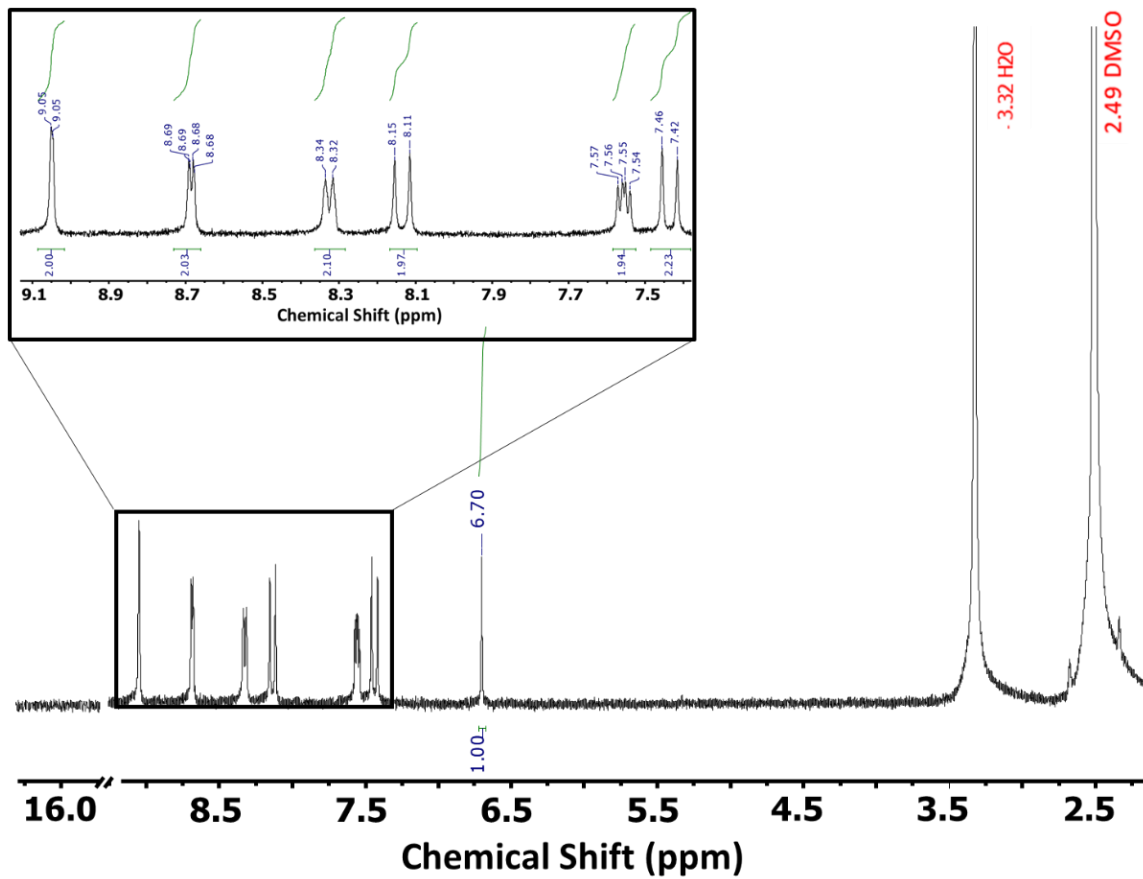


Figure A.2. ^1H NMR spectrum of 3pyCCMoid.

Figure A.3. ^1H NMR spectrum of 3pyCCMoidBF₂

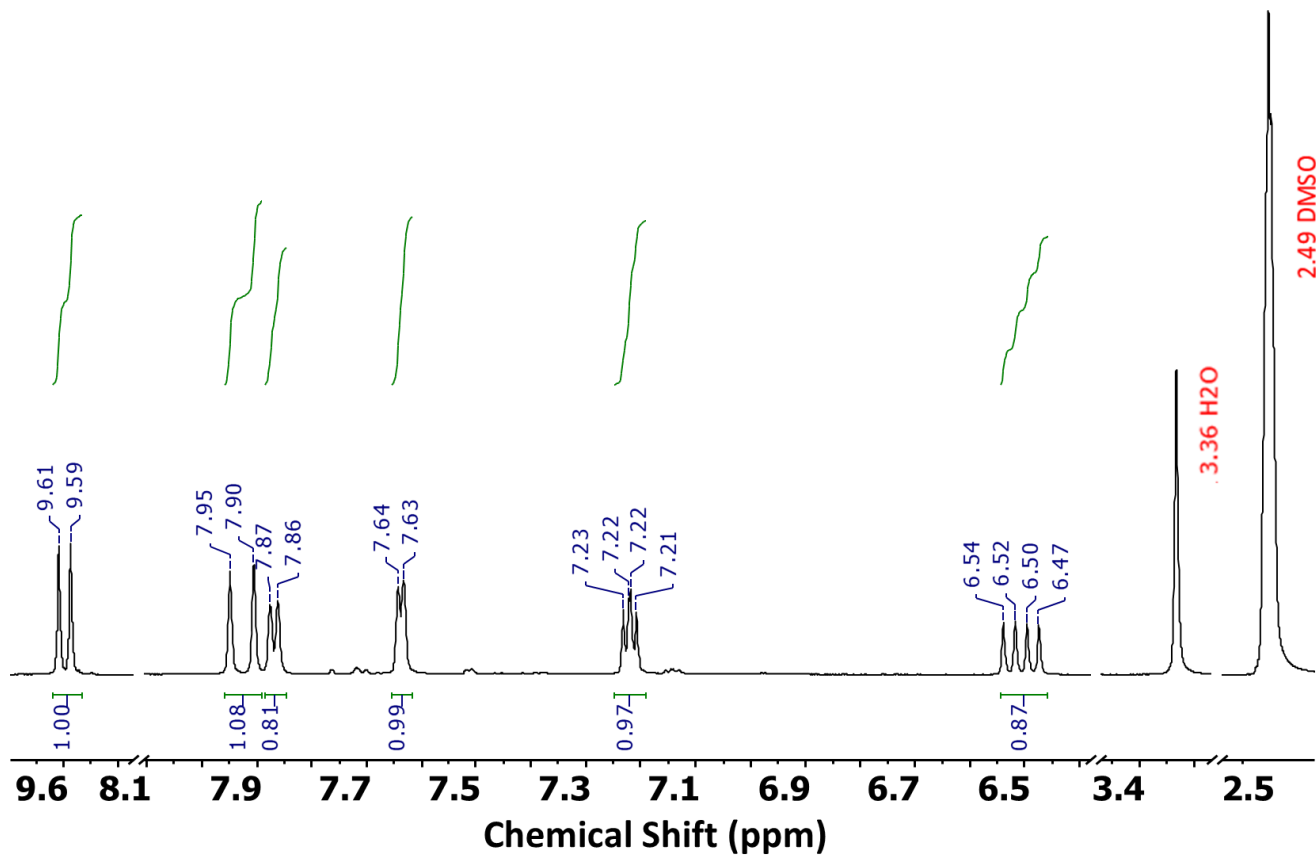


Figure A.4. ^1H NMR spectrum of 3-(2-Thienyl)acrylaldehyde (E isomer)

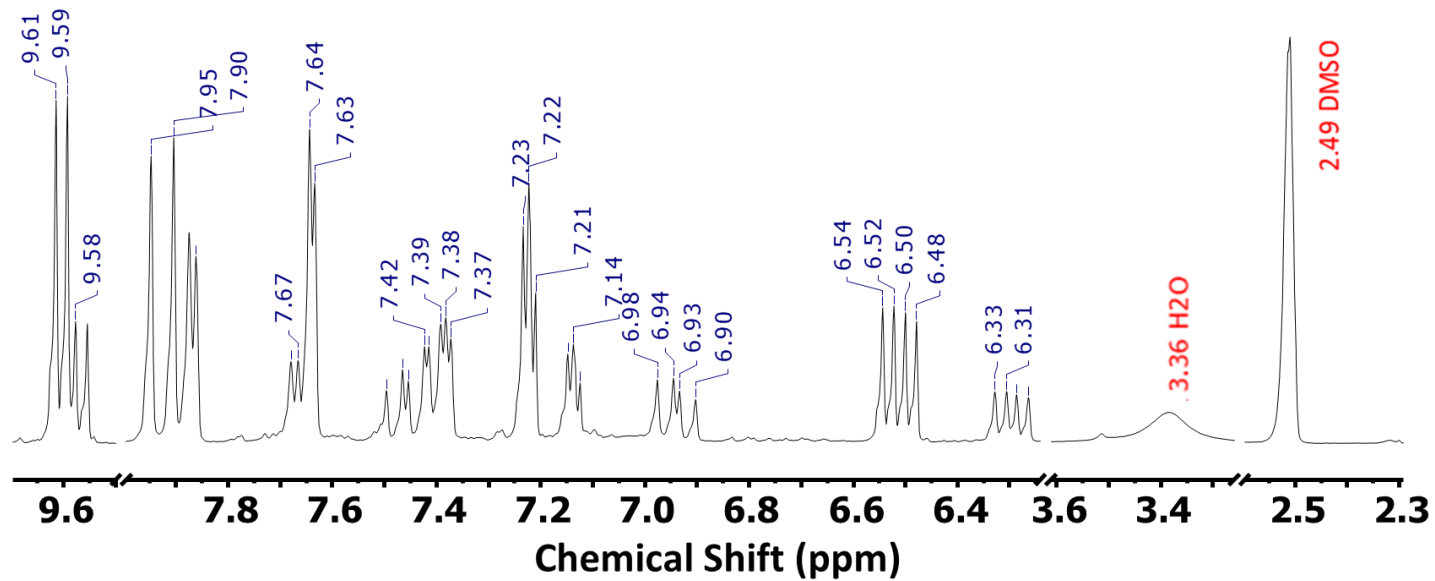


Figure A.5. ¹H NMR spectrum of 3-(2-Thienyl)acrylaldehyde (Mixture of Z and E isomers).

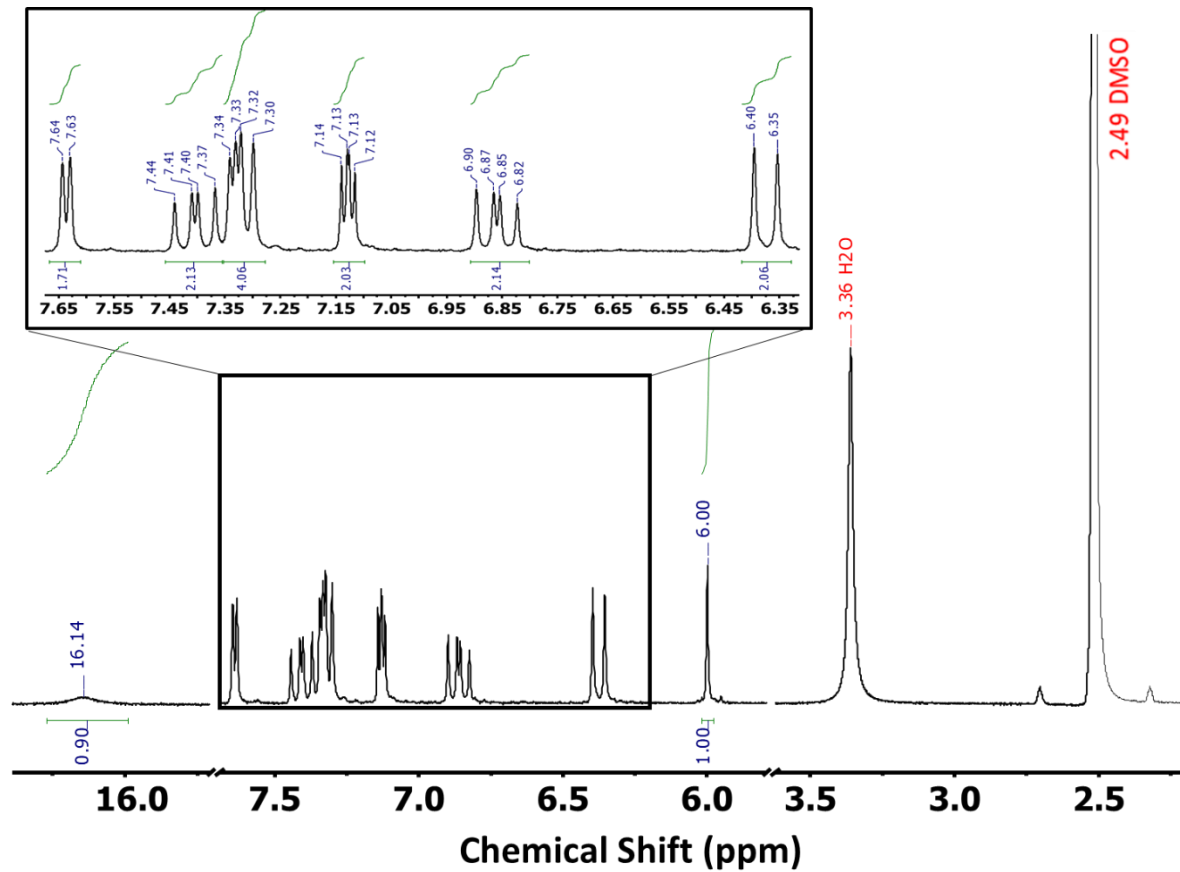


Figure A.6. ^1H NMR spectrum of 2-thphLCCMoid.

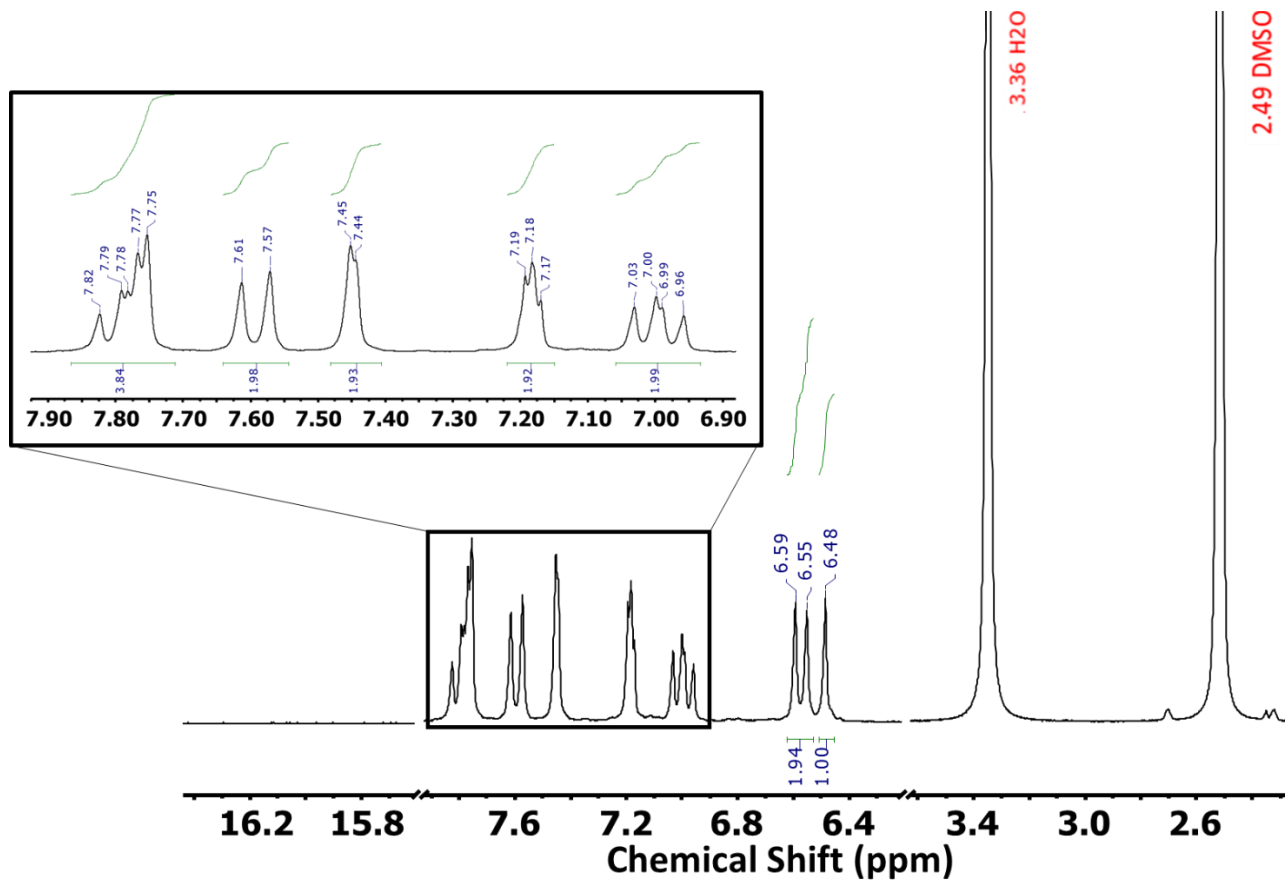


Figure A.7. ^1H NMR spectrum of 2-thphLCCMoidBF₂.

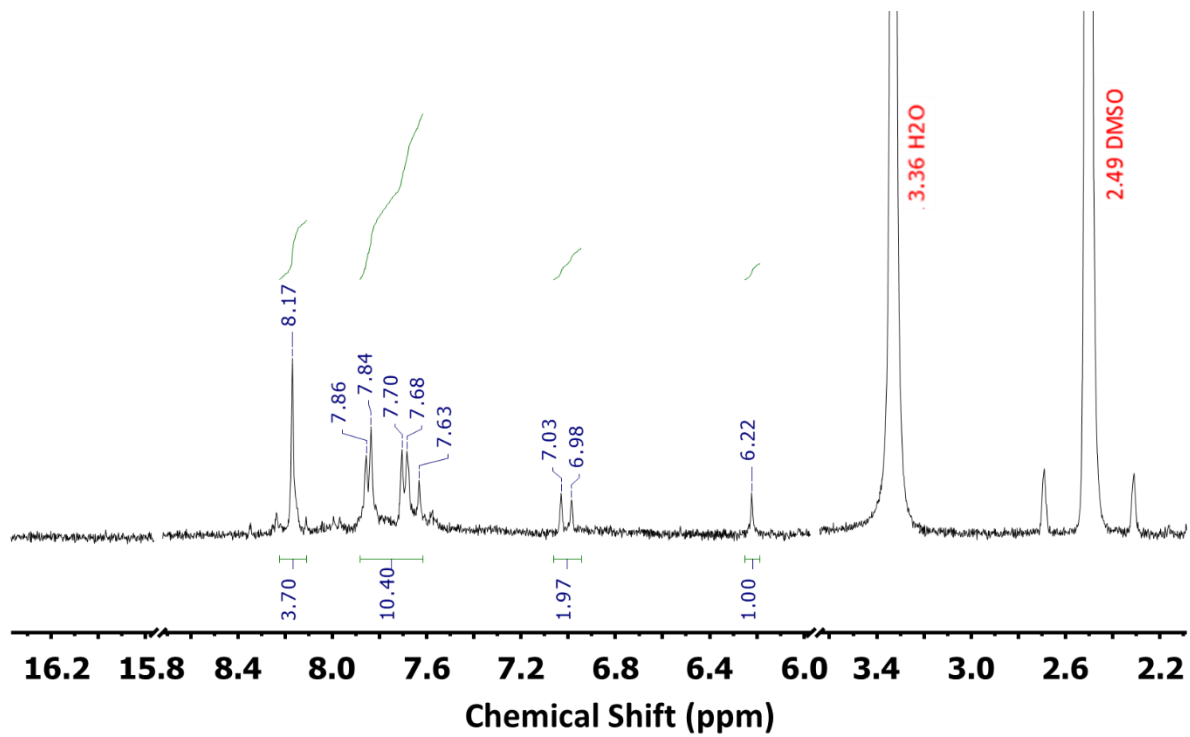


Figure A.8. ^1H NMR spectrum of BOHCCM.

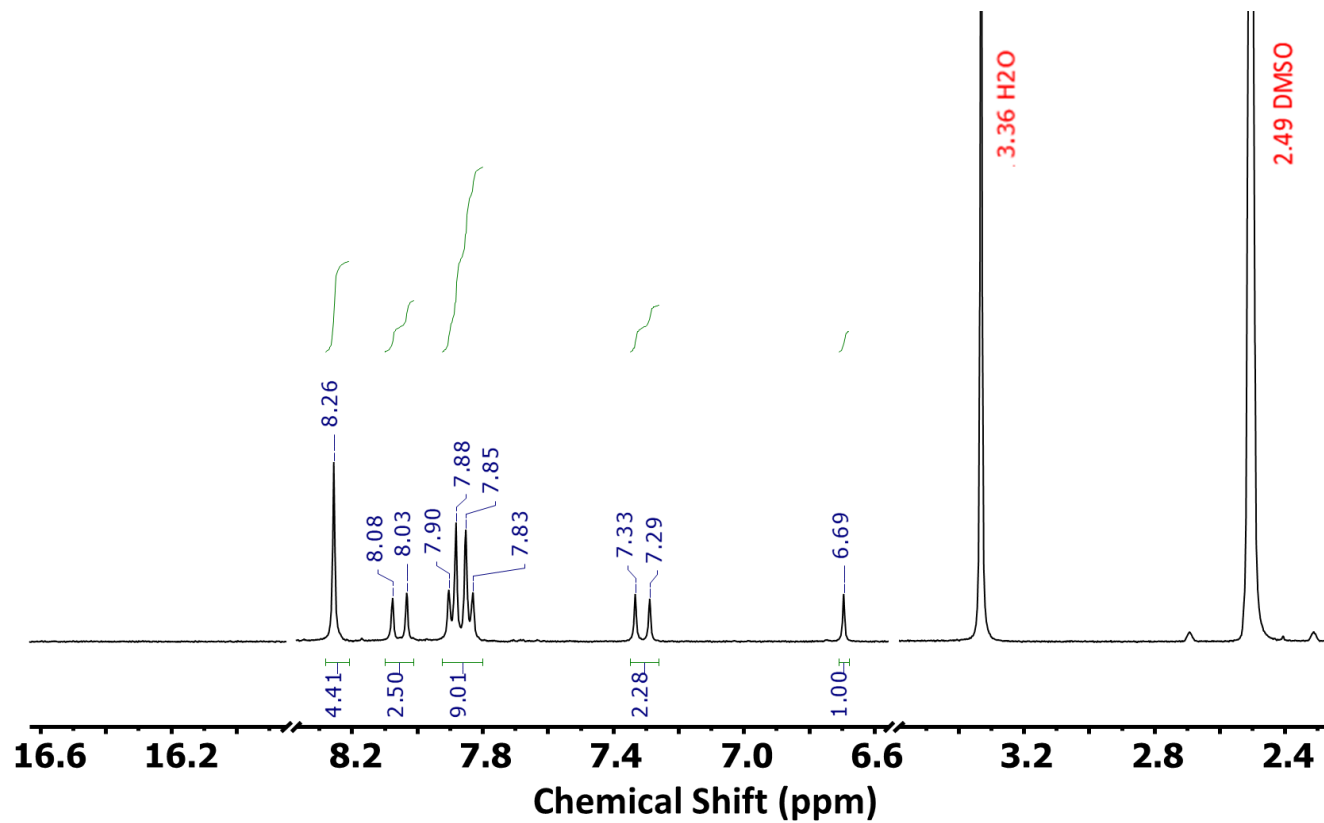


Figure A.9. ^1H NMR spectrum of BOHCCMBF₂.

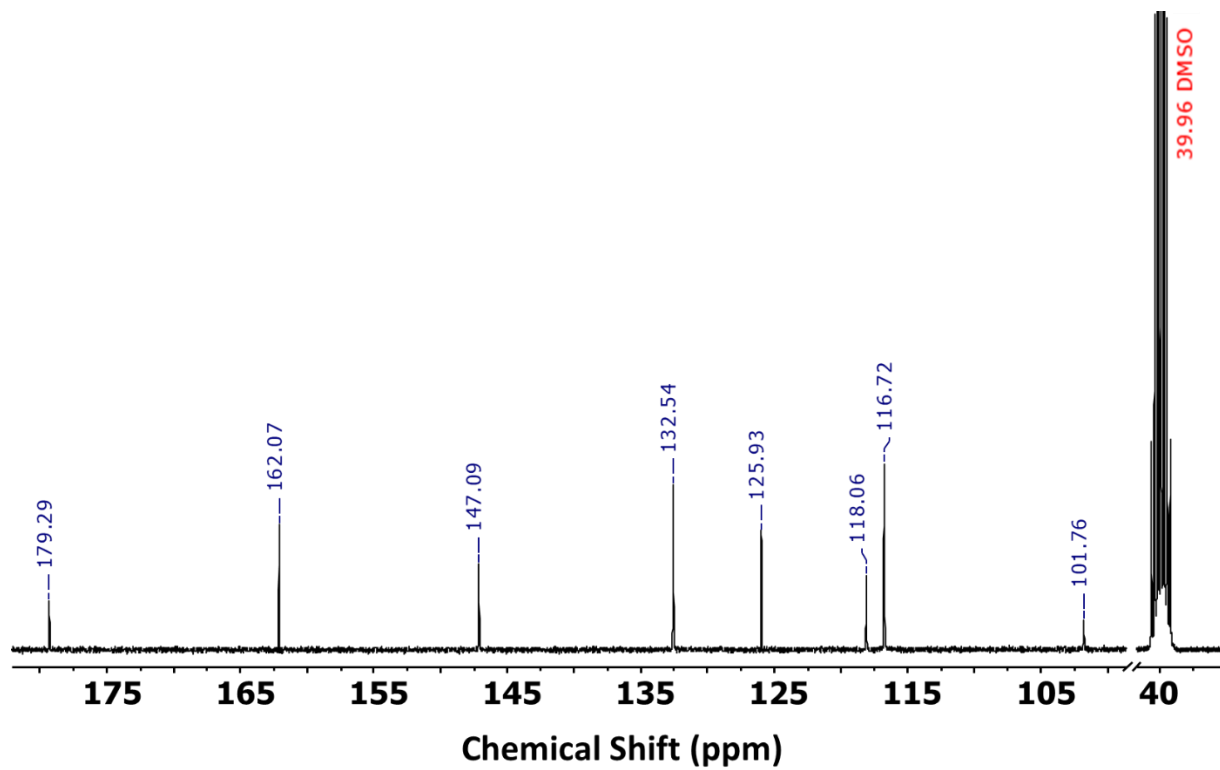


Figure A.10. ^{13}C NMR spectrum of BDMCBF₂.

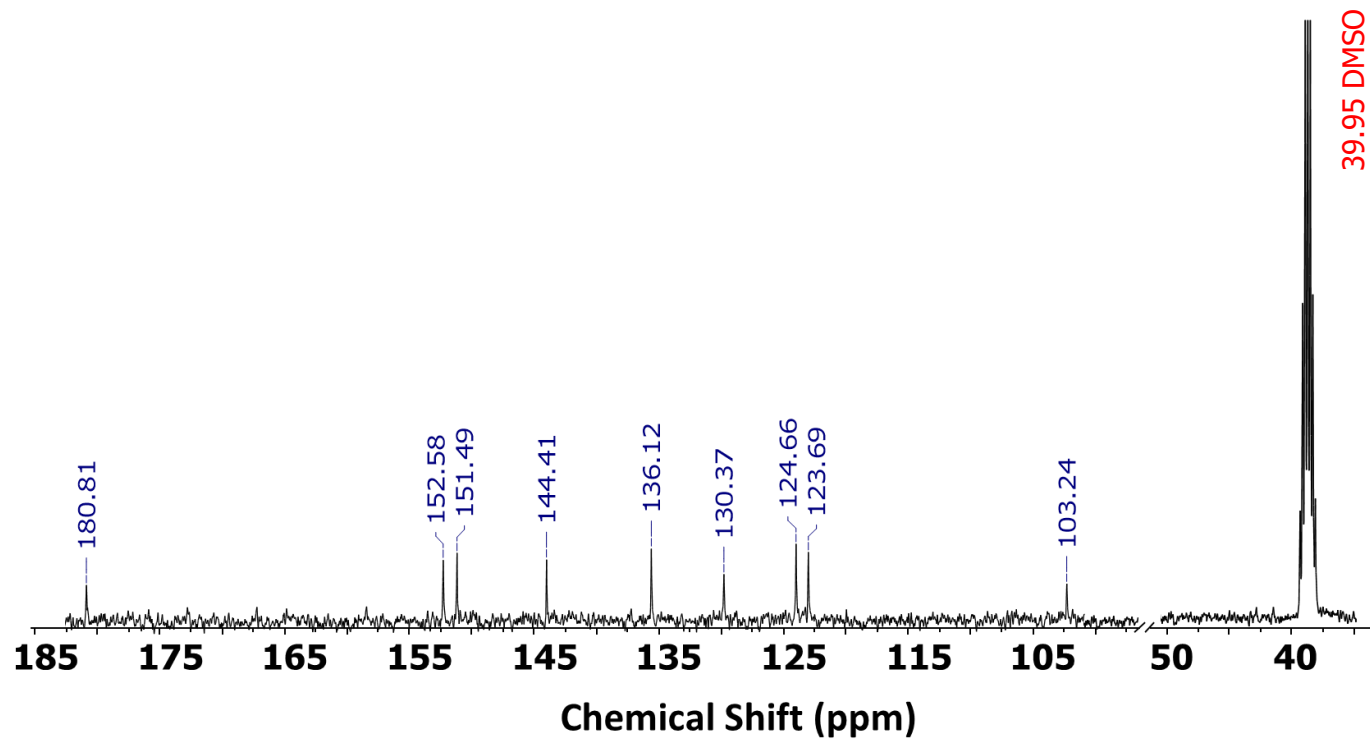


Figure A.15. ^{13}C NMR spectrum of 3pyCCMoidBF₂

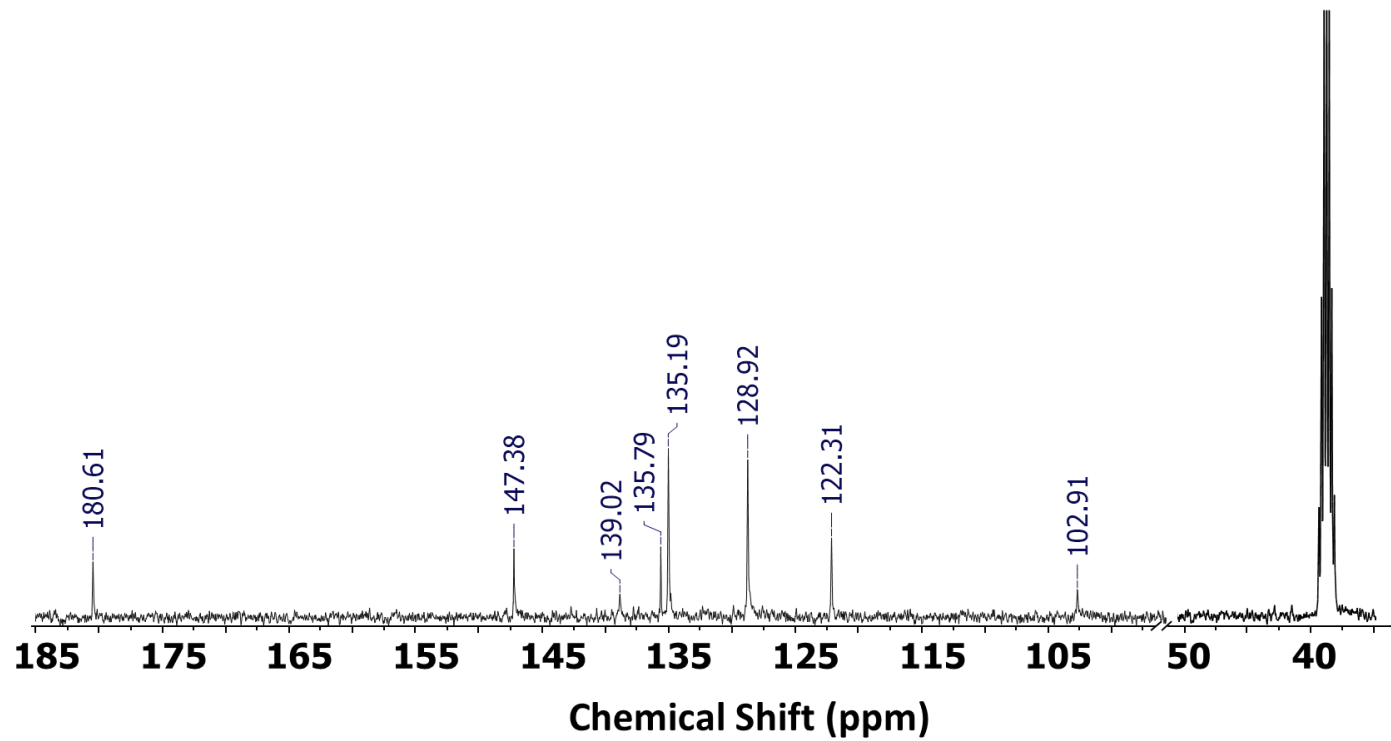


Figure A.16. ^{13}C NMR spectrum of BOHCCMBF

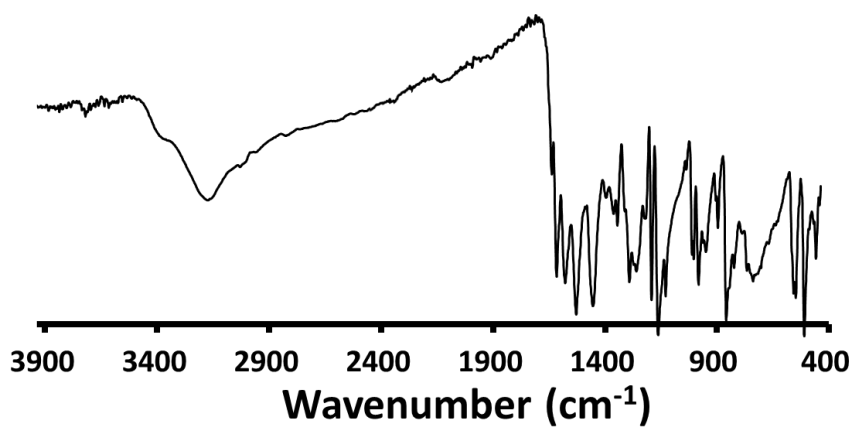


Figure A.17. FTIR-ATR spectrum of BDMC

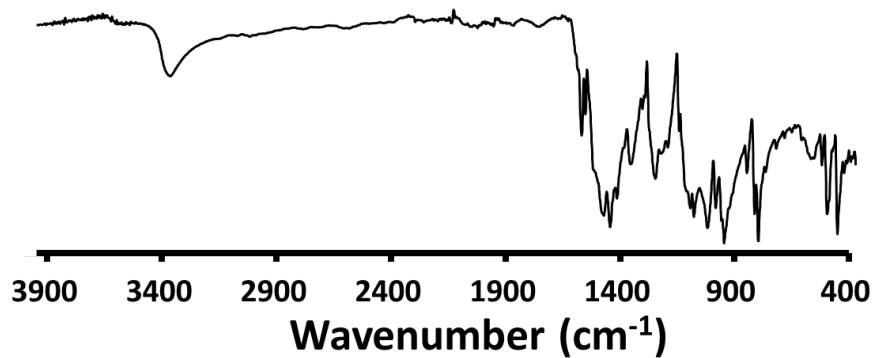


Figure A.18. FTIR-ATR spectrum of BDMCBF₂

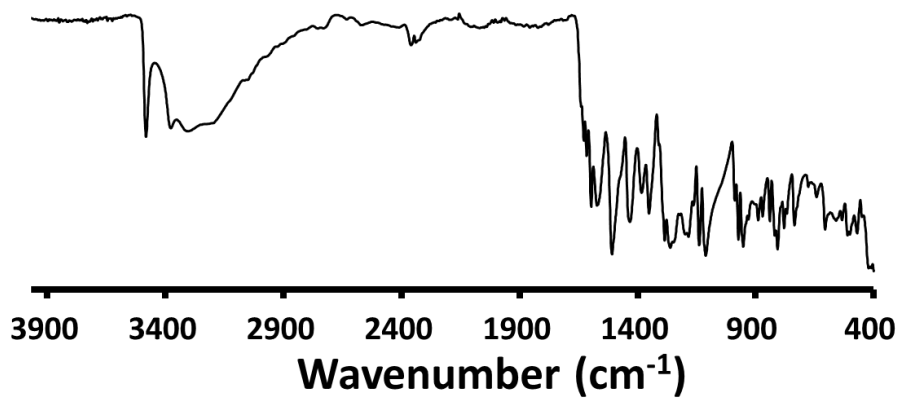


Figure A.19. FTIR-ATR spectrum of BODMC

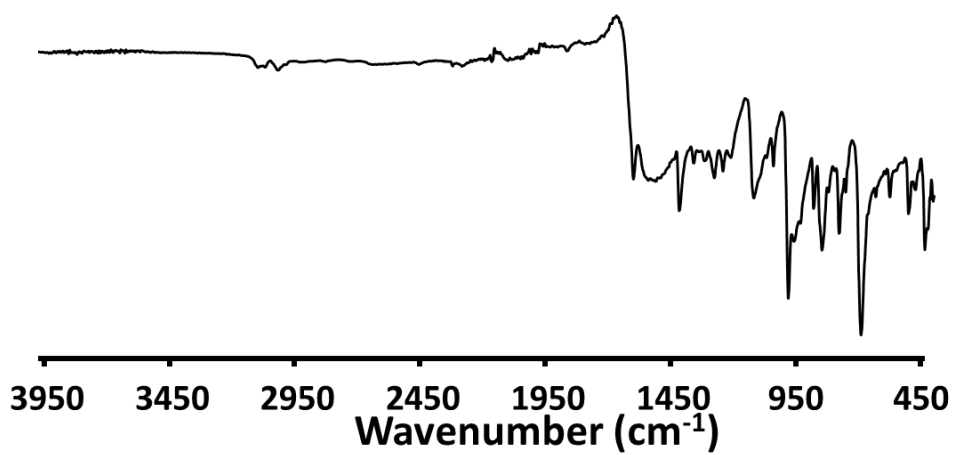


Figure A.20. FTIR-ATR spectrum of 2-thphLCCMoid

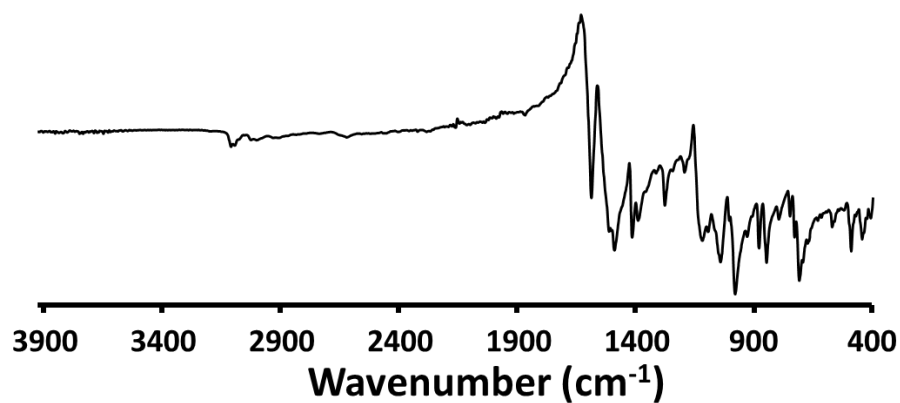


Figure A.21. FTIR-ATR spectrum of 2-thphLCCMoidBF₂

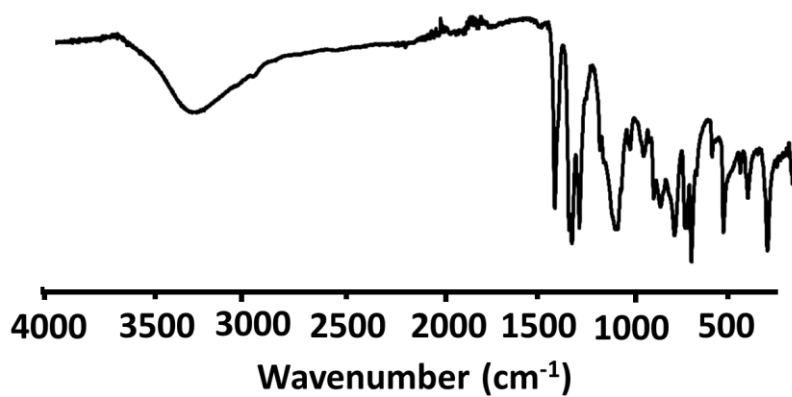


Figure A.22. FTIR-ATR spectrum of BOHCCMoidBF₂

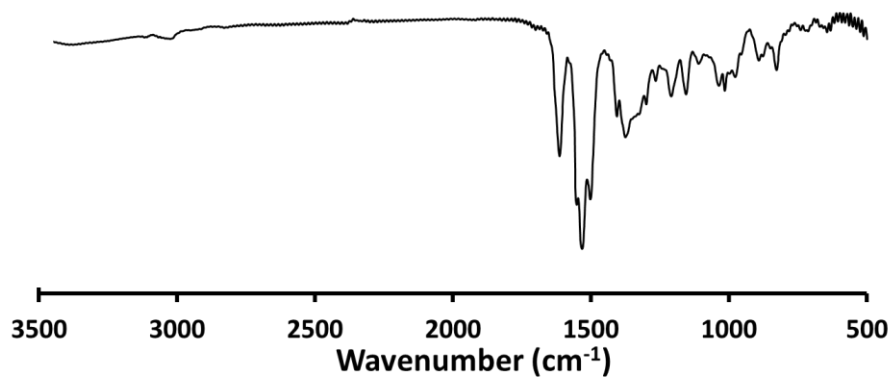


Figure A.23. FTIR-ATR spectrum of BOHCCMoid

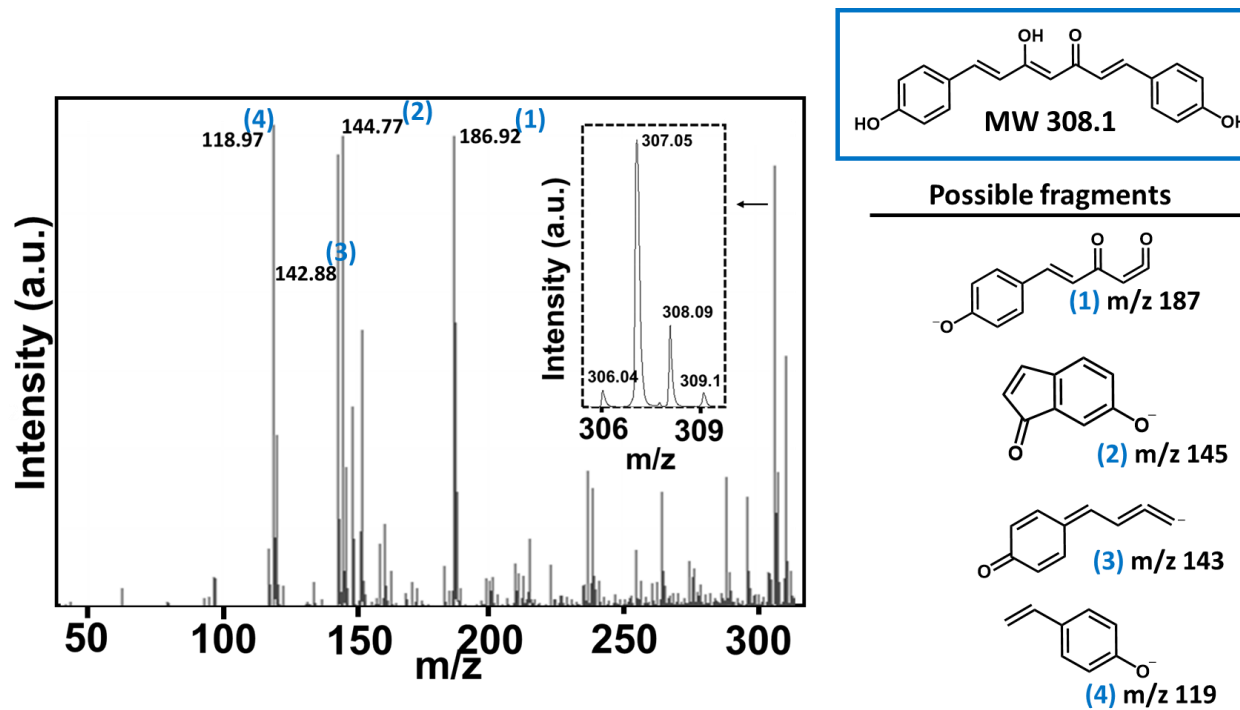


Figure A.24. MALDI-TOF spectrum of BDMC and possible fragments.

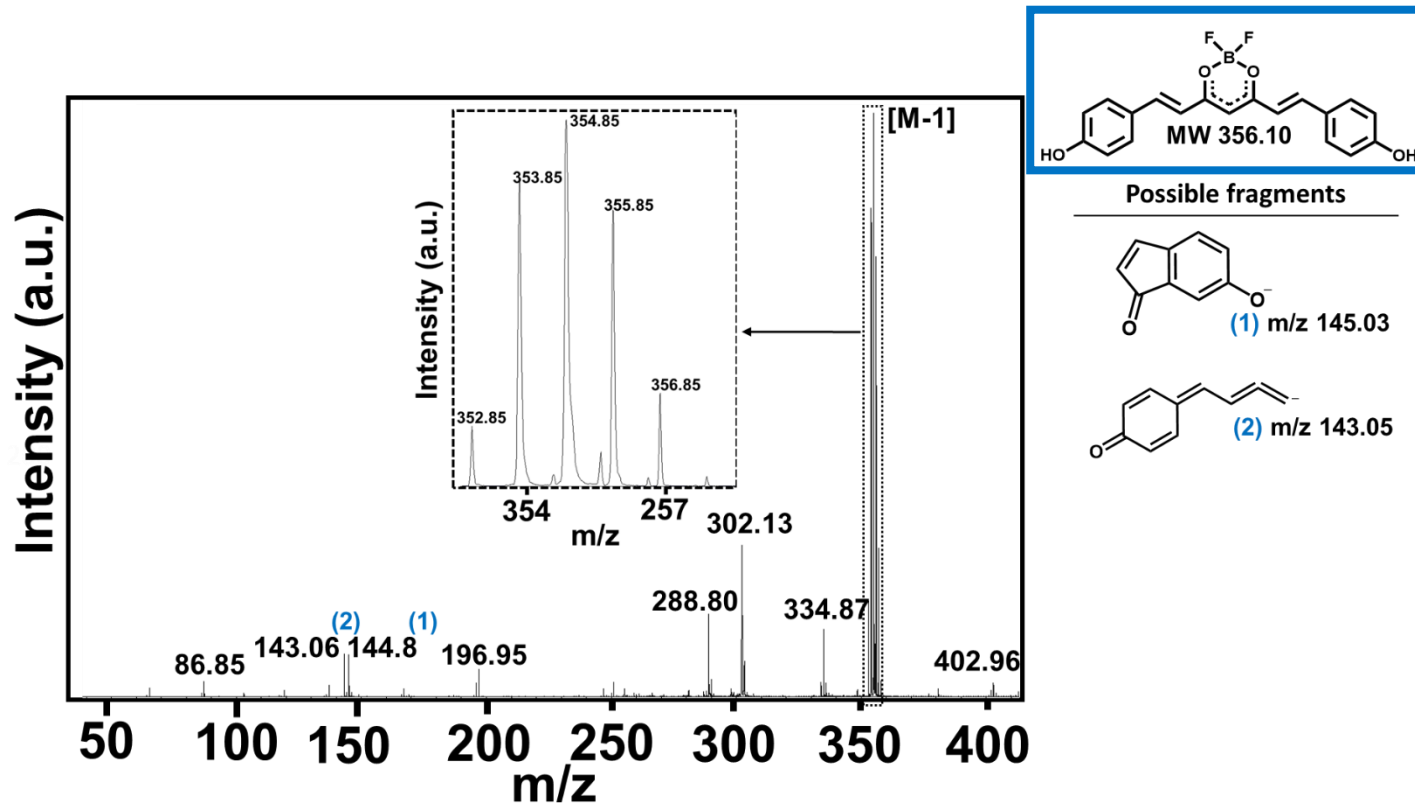


Figure A.25. MALDI-TOF spectrum of BDMCBF₂ and possible fragments.

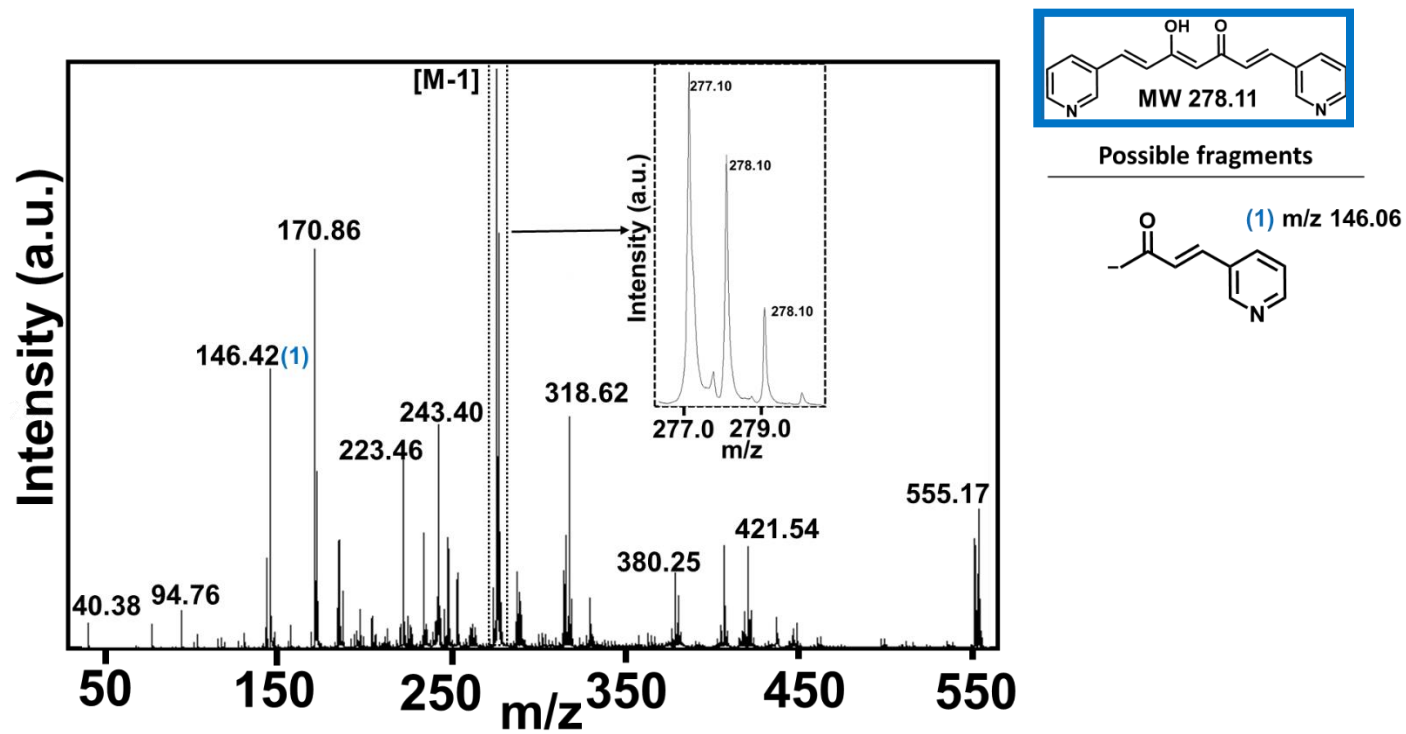


Figure A.27. MALDI-TOF spectrum of 3pyCCMoid and possible fragments.

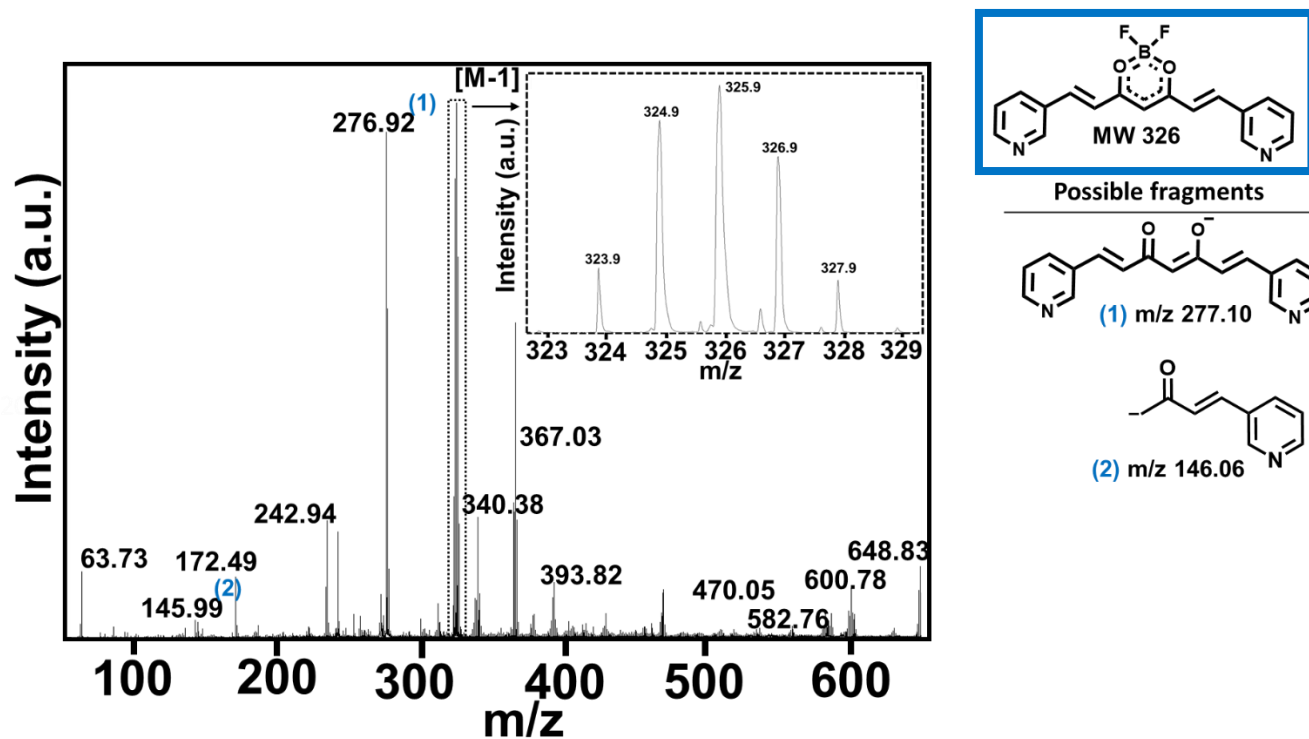


Figure A.28. MALDI-TOF spectrum of 3pyCCMoidBF₂ and possible fragments.

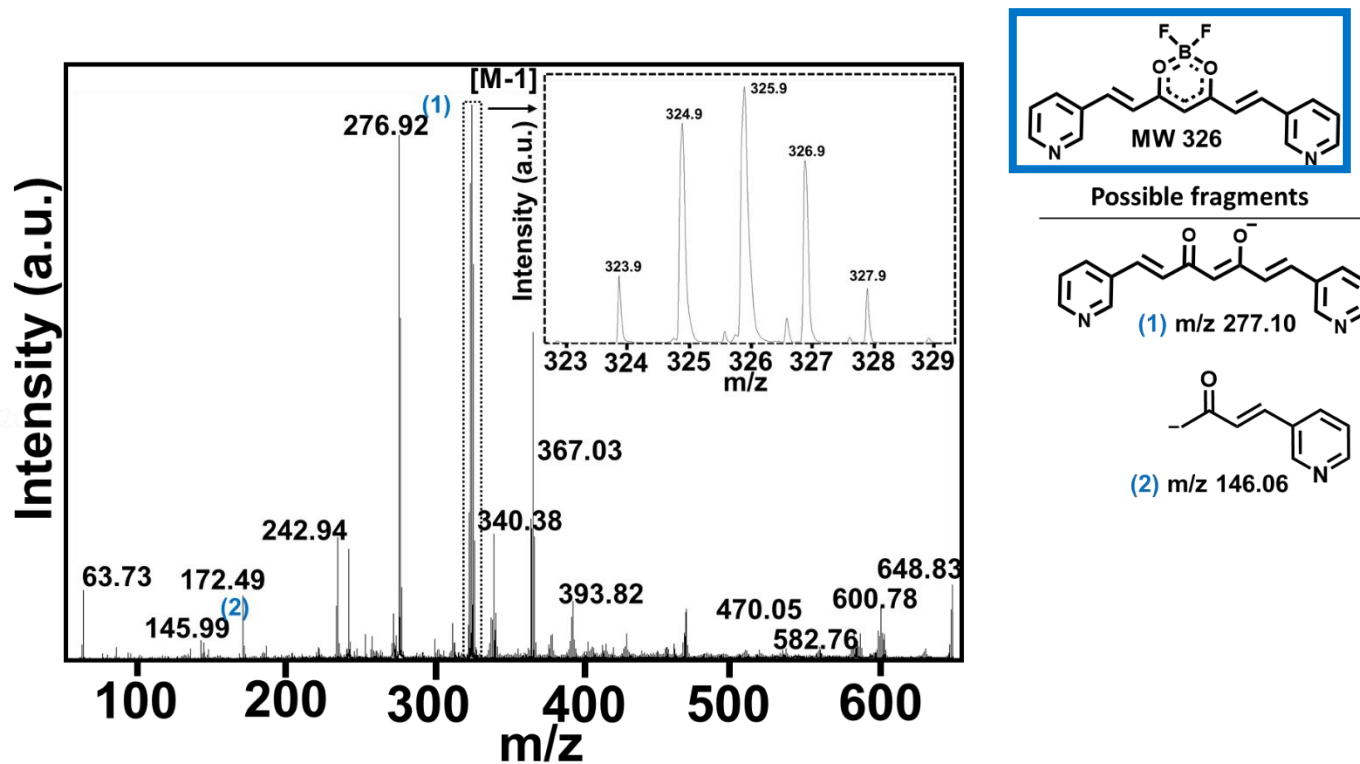


Figure A.29. MALDI-TOF spectrum of 3pyCCMoidBF₂ and possible fragments.

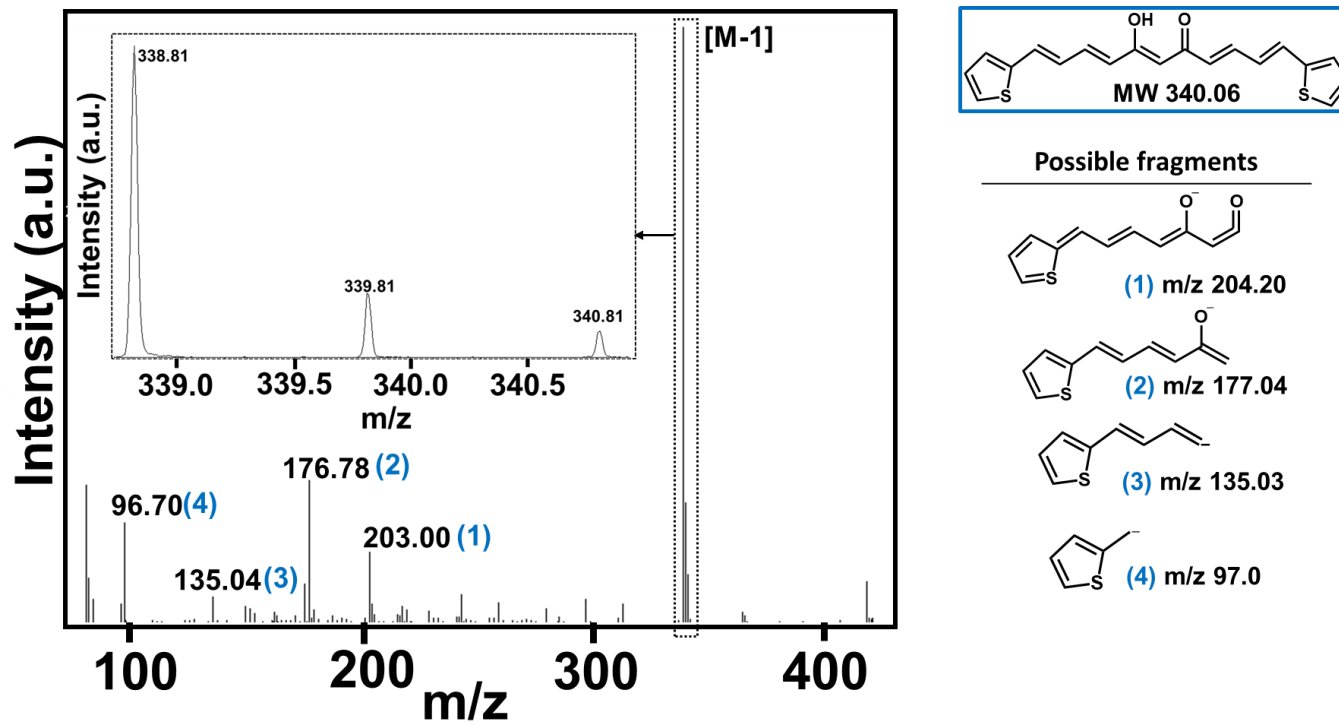


Figure A.30. MALDI-TOF spectrum of 2-thphLCCMoid and possible fragments.

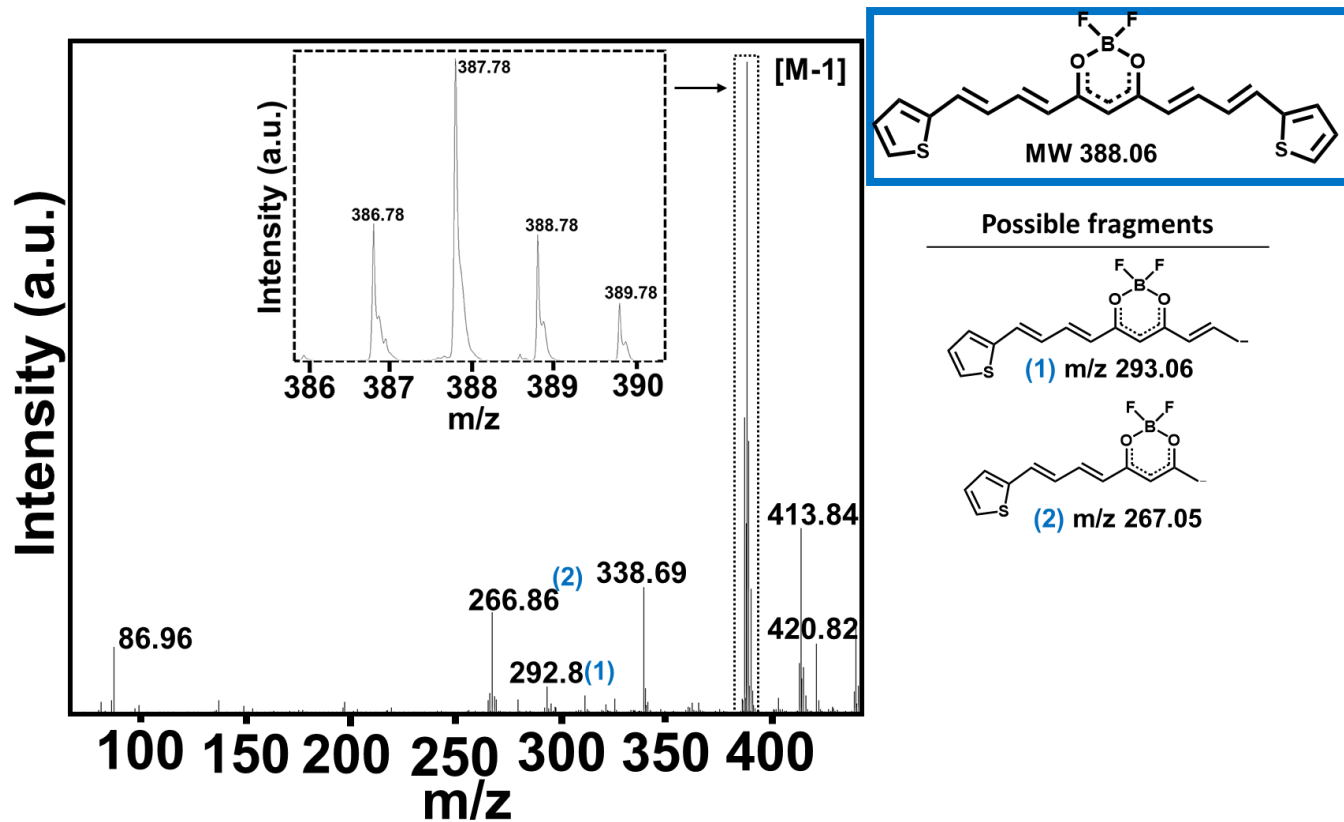


Figure A.31. MALDI-TOF spectrum of 2-thphLCCMoidBF₂ and possible fragments.

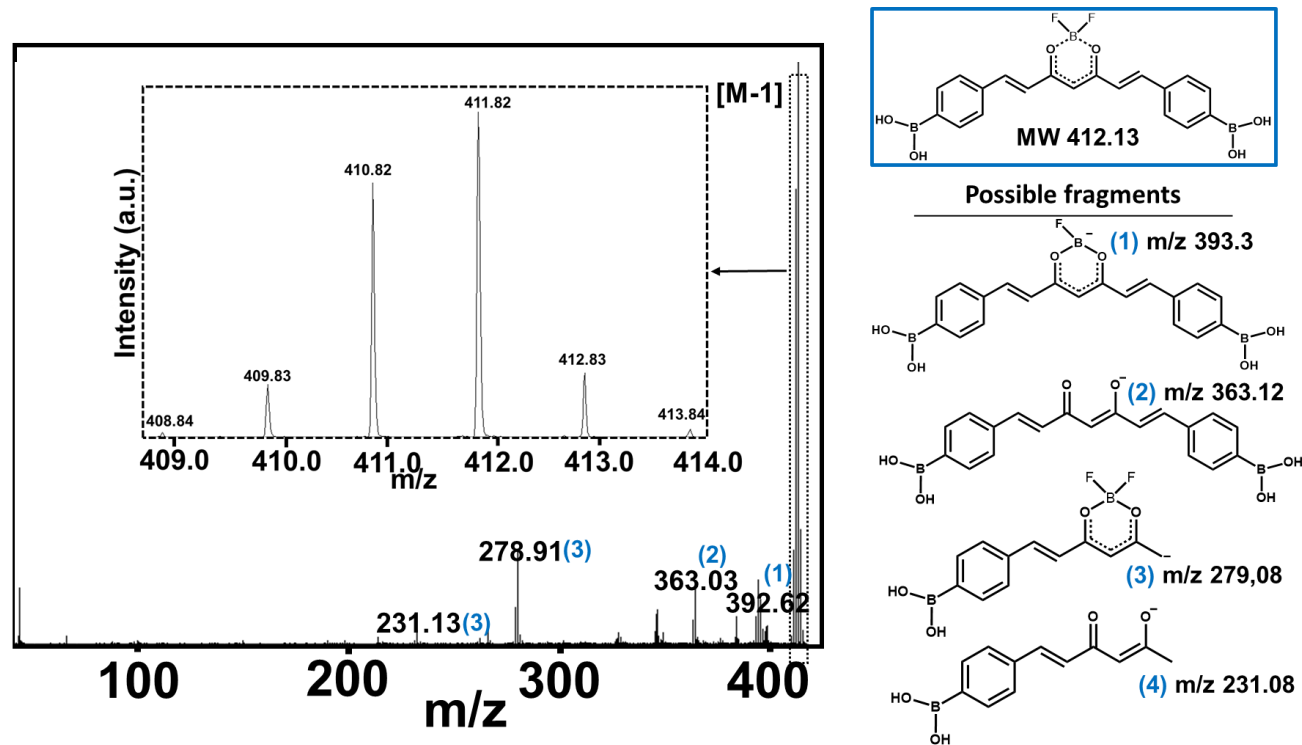


Figure A.34. MALDI-TOF spectrum of BOHCCMBF₂ and possible fragments.

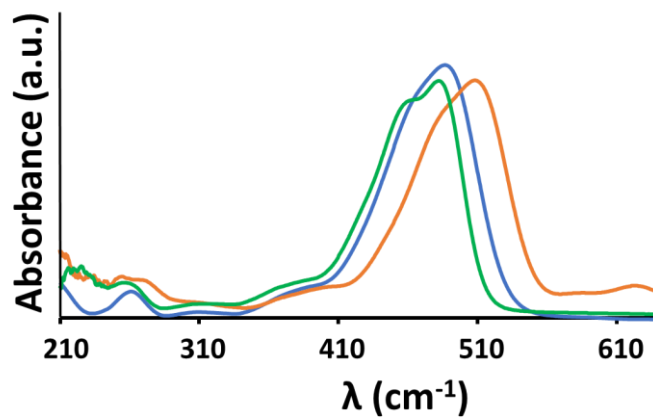


Figure A.35. UV-Vis absorption spectrum of BDMCBF₂ in ethyl acetate (green), methanol (blue) and DMSO (orange).

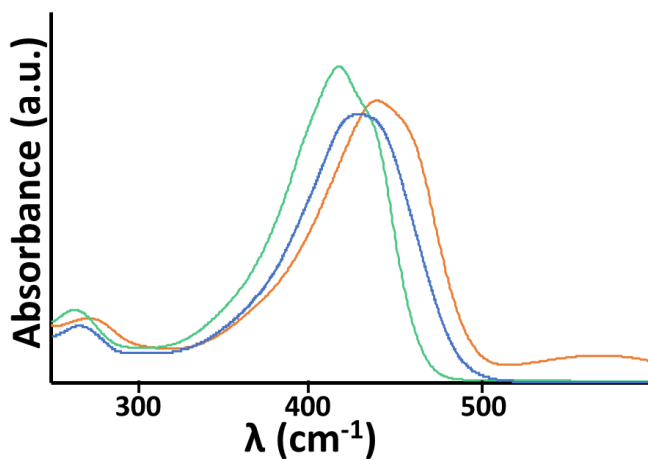


Figure A.36. UV-Vis absorption spectrum of BODMC in ethyl acetate (green), methanol (blue) and DMSO (orange).

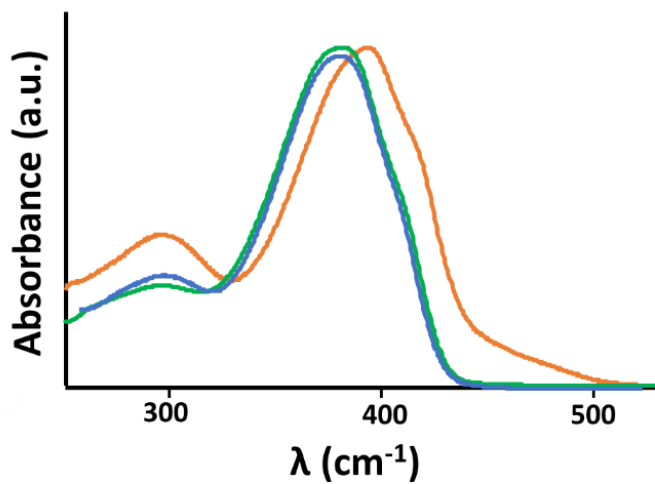


Figure A.37. UV-Vis absorption spectrum of 3pyCCMoid in ethyl acetate (green), methanol (blue) and DMSO (orange).

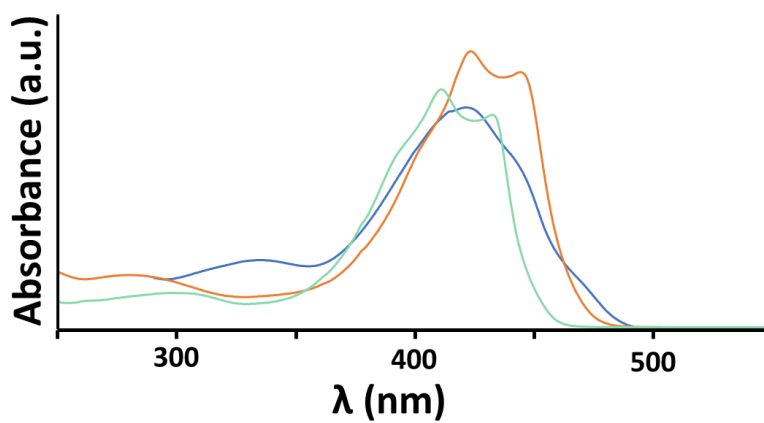


Figure A.38. UV-Vis absorption spectrum of 3pyCCMoidBF₂ in ethyl acetate (green), methanol (blue) and DMSO (orange).

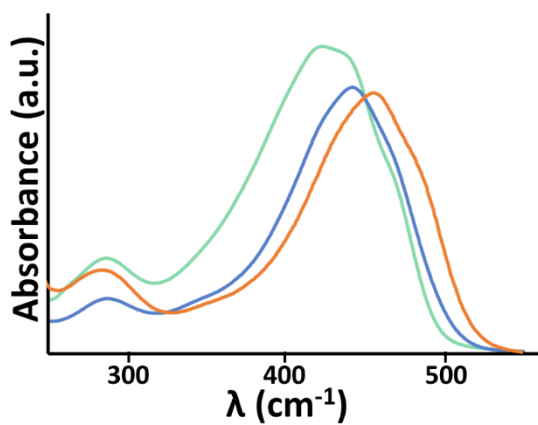


Figure A.39. UV-Vis absorption spectrum of 2-thphLCCMoid in ethyl acetate (green), methanol (blue) and DMSO (orange).

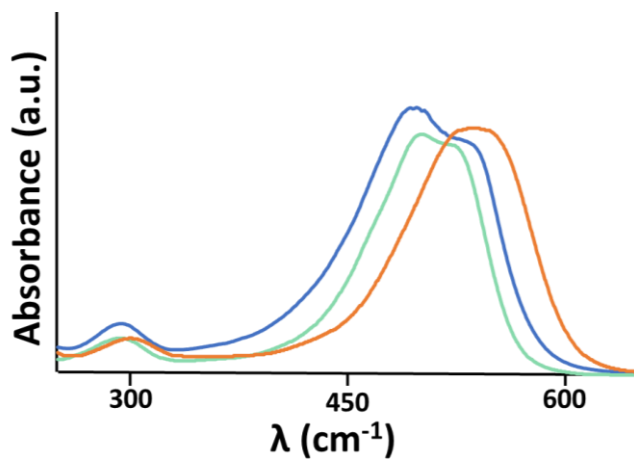


Figure A.40. UV-Vis absorption spectrum of 2-thphLCCMoidBF₂ in ethyl acetate (green), methanol (blue) and DMSO (orange).

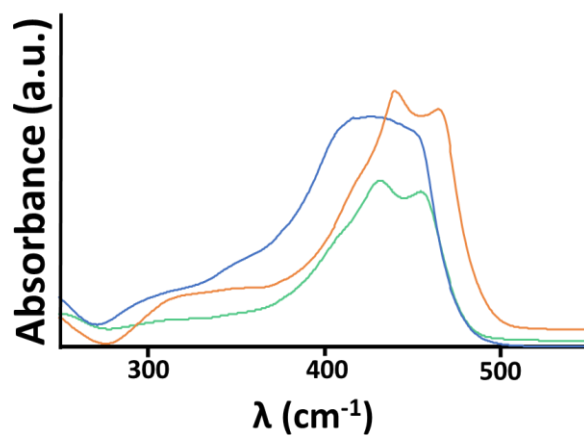


Figure A.41. UV-Vis absorption spectrum of BOHCCMBF₂ in ethyl acetate (green), methanol (blue) and DMSO (orange).

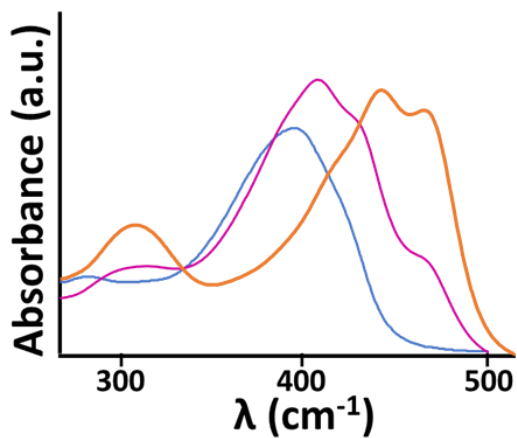


Figure A.42. UV-Vis absorption spectrum of BOHCCM in methanol (blue), chloroform (purple) and DMSO (orange).

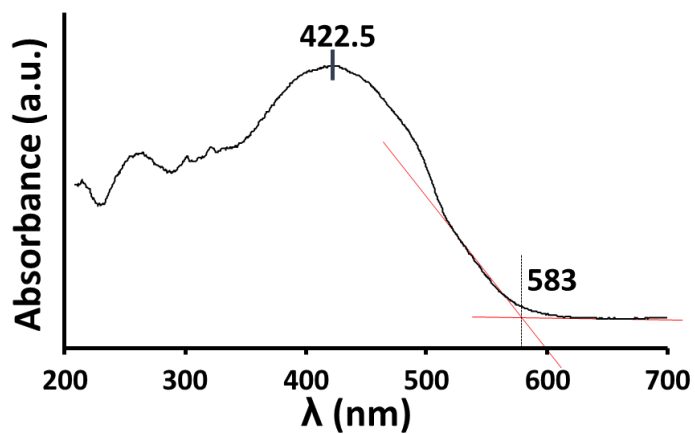


Figure A.43. UV-Vis absorption spectrum of BDMC in solid state.

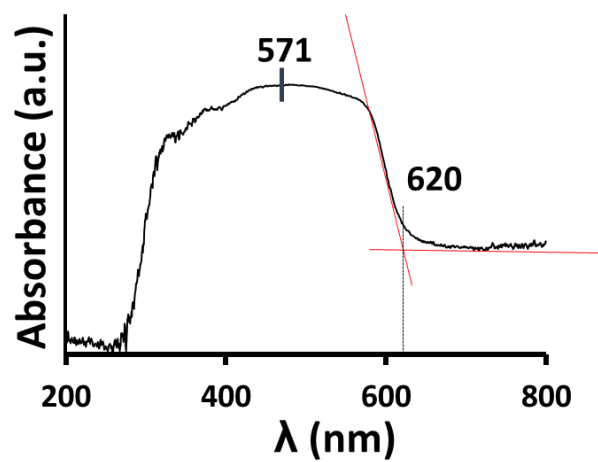


Figure A.44. UV-Vis absorption spectrum of BDMCBF₂ in solid state.

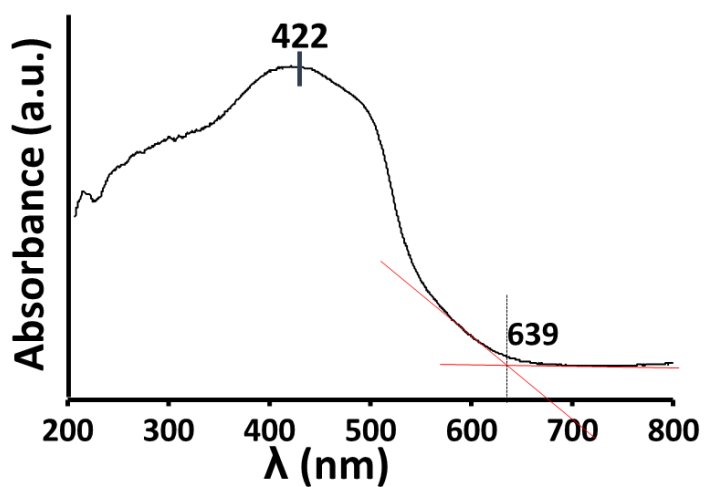


Figure A.45. UV-Vis absorption spectrum of BODMC in solid state

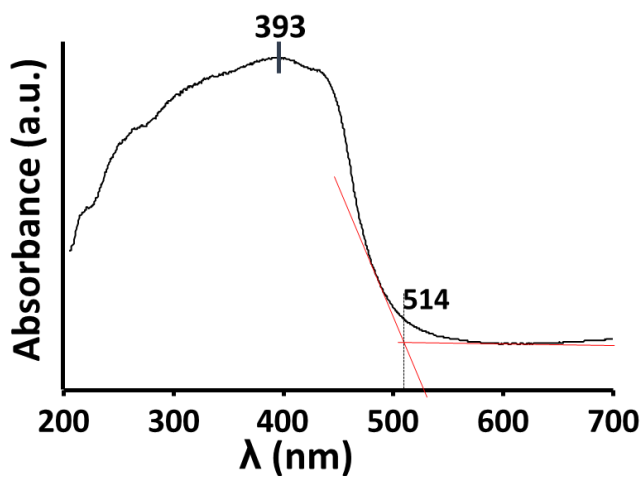


Figure A.46. UV-Vis absorption spectrum of 3pyCCMoid in solid state.

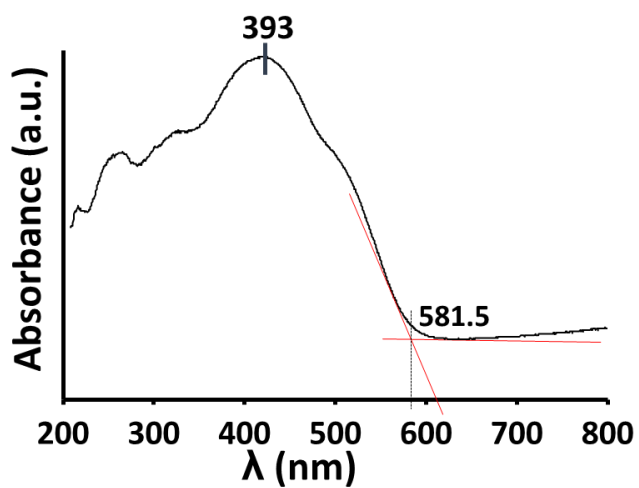


Figure A.47. UV-Vis absorption spectrum of 3pyCCMoidBF₂ in solid state.

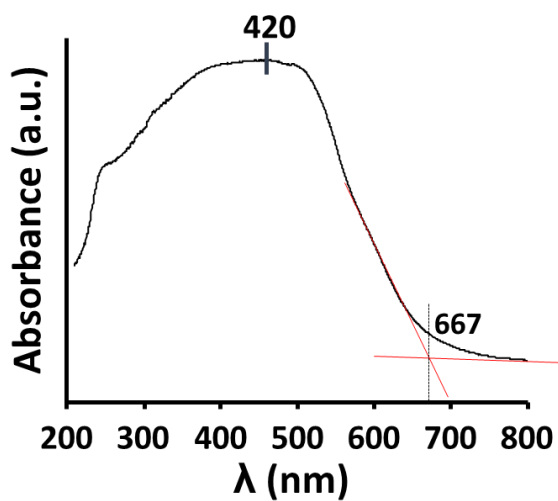


Figure A.48. UV-Vis absorption spectrum of 2-thphLCCMoid in solid state.

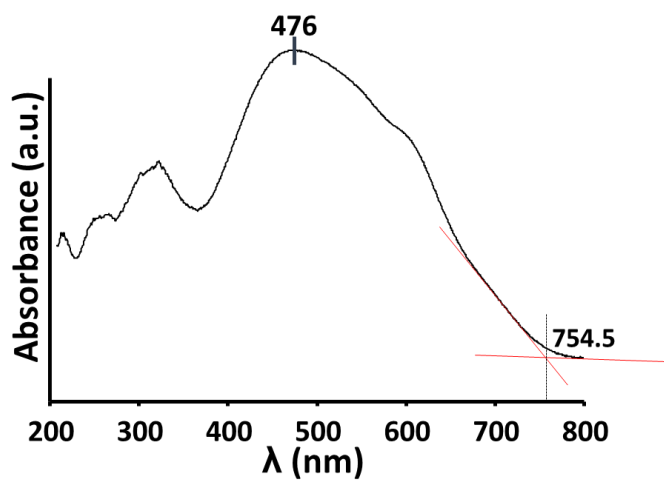


Figure A.49. UV-Vis absorption spectrum of 2-thphLCCMoidBF₂ in solid state.

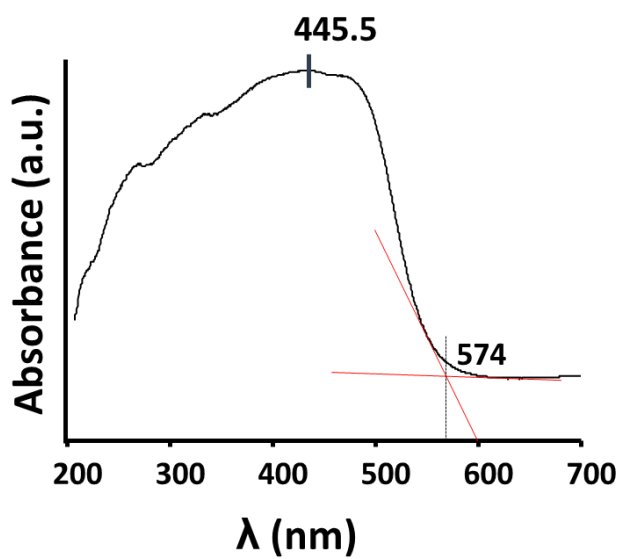


Figure A.50. UV-Vis absorption spectrum of BOHCCMoid in solid state.

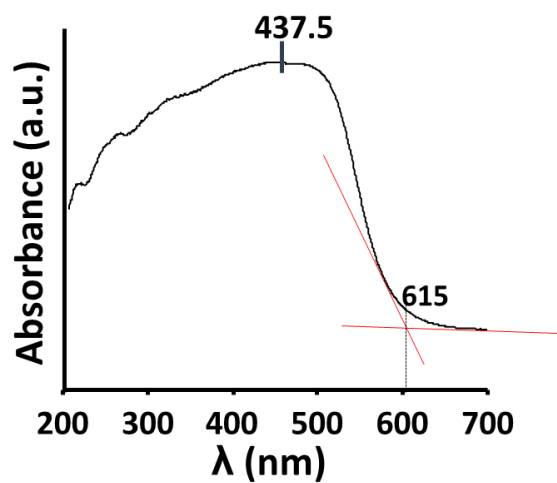


Figure A.51. UV-Vis absorption spectrum of BOHCCMoidBF₂ in solid state.

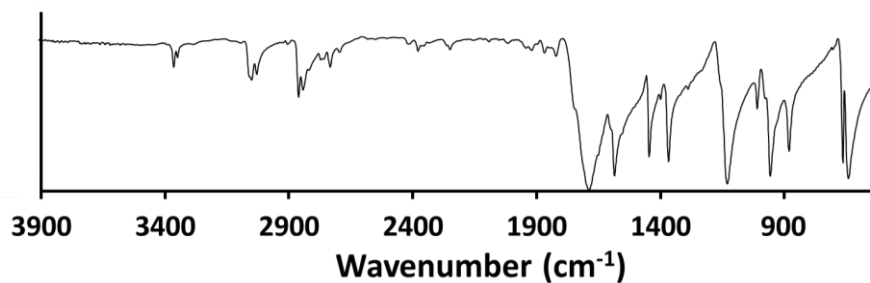


Figure A.52. FTIR spectrum of benzene-1,3,5-tricarbaldehyde.



Appendix II.

Publications

Novel Zn(II) Coordination Polymers Based on the Natural Molecule Bisdemethoxycurcumin

Laura Rodríguez-Cid, E. Carolina Sañudo, Ana M. López-Periago, Arántzazu González-Campo, Núria Aliaga-Alcalde,* and Concepción Domingo*

Cite This: *Cryst. Growth Des.* 2020, 20, 6555–6564

Read Online

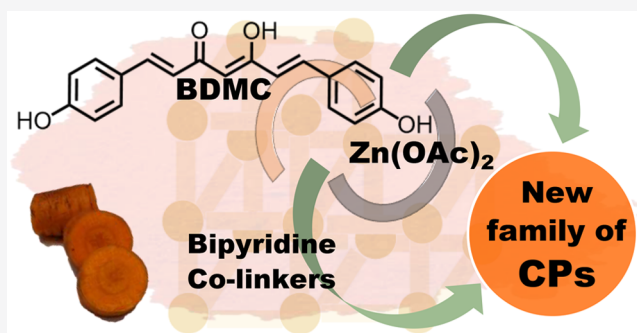
ACCESS |

Metrics & More

Article Recommendations

Supporting Information

ABSTRACT: This article introduces a new family of coordination polymers (CPs) that contains a renewable curcumin derivative, the bisdemethoxycurcumin (BDMC), coordinated to Zn(II) centers. The reaction between BDMC and zinc acetate, performed under mild conditions in ethanol, provides a new 1D phase termed **BDMCZn-1**. In addition, dimensionality and porosity of this network have been expanded by studying the reaction occurring between three species, the BDMC, the Zn(II), and a ditopic colinker: 1,2-bis(4-pyridyl)ethylene, 1,3-bis(4-pyridyl)propane, or 4,4'-bipyridine. In total, seven new CPs are presented, named **BDMCZn-x**. The structures of five of them were elucidated by single-crystal X-ray diffraction. Moreover, we show that the combination of the latest technique with solid-state ^{13}C nuclear magnetic resonance is a powerful tool set to analyze the coordination modes of the BDMC, providing insight into the two unresolved structures. In the achievement of the new CPs, we further discuss the coordination capacity of BDMC, the relevance of solvents, and supramolecular interactions.



INTRODUCTION

According to IUPAC,¹ the chemistry of metal–organic frameworks (MOFs) and coordination polymers (CPs) is in the sixth position of the current list of top emerging technologies, which motivates a large amount of research on this topic. As any newly developed chemistry technology, sustainability criteria must be taken into account from the first stages in the design, regarding both molecular constituent elements and synthetic procedure.² The main ingredients of CPs are the inorganic part, represented by metal ions or clusters, and the organic backbone containing neutral or charged linkers that form different structures in several dimensions. The search for cost-effective and sustainable sources for linkers has led to the study of bio-based natural molecules (vs fossil derived materials) to guarantee element renewability and the attainment of green chemistry. Examples of employed biolinkers for CPs building are peptides, oligopeptides, carbohydrates, amino acids, nucleobases, and porphyrins.^{3–9} In the studied natural linkers, frequent drawbacks are the lack of symmetry factors in the molecule and the presence of considerable flexibility, which make the crystallization of CPs with high dimensionality challenging. In a more extended picture, a pro-active approach to sustainability would involve the consistent addition of new polytopic natural and biorenewable linkers in the creation of 1D–3D polymeric architectures for all kinds of purposes related to energy, gas adsorption, and catalysis.¹⁰ Additionally, the use of biocompat-

ible molecules would option medical purposes, for example, as drug delivery systems or in diagnosis by imaging.^{11,12}

Connected with the above, curcuminoids (CCMoids, Figure 1a) are diarylheptanoid bioderived molecules extracted from the renewable rhizomes of the plant *Curcuma longa*,¹³ although they can also be synthesized using the synthetic methods described by Pabon and others.^{14–16} These species, and particularly curcumin (CCM), the prevalent CCMoid in the turmeric rhizome, have been used since ancient times in food and medicine and as a natural dye.^{17–19} From a structural point of view, natural CCMoids have three potential sites toward metal–ligand coordination, consisting of one β -diketone/enol group and two phenolic rings with different substituents (Figure 1a).²⁰ As polytopic linkers, CCMoids are perfect candidates for the synthesis of CPs, since they retain specific symmetry in the molecule, and possess moderate flexibility. These molecules can exhibit numerous coordination modes with metal ions, giving place to a high structural diversity in the crystallized products. There are many examples of the coordination of CCM and 3d/4f/5d metal centers.²¹

Received: June 1, 2020

Revised: September 10, 2020

Published: September 11, 2020



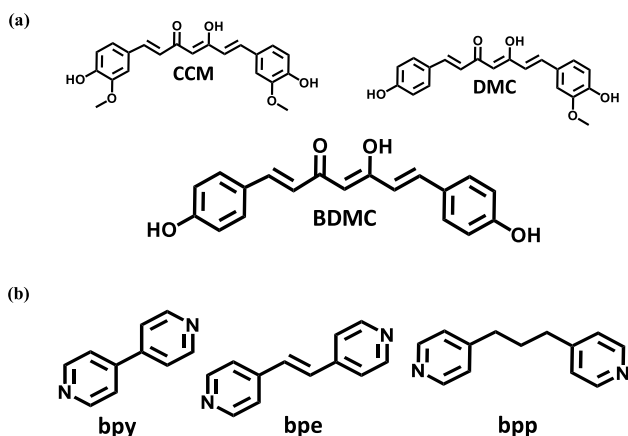


Figure 1. Molecular structures of (a) main CCMoids (CCM = curcumin, DMC = demethoxycurcumin, BDMC = bisdemethoxycurcumin) present in the turmeric root (central image), and (b) dipyrindine colinkers used (bpy = 4,4'-bipyridine, bpe = 1,2-bis(4-pyridyl)ethylene, bpp = 1,3-bis(4-pyridyl)propane).

However, reported reactions regarding the coordination of metals with the rest of CCMoids from the turmeric root, i.e., bisdemethoxycurcumin (BDMC) and demethoxycurcumin (DMC) (Figure 1a), are less common.^{22–25} MOFs and CPs based on CCM^{26,27} have been proposed for drug delivery applications.

Besides the CCM CPs described in the literature by Su et al.²⁶ and us,²⁷ to the best of our knowledge, there are only a few more reported involving transition metals (Co(II) and Ni(II)), also by some of us.²⁸ In this respect, this work presents the first examples of a series of CPs synthesized with a Zn(II) source and the natural CCMoid BDMC. The significant symmetry and conjugated nature of this polytopic renewable biomolecule confer attractive characteristics for CPs synthesis, and to the best of our knowledge, this path remains unexplored. The reaction of BDMC with Zn(II) investigated in this work, performed in EtOH, a green solvent, under solvothermal conditions, resulted in a dense 1D CP (BDMCZn-1). In addition, as a way to increase the dimensionality and porosity of the network, the use of ancillary linkers, chosen from the family of the dipyrindines (1,2-bis(4-pyridyl)ethylene (bpe), 1,3-bis(4-pyridyl)propane (bpp), and 4,4'-bipyridine (bpy)) in Figure 1b), was studied.^{29,30} With this procedure, seven new CPs, with 1D and 3D dimensionalities, were crystallized (BDMCZn1, 2a, 2b, 3, 4a, 4b, and 4c). The structures of five of the newly synthesized compounds could be elucidated by single-crystal X-ray diffraction. Solid-state ¹³C nuclear magnetic resonance (NMR) measurements were performed as a complementary technique to ascertain the different coordination modes of the BDMC molecule within the compounds. This technique is sensitive to small changes in the disposition, environment, and conformation of the analyzed molecules.³¹ The spectral data obtained from the unresolved crystalline materials were correlated to potential crystal topology and composition to outline the structures. This work shows a rich variety of crystallographic structures using a CCMoid aside from CCM, and solid-state ¹³C NMR as a handy characterization tool to discern coordination of such species. Our results aim to show renewable natural CCMoids as powerful polytopic building units toward the creation of future extended structures in CPs,

providing useful characterization tools toward their analysis in the solid state.

■ MATERIALS AND METHODS

Materials. Zn(OAc)₂·2H₂O and the ancillary linkers (bpy, bpe, and bpe) were provided by Sigma-Aldrich. BDMC was synthesized using a modification of Pabon method.¹⁴ EtOH was supplied by Scharlab.

Synthetic Method. Synthesized CPs were obtained using a solvothermal methodology and EtOH as a solvent. Reactions were carried out in 10 mL Pyrex vials with hermetic closures, which were placed in an oven at 80 °C for 3 days. The end products were collected after cooling down the vials to room temperature. Crystals, placed on the walls and at the bottom of the vials, were recovered directly from the mother solution and washed with fresh solvent before drying.

BDMCZn-1. 30.00 mg (0.097 mmol) of BDMC and 21.36 mg (0.097 mmol) of Zn(OAc)₂·2H₂O were mixed in 2 mL of EtOH. The vial was stirred ultrasonically up to the complete solubilization of all reagents to proceed with the solvothermal treatment. Yield 56–60 wt %. ATR-FTIR data (cm⁻¹): 1603 (ν C=C_{aromatic}), 1591 (C=O_{st β -diketone}), 1487 (ν C=C aromatic), 1382 (δ CCH), 1297 and 1234 (C–O_{st β -phenolic}), 1157 (opp CCH_{aromatic} and CCH_{skeletal}), 970 (=CH _{δ} opp). EA (wt %) data for [Zn(BDMC)(EtOH)] or ZnC₂₁H₁₉O₅ (416.74 g·mol⁻¹) calculated C: 60.37, H: 4.89; found C: 60.30, H: 5.16.

BDMCZn-2a and 2b. Both were synthesized as 1 but with an extra reagent added consisting of either 8.86 mg (0.048 mmol) or 17.73 mg (0.097 mmol) of bpe. Yields 52–70 wt %. ATR-FTIR data of BDMCZn-2a (cm⁻¹): 1603 (ν C=C_{aromatic}), 1537 (C=O_{st β -diketone}), 1494 (ν C=C_{aromatic}), 1407, 1240 (C–O_{st β -phenolic}), 1158 (opp CCH_{aromatic} and CCH_{skeletal}), 968 (=CH _{δ} opp). EA (wt %) for [Zn(BDMC)(bpe)(OAc)]_n·2nH₂O or ZnC₃₃H₂₈O₆N₂·2H₂O (649.47 g·mol⁻¹) calculated C: 60.98, H: 4.96, N: 4.31. found C: 61.05, H: 4.76, N: 4.54.

ATR-FTIR data of BDMCZn-2b (cm⁻¹): 1602 (ν C=C_{aromatic}), 1587 (C=O_{st β -diketone}), 1483, 1442 (ν C=N), 1394 (δ CCH), 1298, 1243 (C–O_{st β -phenolic}), 1154 (opp CCH_{aromatic} and CCH_{skeletal}), 981 (=CH _{δ} opp). EA, the best fit of the found data (C: 64.41, H: 4.42, N: 2.91 wt %) was obtained by using a molar ratio for Zn:BDMC:bpe of 1:1:0.5 (C: 64.88, H: 4.14, N: 3.03 wt %), therefore resulting in the formulas [Zn(BDMC)(bpe)_{0.5}]_n or ZnC₂₅H₁₉O₄N (462.79 g·mol⁻¹).

BDMCZn-3. The system was synthesized as -1 but adding either 19.29 mg (0.048 mmol) or 38.58 mg (0.097 mmol) of bpp. Yield 75–80 wt %. ATR-FTIR data (cm⁻¹): 1599 (ν C=C_{aromatic}), 1590 (C=O_{st β -diketone}), 1482 (ν C=C_{aromatic}), 1439 (ν C=N), 1384 (δ CCH), 1262 (C–O_{st β -phenolic}), 1157 (opp CCH_{aromatic} and CCH_{skeletal}), 968 (=CH _{δ} opp). EA (wt %) for [Zn(BDMC)(bpp)_{1/2}]_n/2EtOH or Zn₂C₅₁H₄₂O₈N₂·C₂H₆O (987.68 g·mol⁻¹) calculated C: 64.45, H: 4.9, N: 2.84, found C: 64.03, H: 5.21, N: 2.91.

BDMCZn-4a, 4b, and 4c. The three systems were synthesized as BDMCZn-1 but adding either 15.19 mg (0.048 mmol) or 30.38 mg (0.097 mmol) of bpy. BDMCZn-4c was the only compound obtained in significant quantity, with a yield of 38–54 wt %. ATR-FTIR data (cm⁻¹): 1614 (ν C=C_{ring}), 1590 (C=O_{st β -diketone}), 1483 (ν C=C_{aromatic}), 1382 (δ CCH), 1261 (C–O_{st β -phenolic}), 1155 (opp CCH_{aromatic} and CCH_{skeletal}), 965 (=CH _{δ} opp). EA, the best fit of the data found (C: 58.71, H: 4.07, N: 3.4 wt %) was obtained by using a molar ratio for Zn:BDMC:bpy of 1:1:0.5 (C: 59.33, H: 4.56, N: 2.88 wt %) with 2 H₂O molecules in the structure, therefore resulting in the formulas [Zn(BDMC)(bpy)_{0.5}]_n·2nH₂O or ZnC₂₄H₁₈O₄N·2H₂O (485.8 g·mol).

Characterization. Prepared samples were characterized first by routine powder X-ray diffraction (PXRD) by recording the patterns on a Siemens D-5000 diffractometer with Cu K α radiation. Single-crystal X-ray diffraction (SCXRD) data for BDMCZn-1 were collected on a Bruker APEXII Qazar CCD diffractometer equipped (Grup de Magnetisme i Molècules Funcionals, Universitat de Barcelona) at Mo K α wavelength using ϕ and ω scans at 100 K.

The structures were solved by intrinsic phasing methods (SHELXT)³² and refined on F² (SHELXL). Hydrogen atoms were included on calculated positions, riding on their carrier atoms. Data for the rest of the characterized species (**BDMCZn-2a**, **-3**, **-4a**, **-4b**) were collected at the XALOC beamline³³ at ALBA synchrotron (Spain) K with a 0.72931 Å wavelength using the Dectris Pilatus 6 M detector at 100 K. The ϕ scan was repeated at three different κ angles (0°, 45°, and 90°) and merged afterward to increase the completeness and redundancy when possible. Data were indexed, integrated, and scaled using the XDS software.³⁴ Crystallographic data for all compounds are summarized in Table S1 in the SI, and the corresponding CIF files have been deposited in the Cambridge Crystallographic Data Centre and can be accessed free of charge at <https://www.ccdc.cam.ac.uk/structures/> (CCDC deposition numbers 1991279–1991283).

Sample chemical compositions (C, H, and N) were assessed by elemental analysis (EA, Thermo Carlo Erba Flash 2000). Thermogravimetric analysis (TGA, NETZSCH-STA 449 F1 Jupiter), performed up to 600 °C in air or Ar, was used to determine the thermal stability and composition of some samples. Attenuated total reflectance–Fourier transform infrared (ATR-FTIR) spectra were obtained in a FTIR JASCO 4700LE equipment using the ATR accessory with a resolution of 4 cm⁻¹ and 32 scans. For the measurements, ca. 5 mg of the powdered samples were deposited covering the crystal of the ATR accessory and pressed with the pressure tip. The solid-state ¹³C NMR experiments were performed on a Bruker Avance III at a magnetic field of 9.4 T, equipped with a double channel 4.0 mm MAS probe. Sample spinning was set to 10 kHz. A contact time of 2500 μ s (63 kHz), a recycle delay of 1 s, 27 k scans (overall experimental time 8 h), and a decoupling power of 83.3 kHz were used in all experiments. Pure adamantane was used as external chemical shift reference (CH signal at 29.5 ppm).

RESULTS AND DISCUSSION

The combination of solvothermal conditions and EtOH provides seven new CPs with BDMC as the principal linker and Zn(II) as the metallic node. **BDMCZn-1** could be resolved by SCXRD using a conventional radiation source. Nevertheless, **BDMCZn-2a**, **-3**, **-4a**, and **-4b** compounds precipitated as spherulitic crystals, in which each crystal was composed from small subunits of only a few microns. Consequently, for the SCXRD analysis, a synchrotron source was necessary. Unfortunately, the obtained crystals for **BDMCZn-2b** and **4c** did not present enough quality for SCXRD structural elucidation. Solid-state ¹³C NMR spectral analysis, together with TGA, ATR-FTIR, and EA data, were then used to provide further insight in their structures regarding main formulas, coordination mode, and dimensionality.

Crystal Structures. **BDMCZn-1**, with stoichiometry [Zn(BDMC)(EtOH)]_n, crystallizes in the monoclinic P2₁/c space group. Crystallographic parameters for this structure are detailed in Table S1. In the asymmetric unit, one Zn(II) atom appears tetracoordinated, having the basal plane occupied by the β -diketone of one BDMC linker and one EtOH molecule; meanwhile, in the apical position the metallic center coordinates to the phenolic ring of a neighboring BDMC linker (Figure 2a). The pseudotetrahedral geometry of the Zn(II) is imposed by the coordination with the two oxygen atoms in the β -diketone (angles O–Zn–O between 99° and 120°). Each BDMC is coordinated to two different Zn(II) atoms by the β -diketone and one phenolic ring, while the second phenol remains protonated. As a consequence, the system presents a 1D zigzag chain where successive BDMC molecules form angles of 85.50° (Figure 2b). The chains are held together in a 3D structure by hydrogen bonds established

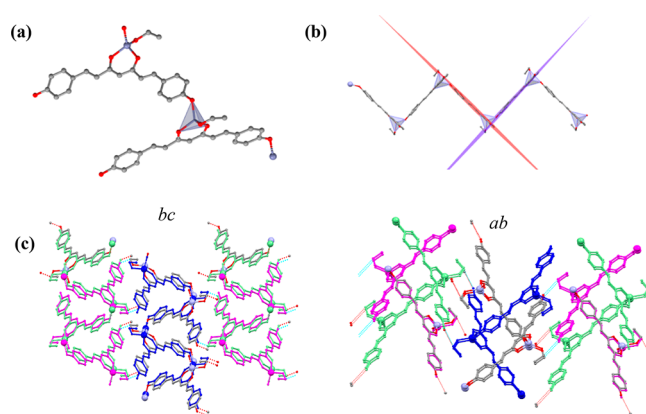


Figure 2. Schematic representation of the crystal structure of compound **BDMCZn-1**: (a) repeating unit showing the coordination mode of Zn(II) and BDMC, (b) zigzag chain in the 1D structure, and (c) extended 3D framework through H-bonding projected in the *a* and *c* directions. Color code: C, gray; O, red; and Zn, blue.

through the coordinated ethanol molecules (Figure 2c). The result is a compact packing with negligible structural porosity. The PXRD pattern obtained for **BDMCZn-1** indicates high purity for the precipitated powder (Figure S1).

BDMCZn-2a presents a [Zn(BDMC)(bpe)(OAc)]_n·2nH₂O stoichiometry. This compound crystallizes in the monoclinic P2₁/c space group (Table S1), as well as **BDMCZn-1**, but its structure involves bpe molecules as colinkers. The asymmetric unit contains a single pentacoordinate Zn(II) atom bonded to the β -diketone of one BDMC, two pyridine N atoms of two additional bpe colinkers, and one oxygen from the acetate ligand. The Zn(II) ion adopts a square-based pyramidal geometry with the β -diketone, the acetate, and one of the bpe colinkers on the basal plane and the second bpe at the apical position (Figure 3a). Overall, the geometry is slightly distorted ($\tau = 0.43$), with angles smaller than 90° in the bonds that implicate the oxygen atoms of the β -diketone (between 85.4° and 88.1°) and larger in the angle between the two N-donor linkers (94.88°). A similar coordination number has been observed in the past in CPs and MOFs, as well as when Zn(II) coordinate to a synthetic CCMoid.^{35–37} In this structure, both

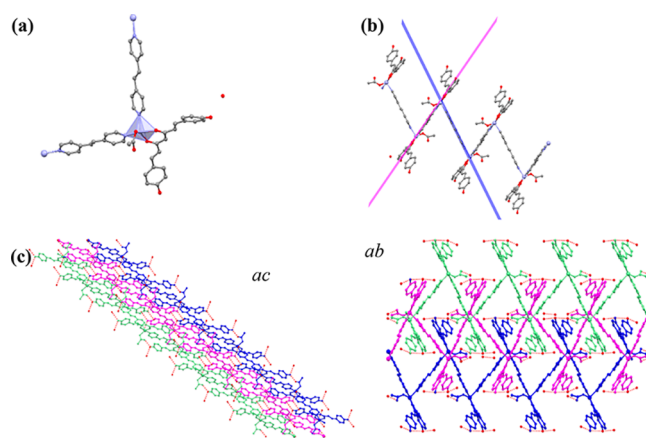


Figure 3. Schematic representation of the crystal structure of compound **BDMCZn-2a**: (a) repeating unit showing the coordination mode of Zn(II) and BDMC, (b) zigzag chain in the 1D structure, and (c) extended 3D framework through H-bonding in the *b* and *c* projections. Color code: C, gray; O, red; N, blue; and Zn, light blue.

phenol groups of the BDMC molecule remain protonated and do not participate in the coordination to the metal, which is exclusively established through the β -diketone. Therefore, a new 1D zigzag array is formed by coordinative bonds established exclusively between the Zn(II) metal centers and the ditopic bpe molecules (with an angle of 64.58° , Figure 3b). In the supramolecular structure, the chains are held together by hydrogen bonds established between the remaining protonated phenol groups in the BDMC molecules and the acetate groups of different chains, with half of those through water bridges (Figure 3c). Again, the result is a dense structure with a negligible porosity (calculated using Mercury). Although the general disposition of Zn(BDMC)(OAc) units attached through the bpe is similar to other CCMoid-CPs published with Co(II) and Ni(II) using bpy,²⁸ the molecular blocks of BDMCZn-2a are unique in the sense that each Zn unit coordinates to BDMC and acetate ligands instead of coordinating only to CCMoid molecules. The comparison between the PXRD of BDMCZn-2a and the pattern calculated from the single crystal structure indicates contamination with a different phase (see peaks at $2\theta = 5.96^\circ$ and 8.62°) (Figure S1). This fact could be related to the low stability of the crystals in the absence of solvent (Figure S2), which produces changes in the structure during the PXRD measurement. Actually, the mixture Zn:BDMC:bpe has a complex crystallization behavior, since the reduction of the molar ratio of bpe (from 1 to 0.5 with respect to Zn(II)) provides the new compound BDMCZn-2b, with a different PXRD pattern (Figure S1) of BDMCZn-2a. Unfortunately, further characterization of the new compound was hampered by the poor quality of the crystals found. Its composition was estimated using EA data and corroborated by solid-state ^{13}C NMR and ATR-FTIR.

BDMCZn-3. This system presents a $[\text{Zn}(\text{BDMC})(\text{bpp})_{0.5}]_n \cdot n/2\text{EtOH}$ stoichiometry and crystallizes in the orthorhombic $P2_1$ space group (Table S1). The repeating unit has a similar composition as BDMCZn-1, but now EtOH groups are replaced with bpp colinkers. As a result, 3D architecture is found in contrast to the 1D observed for BDMCZn-1. The structure of BDMCZn-3 is highly complex, with four crystallographically different Zn(II) atoms, all of them tetracoordinated (Figure 4a), and four independent BDMC units. Each pseudotetrahedral Zn(II) is bonded on the basal plane to the β -diketone of one BDMC linker and to one phenolic ring of a neighbor. The apical position is occupied by the pyridinic moiety of a bpp colinker. Hence, as described in BDMCZn-1, each BDMC is coordinated to two different Zn(II) atoms, through the β -diketone and one phenol ring, while the second phenol group remains protonated. The basic unit is constituted by zigzag $[\text{Zn}(\text{BDMC})]_n$ chains extended in two perpendicular directions with an angle of 86.81° (Figure 4b). These units are attached by the colinker bpp (Figure 4c) that adopts an L-shaped conformation, reducing in a great manner its length. The dense packing of this basic construction leads to interpenetration of the elements within the 3D structure (Figure 4d), giving place to a dense material with null porosity (calculated by Mercury).

BDMCZn-4a, -4b, and -4c. The three compounds display similar stability and precipitate simultaneously from the reagent mixture. Nevertheless, single crystals of BDMCZn-4a and BDMCZn-4b could be resolved by isolating them by hand from the bulk constituted mainly by the unresolved powdered BDMCZn-4c phase. Both compounds (BDMCZn-4a and

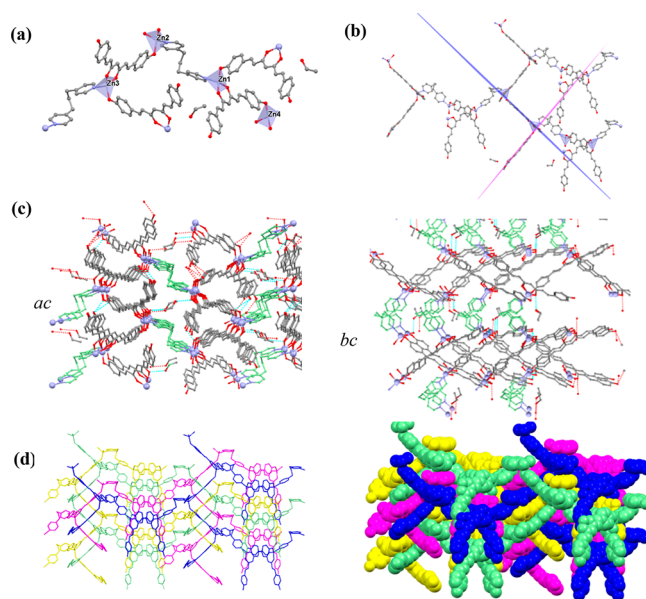


Figure 4. Schematic representation of the crystal structure of compound BDMCZn-3: (a) repeating unit showing the coordination mode of Zn(II) and BDMC, (b) projections of the zigzag basic unit chain, (c) projection of the 3D structures in the b and a directions, and (d) views of the interpenetrated structure, without and with the space filling function in Mercury. Color code: C, gray; O, red; N, blue; and Zn, light blue.

BDMCZn-4b) are rather similar and have alike stoichiometry, with formulae $[\text{Zn}_2(\text{BDMC})_2(\text{bpy})]_n \cdot n\text{H}_2\text{O} \cdot n\text{EtOH}$ and $[\text{Zn}_2(\text{BDMC})_2(\text{bpy})]_n \cdot 2n\text{EtOH}$, respectively, differentiating themselves in the nature and number of adsorbed solvent molecules. Even though these two systems present similarities, they crystallize in different space groups, $C2/c$ and $P2_1/n$ (Table S1), for BDMCZn-4a and BDMCZn-4b, in that order.

Both structures are formed by dinuclear units connected through the ligands. Each dimer displays a Zn_2O_6 core formed by two pentacoordinate crystallographically equivalent Zn(II) atoms (Figure 5a,b)^{37–39} coordinated each to a β -diketone moiety from one BDMC unit and one pyridinic group, from the 4,4'-bpy, in addition to two phenolate groups from neighboring CCMoid molecules that act as the bridging ligands within the dimeric cluster. Therefore, the coordination sphere of the metallic centers in BDMCZn-4a and BDMCZn-4b is the same; however, the geometry of the Zn(II) ions differ between structures. In BDMCZn-4a, each Zn(II) center adopts a square based pyramidal geometry ($\tau = 0.28$) with four oxygen atoms from three different BDMC linkers on the basal plane (depicted in Figure 5a, in which β -diketone is shown in red and phenolate in black) and one N atom from a pyridine moiety in the apical position (Figure 5a displayed in green). In BDMCZn-4a, the angles O–Zn–N are between 96.1° and 108.2° and the angles O–Zn–O are in the range 76.8 – 93.4° . In contrast, the Zn(II) centers in BDMCZn-4b display a bipyramidal trigonal geometry ($\tau = 0.79$) having at the apical positions a phenolate group (Figure 5b, in black) from a CCMoids and a half-coordinated β -diketone moiety from another (Figure 5b, in red). The equatorial positions contain similar fragments and include a pyridinic moiety (Figure 5b, in green). In BDMCZn-4b, the angles are smaller for O–Zn–N (86.8 – 129.3°) and larger for O–Zn–O (79.1 – 98.1°). Again, BDMCZn-4a and BDMCZn-4b present

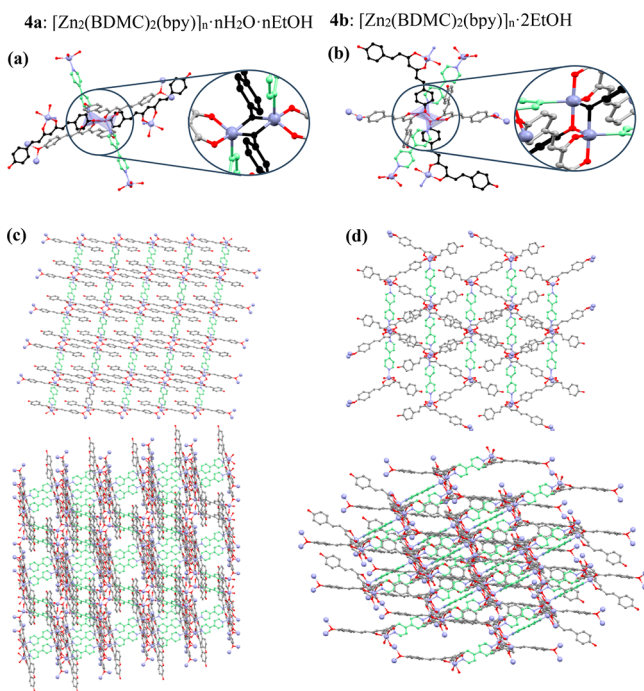


Figure 5. Schematic representation of the crystal structure of compounds **BDMCZn-4a** and **BDMCZn-4b**: (a,b) repeating units showing the coordination modes of Zn(II) and BDMC, and (c,d) two different projections of the 3D structures. Color code: C, gray; O, red; and Zn, light blue; bipyrindine molecules in green and BDMC forming bridges in black.

generally similar trends in the way of expanding and connecting the dimers through the phenolate bridges and the bpy. Both structures display all the BDMC units coordinated through the β -diketone moiety to one Zn(II) ion and one phenolate ring to another center, remaining protonated the second phenolate in the CCMoid unit and giving an overall 3D structure (Figure 5c,d).

Another important difference between these two products resides in the incorporated solvents, H₂O and EtOH in **BDMCZn-4a**, and exclusively EtOH in **BDMCZn-4b**, whose intermolecular interactions add disparity between the two 3D structures (Figure 6a,b). The void space in **BDMCZn-4a** take up 20.2 vol% of the unit cell volume. The porosity is organized in 1D channels extended in the *b* axis. The EtOH/H₂O molecules fill up such porous and are distributed in pairs, relating through an inversion center, having strong hydrogen bonds between one EtOH and one H₂O molecule within the sets (with a O_{H₂O}⋯H—O_{EtOH} distance of 2.630 Å and angle of 164.9°). In addition, each one of these molecules presents several interactions with the surroundings, displaying O _{β -diketone}—O_{H₂O}, C—H_{bpy}⋯O_{H₂O}, and C—H_{CCMoid}⋯O_{EtOH} distances of 2.793, 2.874, and 3.636 Å (showing in the last an angle of 169.64°). This crowded supramolecular network allows the interrelation of separated BDMC linkers through the solvent molecules (Figure S3). For **BDMCZn-4b**, the structural porosity is reduced to 12.6 vol%, constituted by isolated nonconnected pores where the EtOH molecules are placed. The adsorbed EtOH units are disordered, displaying, in the solved structure, the same probability for two opposite positions at the same location. Now, the EtOH is confined in a smaller void, surrounded by pyridinic and CCMoid segments, with not as effective hydrogen bonding as in the former,

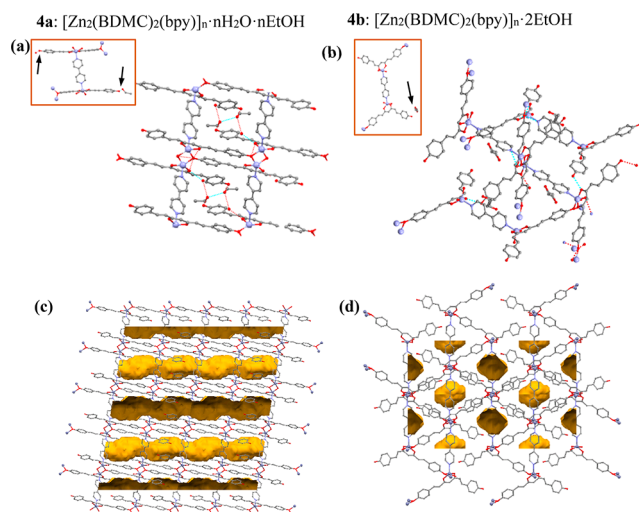


Figure 6. Schematic representation of the crystal and pore structures of compounds **BDMCZn-4a** and **BDMCZn-4b**: (a,b) established H-bonding (arrows indicate the solvent molecules), and (c,d) void maps generated by Mercury showing 1D channels in **BDMCZn-4a** and isolated pores in **BDMCZn-4b**. Color code: C, gray; O, red; N, blue; and Zn, light blue.

presenting short O_{Phenol}⋯H—O_{EtOH} distances (2.941 Å) but small angles; such poor interactions allow the dual disposition of the molecule in the crystal (Figure 6c,d).

In the case of **BDMCZn-4c**, its structure could not be resolved even though it was the major phase obtained in the solvothermal treatment of Zn:BDMC:bpy mixtures. For this compound, knowledge of the composition and formulas was acquired using EA and TGA (SI) data together with solid-state ¹³C NMR studies and ATR-FTIR spectrum.

Solid-State ¹³C NMR. **BDMCZn-1**, **-2a**, **-2b**, **-3**, and **-4c** crystalline phases were further analyzed by solid-state ¹³C NMR. This technique has been successfully used in the characterization of CCM in the solid state,^{38–40} and it is of great assistance in the case of microcrystalline materials, such as MOFs and COFs.^{41,42} Here, the analysis of the free BDMC linker, together with the correlation with the previously elucidated crystal structures by single crystal XRD, was used to provide insight on the unresolved structures (**BDMCZn-2b** and **4c** phases). The solid-state ¹³C NMR spectra of the mentioned species are shown in Figure 7. The assignment of the signals relates by comparison to previous reports on curcumin and solid-state ¹³C NMR studies of the neat BDMC in solution.³⁸

For pristine BDMC, the signal related to the methine carbon (at the center of the CCMoid skeleton, C₁ in Figure 7) at 103.7 ppm, together with the two highly separated β -diketone shifts, C₂ and C_{2'}, at 191.9 and 176.8 ppm, proves the stabilization of the keto–enol form vs the diketone. In addition, the signals of the C₈ and C_{8'} (connected to the hydroxyl groups) appear differentiated, at 160.8 and 157.3 ppm, probably due to effect of the keto–enol form and different surroundings for both endings of the molecule. The rest of the signals, from the diarylheptanoid skeleton and additional aromatic groups, fall in the 115–145 ppm region, where it is feasible to discriminate among them, split in their majority. Taking into account the literature and simulations, they follow a C₇(C_{7'})—C₆(C_{6'})—C₃(C_{3'})—C₅(C_{5'})—C₄(C_{4'})

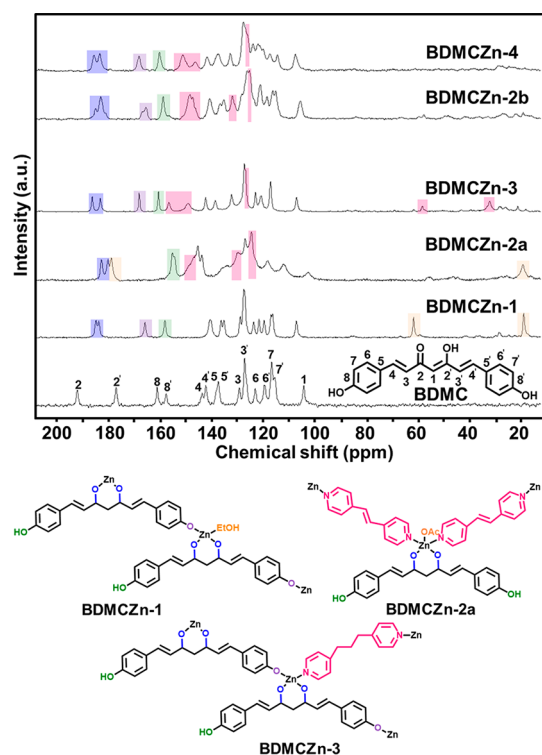


Figure 7. Solid-state ^{13}C NMR of pristine BDMC and compounds **BDMCZn-1**, **BDMCZn-2a**, **BDMCZn-3**, **BDMCZn-2b**, and **BDMCZn-4c**, showing also peak assignments.

order, from highest to lowest field, in the range mentioned above.³⁸

In **BDMCZn-1** and **BDMCZn-3**, the chemical shifts of C_2 and C_2' appear closer now and at lower fields than pristine BDMC (184.6 and 183.5 ppm for **BDMCZn-1** and 186.1 and 182.9 ppm for **BDMCZn-3**, respectively). This alignment is a consequence of the coordination with Zn(II), having C_2 and C_2' similar displacements. For **BDMCZn-2a**, the same thing happens; thus the signals appear at 182.5 and 179.9 ppm, respectively, although here the spectrum displays an additional signal coming from the $\text{C}=\text{O}$ group in the acetate ligand coordinated to the metallic center (at 178.6 ppm, **Figure 7**). In addition, the C_8' chemical displacement for **BDMCZn-1** and **-3** remain similarly to the free BDMC, as this linker also remains free in these structures, while the analogous (C_8) in each system displays shifts to lower fields than BDMC, due to the coordination of this phenol group to a Zn(II) center. If the two phenol groups in the phenyl rings remain free, as it happens in **BDMCZn-2a**, the displacement values of C_8 and C_8' are very similar and closer to those of pristine BDMC.

Additional features, such as the chemical shifts of the coordinated EtOH (18.10 and 60.96 ppm) in **BDMCZn-1**, can also be discriminated, as well as the signals of the coordinated acetate moiety in **BDMCZn-2a** (178.6 and 18.4 ppm). In a similar manner, chemical shifts of the pyridinic colinkers for **BDMCZn-2a** and **BDMCZn-3** appear in the range 120–160 ppm (aromatic groups of bpe and bpy together with the double bond from the bpe system) and 30–60 ppm in the case of the aliphatic groups of **BDMCZn-3**. Their assignment was possible by comparing with the solid-state ^{13}C NMR spectra of the free colinkers, measured in the same conditions as the CPs.

The knowledge acquired on solid-state ^{13}C NMR from the direct comparison of **BDMCZn-1**, **-2a** and **-3**, related to their

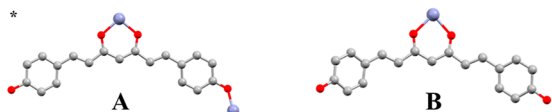
respective crystallographic structures, was used toward the analysis of the spectra of the unresolved systems **BDMCZn-2b** and **-4c**. Unfortunately, the necessity of a substantial amount of sample (ca. 100 mg) limited the use of the technique toward the analysis of the minor phases, such as **BDMCZn-4a** and **-4b**. However, for **BDMCZn-4c**, general trends from the colinkers observed in **BDMCZn-2a** and **BDMCZn-3** (**Table S2**) were applicable for the case of the bpy bridges. In addition, the displacements in the solid-state ^{13}C NMR spectra of **BDMCZn-2b** and **BDMCZn-4c** are similar and point to the coordination of their respective BDMC linkers through the keto/enol moiety and one phenolic ring. In both cases, the displacements of $\text{C}_2-\text{C}_2'$ and $\text{C}_8-\text{C}_8'$ were similar to those found for **BDMCZn-1** and **BDMCZn-3**. Furthermore, both spectra suggest exclusive coordination of the Zn(II) centers with BDMC and bpe or bpy, excluding the possibility of extra coordinated ethanol or acetate molecules. With all of the above taken into account, and the additional characterization data for composition obtained from ATR-IR (**Figure S5b**) and EA, the formation, in **BDMCZn-2b**, of a more extended structure than that found for **BDMCZn-2a** is presumed, due to the double coordination of the BDMC linker and the displacements of the bpe together with the estimated stoichiometry found by EA ($[\text{Zn}(\text{BDMC})(\text{bpe})_{0.5}]_n$). Similarly, for **BDMCZn-4c**, the derived formulas, $[\text{Zn}(\text{BDMC})(\text{bpy})_{0.5}]_n \cdot 2n\text{H}_2\text{O}$, agrees with the TGA analysis that provides similar BDMC weight percentages and shows the existence of solvent within the structure together with coordinated bpy. Hence, the solid-state ^{13}C NMR spectrum also suggests the formation of a structure similar to that found for **BDMCZn-3** (**Figure 7**), which includes the possibility of a different coordination number for the Zn(II) units (e.g., tetra- instead of pentacoordinate) within the structure comparing with **BDMCZn-4a** and **-4b**.

These results are in concordance with the observed in the ATR-FTIR spectra. In the spectra of the CPs, a reduction of the band related with the νOH ($3493-2890\text{ cm}^{-1}$) is observed in comparison with that of the free BDMC, due to the coordination of the β -diketone and one of the phenol groups (**Figure S5a**). This also agrees well with the absence of bands around 1560 cm^{-1} (**Figure S5b**) in the CPs, due to the δCOH in the enol and the hydroxyl groups according with the work of Kolev et al.⁴³ Additionally, the peculiar coordination of **BDMCZn-2a** (which preserves the protonation of the two phenols and coordination of an acetate to the metal center) presents a broad band in the carboxylic region (around 1600 cm^{-1} , **Figure S5b**), related to the acetate, with some of CCMoid nature overlapping with the bands related to the δCOH vibrational mode with a similar intensity as in the pristine CCMoid.

Comparative Analysis and General Trends. Due to the variety of coordination numbers, metal geometries and coordination modes of the ligand BDMC that can be observed in the structures of this work (**Table 1**) and with the novelty in its use as a linker taken into account, a more in-depth analysis of them has been carried out. As mentioned previously, BDMC has three positions for metals to coordinate through the O_2-O_3 in the keto/enol group and through the oxygens O_1 and O_4 in the phenyl rings. However, full BDMC coordination has not been observed in this work (with or without the use of colinkers). Indeed, triple coordination has only been described for CPs based on the pair Zn(II)/CCM precipitated in alcoholic media using solvents with a rather basic nature, such as dimethylacetamide (DMA) or dimethylformamide

Table 1. Metal Coordination, Metal Geometry, and Coordination Mode of the BDMC in the CPs

CP	Zn(II) coordination	Zn(II) adopted geometry	BDMC coordination mode*
BDMCZn-1	Tetracoordinate	Pseudo-tetrahedral	A
BDMCZn-2a	Pentacoordinate	Square-based pyramidal	B
BDMCZn-3	Tetracoordinate	Pseudo-tetrahedral	A
BDMCZn-4a	Pentacoordinate	Square-based pyramidal	A
BDMCZn-4b	Pentacoordinate	Bipyramide trigonal	A

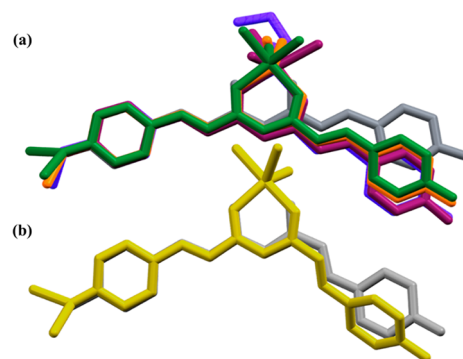


(DMF).⁴⁴ Our first trials indicated that the pair Zn(II)/BDMC was not crystallized in any of these basic solvents.

Remarkably, coordination reactions worked well by using exclusively EtOH, and proof of that is the formation of **BDMCZn-1**. However, in EtOH the number of coordinated sites for the BDMC molecule never reached its maximum, displaying one binding position in **BDMCZn-2a** and two in **BDMCZn-1**, -3, and the -4 series, independently of the use of additional colinkers in the reactions. As expected, in all cases, the most reactive group is the central keto/enol moiety which always appears coordinated.

The obtained structures can be categorized using two features: (i) the absence or use of a dipyrindinic colinker (considering its length and flexibility), and (ii) the adsorbed/coordinated solvent molecules. Both factors affect significantly the coordination and conformation adopted by the main linker, BDMC. The analysis of the results indicates that, as expected, the addition of a dipyrindine based colinker increased the dimensionality of the system with respect to **BDMCZn-1**, going from 1D to 3D. Only for **BDMCZn-2a** a 1D network was obtained, which seems to be favored by the inclusion of the large bpe molecule (distance N₁–N₂ of 9.37 Å) with a limited degree of flexibility. This colinker confers to the Zn(II) metal centers the possibility of being located far away (distance Zn–Zn of 13.49 Å), thus restricting potential interactions between BDMC molecules and Zn(II) atoms, hindering in this way the coordination of the ligand through more than one site. Certainly, in **BDMCZn-2a**, the BDMC did not act as a linker extending the network of the CP, but rather it is essentially a ligand that completes the coordination of Zn(II) center. **BDMCZn-3** and the **BDMCZn-4** series, involving bpp (with an L-shape due to its flexible aliphatic skeleton) and bpy, respectively, had shorter N₁–N₂ distances than **BDMCZn-2a** (6.87 and 7.06 Å, respectively). The length of these colinkers is short enough to allow the BDMC molecules to coordinate through two points (the keto/enol moiety and one phenolate group) to two neighboring Zn(II) atoms. These CPs are extended simultaneously by means of the BDMC and dipyrindinic colinker, resulting in 3D structures with variable complexity.

For the analysis of the crystal structures based on the BDMC linker, the different disposition of the phenolic rings promoted by the conformations should be considered to have originated within the CCMoids skeleton (Figure 8). For that, it is

**Figure 8.** Superimposition of the BDMC moieties in the asymmetric units of the different precipitated compounds, compared to pristine BDMC conformations: (a) BDMC·H₂O (gray), **BDMCZn-1** (blue), **BDMCZn-2a** (purple), **BDMCZn-3** (orange), **BDMCZn-4a** (green), and (b) BDMC (gray), **BDMCZn-4b** (yellow).

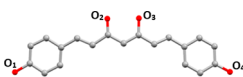
worthwhile to pay attention to the networks described for the pristine and solvated BDMC ligand.⁴⁵ Free BDMC prefers to crystallize together with solvent molecules to lower the crystal free energy, in which the solvent species fill voids and bind efficiently the host molecules providing an extended network with multipoint hydrogen bonding. Typically, adsorbed protic solvents are involved in the formation of the network by acting as bridges between consecutive BDMC units. Therefore, BDMC molecules appear separate enough to adopt a nontensioned near-flat equilibrium conformation. Previous works had shown that the asymmetric units of BDMC·H₂O and BDMC·MeOH are composed of one molecule of BDMC with O₁–O₄ distances of 17.79 and 17.73 Å, respectively.^{46,47}

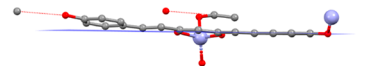

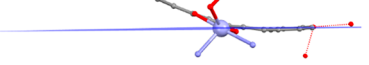
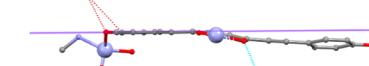

On the contrary, nonsolvated BDMC structures develop a compact packing in which the molecules present strong and direct interactions among them. To achieve this, the BDMC adopts highly distorted conformations presenting curvy forms or segmented molecular backbones not fully extended, presenting in both cases shorter O₁–O₄ phenolate distances between 16.41 and 17.06 Å.⁴⁶

Similarly, the different BDMC conformations found in our CPs can be classified by analyzing the established short interactions and hydrogen bonding created with the solvent or even additional molecules. These interactions affect the overall BDMC architecture, with one side of the molecule remaining planar (typically the one containing the phenolic ring coordinated to the metal), with this being fully extended and defining here the reference plane P1 (which includes C₃ to C₈, Figure 7). The other side of the CCMoid molecule defines the plane P2 (from C_{3'} to C_{8'}, Figure 7), which displays a high degree of possible conformations based on nonextended versions of the CCMoid skeleton adopted to promote improvements in the packing. Significant atomic distances between O₁–O₄ for the coordinated BDMC linkers and P1–P2 angles are shown in Table 2 for each resolved CP.

In **BDMCZn-1**, the CCMoid linker has a quasi-flat conformation with a P1–P2 angle of 10.32° and one of the O₁–O₄ highest lengths (17.32 Å). Here, the BDMC molecules interact through the coordinated EtOH molecule. The context for **BDMCZn-2a** is quite different, since the BDMC coordinates the Zn(II) center through the keto/enol moiety and the network is exclusively extended by the bpe colinker. Hence, the colinker establishes the 3D structure, allowing extra structural degrees of freedom for the BDMC ligand. Therefore,

Table 2. BDMC distances O_1-O_4 and angles P1–P2 in the different compounds. The schematic draw shows the linker conformation in each compound. Color code: C grey, O red N blue and Zn light blue



	O_1-O_4 [Å]	P1–P2 [°]	Schematic draw
1	17.32	10.32	
2a	16.57	38.26	
3	17.05– 17.30	8.76– 11.19	
4a	15.98	17.75	
4b	15.98	44.10	

the latest remains interacting with the surrounding and creates hydrogen bonding through both phenol groups that finally restrain the ligand. As a result, the BDMC displayed a curved geometry with a marked P1–P2 angle of 38.26° , which bring together the O_1-O_4 atoms to a distance of 16.57 \AA . On the other hand, compound **BDMCZn-3** has an elaborated 3D structure with four independent BDMC molecules that interact through bridges of EtOH and H_2O molecules. The result is a low-distortion and almost flat conformation for all the BDMC molecules, with O_1-O_4 distances of $17.05-17.30 \text{ \AA}$ and P1–P2 angles of $8.76-11.9^\circ$. Finally, the **BDMCZn-4** series, involving the bpy colinker, exhibits the strongest influence of the adsorbed solvent in the resulting structure. Note that **BDMCZn-4a** and **BDMCZn-4b** had the same network stoichiometry, $[Zn_2(BDMC)_2(bpy)]_n$, differing in the composition only in the adsorbed solvent molecules (H_2O or EtOH). In **BDMCZn-4a**, strong hydrogen bonds are established through H_2O and EtOH bridges, and here the BDMC adopts a near-planar geometry with a O_1-O_4 distance of 17.42 \AA and a P1–P2 angle of 17.75° . In a totally different scenario, the adsorbed EtOH molecules in **BDMCZn-4b** interact weakly with the crystal network. The lack of interaction of the BDMC linkers through solvent bridges results in a highly tensioned molecule with a distorted conformation. As a result, the O_1-O_4 distance is 15.98 \AA and the P1–P2 angle is 44.10° . Again, the main reason for such a large stretching is the approximation between BDMC molecules to allow short interactions that stabilize the structure with the corresponding

higher distortion of the CCMoid skeleton (through the site that remains uncoordinated).

In **Figure 8**, the structures of the **BDMCZn-1/4b** systems are compared with the conformation of pristine BDMC in either solvated crystal either involving H_2O or unsolvated. Superimposition of the BDMC molecules in the asymmetric unit of each solved structure in this work shows the flexibility of the CCMoid molecule that adopt different conformations. The BDMC disposition in **BDMCZn-1**, **-2**, **-3**, and **-4b** is similar to that found in solvated BDMC (**Figure 8a**), while **BDMCZn-4c** has a conformation similar to unsolvated BDMC (**Figure 8b**).

CONCLUSIONS

The reaction between BDMC and $Zn(OAc)_2$ in EtOH produced the 1D compound $[Zn(BDMC)(EtOH)]_n$ (**BDMCZn-1**). BDMC, Zn(II), and the secondary linker bpe formed either a 1D compound with stoichiometry $[Zn(BDMC)(bpe)(OAc)]_n \cdot nH_2O$ (**BDMCZn-2a**) or an unresolved phase with an estimated $[Zn(BDMC)(bpe)_{0.5}]_n$ formula (**BDMCZn-2b**). On the contrary, the use of either bpp or bpy colinker induced the crystallization of 3D structures with formula $[Zn(BDMC)(bpp)_{0.5}]_n \cdot n/2EtOH$ (**BDMCZn-3**) and $[Zn(BDMC)(bpy)_{0.5}]_n \cdot nSolv$ (Solv = H_2O and EtOH in **BDMCZn-4a**, EtOH in **-4b** and $2H_2O$ in the estimation of **-4c**). The BDMC in these structures is coordinated to Zn(II) by the β -diketone and one phenolic ring (**BDMCZn-1**, **-2b**, **-3**, **-4a**, **-4b**, and **-4c**) or only through the β -diketone (**BDMCZn-2a**). Five of these structures could be structurally elucidated by SCXRD. For unresolved compounds, the main findings obtained by compiling the characterization results achieved by XRD, EA, TGA, ATR-FTIR, and solid-state ^{13}C NMR are (i) **BDMCZn-2b** incorporates only half of the bpe colinker present in **BDMCZn-2a**, with $[Zn(BDMC)(bpe)_{0.5}]_n$ as a feasible formula; (ii) **BDMCZn-4a** and **-4b** have similar stoichiometry $[Zn(BDMC)(bpy)_{0.5}]_n$, but differ in the coordination geometry of Zn(II) driven by different adsorbed H_2O /EtOH molecules; and (iii) **BDMCZn-4c** shows lots of similarities with the corresponding minor phases **BDMCZn-4a** and **-4b**, but also shares features with **BDMCZn-3**. The high mobility present in the arms of the BDMC molecule creates a myriad of possible conformations, giving place to the new family of CPs presented here. The existence of hydrogen bonding stabilizes near-equilibrium conformations, while the absence of these bridges forces the molecule to adopt curved/shrunk conformations. In all cases, the presence of free phenol groups in the structures opens the possibility of post-synthetic reactions that can modify the properties of these CPs. This factor becomes especially important in a compound like **BDMCZn-4a**, in which these phenol groups may be easily accessible, resulting in new potential applications for CPs involving renewable linkers, including biomedical uses that would be examined in a future work. Finally, we would like to remark that our results emphasize the use of mild conditions and green solvent in the synthetic methodology; it shows the unanticipated coordination of the BDMC under such conditions and the assistance of ss ^{13}C NMR toward the analysis of the new CPs. Altogether, this work highlights the potential of BDMC as a polytopic linker and allows a comprehensive understanding of its capabilities for further uses.

■ ASSOCIATED CONTENT

Supporting Information

The Supporting Information is available free of charge at <https://pubs.acs.org/doi/10.1021/acs.cgd.0c00742>.

Additional figures of the structures and crystals, powder X-ray diffraction, thermal characterization, ATR-FTIR spectrum, values of the solid-state ^{13}C NMR, and crystallographic details (PDF)

Accession Codes

CCDC 1991279–1991283 contain the supplementary crystallographic data for this paper. These data can be obtained free of charge via www.ccdc.cam.ac.uk/data_request/cif, or by emailing data_request@ccdc.cam.ac.uk, or by contacting The Cambridge Crystallographic Data Centre, 12 Union Road, Cambridge CB2 1EZ, UK; fax: +44 1223 336033.

■ AUTHOR INFORMATION

Corresponding Authors

Concepción Domingo – Instituto de Ciencia de Materiales de Barcelona (ICMAB-CSIC), Bellaterra 08193, Spain;

orcid.org/0000-0002-6976-8283; Email: conchi@icmab.es

Núria Aliaga-Alcalde – Instituto de Ciencia de Materiales de Barcelona (ICMAB-CSIC), Bellaterra 08193, Spain; ICREA, Institutió Catalana de Recerca i Estudis Avançats, 08010 Barcelona, Spain; orcid.org/0000-0003-1080-3862;

Email: naliaga@icmab.es, nuria.aliaga@icrea.cat

Authors

Laura Rodríguez-Cid – Instituto de Ciencia de Materiales de Barcelona (ICMAB-CSIC), Bellaterra 08193, Spain;

orcid.org/0000-0002-4978-0701

E. Carolina Sañudo – Departament de Química Inorgànica i Orgànica and Institut de Nanociència i Nanotecnologia, Universitat de Barcelona, 08028 Barcelona, Spain;

orcid.org/0000-0001-9647-6406

Ana M. López-Periago – Instituto de Ciencia de Materiales de Barcelona (ICMAB-CSIC), Bellaterra 08193, Spain

Arántzazu González-Campo – Instituto de Ciencia de Materiales de Barcelona (ICMAB-CSIC), Bellaterra 08193, Spain; orcid.org/0000-0002-1209-8119

Complete contact information is available at: <https://pubs.acs.org/doi/10.1021/acs.cgd.0c00742>

Author Contributions

The manuscript was written through contributions of all authors. All authors have given approval to the final version of the manuscript.

Notes

The authors declare no competing financial interest.

■ ACKNOWLEDGMENTS

This work has received funding from the European Research Council (ERC) under the European Union's Horizon 2020 R&D programme (ERC-724981). We also acknowledge the Spanish Government, Ministerio de Ciencia e Innovación (projects CTQ2017-83632, CTQ2015-68370-P and PGC2018-098630-B-I00 - MAT2016-77852-C2-1-R, and Ramon y Cajal grant RYC-2017-22910) and the Generalitat de Catalunya for the grant 2017SGR1277. C.D., N.A.A., A.L.P., A.G.C., and L.R.C. acknowledge the financial support through

the “Severo Ochoa” program for Centres of Excellence in R&D (SEV-2015-0496) under the FUNMAT-FIP-2016 fellowship. Special thanks to the Alba synchrotron for the possibility of carrying out the measurements of the crystals in the experiments AV-2017042211, AV-2018052864, AV-2018072912, and AV-2019023285 at beamline BL13–XALOC. This work (L.R.C.) has been done in the framework of the doctoral program “Chemistry” of the Universitat Autònoma de Barcelona.

■ ABBREVIATIONS

AI, active ingredients; BDMC, bisdemetoxycurcumin; CP, coordination polymers; bpe, 1,2-bis(4-pyridyl)ethylene; bpp, 1,3-bis(4-pyridyl)propane; bpy, 4,4'-bipyridine; CCM, curcumin; CCMoid, curcuminoid; DMC, demethoxycurcumin; EA, elemental analysis; EtOH, ethanol; ATR-FTIR, attenuated total reflectance Fourier transform infrared; MOF, metal organic framework; OAc, acetate; PXRD, powder crystal X-ray diffraction; SCXRD, single crystal X-ray diffraction; solid-state ^{13}C NMR, solid state ^{13}C nuclear magnetic resonance; TGA, thermal gravimetric analysis

■ REFERENCES

- (1) Gomollón-Bel, F. Ten Chemical Innovations That Will Change Our World: IUPAC identifies emerging technologies in Chemistry with potential to make our planet more sustainable. *Chem. Int.* **2019**, *41*, 12–17.
- (2) El-Sayed, E. S. M.; Yuan, D. Waste to MOFs: sustainable linker, metal, and solvent sources for value-added MOF synthesis and applications. *Green Chem.* **2020**, *22*, 4082–4104.
- (3) Abrahams, B. F.; Moylan, M.; Orchard, S. D.; Robson, R. Zinc Saccharate: A Robust, 3D coordination network with two types of isolated, parallel channels, one hydrophilic and the other hydrophobic. *Angew. Chem., Int. Ed.* **2003**, *42*, 1848–1851.
- (4) Navarro-Sánchez, J.; Argente-García, A. I.; Moliner-Martínez; Roca-Sanjuán, D.; Antypov, D.; Campíns-Falcó, P.; Rosseinsky, M. J.; Martí-Gastaldo, C. Peptide metal–organic frameworks for enantioselective separation of chiral drugs. *J. Am. Chem. Soc.* **2017**, *139*, 4294–4297.
- (5) Lillo, V.; Galán-Mascarós, J. R. Transition metal complexes with oligopeptides: single crystals and crystal structures. *Dalt. Trans.* **2014**, *43*, 9821–9833.
- (6) Marabello, D.; Antoniotti, P.; Benzi, P.; Canepa, C.; Diana, E.; Operti, L.; Mortati, L.; Sassi, M. P. Non-linear optical properties of β -D-fructopyranose calcium chloride MOFs: an experimental and theoretical approach. *J. Mater. Sci.* **2015**, *50*, 4330–4341.
- (7) Xie, Y.; Yu, Z.; Huang, X.; Wang, Z.; Niu, L.; Teng, M.; Li, J. Rational design of MOFs constructed from modified aromatic amino acids. *Chem. - Eur. J.* **2007**, *13*, 9399–9405.
- (8) Pratibha; Verma, S. Imine component based modified adenine nucleobase-metal frameworks. *Cryst. Growth Des.* **2015**, *15*, 510–516.
- (9) Wilcox, O. T.; Fateeva, A.; Katsoulidis, A. P.; Smith, M. W.; Stone, C. A.; Rosseinsky, M. J. Acid loaded porphyrin-based metal-organic framework for ammonia uptake. *Chem. Commun.* **2015**, *51*, 14989–14991.
- (10) Smaldone, R. A.; Forgan, R. S.; Furukawa, H.; Gassensmith, J. J.; Slawin, A. M. Z.; Yaghi, O. M.; Stoddart, J. F. Metal–organic frameworks from edible natural products. *Angew. Chem., Int. Ed.* **2010**, *49*, 8630–8634.
- (11) Keskin, S.; Kızılel, S. Biomedical applications of metal organic frameworks. *Ind. Eng. Chem. Res.* **2011**, *50*, 1799–1812.
- (12) Cai, W.; Chu, C.; Liu, G.; Wang, Y. Metal–organic framework-based nanomedicine platforms for drug delivery and molecular imaging. *Small* **2015**, *11*, 4806–4822.

- (13) Reddy, S.; Vasavi, A.; Suresh, J.; Yadav, H.; Singh, A. A Review on Curcuma longa - ProQuest. *Res. J. Pharm. Technol. Raipur*. **2012**, *5*, 2, 158–165.
- (14) Pabon, H. J. J. A synthesis of curcumin and related compounds. *Recl. des Trav. Chim. des Pays-Bas*. **1964**, *83* (4), 379–386.
- (15) Nurfina, A. N.; Reksodiprodjo, M. S.; Timmerman, H.; Jenie, U. A.; Sugiyanto, D.; Van der Goot, H. Synthesis of some symmetrical curcumin derivatives and their antiinflammatory activity. *Eur. J. Med. Chem.* **1997**, *32*, 321–328.
- (16) Pedersen, U.; Rasmussen, P. B.; Lawesson, S. O. Synthesis of naturally occurring curcuminoids and related compounds. *Liebigs Annalen der Chemie*. **1985**, *1985*, 1557–1569.
- (17) Kunnumakkar, A. B.; Guha, S.; Krishnan, S.; Diagaradjane, P.; Gelovani, J.; Aggarwal, B. B. Curcumin potentiates antitumor activity of gemcitabine in an orthotopic model of pancreatic cancer through suppression of proliferation, angiogenesis, and inhibition of nuclear factor- κ B-regulated gene products. *Cancer Res.* **2007**, *67*, 3853–3861.
- (18) Dandawate, P. R.; Vyas, A.; Ahmad, A.; Banerjee, S.; Deshpande, J.; Swamy, K. V.; Sarkar, F. H. Inclusion complex of novel curcumin analogue CDF and β -cyclodextrin (1:2) and its enhanced in vivo anticancer activity against pancreatic cancer. *Pharm. Res.* **2012**, *29*, 1775–1786.
- (19) Maheshwari, R. K.; Singh, A. K.; Gaddipati, J.; Srimal, R. C. Multiple biological activities of curcumin: a short review. *Life Sci.* **2006**, *78*, 2081–2087.
- (20) Claramunt, R. M.; Lavandera, J. L.; Alkorta, I.; Elguero, J. Curcumin and curcuminoids: Chemistry, structural studies and biological properties. *An. Real Acad. Nac. Farm.* **2015**, *81*, 278–310.
- (21) Zhang, Y.; Khan, A. R.; Fu, M.; Zhai, Y.; Yu, A.; Zhai, G. The progresses in curcuminoids-based metal complexes: especially in cancer therapy. *Future Med. Chem.* **2019**, *11*, 1035–1056.
- (22) Pettinari, R.; Marchetti, F.; Condello, F.; Pettinari, C.; Lupidi, G.; Scopelliti, R.; Mukhopadhyay, S.; Riedel, T.; Dyson, P. J. Ruthenium(II)-arene RAPTA type complexes containing curcumin and bisdemethoxycurcumin display potent and selective anticancer activity. *Organometallics* **2014**, *33*, 3709–3715.
- (23) Pettinari, R.; Marchetti, F.; Pettinari, C.; Condello, F.; Petrini, A.; Scopelliti, R.; Riedel, T.; Dyson, P. J. Organometallic rhodium(III) and iridium(III) cyclopentadienyl complexes with curcumin and bisdemethoxycurcumin co-ligands. *Dalton T.* **2015**, *44*, 20523–20531.
- (24) Krishnankutty, K.; Venugopalan, P. Metal chelates of curcuminoids. *Synth. React. Inorg. Met.-Org. Chem.* **1998**, *28*, 1313–1325.
- (25) Li, Y.; Gu, Z.; Zhang, C.; Li, S.; Zhang, L.; Zhou, G.; Wang, S.; Zhang, J. Synthesis, characterization and ROS-mediated antitumor effects of palladium (II) complexes of curcuminoids. *Eur. J. Med. Chem.* **2018**, *144*, 662–671.
- (26) Su, H.; Sun, F.; Jia, J.; He, H.; Wang, A.; Zhu, G. A highly porous medical metal-organic framework constructed from bioactive curcumin. *Chem. Commun.* **2015**, *51*, 5774–5777.
- (27) Portolés-Gil, N.; Lanza, A.; Aliaga-Alcalde, N.; Ayllón, J. A.; Gemmi, M.; Mugnaioli, E.; López-Periago, A. M.; Domingo, C. Crystalline Curcumin bioMOF Obtained by Precipitation in Supercritical CO₂ and Structural Determination by Electron Diffraction Tomography. *ACS Sustainable Chem. Eng.* **2018**, *6*, 12309–12319.
- (28) Diaz-Torres, R.; Menelaou, M.; González-Campo, A.; Teat, S. J.; Sañudo, E. C.; Soler, M.; Aliaga-Alcalde, N. Comparative Magnetic Studies in the Solid State and Solution of Two Isostructural 1D Coordination Polymers Containing CoII/NiII-Curcuminoid Moieties. *Magnetochemistry*. **2016**, *2*, 29.
- (29) Manna, B.; Desai, A. V.; Ghosh, S. K. Neutral N-donor ligand based flexible metal-organic frameworks. *Dalton Trans.* **2016**, *45*, 4060–4072.
- (30) Haldar, R.; Maji, T. K. Metal-organic frameworks (MOFs) based on mixed linker systems: structural diversities towards functional materials. *CrystEngComm* **2013**, *15*, 9276–9295.
- (31) Duer, M. J. *Solid state NMR spectroscopy: principles and applications*, Dier, M. J., Ed.; John Wiley & Sons, 2008; pp 483–485.
- (32) Sheldrick, G. M. Crystal structure refinement with SHELXL. *Acta Crystallogr., Sect. C: Struct. Chem.* **2015**, *71*, 3–8.
- (33) Juanhuix, J.; Gil-Ortiz, F.; Cumí, G.; Colldelram, C.; Nicolás, J.; Lidón, J.; Boter, E.; Ruget, C.; Ferrer, S.; Benach, J. Developments in optics and performance at BL13-XALOC, the macromolecular crystallography beamline at the Alba Synchrotron. *J. Synchrotron Radiat.* **2014**, *21*, 679–689.
- (34) Kabsch, W. Xds. *Acta Crystallogr., Sect. D: Biol. Crystallogr.* **2010**, *66*, 125–132.
- (35) Dong, L.; Chu, W.; Zhu, Q.; Huang, R. Three Novel Homochiral Helical Metal-Organic Frameworks Based on Amino Acid Ligand: Syntheses, Crystal Structures, and Properties. *Cryst. Growth Des.* **2011**, *11*, 93–99.
- (36) Singh, W. M.; Baruah, J. B. Nickel, copper and zinc complexes of (2-methoxycarbonylmethylimino-5-methyl-thiazol-3-yl)-acetic acid. *Polyhedron* **2008**, *27*, 2968–2972.
- (37) Aliaga-Alcalde, N.; Rodríguez, L.; Ferbinteanu, M.; Höfer, P.; Weyhermüller, T. Crystal structure, fluorescence, and nanostructuration studies of the first ZnII anthracene-based curcuminoid. *Inorg. Chem.* **2012**, *51*, 864–873.
- (38) Matlinska, M. A.; Wasylishen, R. E.; Bernard, G. M.; Terskikh, V. V.; Brinkmann, A.; Michaelis, V. K. Capturing elusive polymorphs of curcumin: A structural characterization and computational study. *Cryst. Growth Des.* **2018**, *18*, 5556–5563.
- (39) Pöppler, A. C.; Lübtow, M. M.; Schlauersbach, J.; Wiest, J.; Meinel, L.; Luxenhofer, R. Loading-Dependent Structural Model of Polymeric Micelles Encapsulating Curcumin by Solid-State NMR Spectroscopy. *Angew. Chem., Int. Ed.* **2019**, *58*, 18540–18546.
- (40) Kong, X.; Brinkmann, A.; Terskikh, V.; Wasylishen, R. E.; Bernard, G. M.; Duan, Z.; Wu, G. Proton probability distribution in the O...H...O low-barrier hydrogen bond: a combined solid-state NMR and quantum chemical computational study of dibenzoyl-methane and curcumin. *J. Phys. Chem. B* **2016**, *120* (45), 11692–11704.
- (41) Volkringer, C.; Popov, D.; Loiseau, T.; Guillou, N.; Ferey, G.; Haouas, M.; Taulelle, F.; Mellot-Draznieks, C.; Burghammer, M.; Riekel, C. A microdiffraction set-up for nanoporous metal-organic-framework-type solids. *Nat. Mater.* **2007**, *6*, 760–764.
- (42) Stegbauer, L.; Schwinghammer, K.; Lotsch, B. V. A hydrazone-based covalent organic framework for photocatalytic hydrogen production. *Chem. Sci.* **2014**, *5*, 2789–2793.
- (43) Kolev, T. M.; Velcheva, E. A.; Stamboliyska, B. A.; Spittler, M. DFT and experimental studies of the structure and vibrational spectra of curcumin. *Int. J. Quantum Chem.* **2005**, *102*, 1069–1079.
- (44) Kaljurand, I.; Lilleorg, R.; Murumaa, A.; Mishima, M.; Burk, P.; Koppel, I.; Koppel, I. A.; Leito, I. The Basicity of Substituted N,N-Dimethylanilines in Solution and in the Gas Phase. *J. Phys. Org. Chem.* **2013**, *26* (2), 171–181.
- (45) Yuan, L.; Lorenz, H. Solvate formation of bis (demethoxy) curcumin: Screening and characterization. *Crystals* **2018**, *8*, 407.
- (46) Yuan, L.; Horosanskaia, E.; Engelhardt, F.; Edelman, F. T.; Couvrat, N.; Sanselme, M.; Cartigny, Y.; Coquerel, G.; Seidel-Morgenstern, A.; Lorenz, H. Solvate Formation of Bis (demethoxy) curcumin: Crystal Structure Analyses and Stability Investigations. *Cryst. Growth Des.* **2019**, *19* (2), 854–867.
- (47) Karlsen, J.; Mostad, A.; Tønnesen, H. H.; et al. Structural studies of curcuminoids. VI. Crystal structure of 1,7-bis(4-hydroxyphenyl)-1,6-heptadiene-3,5-dione hydrate. *Acta Chem. Scand.* **1988**, *42*, 23–27.

Cite this: *Dalton Trans.*, 2021, **50**, 7056

Broadening the scope of high structural dimensionality nanomaterials using pyridine-based curcuminoids†

Laura Rodríguez-Cid,^{‡a} Wenjie Qian,^{‡a} Joseline Iribarra-Araya,^b Álvaro Etcheverry-Berrios,^b Eulalia Martínez-Olmos,^a Duane Choquesillo-Lazarte,^c Eva Carolina Sañudo,^{d,e} Olivier Roubeau,^f Ana María López-Periago,^a Arántzazu González-Campo,^a José G. Planas,^a Mònica Soler,^g *^b Concepción Domingo^g *^a and Núria Aliaga-Alcalde^g *^{a,g}

We present a new heteroditopic ligand (**3pyCCMoid**) that contains the typical skeleton of a curcuminoid (CCMoid) decorated with two 3-pyridyl groups. The coordination of **3pyCCMoid** with Zn^{II} centres results in a set of novel coordination polymers (CPs) that display different architectures and dimensionalities (from 1D to 3D). Our work analyses how synthetic methods and slight changes in the reaction conditions affect the formation of the final materials. Great efforts have been devoted toward understanding the coordination entities that provide high dimensional systems, with emphasis on the characterization of 2D materials, including analyses of different types of substrates, stability and exfoliation in water. Here, we foresee the great use of CCMoids in the field of CPs and emphasize **3pyCCMoid** as a new-born linker.

Received 2nd March 2021,
Accepted 14th April 2021

DOI: 10.1039/d1dt00708d

rsc.li/dalton

Introduction

Coordination polymers (CPs) comprise a large variety of crystalline metal–organic architectures extending in one, two or three dimensions.¹ The potential applications of these materials, as gas storage modules, conducting films, drug delivery vehicles, sensing agents and catalysts, among others,² have driven intense research concerning the factors that trigger the assembly between inorganic/organic units, ruling

topology and final properties.^{1–3} In addition, the creation of functional materials that combine the diversity of CPs and tailored dimensions is highly desirable, where the tuning of dimensionality and size aims to overcome the present technological challenges exploiting the optical, electronic and/or biological properties of such nanomaterials.⁴ Toward such goals, special attention has been paid to the design of homoditopic linkers (molecules with identical coordinative sites) with a variety of frameworks (from flexible to rigid)⁵ and binding sites (*e.g.*: linkers with O- or N-donor groups).⁶ Much less information has been gathered about heteroditopic ligands (linkers with more than one type of coordinative ending),⁷ partly due to the difficulties in achieving crystalline materials and predicting final assemblies. Paradoxically, the latter is also one of the strengths of such multifunctional ligands, capable of generating new topological CPs by binding with one type of metal centre or the combination of a few.^{7,8}

A number of naturally occurring molecules are potential heteroditopic linkers, with great projection in the field, adding beneficial features to CPs, such as low toxicity and biocompatibility.⁹ In this sense, curcumin (CCM) fulfills all the criteria, as shown in recent publications by Zhu *et al.*¹⁰ and some of us.¹¹ These studies display the two only crystalline ZnMOF/ZnCP structures based exclusively on the ligand CCM.

Encouraged by the available data on CCM derivatives (the so-called curcuminoids, CCMoids), some of us have recently described a new family of CPs containing a natural CCMoid,

^aInstitut de Ciència de Materials de Barcelona (ICMAB–CSIC), Campus Universitari, 08193 Bellaterra, Spain. E-mail: nuria.aliaga@icrea.cat, conchi@icmab.es

^bDepartment of Chemical Engineering, Biotechnology and Materials, Faculty of Physical and Mathematical Sciences, University of Chile, Beauchef 851, Santiago, 837.0415, Chile. E-mail: msoler@ing.uchile.cl

^cLaboratorio de Estudios Cristalográficos, IACT, CSIC-Universidad de Granada, Avda. de las Palmeras 4, 18100 – Armilla, Granada, Spain

^dDepartament de Química Inorgànica i Orgànica, Universitat de Barcelona, C/Martí i Franqués 1-11, 08028 Barcelona, Spain

^eInstitut de Nanociència i Nanotecnologia, Universitat de Barcelona, Av. Diagonal 645, 08028 Barcelona, Spain

^fInstituto de Nanociencia y Materiales de Aragón (INMA) CSIC and Universidad de Zaragoza, Plaza San Francisco s/n, 50009 Zaragoza, Spain

^gICREA – Institució Catalana de Recerca i Estudis Avançats, Passeig Lluís Companys 23, 08010 Barcelona, Spain

†Electronic supplementary information (ESI) available. CCDC 2044029 (**3pyCCMoid**), 2044078 (1), 2044079 (2) and 2043842 (4). For ESI and crystallographic data in CIF or other electronic format see DOI: 10.1039/d1dt00708d

‡Both authors made equal contributions to this work.



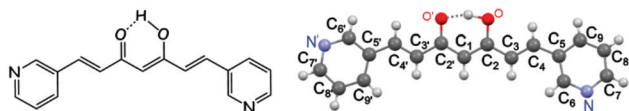


Fig. 1 (Left) General molecular structure of **3pyCCMoid**. (Right) Picture of **3pyCCMoid** from the crystallographic data. H atoms are not labelled for clarity. Colour legend: C, grey; O, red; N, blue; H, light grey.

bisdemethoxycurcumin (BDCM).¹² Now, we describe a synthetic linker that displays CCMoid characteristics (diarylheptanoid chain and central keto–enol moiety), with pyridine groups at the ends of the molecule (**3pyCCMoid**, Fig. 1).

The choice of the latter confers **3pyCCMoid** with: (i) new coordination sites, in comparison with the phenol/methoxide groups of CCM and natural CCMoids^{10–12} (ii) additional chemical properties, such as weak basicity, variations in the solubility together with the ability to generate supramolecular interactions^{6,13} and (iii) possible biological contributions, given that pyridines are chemically stable *in vivo*, present in natural products (vitamins and coenzymes)¹⁴ and used as active components in drugs and pesticides.^{14,15} Connected with these factors, **3pyCCMoid** is partially soluble in H₂O (Fig. S1†) and has not shown cytotoxic activity against SH-SY5Y cells¹⁶ and in *in vivo* tests with mice,¹⁷ properties that encourage its possible use as a biocompatible material. Nevertheless, further applications of this CCMoid exceed the scope of this paper and they will be explored in further work.

Here, we report three novel CPs containing **3pyCCMoid** coordinated to Zn^{II} ions. This manuscript explores the use of solvent mixtures in combination with layering and soft solvothermal methods for the creation of 1D, 2D and 3D species (systems **1**, **2** and **4**, respectively), including crystallographic data for the three systems. We concentrate on the synthesis and physico-chemical characterization of the new species, emphasizing the heteroditopic nature of **3pyCCMoid** and its versatile coordination (two/three coordinated sites). These CPs are achieved under mild conditions using straightforward methodologies and purification processes. Furthermore, these systems assert synthetic CCMoids as optimal molecular platforms, being the first examples of the foreseen broad production of CPs based on this family of molecules. In particular, the exfoliation of 2D layered metal–organic hybrid materials,¹⁸ such as **2**, has attracted attention in recent years due to the different properties shown by a few layers of these materials (nanosheets) when compared to the bulk product. In this work, we present an effective methodology for the exfoliation of **2** in H₂O as well as the characterization of the nanosheets.

Results and discussion

Synthesis

3pyCCMoid was prepared in high yield using the classic method described by Pabon.¹⁹ Specifically, the intermediate

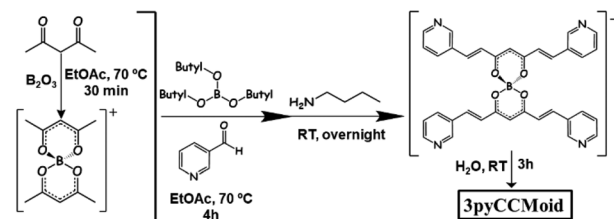


Fig. 2 Scheme of the synthetic path to achieve **3pyCCMoid**.

boron complex was isolated and water was used to achieve the free ligand, avoiding this way diluted acidic solutions in the last step that protonate the pyridine moieties and make the extraction of the final system difficult (Fig. 2). Recrystallization with hot MeCN provided the crystals of **3pyCCMoid**.

We tested the capability of **3pyCCMoid** as a heteroditopic ligand to produce new CPs through the reaction with Zn(NO₃)₂·6H₂O; the latter is a biocompatible metallic source²⁰ that presents a versatile coordination and is well known in the fields of bio-MOFs and CPs.^{9–12,21} Table 1 shows the interplay of solvents as well as the two methodologies studied to afford **1–2** and **4**, respectively. A mixture of alcohols (MeOH/EtOH) with high boiling point solvents (DMF/DMA), together with subtle differences in their combinations, provides partial or full coordination of **3pyCCMoid** showing penta- or hexacoordination modes for the Zn^{II} centres, as seen in the structures. As a result, the attained crystalline materials display a variety of structural dimensionalities, from 1D to 3D, pointing to the plurality that the design of CCMoids can add in the field of CPs.

Structural descriptions

The single crystal X-ray crystallographic resolution of **1**, **4** and **3pyCCMoid** required the use of a synchrotron source, while for **2** routine equipment could be used. Table S1† shows the general crystalline structural data for all the species and Fig. S2–S4† show the enlarged views, for clarity, of the images shown in this section. The selected bond lengths and angles for each system are listed in Tables S2, S3 and S4,† respectively. Compound **3** did not provide suitable crystals for crystallographic resolution, which is the reason why the analysis of its structure is still elusive. This compound was achieved together with **1** and provides some insights into the effects of solvents and the synthetic methodology. Fig. S5† shows the X-ray diffraction (XRD) patterns generated from the three single crystal datasets compared with those measured from the powdered samples, except for **4**, with reproducible synthesis but low yield, not enough to record the experimental XRD data, therefore only the simulated ones from single X-ray diffraction are shown.

3pyCCMoid. This CCMoid (Fig. 1) crystallizes in the monoclinic space group *P2₁/c*. The molecule presents a diarylheptanoid skeleton that contains alternating conjugated bonds on both sides of the β-diketone moiety (C=C and C–C distances range between 1.336–1.385 Å and 1.454–1.469 Å, respectively). Distances of 1.315 Å and 1.281 Å were found for the C–OH and



Table 1 Summary of methodologies/conditions used to achieve 1–4 CPs. System 3 was crystalline but not suitable for single-crystal X-ray diffraction; it was found in a mixture together with 1 and has been added to the table for comparative purposes

CP	Ligand	Metal salt	Method	Solvent	Conditions
1	3pyCCMoid 0.018 mmol	Zn(NO ₃) ₂ ·6H ₂ O 0.054 mmol	Solvothermal	DMF : MeOH (1 : 4)	80 °C 72 h
2	3pyCCMoid 0.018 mmol	Zn(NO ₃) ₂ ·6H ₂ O 0.054 mmol	Solvothermal	DMA : EtOH (1 : 4)	80 °C 72 h
1 & 3	3pyCCMoid 0.018 mmol	Zn(NO ₃) ₂ ·6H ₂ O 0.054 mmol	Solvothermal	DMF : EtOH (1 : 4)	80 °C 72 h
4	3pyCCMoid 0.108 mmol	Zn(NO ₃) ₂ ·6H ₂ O 0.215 mmol	Layering	DMF : EtOH (3 : 7)	RT 2–3 weeks

C=O groups, in this order, and the intramolecular hydrogen bond displayed an angle of 158.68°, similar to alike systems in the literature.^{10,12,22} The molecule is almost flat, and only the pyridine arms show slight deviations from the plane that contains the linear framework (6.78°).²³ Such units are placed at the ends, having the N atoms at the *meta*-positions and facing opposite directions with respect to each other. A rich supramolecular environment leads the packing arrangement (not shown). The pseudo-hydrogen bonds between each pyridine moiety and neighbours appear to be weak (C_{py}–H...N) but numerous, displaying angles of 152.83° and 158.84° and distances of 3.384 Å and 3.441 Å. Additionally, the C=O...H–C_{py} interactions assist the network extension, with a distance of 3.350 Å and an angle of 150.45°. The final assembly displays negligible π–π interactions.

[Zn_{0.5}(3pyCCMoid)]_n (**1**). **1** crystallizes in the monoclinic space group *C2/c*. The asymmetric unit includes one 3pyCCMoid molecule and one-half of the Zn ion. The Zn^{II} centres are hexacoordinated, where each unit binds to two 3pyCCMoids through their β-diketone moieties (Zn–O distances between 2.026 and 2.132 Å) and two pyridine groups (Zn–N distances of 2.211 Å) from neighbouring CCMoids (Fig. 3a). In this arrangement, the β-diketone groups are contained in crossed planes, disposing in a *cis* configuration the

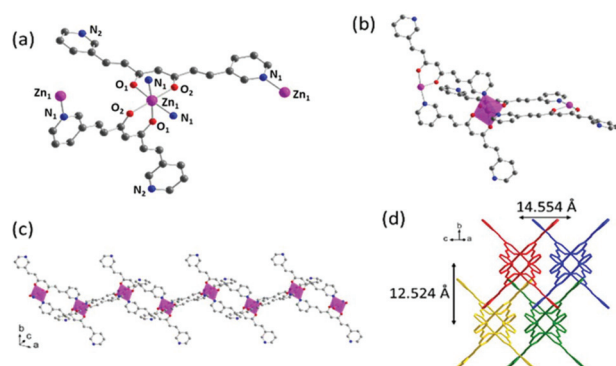


Fig. 3 Crystal structure of **1**: (a) Representation of the coordination sphere of a Zn^{II} centre and the coordination modes of 3pyCCMoid molecules; (b) representation of two loops connected through the intermediate Zn(II) centre; (c) extended view of one chain; (d) arrangement of four chains in the crystal. Colour legend: Zn, pink; C, grey; O, red; N, blue; H atoms are omitted for clarity.

two pyridine moieties (Fig. 3a). Regarding each 3pyCCMoid ligand, one of the pyridine moieties remains always free (Fig. 3a–c). Compared with the free CCMoid, here the CCMoid skeletons are slightly bent (23.16°, Fig. S6†)²³ with the pyridine groups facing in opposite directions as seen before. The framework spreads forming loops through the coordination of the adjacent unit, similar to Fig. 3a, by pyridine endings (Zn...Zn distance 9.271 Å, Fig. 3b and c). In addition, the Zn^{II} centres act as nodes among the loops, displaying them in a nearly perpendicular way (angles of 87.52° and 93.77°) and as a result, the system evolves into a staircase shaped 1D net. The chains are aligned and efficiently packed (Fig. 3d), with Zn...Zn distances of 14.5 Å and 12.5 Å among the closest neighbours.

[Zn₂(3pyCCMoid)₂(NO₃)₂]_n (**2**). System 2 crystallizes in the monoclinic space group *P2₁/n*. The asymmetric unit cell contains two [Zn(3pyCCMoid)(NO₃)] fragments, each presenting 3pyCCMoid molecules with slightly different distances and conformations. As in **1**, the Zn^{II} ions adopt a pseudo-octahedral geometry, but now there is only one 3pyCCMoid chelating the metal centre together with one NO₃[−] anion. The two remaining sites, within the Zn^{II} unit, are occupied by pyridine moieties from nearby CCMoids. Here again, the disposition of the chelating groups, CCMoid and NO₃[−], is in the *cis*-configuration (Fig. 4a). The 3pyCCMoid ligand is now fully coordinated, bringing into play its three coordinative sites. Each

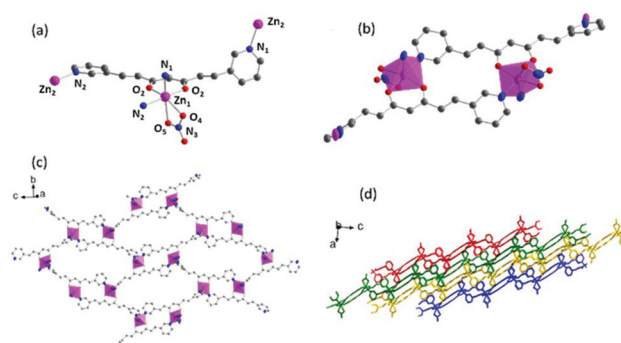


Fig. 4 Crystal structure of **2**: (a) Representation of the coordination sphere of a Zn^{II} centre and the coordination mode of 3pyCCMoid; (b) picture of the smallest loop in the layer; (c) single 2D layer; (d) framework consisting of packed 2D layers (each layer represented by a different colour). Colour legend: Zn, pink; C, grey; O, red; N, blue; H atoms are omitted for clarity.



3pyCCMoid coordinates through the β -diketone moiety to one of the Zn^{II} ions in the fragment, binding the pyridine groups to two neighbouring Zn^{II} centres (Fig. 4a). The assembly of two asymmetric units forms loops too ($\text{Zn}\cdots\text{Zn}$ distance of 9.028 Å, Fig. 4b). Within such dimers, everything relates by an inversion centre, making the NO_3^- groups point out in opposite directions. The connection of four of these loops through the remaining pyridine groups creates a bigger cavity (Fig. 4c). Now the void displays a rhomboid shape, being the longest $\text{Zn}\cdots\text{Zn}$ distance of 22.060 Å. This implies a greater twist of the skeletons of the CCMoids (60.42° and 75.52°),²³ where the pyridine moieties face almost perpendicularly allowing the extension in two dimensions and forming infinite layers (Fig. 4b and c). Despite the presence of several cavities in each single layer, the material presents a dense arrangement, where two NO_3^- groups, from adjacent layers, are inserted in the bigger voids resulting in a compact material (Fig. 4d).

$[\text{Zn}(\text{3pyCCMoid})(\text{NO}_3)(\text{EtOH})_2]_n$ (**4**). System **4** crystallizes in the orthorhombic $P2_12_12_1$ space group. The asymmetric unit is formed by one $[\text{Zn}(\text{3pyCCMoid})(\text{EtOH})]\cdot\text{NO}_3\cdot\text{EtOH}$ fragment. Here, the Zn^{II} ions are pentacoordinated adopting a trigonal bipyramidal geometry ($\tau = 0.85$). Their coordination sphere chemically resembles the previous one, with every metallic centre coordinated to one β -diketone group from one CCMoid and two pyridine moieties from two other neighbours. However, the remaining position is now occupied by an EtOH molecule leaving uncoordinated the NO_3^- ion (Fig. 5a). In the structure, the CCMoid shows deviations from planarity (35.25°)²³ but less pronounced than for compound **2**, having here the pyridine groups oriented in opposite directions as in the pristine **3pyCCMoid** and in **1**. A remarkable difference with previous CP structures is the absence of loops. The shortest $\text{Zn}\cdots\text{Zn}$ distance is now 9.31 Å. In this case, the pyridine groups of the neighbouring CCMoids do not promote the formation of dimers, exhibiting their rotational freedom and

spreading of the net (Fig. 5b) assisted by the Zn^{II} centres. This, together with the fact that all the active sites of the **3pyCCMoid** ligands are coordinated, favours the formation of a compact 3D structure (Fig. 5c). The new CP displays small voids occupied by one extra molecule of EtOH and the NO_3^- ion (Fig. 5c), both promoting supramolecular interactions with adjacent CCMoid residues.

Comparative structural analysis of 3pyCCMoid

Compounds **1**, **2** and **4** show that **3pyCCMoid** is an excellent heteroditopic ligand that always binds through the β -diketone group with partial or total coordination of the pyridine moieties. It is worth noting that the description of our experimental combinations, regarding the metallic salt, solvents, and methods, was restricted for comparative purposes in contrast to the variety of results. Still, we focus on **3pyCCMoid**, where the reasonable study of all variables would be highly complex. Nevertheless, some facts are highlighted for the general overview.

Briefly, solvents have a regulative role in the assembly process of different CPs, acting as orchestrators of the final coordination of the metal and/or as guest molecules, although it is difficult to assert the specifics of their performance.^{12,24,25} In this regard, the solvents used in this work (high boiling points, DMA and DMF, and alcoholic solvents, EtOH and MeOH) present excellent coordination abilities ($\text{DMF} > \text{MeOH} > \text{DMA} > \text{EtOH}$)²⁶ and the synthetic procedures of the three systems, **1–2** and **4**, display different combinations of them. This coordination ability is even more remarkable in **4**, where EtOH forms part of the structure. Considering the metal centre, the Zn^{II} ions can show a variety of coordination numbers (from 4 to 6) optimal to stabilize the coordination segments that the latter can connect and expand, increasing the dimensionality.^{25,27} Nevertheless, the arrangement among the units (Table S5†) is responsible for the final dimension (**4** is a 3D system that displays pentacoordinated Zn^{II} ions, while **1** and **2** show hexacoordinated metal centres, being 1D and 2D systems, respectively). With reference to the methodology, the achievement of a mixture of crystals, **1** & **3**, instead of **4** (Table 1) is a clear example of the effects of temperature, pressure and time on the creation of fragments that grow and organize. System **3**, although crystalline, could not be resolved. This together with the achievement of **1**, with two different mixtures of solvents, indicates that independent of the methodology, similar coordination entities may be possible or even coexist in solution, the solvent mixture being responsible for favouring one over the others.

On the basis of the CCMoid structures, Fig. 6 shows the crystallographic variations among the coordinated **3pyCCMoid** in the CPs compared with the pristine ligand. The uncoordinated **3pyCCMoid** (in grey) shows a quasi-planar disposition that appears slightly disturbed in **1** and **4** (Fig. 6, magenta and blue, respectively). System **2** shows the highest distortion, having two crystallographically different CCMoids with twisted skeletons (yellow and green, Fig. 6), showing a clear predisposition towards the perpendicular orientations of the pyridine

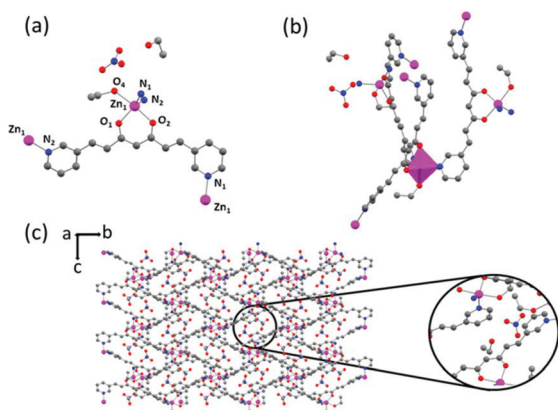


Fig. 5 Crystal structure of **4**: (a) Representation of the coordination sphere of a Zn^{II} centre and the coordination mode of **3pyCCMoid**; (b) picture of the connection of two neighbouring CCMoids; (c) 3D structure with molecules of the solvent and magnification of their disposition in the cavity. (Zn, pink; C, grey; O, red; N, blue; H atoms are omitted for clarity).



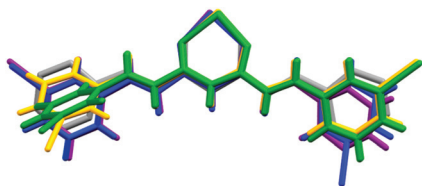


Fig. 6 Superimposition of **3pyCCMoid** in the asymmetric units of the different compounds, compared to pristine **CCMoid**: **3pyCCMoid** (grey), **1** (purple), **2** (yellow and green) and **4** (blue).

groups in the same ligand (green). Comparing **1** and **2**, it can be observed that the dimers that provide small loops do not relate to the framework differences, although the higher distortion observed in **2** allows the connection among dimers creating additional bigger loops (Fig. 4d).

Hence, the gentle conformational changes in the **CCMoid** skeleton, together with the rotation of the pyridine groups, allow further coordination to the Zn^{II} units, increasing the variety of possible arrays and, therefore, the dimensionality. In this context, the N atoms in their pyridine groups appear always facing opposite directions.

Studies on the 2D material (compound 2)

Encouraged by the known biocapabilities of **3pyCCMoid** and that the synthesis of nano-sized 2D CPs is highly desired for a number of applications, including membrane sensors and biomedicine,^{10,28,29} we further characterized our 2D system (compound **2**). In this way, exfoliation was pursued towards the achievement of few-layered sheets from the hybrid material, together with the analysis of their thickness and stability. The physico-chemical properties of **2** were studied, together with the assessment of the number of layers after exfoliation, among others.^{30,31} Regarding this matter, compound **2** is an appealing system due to its arrangement and composition, although limitations such as constrain, thermal and/or solvent instability had to be tested.³² The powder XRD spectrum of **2** before (crystals) and after grinding (fine powder) displays a consistent pattern (Fig. S7†). STA(TG-DSC) experiments (Fig. S8†) show that **1** and **2** start decomposing at 325/262 °C, temperatures higher than the one found for the neat **3pyCCMoid**, which starts to show a remarkable loss of weight at 185 °C. Regarding the two CPs, the lower thermal stability of **2** with respect to **1** could be related to the lability of the NO_3^- ions and further instability of the remaining system.

Solvent studies. **2** is stable in EtOH at RT for long periods of time (>1 month). The powder XRD patterns, shown in Fig. S9,† demonstrate that the treatment with this solvent, which includes washing and conservation, does not affect its general structure, although the intensity of some peaks changes which is especially noticeable in the peak around 6.4°. These small changes can be related to the labile nitrate group or changes in the preferential growth direction of the crystals. However, when neat DMA is used to keep the crystals, the material loses crystallinity and the solution becomes yellowish, indicating partial re-dissolution. The remaining solid and solution were

studied in parallel. First, in an attempt to identify the components of the yellowish solution, DMF-d_7 was used to partially dissolve the crystals and the filtered solution was studied by ^1H NMR to compare with the spectrum of the pristine ligand (Fig. S10†). The spectrum of **2** displayed a set of well-defined shifts that agreed with the presence of one fragment different from the free ligand, pointing to the existence of a Zn^{II} -**CCMoid** compound, similar to other mononuclear Zn^{II} species previously published.²² Nevertheless, the putative structure is still elusive (*e.g.*: mononuclear or some sort of dinuclear/short polynuclear systems). Beyond the singularity of its NMR in DMF, ESI studies in DMA did not show traceable molecular weight patterns (Fig. S11†). In addition, unfiltered solutions of **2** in DMA and the remaining solid were studied by SEM and AFM after deposition on different substrates (drop casting on SiO_2/Si wafers, HOPG and mica). EDX experiments corroborated the existence of Zn and expected C and N atoms in the samples (Fig. S12†). Drop casting of the unfiltered solution after the complete evaporation of the solvent on SiO_2/Si shows flakes of **2** and aggregation (Fig. 7, right). Here, there is a significant effect on the final morphology depending on the surface. Similar organization is observed for HOPG, although on mica the molecules spread out in a distinct manner, presenting less aggregates and, therefore, affinity for the substrate and higher disorder in their disposition (Fig. S13†). The morphologies found in all the cases for the unfiltered solution are dramatically different from those found for **3pyCCMoid** under the same conditions and substrates (Fig. S14†), emphasizing, once more, the idea that the dissolved systems from DMA do not relate to the free ligand. On the other hand, the remaining solid from DMA is dispersed on the different substrates in a similar manner, displaying homogeneous cubes with an average size of 1 μm , (Fig. 7, left and S14†). Related types of shapes are reported studying the effect of solvent and surfaces on some CP dispersions, showing that crystals are formed by domains that can disaggregate.³³

AFM topographic images, using the tapping mode for the SiO_2/Si wafers, are shown in Fig. 8. The so-called flakes from solution appear as amorphous aggregates of different heights (average 1 μm , Fig. 8, top). In contrast, the AFM images of the remaining solid show the robustness of the cubes with dimensions of 1 to 1.5 μm and a height of 0.5 μm (Fig. 8, bottom). Within the cubes, no further information regarding the orien-

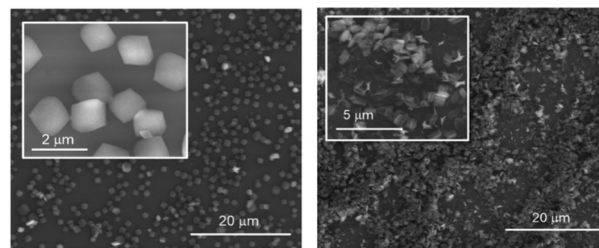


Fig. 7 SEM images of different substrates of **2** after treatment with DMA on silicon wafer: (left) solid sample and (right) solution.



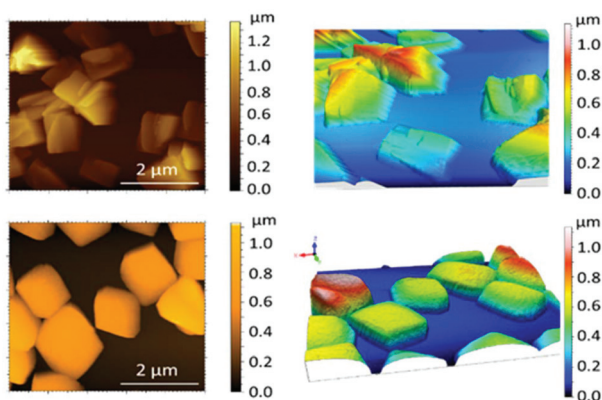


Fig. 8 AFM images of the cubes of **2** (left) and 3D representations (right) obtained with the tapping mode for solution samples (top) and solid (bottom).

tation of the sheets with respect to the surface was extracted; further work may require functionalization of the cubes/surfaces to promote their alignment with the working surfaces. Overall, the cubes appear as intermediate forms between the crystals and the amorphous flakes that segregate, at the same time, in the units observed by NMR; overall, these experiments show the steps into the formation/aggregation of the 2D system.

Exfoliation studies. Several sets of experiments in H₂O were performed with **2**, by varying sonication and resting times, as well as sample collection modes. A complete description of the most reproducible methodology is provided in the Experimental section. The Tyndall effect (Fig. S15[†]) proved the presence of nanosheets in suspension. Statistical analysis by AFM of the height profile using 100 measurements of these nanosheets deposited on SiO₂/Si (Fig. 9) shows that approxi-

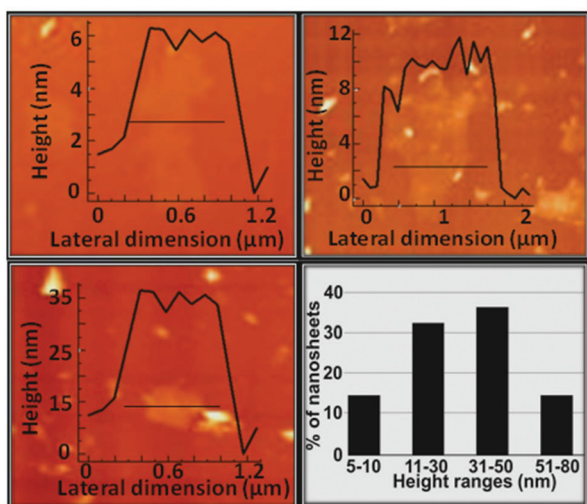


Fig. 9 AFM height profile of three different nanosheets showing the most abundant height ranges and the statistical analysis of the nanosheet thickness.

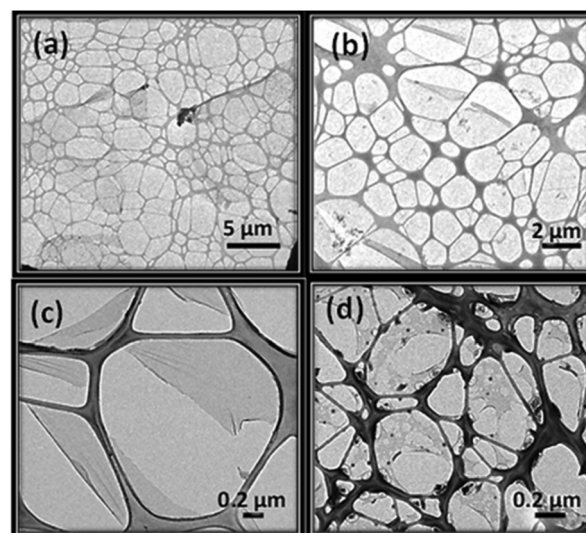


Fig. 10 TEM images of nanosheets (a) after the evaporation of the drop on the TEM grid, (b) magnification of (a), (c) after 3 days in the TEM grid, and (d) after the addition of more water.

mately 70 of the measured nanosheet heights were between 11–50 nm (approximately: 12% of 11–20 nm, 21% of 21–30, 22% of 31–40 nm and 15% of 41–50 nm) followed by 15 measures that show values under 10 nm and in the same number of nanosheets higher than 50 nm.

In contrast, the extension of the nanosheets is dramatically large (average 1–5 μm, Fig. 10). Nanosheet deposition on the TEM grids showed transparent layers and continuous surfaces (Fig. 10a and b). After three days of sample deposition, the setups displayed breaks on the edges and folding of the sheets (live phenomenon in the ESI[†] video), due to surface tension effects and the low thickness of the material (Fig. 10c). Attempts to decrease the height of the sheets were made by applying longer resting periods, from 7 to 12 h. However, as a result, degradation of the material was observed, where the TEM grids presented black aggregates together with nanosheets that displayed evident holes. We postulate that at the interface between the nanosheets and the solvent, due to the labile nature of the NO₃[−] groups coordinated to the Zn^{II} centres, together with sonication and long periods in contact with H₂O molecules, must trigger the segregation of the units which in H₂O deteriorate, creating the holes in the nanosheets.

A similar nanosheet appearance is observed when more water is added to the nanosheets after 6 hours of resting, proving the important role that this solvent plays in the degradation (Fig. 10d). The composition of the nanosheets deposited on the TEM grids was analysed by EDX showing the same elements as the original crystals (Fig. S16[†]).

Solid state fluorescence studies

The luminescence properties of **3pyCCMoid** together with compounds **1** and **2** were analysed in the solid state at room temperature (Fig. S17[†]). **3pyCCMoid** shows an emission band



at 527 nm, expected in part from the CCMoid dye nature. However, compound **1** does not show fluorescence, and **2** compared with the neat ligand displays an attenuated band at the same wavelength. These results were somehow unexpected, taking into account that the chelation enhancement of fluorescence (CHEF)³⁴ is normally observed when Zn^{II} ions coordinate to dyes, which is our past experience with different Zn-CCMoid coordination compounds, although coordination in the latter was exclusively through the β -diketone group.²² Conversely, here the outcome indicates that the coordination of Zn^{II} units to the pyridine moieties of the skeleton may have an adverse effect on the fluorescence.

Experimental section

Materials and methods

Experiments were carried out using commercial HPLC grade solvents. The chemicals were purchased from Sigma and used as received. The oven used for the CP synthesis is an Ecocell comfort.

Synthesis

Synthesis of 3pyCCMoid.³⁵ 0.7 g of acac (7 mmol) and 0.35 g of B₂O₃ (5 mmol) were dissolved in 8 mL of EtOAc. The reaction mixture was heated at 70 °C for 30 min until a white paste was formed. Then, a solution of 1.5 g of 3-pyridine carboxaldehyde (14 mmol) and 3.22 g of tributyl borate (14 mmol) in 3 mL of EtOAc was added. The mixture was stirred and refluxed (70 °C) for an additional 4 h. After cooling down, a solution of *n*-butylamine (0.4 mL, 4 mmol) in EtOAc (1 mL) was added dropwise, and the final reaction mixture was kept stirring at room temperature overnight. The reaction mixture turned yellow with the precipitate on the next day. This suspension was filtered, washed with EtOAc and dried to afford a yellow solid. Then, the solid was suspended in 30 mL of H₂O and stirred for 3 h at room temperature, followed by filtering, washing with H₂O and finally vacuum drying. Pure **3pyCCMoid** was achieved by recrystallization from hot MeCN. Yield: 1.56 g, 80%. ¹H NMR (400 MHz, DMSO-*d*₆) δ 15.96 (s, 1H), 8.91 (d, *J* = 1.7 Hz, 2H), 8.59 (dd, *J* = 4.8, 1.7 Hz, 2H), 8.19 (d, *J* = 8.0 Hz, 2H), 7.69 (d, *J* = 16.1 Hz, 2H), 7.48 (dd, *J* = 7.9, 4.8 Hz, 2H), 7.13 (d, *J* = 16.1 Hz, 2H), 6.22 (s, 1H). Elemental analysis (%) calculated for C₁₇H₁₄N₂O₂·0.15 H₂O: C 72.66, H 5.13, N 9.97; found C 72.18, H 4.43, N 10.07. MALDI-MS *m/z* (%): 277.04 ([M - H]⁻), 279.03 ([M + H]⁺). FTIR data (KBr, cm⁻¹): 1626 (ν C=C_{aromatic}), 1579 (C=O_{st, β -diketone}), 1509 (ν C=N) 1476 (ν C=C_{aromatic}), 1383 (δ CCH), 1295, 1145 (opp CCH_{aromatic} and CCH_{skeletal}), 973 (=CH _{δ ,opp}). Elemental analysis (%) calculated for C₁₇H₁₄N₂O₂·0.15 H₂O (281.01 g mol⁻¹) calculated: C 72.66, H 5.13, N 9.97; found: C 72.18, H 4.43, N 10.07.

Synthesis of 1.³⁵ **3pyCCMoid** (5 mg, 0.0180 mmol) and Zn(NO₃)₂·6H₂O (16 mg, 0.054 mmol) were added to a mixed solvent involving DMA (0.5 mL) and methanol (1.5 mL). After blending well by sonication at RT, the solution was heated in a

closed vessel at 80 °C for 3 days to obtain orange crystals with a size of about 1 mm. The crystals were washed and kept in MeOH. FTIR data (KBr, cm⁻¹): 1633 (ν C=C_{aromatic}), 1548 (C=O_{st, β -diketone}), 1509 (ν C=N) 1462 (ν C=C_{aromatic}), 1383 (δ CCH), 1298, 1160 (opp CCH_{aromatic} and CCH_{skeletal}), 970 (=CH _{δ ,opp}). Elemental analysis (%) calculated for [Zn(3py-CCM)₂]_{*n*}/2ZnO or C₃₄H₂₈N₄O_{5.5}Zn_{0.5} (659.6 g mol⁻¹) calculated C:61.8, H:3.96, N:8.48; found: C:61.56, H:4.055, N:8.6.

Synthesis of 2.³⁵ The amount of the ligand and metal salt used to synthesize **2** was the same as that for **1**. The reaction was performed in a mixed solvent involving DMA (0.5 mL) and absolute ethanol (1.5 mL), following the procedure previously described for **1**. The obtained orange crystals were washed and kept in EtOH. FTIR data (KBr, cm⁻¹): 1641 (ν C=C_{aromatic}), 1550 (C=O_{st, β -diketone}), 1512 (ν C=N) 1463 (ν C=C_{aromatic}), 1384 (δ CCH), 1295, 1160 (opp CCH_{aromatic} and CCH_{skeletal}), 970 (=CH _{δ ,opp}). EA (wt%) data for [Zn(3py-CCM)]_{*n*}/1/2nH₂O or C₁₇H₁₄N₃O_{5.5}Zn (413.68 g mol⁻¹) calculated C: 49.35, H: 3.41, N:10.15; found C:49.33, H:3.33, N:9.8.

Synthesis of 4. 3pyCCMoid (30 mg, 0.108 mmol) was dissolved in 1.5 mL of DMF and placed at the bottom of an elongated vial. Then 1 mL of EtOH was placed on the top. Finally, 64 mg (0.215 mmol) of Zn(NO₃)₂·6H₂O, dissolved in 2.5 mL of EtOH, were added. After the system set-up, it can be observed that the clean EtOH was forming a clearly visible boundary between the solvents keeping the two reagents. After 2–3 weeks, the formation of crystals was observed on the vial walls. These crystals were cleaned several times with fresh EtOH and kept in this solvent. The characterization of **4** by IR spectroscopy and elemental analysis was not possible because only a few crystals are obtained.

Exfoliation of 2. A suspension of 1 mg of the crystalline sample of **2** was prepared in 1 mL of Milli-Q H₂O and added to 2 mL vials, which were sonicated for 1 h. Then, the vials were left undisturbed for 6 h. During this time, the deposition of the largest multi-layer nanosheets is expected, while those with only a few layers remain dispersed in the solvent. The presence of residual nanosheets in the solvent is proved by the Tyndall effect using a conventional laser. In the experiment where the effect of H₂O on the degradation of the nanosheets is tested, 10 μ L of the solvent was placed on the top of a vial containing 50 μ L of fresh Milli-Q H₂O. The liquids were mixed using a vortex. For analysis, 10 μ L of the solvent on the top of the vial was placed on a TEM grid or on a SiO₂/Si surface.

Characterization

Single crystal X-ray diffraction data for **1** and **4** were collected at the XALOC beamline 13 of Alba-CELLS Synchrotron (Spain) (*T* = 100 K, λ = 0.82654 Å for **1** and 0.729 Å for **4**), data for **3pyCCMoid** at the ALS Synchrotron (Berkeley, USA) (*T* = 100 K, λ = 0.7749 Å) and data for **2** using a Bruker D8 Venture diffractometer at 293(2) K (λ = 0.71073 Å). The structures were solved by intrinsic phasing methods (SHELXT using the XIA package for the data collected on the beamline) and refined on *F*².³⁶ Hydrogen atoms were included at the calculated positions, riding on their carrier atoms. Powder X-ray diffraction (PXRD)



patterns were collected on a Panalytical X'PERT PRO MPD diffractometer using Cu K α radiation ($\lambda = 1.5418 \text{ \AA}$) at 295 K. The simulated powder patterns were calculated from the single crystal crystallographic data using Mercury 3.7 programme. Fourier transform infrared (FTIR) spectra were obtained using an FT-IR JASCO 4700LE using the ATR (attenuated total reflectance) accessory in the range between 600 and 4000 cm^{-1} . Elemental analyses were carried out using a PerkinElmer 2400 series II analyser. $^1\text{H-NMR}$ spectra were obtained on a Bruker Advanced at 300 MHz and 298 K. Thermogravimetric analysis was performed under a N_2 atmosphere from room temperature to 1000 $^\circ\text{C}$ at a heating rate of 10 $^\circ\text{C min}^{-1}$, using a simultaneous thermogravimetric analysis (TG)-differential scanning calorimetry/differential thermal analysis (heat flow DSC /DTA) system NETZSCH-STA 449 F1 Jupiter. Images of the nanosheets for the morphological analysis were obtained with a TEM 120 kV JEOL 1210. The composition of the nanosheets was roughly estimated using a SEM Magellan 400L working in STEM mode and equipped with an X-Max Ultim Extreme EDX (Oxford Instruments). The determination of the nanosheet thickness was performed by analysing the topographic images obtained with a Keysight 5100 using the software WSxM 5.0.³⁷

Conclusions

This work presents the ligand **3pyCCMoid** as a promising heteroditopic ligand in the field of CPs. The synthesis of this molecule together with three new CPs, **1–3**, containing exclusively **3pyCCMoid** as a linker among the Zn^{II} centres, provides structures that extend from 1D to 3D. This work illustrates the versatile architectures that are possible thanks to this ligand and presents CCMoids as reliable connectors, emphasizing that their use in coordination chemistry should not be limited to curcumin. Our work describes the structures and basic physicochemical properties of the three new CPs, as well as pays great attention to the study of compound **2**, due to its 2D nature. Here, stability studies in organic solvents and exfoliation in H_2O have been introduced finding a way to achieve extended few-layered materials and analysing the factors that could degrade the system. We would like to extend our studies to other metals as well as heterometallic systems. In addition, extended biocompatibility studies of **3pyCCMoid** and CPs will be analysed toward their possible use as active ingredients in therapeutic uses and/or nano-/microdevices.

Author contributions

Conceptualization and writing, N. A.-A, C. D and M.S.; experimental part CPs, L. R.-C., W. Q., J. I.-A. and E. M.-O.; L. R.-C. and W. Q. made equal contributions to this work; experimental part 3-pyCCMoid, A. E.-B.; supervision of experimental work, A. G.-C and A. L.-P.; acquisition and/or resolution of crystallographic data, D. C.-L., E. C. S., O. R. and J. G. P. All authors have read and agreed to the published version of the manuscript.

Conflicts of interest

There are no conflicts to declare.

Acknowledgements

This work has received funding from the European Research Council (ERC) under the European Union's Horizon 2020 R&D programme (ERC-724981). We also acknowledge the Spanish Government, Ministerio de Ciencia e Innovación (projects CTQ2017-83632, CTQ2015-68370-P, PGC2018-098630-B-I00, MAT2016-77852-C2-1-R, CTQ2016-75150-R, PGC2018-098630-B-I00, PGC2018-102047-B-I00 and Ramon y Cajal grant RYC-2017-22910) and the Generalitat de Catalunya for the grant 2017SGR1277. The work at the University of Chile was supported by ANID, Fondecyt Regular Project 1201962 and 1161775 (M. S.). C. D., N. A.-A., A. L.-P., A. G.-C., and L. R.-C. acknowledge the financial support through the "Severo Ochoa" program for Centres of Excellence in R&D (SEV-2015-0496) under the FUNMAT-FIP-2016 fellowship. Some of the experiments were performed at the XALOC46 and NCD-SWEET beamlines of the ALBA synchrotron with the support of ALBA staff and at the Advanced Light Source (ALS) synchrotron. The Advanced Light Source is supported by the Director, Office of Science, Office of Basic Energy Sciences of the U.S. Department of Energy under contract no. DE-AC02-05CH11231. This work (L. R.-C.) has been done in the framework of the doctoral program "Chemistry" of the Universitat Autònoma de Barcelona.

Notes and references

- (a) K. Ariga, M. Nishikawa, T. Mori, J. Takeya, L. K. Shrestha and J. P. Hill, *Sci. Technol. Adv. Mater.*, 2019, **20**, 51–95; (b) S. Kitagawa, R. Kitaura and S. Noro, *Angew. Chem., Int. Ed.*, 2004, **43**, 2334–2375; (c) B. Moulton and M. J. Zaworotko, *Chem. Rev.*, 2001, **101**(6), 1629–1658.
- (a) J. L. Wang, X. Y. Wang, Y. Wang, X. Y. Hu, J. R. Lian, Y. L. Guan, H. Chen, Y. He and H. S. Wang, *Coord. Chem. Rev.*, 2020, **411**(213256), 1–21; (b) W. L. Leong and J. J. Vittal, *Chem. Rev.*, 2011, **111**, 688–764.
- C. Janiak, *Dalton Trans.*, 2003, 2781–2804.
- (a) M.-A. Haga, K. Kobayashi and K. Terada, *Coord. Chem. Rev.*, 2007, **251**, 2688–2701; (b) F. Novio, J. Simmchen, N. Vázquez-Mera, L. Amorín-Ferré and D. Ruiz-Molina, *Coord. Chem. Rev.*, 2013, **257**, 2839–2847.
- (a) K. Uemura, R. Matsuda and S. Kitagawa, *J. Solid State Chem.*, 2005, **178**, 2420–2429; (b) C. R. Murdock, B. C. Hughes, Z. Lu and D. M. Jenkins, *Coord. Chem. Rev.*, 2014, **258**, 119–136.
- (a) A. Y. Robin and K. M. Fromm, *Coord. Chem. Rev.*, 2006, **250**, 2127–2157; (b) B. H. Ye, M. L. Tong and X. M. Chen, *Coord. Chem. Rev.*, 2005, **249**, 545–565.



- 7 (a) T. S. Basu Baul, A. Chaurasiya, A. Duthie, P. Montes-Tolentino and H. Hopfl, *Cryst. Growth Des.*, 2019, **19**, 6656–6671; (b) F. Wang, J. Zhang, X. Ding, S. Dong, M. Liu, B. Zheng, S. Li, L. Wu, Y. Yu, H. W. Gibson and F. Huang, *Angew. Chem., Int. Ed.*, 2010, **49**, 1090–1094.
- 8 C. Maxim, D. Branza, M. Allain, M. Andruh, R. Clerac, B. Iorga and N. Avarvari, *CrystEngComm*, 2012, **14**, 3096–3102.
- 9 (a) S. Rojas, T. Devic and P. Horcajada, *J. Mater. Chem. B*, 2017, **5**, 2560–2573.
- 10 (a) H. Su, F. Sun, J. Jia, H. He, A. Wang and G. Zhu, *Chem. Commun.*, 2015, **51**, 5774–5777; (b) X. Feng, Y. Wang, F. Muhammad, F. Sun, Y. Tian and G. Zhu, *Cryst. Growth Des.*, 2019, **19**, 889–895.
- 11 N. Portoles-Gil, A. Lanza, N. Aliaga-Alcalde, J. A. Ayllon, M. Gemmi, E. Mugnaioli, A. M. Lopez-Periago and C. Domingo, *ACS Sustainable Chem. Eng.*, 2018, **6**, 12309–12319.
- 12 L. Rodríguez-Cid, E. C. Sañudo, A. M. López-Periago, A. González-Campo, N. Aliaga-Alcalde and C. Domingo, *Cryst. Growth Des.*, 2020, **20**(10), 6555–6564.
- 13 E. A. Philip, *Progress in Heterocyclic chemistry*, ed. G. Gribble and J. A. Joule, Elsevier Ltd, 2011, vol. 22, pp. 349–391.
- 14 Y. Hamada, *Pyridine*, ed. P. P. Pandey, IntechOpen, 2018, vol. 9, pp. 9–25.
- 15 A. Y. Guan, C. L. Liu, X. F. Sun, Y. Xie and M. A. Wang, *Bioorg. Med. Chem.*, 2016, **24**, 342–353.
- 16 N. N. Jha, D. Ghosh, S. Das, A. Anoop, R. S. Jacob, P. K. Singh and S. K. Maji, *Sci. Rep.*, 2016, **6**, 1–15.
- 17 R. J. Anto, G. Kuttan, K. D. Babu, K. N. Rajasekharan and R. Kuttan, *Pharm. Pharmacol. Commun.*, 1998, **4**, 103–106.
- 18 M. Zhao, Y. Huang, Y. Peng, Z. Huang, Q. Ma and H. Zhang, *Chem. Soc. Rev.*, 2018, **47**, 6267–6295.
- 19 H. J. J. Pabon, *Recl. Trav. Chim. Pays-Bas*, 1964, **83**, 379.
- 20 Y. Chen, P. Huang, H. Chen, S. Wang, H. Wang, J. Guo, X. Zhang, S. Zhang, J. Yan, J. Xia and Z. Xu, *ACS Biomater. Sci. Eng.*, 2018, **4**, 4095–4103.
- 21 C. Tamames-Tabar, E. Imbuluzqueta, N. Guillou, C. Serre, S. R. Miller, E. Elkaïm, P. Horcajada and M. J. Blanco-Prieto, *CrystEngComm*, 2015, **17**, 456–462.
- 22 N. Aliaga-Alcalde, L. Rodríguez, M. Ferbinteanu, P. Höfer and T. Weyhermüller, *Inorg. Chem.*, 2012, **51**, 864–873.
- 23 The two planes used to measure planarity were made using the *meta*-positions of the aromatic rings and the central carbon of the studied **3pyCCMoid**, hence N'–C8''C1 and N–C8–C1 atoms from Fig. 1.
- 24 R. Seetharaj, P. V. Vandana, P. Arya and S. Mathew, *Arabian J. Chem.*, 2019, **12**, 295–315.
- 25 Y. Q. Lan, H. L. Jiang, S. L. Li and Q. Xu, *Inorg. Chem.*, 2012, **51**, 7484–7491.
- 26 R. Díaz-Torres and S. Alvarez, *Dalton Trans.*, 2011, **40**, 10742–10750.
- 27 (a) A. Krężel and W. Maret, *Arch. Biochem. Biophys.*, 2016, **611**, 3–19; (b) H. Vahrenkamp, *Dalton Trans.*, 2007, 4751–4759; (c) A. Erxleben, *Coord. Chem. Rev.*, 2003, **246**, 203–228.
- 28 Y. Song, J. Yang, L. Wang and Z. Xie, *ChemMedChem*, 2020, **15**, 416–419.
- 29 M. Zhao, Y. Huang, Y. Peng, Z. Huang, Q. Ma and H. Zhang, *Chem. Soc. Rev.*, 2018, **47**, 6267–6295.
- 30 P. Amo-Ochoa and F. Zamora, *Coord. Chem. Rev.*, 2014, **276**, 34–58.
- 31 M. Bazargan, M. Mirzaei and M. Akbari, *J. Mol. Struct.*, 2019, **1188**, 129–141.
- 32 C. L. Tan, X. H. Cao, X.-J. Wu, Q. Y. He, J. Yang, X. Zhang, J. Z. Chen, W. Zhao, S. K. Han, G.-H. Nam, M. Sindoro and H. Zhang, *Chem. Rev.*, 2017, **117**, 6225.
- 33 W. Qian, A. González-Campo, A. Pérez-Rodríguez, S. Rodríguez-Hermida, I. Imaz, K. Wurst, D. MasPOCH, E. Ruiz, C. Ocal, E. Barrena, D. B. Amabilino and N. Aliaga-Alcalde, *Chem. – Eur. J.*, 2018, **24**, 12950–12960.
- 34 E. V. Antina, N. A. Bumagina, A. I. Vyugin and A. V. Solomonov, *Dyes Pigm.*, 2017, **136**, 368–381.
- 35 W. Qian, PhD thesis, Universitat Autònoma de Barcelona, Spain, 2018, https://ddd.uab.cat/pub/tesis/2018/hdl_10803_664220/weqi1de1.pdf.
- 36 G. Sheldrick, *Acta Crystallogr., Sect. C: Struct. Chem.*, 2015, **71**, 3–8.
- 37 I. Horcas, R. Fernández, J. M. Gomez-Rodriguez, J. W. Colchero, J. W. Gómez-Herrero and A. M. Baro, *Rev. Sci. Instrum.*, 2007, **78**, 013705.



